TECHNISCHE UNIVERSITÄT WIEN
Vienna | Austria

Master`s thesis

Airborne particulate matter in the subway system of Vienna

Under the Supervision of

Ao. Univ. Prof. Dipl.-Ing Dr. techn. Anne Kasper-Giebl

(E164 Institute of Chemical Technologies and Analytics)

Submitted to TU Wien

Faculty of Technical Chemistry

By

Aron Göndör

Vienna, 2021

"...

I`ve got to experiment to get data,

To analyze them later,

Statistical relationship,

Linear, expo, logarithmic

L A B, laboratory

that`s the place where I like to be.

Unknown territories I explore,

Wow, I`ve never seen this before.

Eco-systemic influences,

not a lot of differences

between nature and urban systems

I`ve got to analyze similarities

..."

SHP – *"My research"* (Pupajim et al., 2017)

Acknowledgements

I wish to express my greatest gratitude to my supervisor, Prof. Anne Kasper-Giebl, for all the continuing support and guidance I got throughout the journey leading to this thesis. She granted me the opportunity of working at her research group, which proved to be a truly inspiring time of my life, steering and amplifying my interests towards the field of atmospheric chemistry.

I would also like to praise the know-how and instructor skills of Magdalena Berger, who taught me the appropriate techniques, regarding the handling and operation of the monitoring and sampling instruments. She was also a fantastic company during this endeavor, allowing me to ask many questions and showing me great patience on all accounts.

I am also deeply and equally grateful to all the further members of the Environmental Analytics research group, especially to Bernadette Kirchsteiger, Daniela Kau, Thomas Steinkogler, Peter Redl, Karoline Rieger and Hong Huang who kindly welcomed me as their colleague and created a delightful work environment. They taught me not only the handling of all the required lab instruments but helped me with the distillation of the relevant information, data interpretation and visualization, providing me with their open feedbacks. Additionally, I would like to thank Bernadette, Daniela, and Hong for the proofreading of the thesis.

I also wish to thank Christopher Herzig and Andreas Limbeck for their enduring support in the elemental analysis. Additionally, I would like to express my thanks to Manuel Hahn, Philipp Aschenbrenner and Johann Fellner for providing me with the tools for the sample digestions. Further I want to thank Hans Lohninger for supplying me with a free license of DataLab for performing the statistical analysis presented in this work.

I would also like to thank the Wiener Linien for financing part of the work presented within this thesis. Further on, I would like to thank, in particular, Irene Popp and Claudia Ramskogler-König for the organization, and their personal participation in the measurements.

Abstract

Since its opening more than 40 years ago, the subway system in Vienna affirmed itself as an elemental part of the capital`s infrastructure. While subway systems are offering a convenient and environmentally friendly option of getting around in major cities all around the world, recent studies of air quality in these microenvironments focused on the elevated particulate matter (PM) concentrations.

In addition to a comprehensive literature survey a measurement campaign was performed at four different stations in six platform and tunnel locations to evaluate and characterize the PM_{10} levels using a Low Volume Sampler for gravimetric and chemical analysis, side by side with an Optical Particle Counter and an Electric Low-Pressure Impactor to identify the impact on air quality.

The findings of the present study display elevated degrees of airborne ferruginous dust, depending predominantly on the rate of passing trains and number of commuters, producing daily repetitive trends of PM_{10} mass concentration variations. The mean PM_{10} concentrations ranged between 97 µg/m^3 and 341 µg/m^3 in the Viennese subway system, thereby placing it in an average position, with respect to subway PM concentrations in other European cities, described in the literature. A unique feature of the current work is that measurements were conducted within the tunnels and not only on the platforms. Within the dataset collected during this work, marked concentration differences between platform and tunnel locations couldn`t be confirmed. The proportionately coarse $PM_{10\text{-}2.5}$ mode contributed a major share, with relative contributions between 45 % to 70 % to the PM_{10} mass concentrations. Meanwhile, the particle number concentrations were not elevated regarding common urban concentration values, reaching 1-2*10^4 #/cm^3, influenced mainly by particles with a mean aerodynamic diameter less than 0.3 µm. Spatial and temporal concentration variations, monitored on the platform levels, were analyzed, and discussed with regard to factors like station designs and train frequencies, inter alia. Further on, source analysis could identify PM sources within the subway system and, to a smaller extent, ambient influences as well.

Table of contents

Chapter 1) Introduction

1.1 Task formulation

The investigation of the air quality in the subway microenvironment was done by aerosol collection on filter samples and simultaneous monitoring of PM levels via continuously registering instruments. The collected filter samples enabled the evaluation of four-hour mean PM_{10} mass concentration levels and a subsequent chemical analysis. At the same time the high-resolution monitoring instruments registered additional information regarding the brief temporal and spatial changes in the particulate matter concentration levels along the Viennese subway system. The measurement campaign was undertaken between October 2019 and in March 2020.

The evaluation of the collected data focused on discussing and answering the following questions:

- What are the particulate matter concentration levels encountered in the platform and tunnel areas of the subway system of Vienna?
- What conclusions can be drawn from the spatial and temporal subway PM variations of concentration values?
- What is the chemical composition of the subway PM samples?
- How does the particle size distribution look like?

1.2 The subway system of Vienna

The construction of the Viennese subway, the partial inheritor of the Viennese "Stadtbahn", started in 1969, while the initial operation of the first section to the public was opened in 1978 (Bensch, 2013). The construction of new lines and the expansion of old ones hasn`t stopped ever since (excluding minor breaks), earning its designation to "high-performance urban arteries", connecting other transport modes, and thus absorbing a great share of the urban commuting load. The total operating length of the underground system is 83,4 km consisting of 109 stations, with a ridership of almost 460 million in 2019 (Wiener Linien, 2020). The station Altes Landgut U1 lies approximately 30 meters underground and is currently the deepest platform of the Viennese metro system (Wiener Linien, 2018).

The global trend of urbanization and thus rapid population growth in cities shaped the last 25 years of Vienna as well. The net population growth observed since 1995 is around 369k, thereby reaching an inhabitant size of approximately 1.9 million at the beginning of 2020 (City of Vienna, 2020). However, Vienna topped for the 10^{th} consecutive time the Mercer ranking list in 2019, entitling the Austrian capital as "the city with the highest quality of living worldwide", justified by the organized and trustworthy public transport network next to the exceptional tap water quality, healthcare, and cultural opportunities, amongst other criteria (City of Vienna, 2019). On the other hand, urban development frequently entails negative impacts on air quality in cities and agglomerations around it, due to the enhanced motorized traffic emissions, including greenhouse gases (Wen et al., 2020). Thus, from an environmental point of view, the commutation via low-carbon transport modes, like underground subway systems, has the qualities of the cleanest forms of transportation next to e-mobility and active transport modes in cities (Querol et al., 2012).

1.3 Particulate Matter

Particulate matter (PM) counts as a key factor for the estimation of air quality levels worldwide, being one of the six major air pollutants, next to ground-level ozone, carbon monoxide, sulfur dioxide, nitrogen dioxide and lead, listed by the Environmental Protection Agency (EPA) of the U.S., for which Air Quality Indices (AQI) were established and National Ambient Air Quality Standards (NAAQS) were set in the United States.

EPA`s Integrated Science Assessments (ISA) report on Particulate Matter defines PM as a collective terminology for chemically and physically diverse substances, consisting of a mixture of solid and liquid particles suspended in the air. The characteristics of particulate matter, including the differing aerodynamic sizes, shapes, and chemical compositions, are mainly framed by their generation and subsequent transformation processes, and vary broadly according to the seasons, time of the day, region, meteorology, and source category (EPA, 2019). The origins of airborne particles can be allocated according to different aspects regarding their sources and formation processes, thereby grouping them either into anthropogenic/natural, or into primary/secondary aerosols. Aerosols directly emitted into the air are called primary PM and can have both anthropogenic and natural sources. Major anthropogenic sources of primary particulate matter include, amongst others, combustion of wood and fossil-based fuels for energy or commutation purposes, agricultural operations, and construction activities. Meanwhile, natural sources of primary particulate matter involve vegetational pollen sources, wildfires, and emission of sea salt aerosols. In comparison, secondary particles are formed in the atmosphere by gaseous precursors such as sulfur oxides (SO_X), oxides of nitrogen (NO_X), ammonia (NH_3) and volatile organic compounds (VOCs) originating from both natural (e.g., microbial and biogenic VOCs) and human-made sources (e.g., vehicle or industrial emission sources) (World Health Organization, 2013). The Directive 2008/50/EC of the European Parliament defines PM_{10} as the particulate matter fraction which passes through a size-selective inlet as defined in the reference method for the sampling and measurement of PM_{10}, EN 12341, with a 50 % cut-off efficiency at an aerodynamic diameter of 10 µm. Consequently, the $PM_{2,5}$ and PM_1 size fractions can be formalized in an identical manner (The European Commission, 2008). A simplified definition characterizes PM_{10} as particulate matter with a nominal mean aerodynamic diameter less than or equal to 10 µm.

Over the years of collecting data for epidemiologic studies concerning the health effects related to air pollution, a scientific consensus emerged about the importance regarding the distinction of fine and coarse particulate matter fractions, encouraging the concept of size selective particulate matter sampling (Brown et al., 2013). The PM_{10} aerosol fraction can be divided into the coarse sub-fraction of inhalable particulates with a nominal mean aerodynamic diameter greater than 2.5 µm and less than or equal to 10 µm ($PM_{10-2.5}$) and the $PM_{2.5}$ fraction, which furtherly encompasses the ultrafine particle fraction (UFP), usually considered as aerosols with an aerodynamic diameter less than or equal to 0.1 µm (P. Kumar et al., 2014).

Generally, both the coarse and the two finer particle modes contribute to the PM concentration levels encountered in the urban environments of most cities, although the ratios comparing the three aerodynamic size fractions tend to alter according to the parameters mentioned previously, such as the local geography, meteorology, and specific PM sources, amongst further criterions (World Health Organization, 2005). Aerosol particles part of the coarse $PM_{10-2.5}$ mode usually originate either from natural sources and processes like wind erosion and mechanical abrasion of materials derived from crustal origin, or natural activity emitting organic substances in the form of biological material, such as bacteria, endotoxins, or pollen. Meanwhile, the combustion-based processes, employed for the sustenance of the motorized traffic, industrial production, and power generation in urban areas, emit primary and secondary aerosol particles within the finer $PM_{2,5}$ size mode. The UFP particle mode owns only a limited residence time in the atmosphere, principally due to accumulation and coagulation processes merging them into fine particles with increased aerodynamic diameter sizes (Pope, 2000). Even though the influence of UFP on PM mass concentrations are rather moderate, they dominate the total particle number concentration with a contribution of over 80 % (Hussein et al., 2004; Moore et al., 2009).

1.3.1 Health effects

Since the 1970s, high concentration levels of PM air pollution have been linked to various health impacts by different research teams employing diverse analytical methods (Pope & Dockery, 2006). As the process of urbanization is still a globally ongoing trend with the expected urban population to rise to 66 % by 2050 (United Nations, 2015), the assessment of the health-risks posed by air pollution to urban dwellers is becoming more vital than ever.

One aspect for the estimation of the pathogenic potential of the inhaled PM is through the evaluation of the regional pattern of the particulate deposition in the human respiratory tract (HRT), which can be principally partitioned into three segments, regarding personal exposition: extrathoracic, tracheobronchial, and alveolar (pulmonary) region (Patwa & Shah, 2015). On the other hand, most particulate matter sampling methods are specified in relation to the aerosols` penetration depth into the HRT instead of the anticipated regional particle deposition rate (Brown et al., 2013), whereby three specific particle mass fractions were defined by the European Committee for Standardization (CEN), accordingly. Therein the inhalable fraction is characterized as the aerosol fraction which can be inhaled over nose and mouth. The mass fraction of inhalable particles that is capable of trespassing the larynx is defined as the thoracic fraction, which can be further on subdivided into the respiratory fraction, incorporating particles penetrating to the gas-exchange region. Regarding the penetration efficiency of the inhaled PM, particles with an aerodynamic diameter size of 10 µm and 4 µm possess a 50 % penetration rate into the thoracic and respiratory fractions, respectively (CEN, 1993). Albeit, the actual deposition and retainment load of the inhaled PM is determined by further aspects, on the one hand by factors as the exposure concentration and duration, the particular state of physical activity; ranging from resting to physical labor and sport, the inhalation pattern either through the oral or nasal passage; with the nasal airway marked as a more efficient particle filtration route (Lippmann et al., 1980), and on the other hand by particle characteristics (e.g., particle size, hygroscopicity, solubility in airway fluids ,and cellular components). In line with the age group, gender, activity level and health condition, the proportion of oral versus nasal breathing is differing in individuals, thereby adding extra perplexity to the general assessment of PM deposition in the HRT (EPA, 2019). Even so, modern computational models have been recently emerging in order to give further insights into the behavior of aerosol particles entering the respiratory tract (Bui et al., 2020).

The key findings of the 2019 Integrated Science Assessment for Particulate Matter, based on the review of decades-long scientific data conducted by the EPA, confirm the negative health impacts connected to both long-term and short-term PM exposure, with the most compelling indications assigned to the link between various health effects and $PM_{2.5}$. The ISA investigation of epidemiological studies indicated causal relation of both short and long-term $PM_{2.5}$ exposure to cardiovascular effects and non-accidental mortality rate, further on likely to be causal relationship to respiratory effects and cancer, while the evidence on metabolic effects, procreative effects and short-term exposure and nervous system effects showed suggestive linkage, but not sufficient to infer a causal connection. It was also stated that the fluctuations regarding the risk assessments by public health investigations may not be solely connected to differences in the composition of $PM_{2.5,}$ but rather mirror the region-specific exposure conditions, shaped mainly by habitation and commutation characteristics. The information regarding the dose-response correlation suggests a linear, no-threshold concentration-response relationship, with less confidence about the curve`s form at lower $PM_{2,5}$ concentrations. Epidemiological studies on the coarse $PM_{10-2.5}$ fraction are less straightforward, partly due to the greater spatial variability of $PM_{10-2.5}$ concentrations, increasing the uncertainty of the interpretation of the health impact investigations, which have been examined to a lesser extent only, compared to the studies inspecting the effects caused by the finer $PM_{2.5}$ fraction. Hence, these limitations on the latest evidence base for short and long-term $PM_{10-2.5}$ exposure levels hinder an adequate causality determination regarding the induced adverse health impacts. Similarly, the spatial and temporal variations of the UFP fraction complicate the interpretation of the limited epidemiological studies, providing inconsistent information on the effects due to short-term and long-term ultrafine particle exposure on humans. Still, there is strong evidence regarding the translocation of UFP exterior to the HRT, thereby presumably possessing the ability of entering the circulation and reaching various organs, thus bearing potentially hazardous capabilities. (EPA, 2019)

1.3.2 Air quality monitoring networks and guidelines

Over the last 50 years, wealthier nations achieved to enact a robust system of air quality supervision, consisting of large-scale ambient monitoring, emission source identification, and emission reduction projects, operated in a decentralized manner through a large number of initiatives run by citizens, communities, companies, non-profit organizations, and governments. Although these actions proved to generate positive trends in developed countries, apparent through a general declining tendency in emissions and ambient air pollution concentrations in spite of the ever-growing economic development and motorized vehicle usage (Awe et al., 2017), the contrary effect can be seen for social-economically less developed nations with less widespread monitoring capabilities, where the inhabitants are up to encounter $PM_{2.5}$ exposure levels that can be four to five times those of more-developed countries (Health Effects Institute, 2019). For these regions without available measurement data, exposure estimations have been mainly provided by means of modelling techniques, like spatial interpolation methods, land use regression, dispersion models, and chemical transport models (EPA, 2019).

1.3.2.1 Outdoor PM limit values

In 1987, the first outdoor air quality guidelines (AQGs) were produced by the WHO, covering the four key air pollutants (PM, NO_2, SO_2, O_3), with the aim of giving guidance for governments in reducing the health impacts of air pollution worldwide. Following the principle of subsidiarity, air quality standards are established separately by each country around the globe, mirroring the national capacity of air quality control, dependent mainly on the technological feasibility, economic considerations, and other political and social factors (World Health Organization, 2005). Hence, the European Union implemented its own air quality standards, with current limit values set in the Ambient Air Quality Directives 2004/107/EC and 2008/50/EC for all the Member States (The European Commission, 2004)(The European Commission, 2008).

In Austria, the Air Pollution Control Act (Immissionsschutzgesetz – Luft, IG-L) is responsible as the central law to enforce the threshold values set by the EU Directives. The contemporary Air Quality Guidelines and Standards are summarized in Table 1.1, where different averaging periods have been applied in alignment with the observed dependence of the associated adverse health effects and exposure time. The European Ambient Air Directive permits an annual maximum of 35 exceedance days regarding the daily limit values, while the Austrian Air Pollution Control Act (IG-L) allows 25 days. The supervision of the air quality levels is managed by the Member States by dividing its territories into zones and agglomerations, where air pollution levels are assessed through measurements by air monitoring stations and modelling techniques, and the collected data is reported to the European Commission respectively (The European Commission, 2015).

Table 1.1 Existing Air Quality Guideline and Air Quality Standard limit values set by the World Health Organization and the European Commission, respectively

Air Quality Guideline		**WHO**	**EU**	**Austria (IG-L)**
Allowed annual exceedance (regarding daily values)			*(35 days)*	*(25 days)*
			[μg/m³]	
$PM_{2,5}$	*annual*	10	25	25
	daily	25		
PM_{10}	*annual*	20	40	40
	daily	50	50	50

The 2019 report on the air quality of Europe, conducted by the European Environment Agency (EEA), revealed the continuous violation of the EU limit values and of the values stated in the WHO AQGs for substantial parts of Europe in 2016. According to this report, 17 % of the EU`s urban population experienced PM_{10} exposure levels above the daily limit value and roughly 44 % was exposed to PM_{10} levels surpassing the more stringent annual limit values set by the WHO. Concerning the finer $PM_{2,5}$ fraction, 8 % of the urban population, native in the EU, were exposed to concentration levels above the annual EU threshold value, while this proportion amounts to approximately 77 %, considering the Air Quality Guidelines established by the WHO (EEA, 2019). Still, a decreasing trend in air pollution levels can be noticed in the European Member

States, when the collected, publicly accessible air quality monitoring data since the year 2000 is considered. This trend is further on confirmed by the annual Austrian Air Quality report published by the Environmental Agency of Austria, even though significant fluctuation of air quality levels is occurring throughout the years, shaped mainly by meteorological factors next to the current emission behavior. Until 2018, exceedances of the limit values were still recorded regularly at specific air monitoring stations every year (Spangl & Nagl, 2018), despite the progressing tendency of decreasing emission trends in Austria and its eastern neighboring states (Spangl, 2018). 2019 was the first year in Austria since the start of the air monitoring operations in 2000, where no violation of the PM_{10} limit values could be registered. Regarding the various components of the ambient particulate matter, the Austrian Air Pollution Control Act (IG-L) sets annual threshold values for selected pollutants, that is 0.5 $\mu g/m^3$ for Lead, 6 $\mu g/m^3$ for Arsenic, 5 $\mu g/m^3$ for Cadmium, 20 $\mu g/m^3$ for Nickel and 1 ng/m^3 for Benzo(a)pyrene. The limit value (IG-L) of Benzo(a)pyrene was violated only at one, while the threshold value for lead was exceeded at two monitoring stations in 2019 (Nagl & Spangl, 2020).

1.3.2.2 Indoor PM limit values

In Germany, additional general indoor airborne dust limit values have been defined for the protection of the respiratory organs of laborers in the Technical Regulations for Hazardous Materials (Technische Regeln für Gefahrenstoffe-TRGS 900) by the German Federal Ministry of Labor and Social Affairs (Bundesministerium für Arbeit und Soziales, Deutschland – BMAS), where the threshold values were set for poorly or non-soluble particulate matter compounds without further regulations elsewhere. Thereby, the mean mass concentration value for an eight-hour work period was regulated to 1.25 mg/m^3 (based on particles with a density of 2.5 g/cm^3) and 10 mg/m^3 (without reference to particle density) concerning the respirable and inhalable fractions, respectively (BMAS, 2021).

Further on, specific maximum allowable concentration (Maximale Arbeitsplatz Konzentrationswerte - MAK) values were set for several components of airborne particulate matter, and guideline values were set for biologically inert airborne dust concentrations for the workplace in the Austrian Limit Value Ordinance (Grenzwertverordnung – GKV), additionally. Here, the threshold values for the inert PM were set to a daily mean concentration of 5 mg/m^3 and 10 mg/m^3 for the respirable and inhalable fractions, correspondingly. An overview of the maximum allowable concentration values, regarding the relevant compounds found in the microenvironment of subway systems, is presented in Table 1.2, with a noteworthy value of 10 mg/m^3 for iron oxides, as they have the highest contribution to the subway PM (further discussion in section 1.4).

Table 1.2 Overview of the maximum allowable concentration values relevant for the subway microenvironment (Maximale Arbeitsplatz Konzentrationswerte - MAK)

		MAK value [mg/m^3]	
Compound-type	*Fraction*	*inhalable*	*respirable*
Iron oxides		10	
Chromium		2	
Manganese and its inorganic compounds		0.2	0.05
Zinc oxide-smoke		5	
Antimony		0.5	
Cadmium and its compounds		0.004	
Nickel and dust generated from nickel-compounds and -alloys		0.5	
Lead and its compounds		0.1	
Copper and its compounds		1	
Beryllium and its compounds		0.0006	

1.4 PM in the microenvironment of subway systems

The burdens of poor air quality may not be comprehensively portrayed by the health impacts on society without the resulting economical load and drag on development, manifesting primarily in monetary expenses regarding the treatment and management of air pollution related health problems and the productivity loss due to the consequential absence of work (World Bank and Institute for Health Metrics and Evaluation, 2016). According to recent estimations, 91 % of the world`s population and 96 % of EU citizens live in areas with air pollution levels exceeding the WHO`s global air quality guidelines (World Health Organization, 2016)(ECA, 2020). An impact assessment produced by the European Commission in 2013 estimated the annual costs of total health related expenses, caused by air pollution, to range between € 330- 940 billion (The European Commission, 2013), while a 2020 report by the Centre for Research on Energy and Clean Air, focusing merely on the air pollution generated by the combustion of fossil fuels, suggests an international daily cost of US$ 8 billion (approximately € 6.8 billion based on the exchange rate on 12th of August 2020), equivalent to 3.3 % of the global GDP, among which the greatest financial cost was attributed to $PM_{2.5}$, next to NO_X and ozone, considered in the study (Farrow & Miller, 2020).

Over the last two decades, researchers started to report particulate matter mass concentration levels in the underground microenvironments of subway systems in cities all around the world. A wide range of studies evolved, focusing primarily on the characterization of the factors shaping the air quality dynamics present in these semi-isolated structures, on the possible mitigation and improvement efforts regarding the management of indoor pollutants in existing infrastructures, and on the invention of improved design concepts for future underground rail projects (Xu & Hao, 2017)(Hyeong et al., 2018)(Wen et al., 2020). Due to the inherent character of these semi-enclosed underground systems and the presence of PM emission sources, the accumulation of particulate matter turns out to be the most crucial factor in the determination of a potential detrimental impact on the common health. On the one hand of the public, with comparably short-term commuting exposure periods, and on the other hand of workers, with significant and regular residence time in these underground environments have to be considered (Nieuwenhuijsen et al., 2007).

1.4.1 Global subway PM concentration levels

Numerous studies were conducted to assess the air quality levels inside existing metro systems. Several of the thereby determined mean PM mass concentration values of cities from Europe and of other metropoles from around the globe are presented in Table 1.3 and Table 1.4, respectively. The significant variance of air quality, not only among different subway systems, but also within the corresponding metro lines and individual sampling sites, can be noticed. In addition, the relatively high PM mass concentration levels, compared to typical outdoor concentrations, can be noted in these underground subway systems. In Europe, measured PM_{10} concentrations of subway particulate matter ranged between 24 µg/m^3 and 1500 µg/m^3, with the lowest values determined in Prague, Czech Republic, and the highest in London, United Kingdom, while the detected $PM_{2.5}$ concentrations spread from 11 µg/m^3 in Barcelona, Spain to 421 µg/m^3 in Istanbul, Turkey. Meanwhile, looking at the studies conducted in metro systems at the rest of the world, the marginal extreme PM levels for both the coarse and fine size fractions were found in Shanghai, China, with PM_{10} and $PM_{2.5}$ values ranging between 6 – 975 µg/m^3 and between 5 – 731 µg/m^3, correspondingly. These PM levels were determined in the course of separate studies with a differing instrumental analysis approach, thereby demonstrating some aspects impacting a seamless comparison of conflicting results from different subway PM studies with different monitoring conditions, intervals and seasons. (Qiao, Xiu, Zheng, Yang, Wang, et al., 2015)(Nieuwenhuijsen et al., 2007)(Moreno et al., 2014).

Table 1.3 . Comparison of measured PM concentrations in subway stations from various studies (part 1)

	Country	City	Measurement position	Concentration		Reference
				PM_{10}	$PM_{2,5}$	
Europe	**Czech**	Prague	*Underground*	103	-	*(Braniš, 2006)*
			Train	114 (24-218)	-	
	Finland	Helsinki	*Underground inner subway*	-	23-103	*(Aarnio et al., 2005)*
	France	Paris	*Station platform*	200	61	*(Raut et al., 2009)*
	Germany	Frankfurt	*Station Platform*	101-166	59-85	*(Gerber et al., 2014)*
	Greece	Athens	*Subway platform*	-	68	*(Martins, Moreno, Mendes, et al., 2016)*
	Hungary	Budapest	*Underground*	180 (85-234)	-	(Salma et al., 2007)
				155 (25-322)	-	
	Italy	Milan	*Station platform*	188 (137-239)	-	*(Colombi et al., 2013)*
		Naples	*Station platform*	172-262	45-60	*(Cartenì et al., 2015)*
			Train	58-138	18-36	
		Rome	*Underground*	407 (71-877)	-	*(Ripanucci et al., 2006)*
	Portugal	Lisbon	*Train*	40	13	*(M. J. Ramos et al., 2015)*
		Porto	*Subway platform*	-	84	*(Martins, Moreno, Mendes, et al., 2016)*
	Spain	Barcelona	*Subway platform*	-	58	*(Martins, Moreno, Mendes, et al., 2016)*
			Subway platform (PSDs)	134 (77-192)	41 (22-60)	(Querol et al., 2012)
			Station platform	346 (289-403)	125 (102-148)	
			Train	65 (49-81)	21 (16-26)	
			Platform	-	48 (12-154)	*(Martins et al., 2015)*
			Train	-	33 (11-99)	
			Platform (warmer period)	-	36 (21-52)	*(Martins, Moreno, Minguillón, et al., 2016)*
			Platform (colder period)	-	65 (32-93)	
	Sweden	Stockholm	*Platform*	302-469	165-258	*(Johansson & Johansson, 2002)*
			Platform	357	-	*(Karlsson et al., 2005)*
	Turkey	Istanbul	*Station platform*	170 (72-294)	105 (20-421)	*(Şahin et al., 2012)*
			Underground	-	49-182	*(Onat & Stakeeva, 2014)*
			Train	-	71 (46-161)	
	UK	London	*Underground*	-	247 (105-371)	*(Adams et al., 2001)*
				-	157 (12 - 263)	
			Station platform	1000-1500	270-280	*(Seaton et al., 2005)*
			Inner Subway	-	130-200	
			Train	-	170 (118-201)	

Table 1.4 . Comparison of measured PM concentrations in subway stations from various studies (part 2)

Region	Country	City	Measurement position	Concentration PM_{10}	Concentration $PM_{2,5}$	Reference
Americas	**Argentina**	Buenos Aires	*Platform*	-	152-270	*(Murruni et al., 2009)*
Americas	**Chile**	Santiago	*Train*	-	17	*(Suárez et al., 2014)*
Americas	**Mexico**	Mexico City	*subway platform*	88-145	60-93	*(Mugica-Álvarez et al., 2012)*
Americas	**Mexico**	Mexico City	*Train*	-	38 (8-68)	*(Gómez-Perales et al., 2004)*
Americas	**USA**	Boston	*Train*	-	65 (36-104)	*(Levy et al., 2002)*
Americas	**USA**	Los Angeles	*Station*	78	57	*(Kam et al., 2011)*
Americas	**USA**	Los Angeles	*Train*	32	24	*(Kam et al., 2011)*
Americas	**USA**	New York	*Underground*	-	56	*(Grass et al., 2010)*
Americas	**USA**	New York	*Train*	-	62	*(Chillrud et al., 2011)*
Americas	**USA**	New York	*Train*	-	40 (34-44)	*(X. R. Wang & Oliver Gao, 2011)*
Americas	**USA**	New York	*Subway platform*	-	68 (60-77)	*(X. R. Wang & Oliver Gao, 2011)*
Asia	**China**	Beijing	*Underground*	325	113	*(Li et al., 2007)*
Asia	**China**	Guangzhou	*Subway compartment*	55	44	*(Chan, Lau, Zou, et al., 2002)*
Asia	**China**	Hong Kong	*Subway compartment*	68	21	*(Chan, Lau, Lee, et al., 2002)*
Asia	**China**	Hong Kong	*Train*	120	10	*(Yang et al., 2015)*
Asia	**China**	Shanghai	*Platform*	366 (81-975)	287 (98-731)	*(Ye et al., 2010)*
Asia	**China**	Shanghai	*Tunnel*	69 (6-156)	57 (5-137)	*(Qiao, Xiu, Zheng, Yang, & Wang, 2015)*
Asia	**China**	Shanghai	*Tunnel*	71 (14-234)	61 (13-190)	*(Qiao, Xiu, Zheng, Yang, Wang, et al., 2015)*
Asia	**China**	Shanghai	*Platform*	-	49-66	*(Lu et al., 2015)*
Asia	**China**	Tianjin	*Train*	-	151	*(B. Q. Wang et al., 2016)*
Asia	**India**	Delhi	*Train*	-	78	*(Goel et al., 2015)*
Asia	**Iran**	Tehran	*Underground station platform*	94 (33-126)	52 (24-85)	*(Kamani et al., 2014)*
Asia	**South Korea**	Seoul	*Station platform*	359 (171-480)	129 (83-176)	*(Youn et al., 2008)*
Asia	**South Korea**	Seoul	*Train*	312 (29-356)	126 (115-136)	*(Youn et al., 2008)*
Asia	**South Korea**	Seoul	*Underground station*	123-145	105-122	(D. U. Park & Ha, 2008)
Asia	**South Korea**	Seoul	*Platform*	-	105	(D. U. Park & Ha, 2008)
Asia	**South Korea**	Seoul	*Train*	-	117	(D. U. Park & Ha, 2008)
Asia	**South Korea**	Seoul	*Platform*	116 (76-164)	66 (39-129)	*(K. H. Kim et al., 2012)*
Asia	**South Korea**	Seoul	*Platform with PSD*	97 (37-247)	58 (20-166)	*(K. H. Kim et al., 2012)*
Asia	**South Korea**	Seoul	*Platform*	108	64	*(Kwon et al., 2015)*
Asia	**Taiwan**	Taipei	*Platform*	49 (11-137)	35 (7-100)	*(Cheng et al., 2008)*
Asia	**Taiwan**	Taipei	*Train*	31 (19-51)	40 (22-71)	*(Cheng et al., 2008)*
Oceania	**Australia**	Sydney	*Train*	-	36	*(Knibbs & de Dear, 2010)*

1.4.2 Subway PM controlling factors and mitigation measures

Widely recognized factors assigned to the high variability concerning PM concentrations of different subway systems worldwide are mainly differences in station design, construction year, train frequency, passenger numbers, station depth and ventilation system (Xu & Hao, 2017)(Moreno et al., 2014). Train frequency and the rate of passengers were confirmed as the dominant cause of the erratic, promptly fluctuating particulate matter levels seen during the operating hours of subway systems, with a rapid increase of PM concentration levels from the onset of train operations in the early morning, reaching the highest pollution values around the morning and afternoon rush hours, characterized by increased train frequency and passenger numbers (Nieuwenhuijsen et al., 2007). Moreover, differing spatial variation patterns were found in relation to the PM concentration levels in different stations with varying designs. At single track platforms, the highest concentration levels were detected mostly on the one end of the platform where the train enters, while at double-track platforms the two directional train movements produced complex airflows, thereby prohibiting the identification of a clear spatial concentration trend linked to train arrival and departure (Moreno et al., 2014).

Further on, a commonly recognized trend is the rise of PM concentration levels with increasing underground deepness, thereby influencing the efficiency of the air exchange between the indoor and outdoor environment, furtherly determined by the presence or absence of a mechanical ventilation system and the seasonal variation of colder and warmer periods (Martins, Moreno, Minguillón, et al., 2016)(Querol et al., 2012). Some of the older metro systems are only equipped with natural ventilation, utilizing the piston effect generated by the train`s motion through the underground tunnel, where the airmass in front of the train is forced forwards along the subway tunnel and a suction is created behind the moving train, thereby performing a regular airing (Moreno et al., 2014)(Pan et al., 2013). Albeit, studies showed that this piston wind isn`t able to maintain the desired air quality levels in underground rail systems, with especially low ventilation efficiency at narrow platforms and tunnels (Martins et al., 2015). Therefore, the employment of forced mechanical tunnel ventilation (FMTV) systems is crucial for the management of air pollutants inside these semi-isolated underground systems, although an appropriate operation set-up, with installed and maintained filtration system, is further on essential to reach the desired PM concentration reductions. On the other hand, mechanical ventilation systems are characterized by elevated operation costs, followed by further potential health risks posed by poor ventilation hygiene, transmission of air pollutants and formation of uncomfortable draft sensations, if the system is managed inadequately (Wen et al., 2020). As a potential solution, new technologies, like the utilization of artificial neural network techniques in the operation of the ventilation facilities, are being designed and tested to reach improved indoor air quality levels with a simultaneous reduction of energy consumption (Hyeong et al., 2018).

In addition to the improvement of passenger safety, the installation of platform screen doors (PSDs) at recently constructed metro stations proved to have a high potential as a further reduction measure for platform PM concentration levels and for energy consumption, related to air conditioning. Stations equipped with PSDs showed a significant reduction in PM_{10} levels and relative abundance of Fe-containing particles in the platform area (K. H. Kim et al., 2012)(Jung et al., 2010), even though the inverse effect on the air quality levels inside the tunnel and trains can result from the positioning of PSDs without the employment of a suitable tunnel ventilation procedure, plainly due to the accumulation of particulate matter in the underground tunnels (Son et al., 2013)(Son et al., 2014) (Ryu & Juraeva, 2012).

1.4.3 PM emission sources and physico-chemical properties

While some part of the subway particulate matter originates from the outdoor, urban environment, the major share of the underground PM loading is generated by indoor sources, produced for example by the friction induced mechanical abrasion of metro system compartments, like rails, wheels, brakes and third rail collector shoes used for the power supply, and further on by the resuspension of formerly generated dust, due to air turbulence produced by the movement of the trains, passengers and by the maintenance works or cleaning activities conducted in the operational downtime (Querol et al., 2012). Consequently, there are substantial dissimilarities in the concentration, chemical composition, and aerodynamic size mode of the subway airborne particles, compared with outdoor urban particulate matter characteristics. (Reche et al., 2017)

Due to the aforementioned complex interaction between the indoor and outdoor microenvironments, a consistent particulate matter composition can`t be appointed to different subway systems. Having said this, the largest contribution to the measured metro PM mass concentrations is generally produced by iron rich, also known as ferruginous, particles in the coarse mode, originating from mechanical wear down at the rail-wheel contact surface, accompanied by trace elements, such as Mn, Cr, Cu, Sb, Ba, Zn, Mo, Ni, Cd, emitted during the operation hours from the same alloys, or additional sources like brake wear and electrical cable erosion (Cusack et al., 2015). It was further on determined, that the metals incorporated in these emitted particulate fragments can undergo a subsequent oxidation process, whereby the elemental iron portion may be converted into magnetite (Fe_3O_4), maghemite (γ-Fe_2O_3) and hematite (α- Fe_2O_3) to a large extent (Moreno, Martins, et al., 2015) (Jung et al., 2012). Other components are secondary inorganic aerosols, aluminosilicates, and carbonaceous particles introduced primarily by outdoor emission sources, including combustion processes and crustal origins, amongst others (B. W. Kim et al., 2010). Further on, the finer $PM_{2,5}$ fraction is differing from ambient airborne dust in terms of mass concentration levels and is mainly dominated by Fe as the most abundant element as well, next to the before mentioned accompanying trace elements, with significantly enriched Cu, Ba, Mn, Cr, Ni concentrations (Martins, Moreno, Mendes, et al., 2016)(Aarnio et al., 2005). While the ultrafine particle fraction of urban environments is characterized by low metal abundancy and contains mainly carbonaceous particles alongside secondary inorganic aerosols, it was shown that the UFP of subway dust encompasses relatively high concentrations of iron and trace metals, generated likely due to high temperatures amid the friction of the train system compartments during operation and a subsequent vaporization (Loxham et al., 2013).

As already mentioned above, the major contribution to the particulate mass concentrations measured in previous studies is produced by the coarse $PM_{10-2.5}$ fraction, although intercomparisons in this regard tend to be difficult, as most measurement campaigns only collected one specific size fraction (generally either PM_{10} or $PM_{2.5}$). Regarding the ones where various size fractions were monitored simultaneously by optical particle counters, the results were either not corrected by the comparison with an accompanying gravimetric measurement, or the same correction factor was used for the all the differing size fractions, thereby yielding $PM_{2.5}/PM_{10}$ ratios ranging from 0.3 to 0.8. Regarding the subway system of Barcelona, two separate studies provided mass concentration ratios of different size fractions. Querol et al. measured PM_{10} and $PM_{2,5}$ mass concentration levels with optical counting devices in platform areas and inside the trains, where both size fractions were corrected via the results of simultaneous gravimetric measurements, providing a $PM_{2.5}/PM_{10}$ ratio of 0.3 - 0.4 and 0.3 at the platform locations and inside the subway trains, respectively (Querol et al., 2012). The measurement campaign of Moreno et al., which took place likewise in various stations of the subway of Barcelona under different ventilation modes, monitored the PM_{10}, PM_3 and PM_1 fractions also with an optical particle counter and corrected the results through the in situ gravimetric measurements with a high-volume sampler collecting PM_{10} and PM_3 samples. The resulting correction factor from the PM_3 gravimetric measurements was then also used for the adjustment of the PM_1 fraction, providing an mean PM_1/PM_{10} and PM_3/PM_{10} ratio of 0.3 and 0.8 for all stations, respectively (Moreno et al., 2014).

In opposition to the particulate mass concentration, the particle number concentration (PNC) distribution is dominated by the fine particle size mode, with loads comparable to urban background particle number concentrations, thereby indicating street traffic and natural sources as primary determinants of PNC levels in the underground systems (Aarnio et al., 2005). The contemporary literature on subway air quality studies offers slightly less insight on particle number concentrations than on mass concentrations, whereby the focus is centered on assessing the number concentration levels of the dominating UFP size mode. Assessed mean number concentrations in various subway microenvironments ranged from 9000 to 37000 particles/cm^3 and are listed in Table 1.5.

Table 1.5 Comparison of measured particulate number concentrations in subway stations from various studies

Country	City	Measurement position	Pollutant size fraction	Concentration (cm^{-3})	Reference
Austria	Vienna	*Subway station (U2)*	10nm-300nm	**1,00E+04**	(Posselt et al., 2019)
Chile	Santiago	*Subway trip*	20nm-1µm	**1,62E+04**	(Suárez et al., 2014)
China	Hong Kong	*Subway trip*	10nm-1µm	**9,00E+03**	(Yang et al., 2015)
Italy	Milan	*Subway trip*	20nm-1µm	**1,30E+04**	(Ozgen et al., 2016)
Spain	Barcelona	*Subway trip*	10nm-300nm	**2,30E+04**	(Moreno, Reche, et al., 2015)
USA	New York City	*Subway trip*	5nm-3µm	**1,74E+04**	(X. R. Wang & Oliver Gao, 2011)
USA	New York City	*Subway station*	5nm-3µm	**3,77E+04**	(X. R. Wang & Oliver Gao, 2011)
USA	Boston	*Subway trip*	20nm-1µm	**2,00E+04**	(Levy et al., 2002)

1.4.4 Subway PM exposure and health impacts

One of the first studies, providing findings suggestive of elevated metal exposure levels of subway commuters, was conducted by Pfeifer et al. in London between 1995 and 1996. The goal of this study was to assess the impacts on exposure levels of the then introduced diesel fuel additive MMT (methylcyclopentadienyl manganese tricarbonyl), by measuring and comparing the personal exposure levels of taxi drivers, with relatively high exposure levels to traffic-related emissions, and office workers, of whom approximately half commuted via the underground rail system. The results indicated that the commutation by the underground train system posed as a significant source of aerosol exposure, with particulate matter substantially enriched in manganese and other metals, in comparison with outdoor aerosol compositions (Pfeifer et al., 1999). These results were thereafter confirmed by follow up studies in various cities around the world (Chillrud et al., 2011)(Seaton et al., 2005)(Aarnio et al., 2005)(Branǐs, 2006), thereby acting as incentive for further research on the topic.

The existing studies focusing on the health impacts of subway dust resulted in mixed conclusions, depending on the respective approaches, summarized in a review by Loxham and Nieuwenhuijsen (2019). Although in vitro studies suggest elevated endpoint risks of carcinogenicity and non-cancer health effects, derived mainly from the high transition metal content of underground PM, the bioavailability of these elements is still of question due to their low water solubility in comparison with ambient PM. Further on, other ambient PM parameters associated with severe impacts on health, like the polycyclic aromatic hydrocarbon (PAH) ratio, higher UFP number concentration loads or gaseous co-pollutants like NOx, generated by motorized vehicles aboveground, seem to surpass the potential negative impacts of elevated mass concentration levels of metal-enriched PM found in the subway microenvironments. (Loxham & Nieuwenhuijsen, 2019)

1.4.5 Exposure comparison with alternative commutation modes

According to a study from 2020, based on data from the European Working Condition Surveys from 1995 to 2015, Austrian citizens generally spend an mean time of approximately 34.5 minutes per day on commuting (No et al., 2020). Even though this travelling period only covers a fraction of their daily schedules, its contribution to the commuters` overall daily exposure may be significant (Zuurbier et al., 2010). Hence, several studies were conducted in the last 15 years, assessing the exposure levels of mostly urban travelers in various transport microenvironments (TMEs) focusing on different air pollutants and their health impacts (Mitsakou et al., 2021)(Brugge et al., 2007)(Cepeda et al., 2017)(Nazelle et al., 2017). As these exposure assessments were derived from data collected by varying measuring equipment (concentrating on diverse pollutants) and sample size with studies conducted in different cities characterized by alternating properties regarding passenger behavior, urban pollution loadings and meteorological conditions, the deduced results in search for the “cleanest” transportation mode are not quite consistent (Borghi et al., 2020).

Common urban transportation modes can be divided into two groups: motorized transport (MT); encompassing personal motorized vehicles (cars, vans, and motorbikes) along with public transportation (bus, tram, subway, rail), and active travel (AT); covering non-motorized vehicles like bicycles, skateboards and roller skates, as well as the aboriginal bipedal transportation mode known as walking. The advantages of active transportation are well known; stretching from its reduction role in relation to congestion, air pollution, noise pollution and energy use (accompanied by subsequently lowered greenhouse gas emissions), all the way to stimulating benefits regarding physical and mental health (Hunkin & Krell, 2019). Nevertheless the absence of spatially well separated cycling and pedestrian routes from motorized traffic may increase exposure concentrations and in addition inhalation doses due to the enhanced respiratory rates of active travelers (C. A. Ramos et al., 2016).

As already mentioned, the evidence regarding PM exposure of the different TMEs are mixed, still most studies typically found lower concentrations for active travelers, rather than in the microenvironments of motorized vehicles with open windows (Mitsakou et al., 2021). Still, car commuters with closed windows and adequate ventilation systems experienced lower concentration loadings than active travelers (Cepeda et al., 2017). Varying results were reported for bus commuters, depending on the bus age, fuel, catalysts, ventilation settings and resuspensions caused by passengers (Adar et al., 2008)(Nazelle et al., 2017). Commuters using massive motorized transport (MMT), including trains and subway, also tend to experience higher exposure levels than active travelers, although higher inhalation rates and travel time can produce elevated inhalation doses compared to motorized personal and public transport modes (Cepeda et al., 2017).

Strasser et al. compared exposure levels for commuters by car, bus, tram, subway and bicycle in Vienna. They found higher $PM_{2.5}$ and PM_1 mass concentration levels during travelling by the subway in comparison to measurements amid travelling by bus. In contrast, the lowest UFP particle number concentrations were measured in the subway carts, followed by the air-conditioned car measurements with closed windows. Particle number concentrations in buses and trams were significantly higher than in the subway or car microenvironments. Further on, the results regarding the lung deposited surface area (LDSA) of cyclists was approximately 9 times higher, compared to measurements in the subway. In summary, commuting by subway was suggested as the preferred motorized transport in Vienna, while still encouraging active travel by bicycle due to its positive impacts induced by physical exercise. (Strasser et al., 2018)

After the first reports of a novel coronavirus in late December 2019 in Wuhan (China) (Zhu et al., 2020), the subsequent worldwide spread reached Austria on 25th of February 2020 (Mattha Busby, Martin Belam, Sarah Marsh, Alison Rourke, 2020), whereas the outbreak`s classification as a global pandemic wasn't implemented until the 11th of March 2020 by the WHO (Munster et al., 2020). Alike to the virtually uniform, global governmental responses (Tirachini & Cats, 2020), the Austrian state introduced next to the closure of economic sectors also travel restrictions regarding public and personal transport (Badelt, 2021), producing major impacts on people`s mobility (Heiler et al., 2021). Since then, there have been subsequent lockdowns and periods of easing interchangeably, based on the actual trends and statistics. In this process, the usage of personal protective equipment or PPE (in the beginning cotton masks, later FFP2 masks), became obligatory and prevalent, inter alia, for the public transport services. Although the amount of risks associated with a COVID-19 contagion cluster in public transport microenvironments is still uncertain, the usage of PPE appears to mitigate the possibility of droplet and aerosol transmission significantly (Tirachini & Cats, 2020; Vitrano, 2020). Further on, Ji et al. estimated that the use of PPE among subway commuters could result in significant exposure cutbacks concerning the exposure to Fe, with exposure reductions from 16 % up to 35 % using cotton masks and FFP2, respectively (Ji et al., 2021). Thus, some of these new norms may have several benefits worth to uphold even in a post-pandemic world.

Chapter 2) Experimental section

2.1 Sampling methodology

The fieldwork consisted of stationary measurements on three different platform and tunnel locations, respectively, in four underground subway stations of the subway lines U1, U2 and U3. The installation of the monitoring site at station Stubentor U3 as well as a close-up of the impaction plate segregating the PM_{10} fraction are shown in Figure 2.1 and Figure 2.2, respectively.

Figure 2.1 Employees of the Wiener Linien setting up the grid wall around the measurement setup at station Stubentor U3

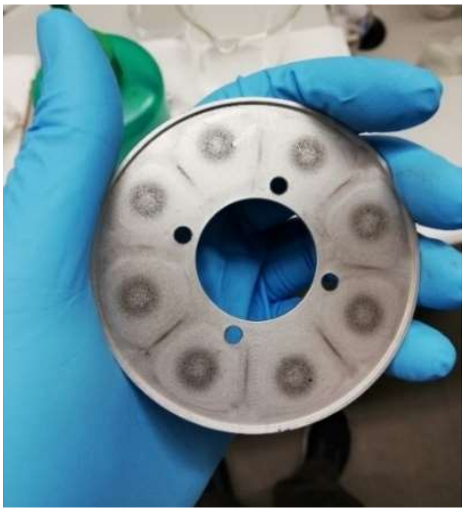

Figure 2.2 Impactor plate of the Low volume sampler with the collected dust (aerodynamic diameter >10µm)

After completion of each measurement, the inlet of the LVS was dismantled and the impactor plate (Figure 2.1) was cleaned before proceeding to the next monitoring site.

2.1.1 Stationary measurements

In terms of station-design, -depth and -age, four contrasting underground stations were chosen for the measurement campaign to evaluate the impacts of these parameters on the air quality of the microenvironments at the platforms and tunnels. There were three sampling periods conducted, both for the tunnel and for the platform evaluations.

For the platform measurements, the selected locations were Karlsplatz U1, Rochusgasse U3 and Stubentor U3, while the chosen tunnel stations were Praterstern U2, Karlsplatz U1 and Rochusgasse U3. Table 2.1 presents the analysis plan for all the stationary measurement sites with the number of filters sampled by the Low Volume Sampler and the additional instruments used. Subsequently all the various sampling sites are going to be characterized in detail.

Table 2.1 Analysis plan of the stationary measurements

Date	Location	Instruments	# of filters sampled
28.-31.10.2019	**platform Stubentor U3**	LVS OPC ELPI*	14
04.-07.11.2019	**platform Karlsplatz U1**	LVS OPC ELPI*	14
11.-14.11.2019	**tunnel Karlsplatz U1**	LVS OPC	16
15.-18.11.2019	**tunnel Rochusgasse U3**	LVS OPC	14
19.-22.11.2019	**platform Rochusgasse U3**	LVS OPC ELPI*	14
26.-29.11.2019	**tunnel Praterstern U2**	OPC ELPI	14
18.-20.02.2020	**tunnel Praterstern U2**	LVS OPC	14

*Operated only during selected time periods (approximately 4 hours for each site)

The measurement setup of the stationary measurements (Figure 2.3) consisted of a Low Volume Sampler (LVS), an optical particle counter (OPC) and an electrical low-pressure impactor (ELPI). The LVS was equipped with quartz fiber filters (Pallflex® Tissquartz™ 2500 QAT-UP/ #7202/ ø47mm) and was programmed to sample PM_{10} in four-hour intervals at every stationary measurement site for the gravimetric evaluation of the mass concentration values and for the subsequent chemical analysis. Additionally, an OPC and an ELPI were operated as online instruments with higher time resolution. The data, consisting of minute means, collected by the OPC was used to study temporal mass concentration variations after their conversion into 15 min mean values and additionally using site-specific correction factors obtained by a calibration using the parallel LVS datapoints (see section 3.2.1). The evaluation of the mass- and number concentration distributions were conducted using the data obtained by the ELPI. The ELPI collected data for approximately 4 hours at all the platform sites, and was operated for 68 hours at one tunnel location, i.e. at the station Praterstern U2.

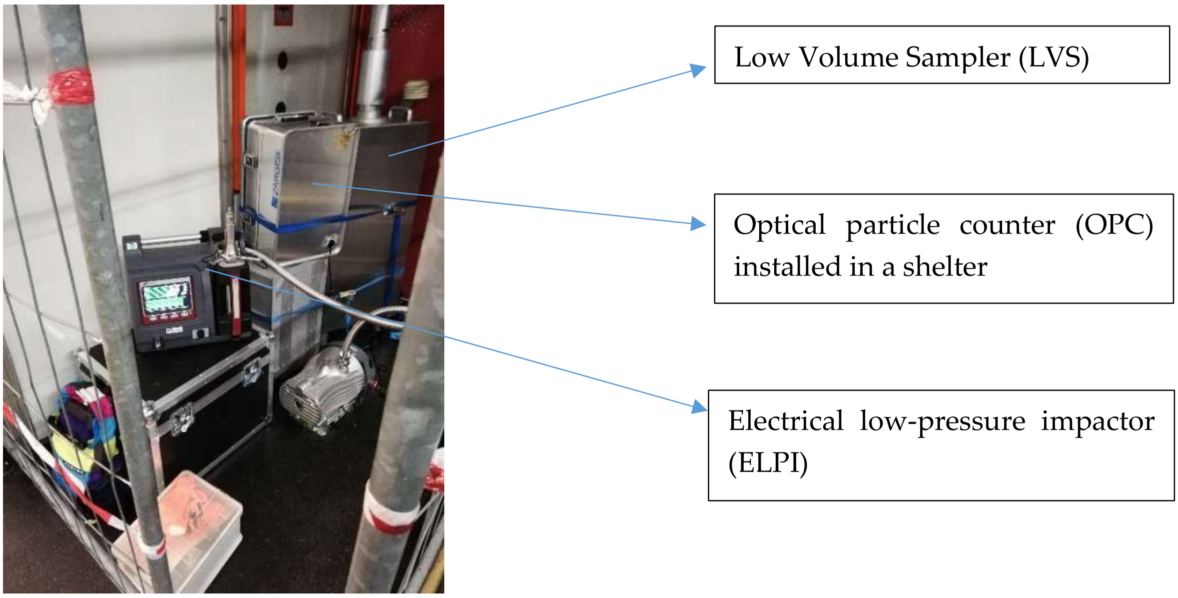

Figure 2.3 Measurement setup

2.1.1.1 Platform measurements

During the measurements on the platforms of the stations Karlsplatz U1, Rochusgasse U3 and Stubentor U3, the sampling resolution of the optical particle counter was set to 6 seconds for a period of 2 hours in order to investigate the spatial variability of the particulate matter concentrations on distinct platform sections and the influences of the arriving and leaving trains.

The station Stubentor U3 consists of a single platform next to a single rail, while there are two separate tunnels with a central platform consisting of a partially divided wall-structure along its length at the stations Karlsplatz U1 (Figure 2.4) and Rochusgasse U3. In the following illustrations (Figure 2.5, Figure 2.6, Figure 2.8), the sketches of the cross-sections of the stations` architectural designs are presented.

Figure 2.4 Access to the subway platform at the station Karlsplatz U1

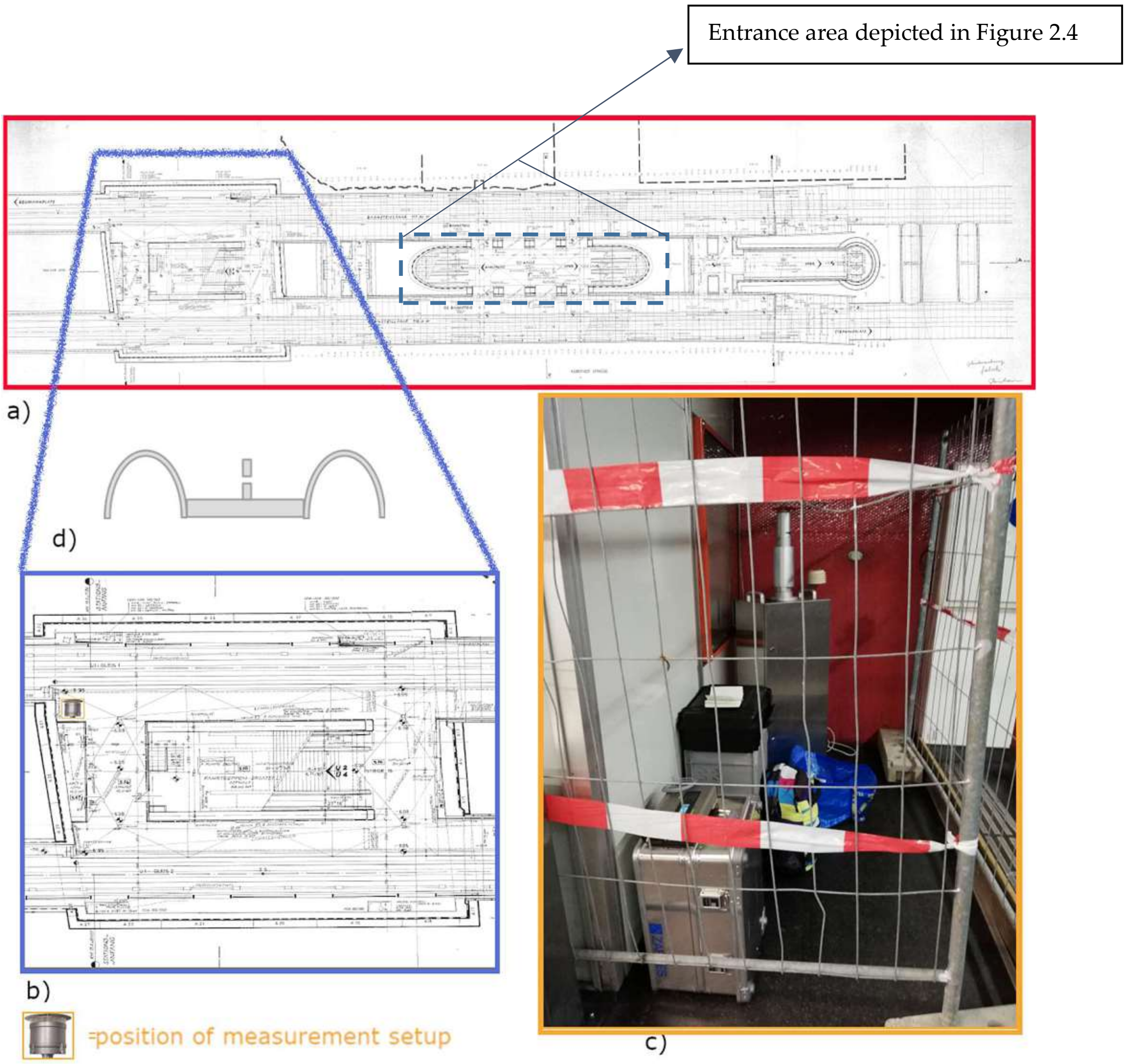

Figure 2.5 Position of the measurement setup at platform Karlsplatz U1
a) + b) blueprint of the platform area of the station Karlsplatz U1
c) measurement setup consisting of LVS and OPC
d) sketch of the cross-section of the station Karlsplatz U1

The collection of the platform air samples of the station Karlsplatz U1 was conducted from 4th to 7th of November in 2019 (from Monday to Thursday). The air monitoring equipment was installed approximately in a distance of 3 meters from track #1, at the end of the platform in the travel direction to Reumannplatz. The platform of the station Karlsplatz U1 lies roughly 24 meters underground, being the deepest station analyzed during this project.

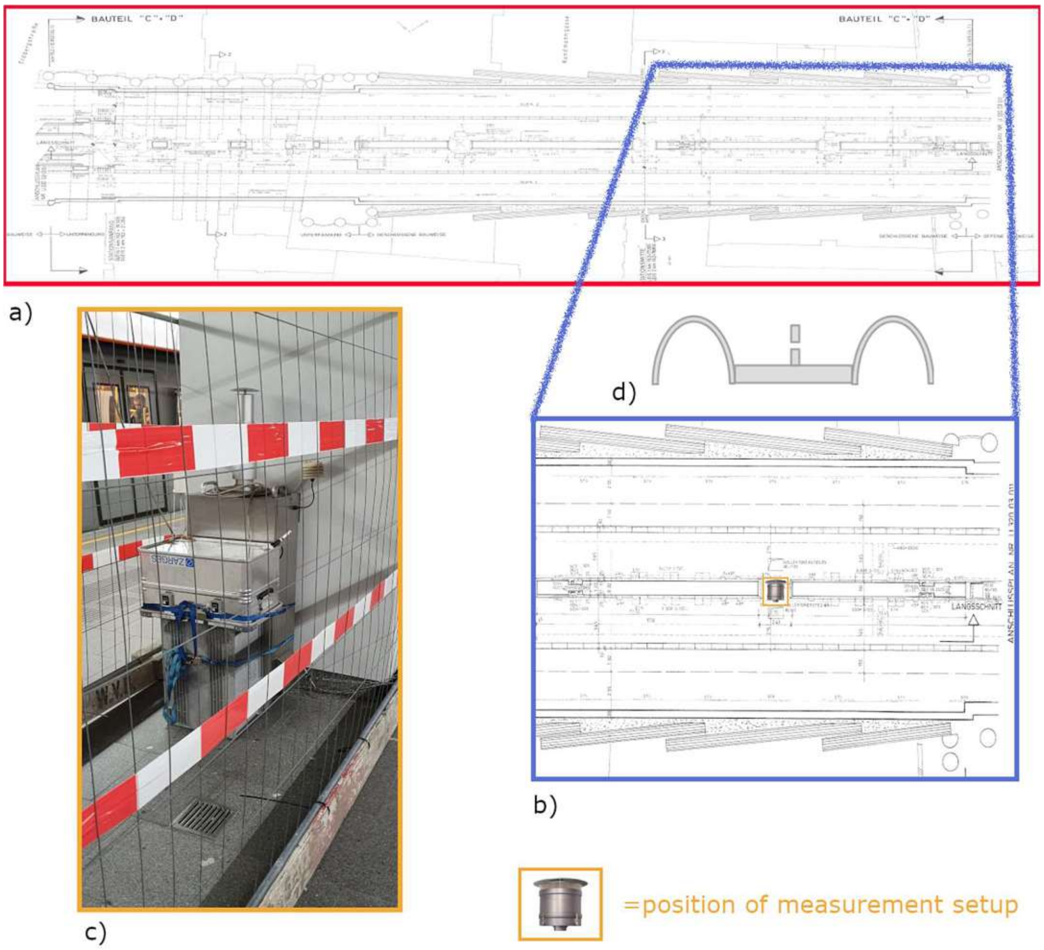

Figure 2.6 Position of the measurement setup at platform Rochusgasse U3
a) + b) blueprint of the platform area of the station Rochusgasse U3
c) measurement setup consisting of LVS and OPC
d) sketch of the cross-section of the station Rochusgasse U3

At the station Rochusgasse U3, the equipment was placed in the front region of the platform in the travel direction of Simmering in a passage between the two tracks, approximately 3.5 meters away from the rails. The measurements were performed between 19^{th} and 22^{nd} of November 2019 (from Tuesday to Friday).

Figure 2.7 LVS filter sampled at platform Rochusgasse U3 during the night hours between 12am and 4am (left)
LVS filter sampled at platform Rochusgasse U3 during the rush hour period in the morning between 8am and 12pm (right)

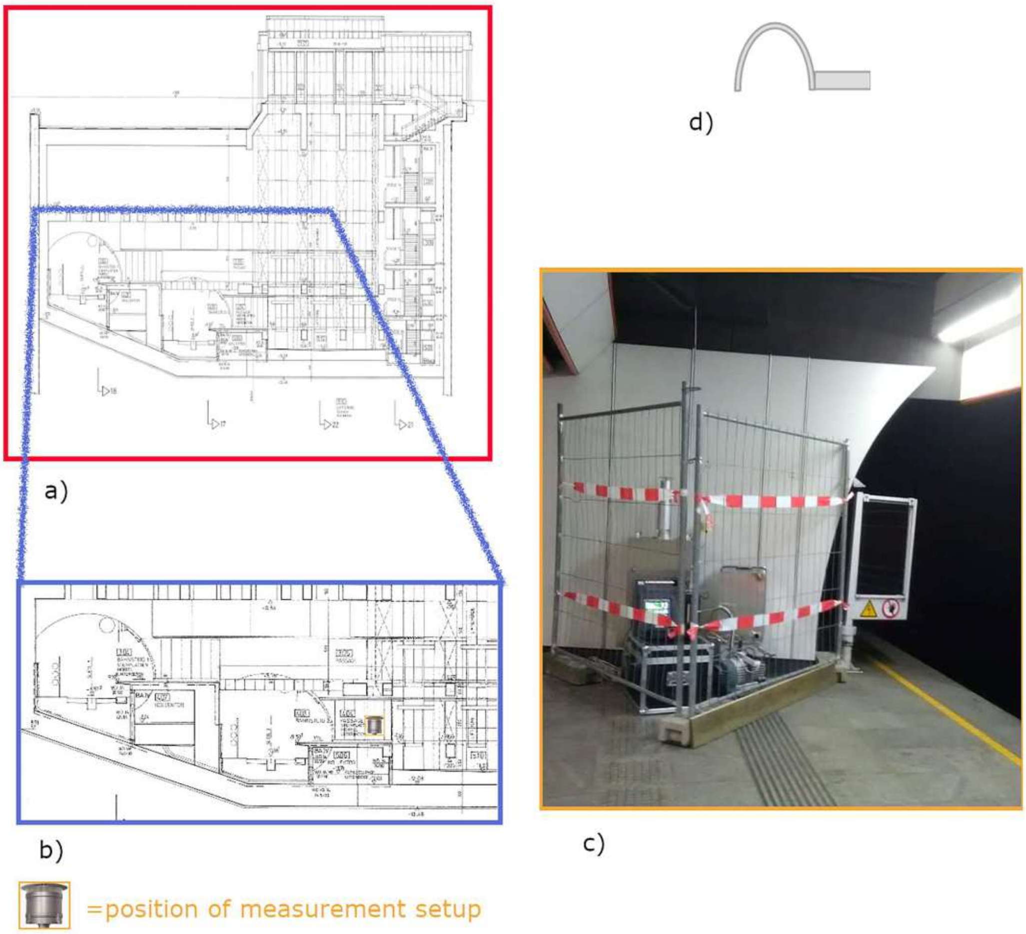

Figure 2.8 Position of the measurement setup at platform Stubentor U3
a) + b) blueprint of the platform area of the station Stubentor U3
c) measurement setup consisting of LVS, OPC and ELPI
d) sketch of the cross-section of the station Stubentor U3

The platform measurements of the single platform station at Stubentor U3 took place in the travel direction Ottakring at the front end of the platform, roughly 3.5 meters from the track. They were conducted from the 28th to the 31st of October 2019 (from Monday to Thursday).

2.1.1.2 Tunnel measurements

The measurement setup and locations of the tunnel measurements are illustrated in the following section from Figure 2.9 to Figure 2.11.

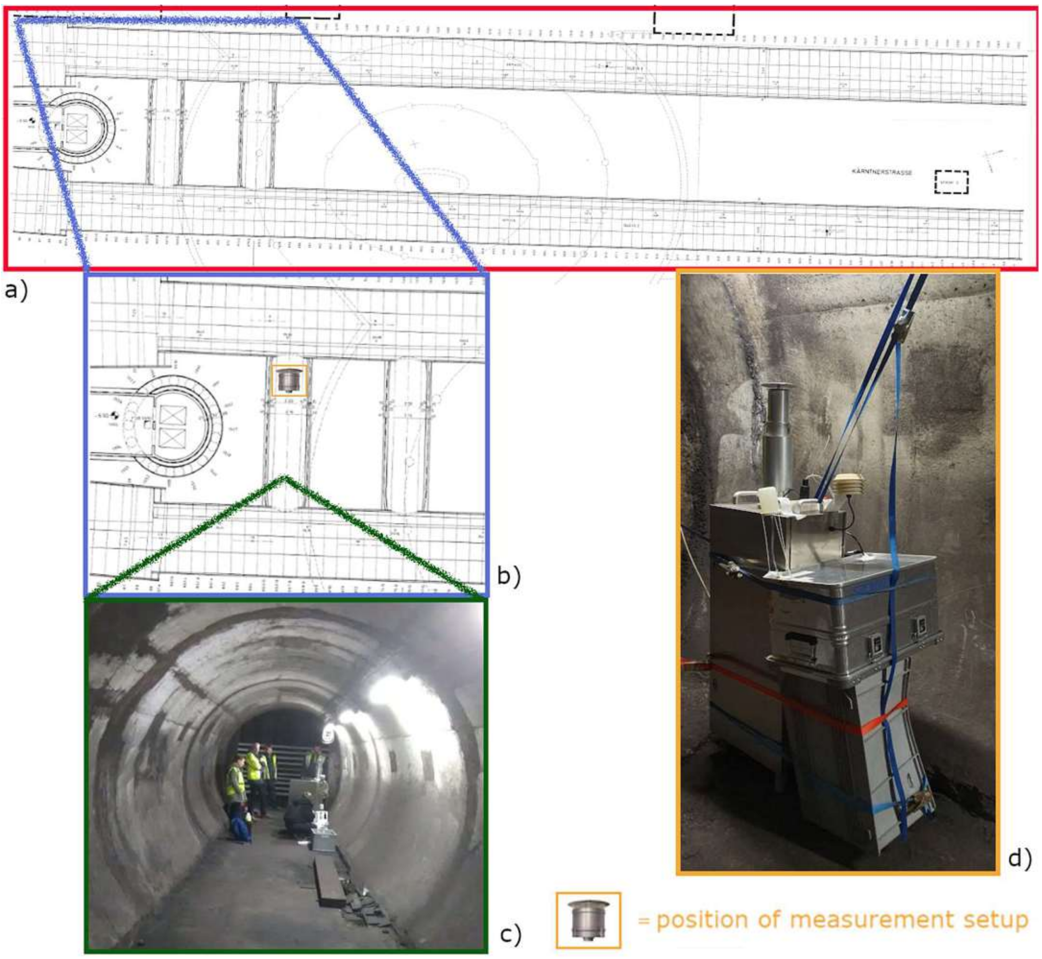

Figure 2.9 Position of the measuring setup at tunnel Karlsplatz U1
a) + b) blueprint of the tunnel area of the station Karlsplatz U1
c) view through the connection channel
d) measurement setup consisting of LVS and OPC

The tunnel measurements near the station Karlsplatz U1 were performed from the 10th to the 14th of November 2019 (from Sunday 4 am to Thursday 8 pm). The air monitoring instruments (LVS and OPC) were placed in the first connection channel, between the two separated narrow tunnels, approximately 3.5 meters from track #1 and 12 meters from track #2.

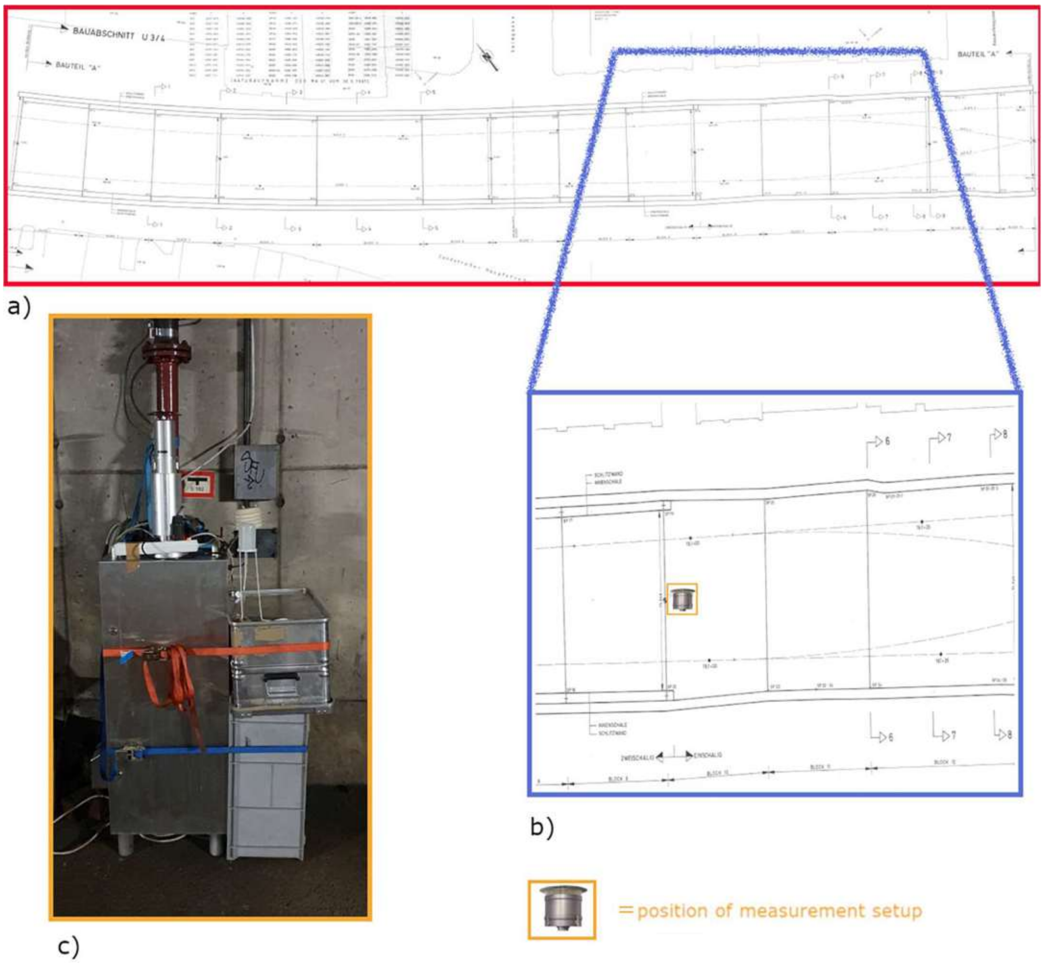

Figure 2.10 Position of the measuring setup at tunnel Rochusgasse U3
a) + b) blueprint of the tunnel area of the station Rochusgasse U3
c) measurement setup consisting of LVS and OPC

For the air quality measurements of the tunnel in the travel direction of Simmering in the station Rochusgasse U3, the equipment was installed right between the two tracks at a distance of 4.5 meters from the rails. The sampling period was from the 15th to the 18th of November 2019 (from Friday 4 pm to Monday 12 pm), representing the only samples collected during continuous operation of the subway system over a weekend period with reduced train frequency.

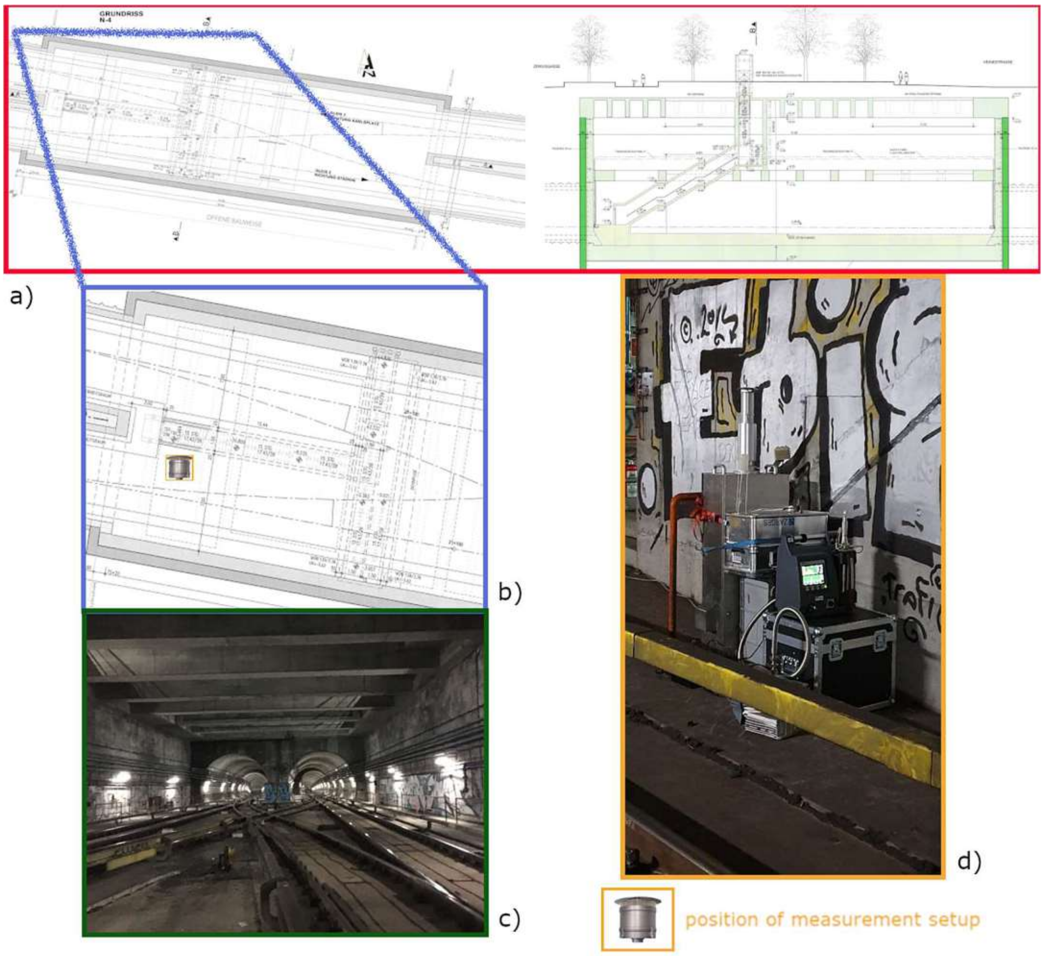

Figure 2.11 Position of the measuring setup at tunnel Praterstern U2
a) + b) blueprint of the tunnel area near the station Praterstern U2
c) view through the tunnel hall
d) measurement setup consisting of LVS, OPC and ELPI

The first attempt for the last stationary measurement, which was located roughly 440 meters from the station Praterstern U2, took place from the 26th to the 28th of November 2019 (from Tuesday 4 pm to Thursday 12 pm), wherein a failure of the LVS occurred. This outage allowed only the evaluation of the data collected by the electrical low-pressure impactor, while the LVS and the OPC measurements were repeated in February 2020 (between the 18th [Tuesday] and the 20th [Thursday]). The instruments were placed roughly 1.7 meters away from the rails, around 19 meters below the surface for both measurements.

2.2 Instruments

2.2.1 Low volume sampler

The model named SEQ47/50 produced by the firm "Sven Leckel Ingenieurbüro GmbH" was utilized as an automated Low Volume Sampler (LVS) for the gravimetric evaluation and chemical analysis of airborne particulate matter. The air sample is drawn through an inlet onto a quartz fiber filter (ø 47mm) by a vacuum pump at a flow rate of 2.3 m^3/h. The inlet is situated at the height of 1.6 meters above the ground and is equipped with a sampling head consisting of an inertial impactor with a PM_{10} cut-off. This inertial impactor removes particles with an aerodynamic diameter greater than 10 µm by making use of their inertia, this way only particles with an aerodynamic diameter smaller than 10 µm are collected on the filters.

The sampling intervals of the stationary measurements were set to a period of four hours and were started at 4 am for the tunnel measurements and at 12 am or 4 pm for the platform measurements. These monitoring intervals were set this way to sample in the night hours between 12 pm and 4 am (characterized by a profoundly reduced train frequency until 1 am and a total suspended train service between 1 am and 4 am) and in order to be able to calculate the daily mean values from six gravimetric filter measurements.

2.2.2 Optical particle counter

The Mini-LAS 11E model, produced by the firm GRIMM Aerosol Technik Ainring GmbH & Co. KG (Software: Lab View Software 1178, Version 8-1 Rev I (09-05-2019)), was used as an online portable optical particle counter (OPC), carrying out the data collection with high temporal resolution. Particle measurements using optical particle counters are based on the measurement of the light scattered on the surface of the sampled particles. The air is drawn through the aerosol inlet provided with the instrument and the sampled particles are led into a measuring chamber equipped with a laser diode (with an emission wavelength of 660 nm as the light source) in a way that only one particle at a time is measured. Using the intensity of the scattered light, the particle size of the aerosols can be calculated, even though the non-monotonic size dependence of the scattered light intensity and its variability with changing refractive indices affect the accurate particle sizing capability of these instruments. This model can count every single particle in a size range from 0.25 to 32 µm and classify them into 31 separate size channels, which can be converted into particle mass concentrations.

The Mini-LAS 11E is designed for environmental air quality measurements, thus the instrument`s automatic internal correction factors cannot be applied to the particles found in the subway microenvironment without compromising the reliability of the observations based on this method. The main difference from the typical ambient particles is due to the high iron content of the aerosols found in the subway systems, which manifests mainly in different refractive indices and densities, altering the size classification efficiency and its correctness. To adjust the collected data, correction factors were determined by the gravimetric evaluations of the integrated PTFE-filters, as well as through the separate gravimetric data collected by the Low Volume Sampler (see 3.2.1). This approximation was only possible for the PM_{10} size fraction, since the deployed LVS was only equipped with a single cut-off stage for this size range.

2.2.3 Electrical low-pressure impactor

As the measurements with the optical particle counter can be biased due to the nature of the subway aerosols, an electrical low-pressure impactor (ELPI) of the company Dekati (model: 2E10-10; Software Version: ELPI+ VI 2.0 rev. 898) was employed as an independent method using an alternative, more robust operating principle. This instrument was installed at the stationary measurements in a way that the air inlet sampled the airborne particles at 0.9 m above the ground.

The operating principle is based on the charging of the sampled particles with a corona charger into a known charge level. Afterwards, the charged particles are transferred in a low-pressure cascade impactor, where the particle size allocation is taking place. Depending on the aerodynamic particle size of the inspected aerosols, the particles are collected on 14 separated electrically insulated impactor stages (Figure 2.12 illustrates two dismounted stages with different aerodynamic fractions of PM collected), which are connected to sensitive electrometers, registering the electric current produced by the impacting particles. The recorded current is directly proportional to the number concentration of the impacted PM on that stage.

This detection principle allows the evaluation of particle number concentrations and distributions, classifying the sampled aerosols in the size range of 6 nm to 10 µm into 14 size channels (corresponding to the 14 impactor stages), as well as their conversion into mass concentration values for the PM_{10}, $PM_{2.5}$ and PM_1 fractions.

Figure 2.12 Impactor stage 7 with particles of an aerodynamic diameter between 155 and 256 nm (left) and stage 9 with particles with an aerodynamic diameter between 382 and 603 nm (right) of the electrical low-pressure impactor after the measurement at tunnel Praterstern U2

2.3 Chemical analyses and LOD values

Before and after the sampling, the quartz fiber filters, sampled by the LVS, were stabilized at 20-22 °C and a relative humidity of 42 - 49 % for a period of 48 hours before weighing. Once the PM_{10} and $PM_{2.5}$ mass concentrations were obtained by gravimetric measurements, the filter samples were punched and prepared (Figure 2.13) for chemical analysis described in the following chapters.

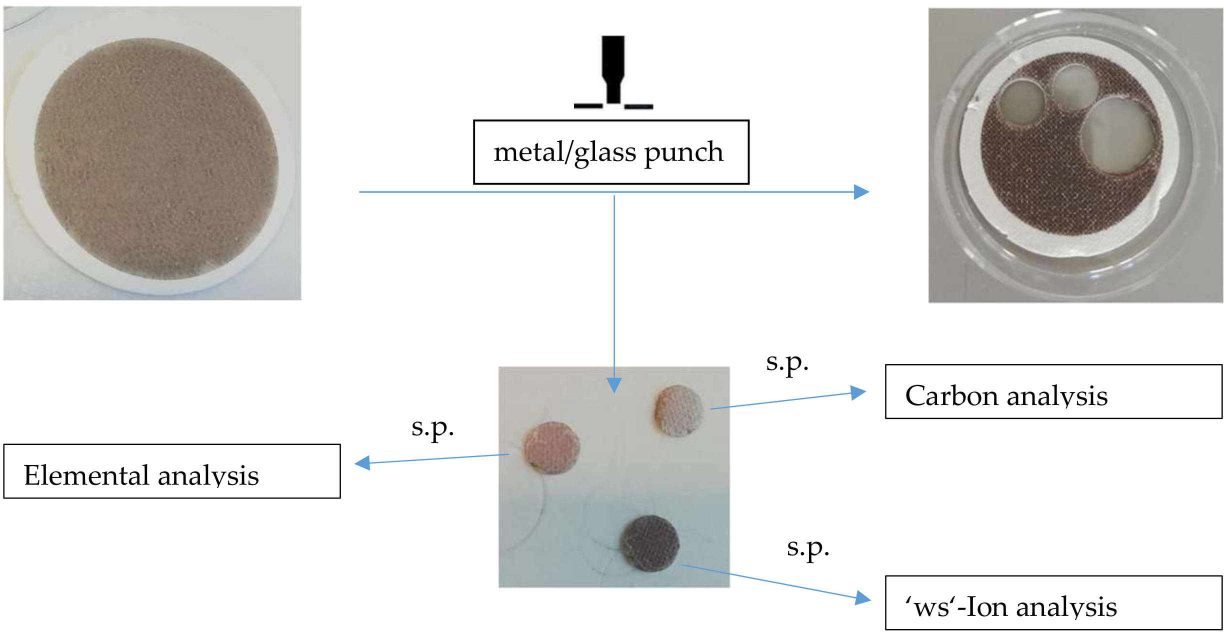

Figure 2.13 Schematic illustration of the division of the sampled filter materials for the chemical analysis methods conducted (s.p – sample preparation)

As the first attempt at the collection of the particulate matter using the LVS at the location tunnel Praterstern U2 failed due to a power outage, the non-sampled filters, which stayed in the subway tunnel environment for 48 hours, were used as an extended set of field blanks. Therefore, they were prepared for the chemical analysis methods the same way as the sampled filters and their measured mean concentration values were used for the blank value adjustments and their threefold standard deviations as the limit of detection values (LOD).

2.3.1 <u>Water-soluble ('ws') Ion analysis</u>

2.3.1.1 Methodology

For the determination of the water-soluble anions and cations, a circular aliquot of each filter with a diameter of 10 mm was punched with a metal punch (Figure 2.14) and eluted in 3 ml de-ionized water (ultrapure water of "Type 1") in an ultrasonic bath for 20 minutes. The extract obtained was centrifuged, the solution decanted and analyzed by ion chromatography using conductivity detection. For anion chromatography (Thermo Scientific Dionex ICS1100) a buffer solution of 4.5 mM Na_2CO_3 and 1.4 mM $NaHCO_3$ was used as an eluent. The separation was performed using a Dionex IonPac AS22 column and a Dionex IonPac AG22A pre-column at a flow rate of 1 ml/min. For the electrolytic regeneration, a Dionex ASRS 300 (4 mm) suppressor was applied, operating in recycle-modus. The concentration determination of the water-soluble cations was completed using a Dionex Ion Pac CS16A separation column, with a Dionex Ion Pac CG16A pre-column connected upstream and a Dionex CDRS 500 (4 mm) Suppressor in recycle-modus attached downstream. A solution of 38 mM methane sulfonic acid was employed as the eluent with a flow rate of 1 ml/min. The determination of both the anion and cation concentrations was realized using seven external standards, ranging from 0.05 mg/l to 7 mg/l, diluted from Certified Reference Material (CRM) standards.

Figure 2.14 Metal punch used for the partition of the filter material for the `ws`-ion and carbon content analysis

2.3.1.2 Limit of detection values of the water-soluble Ion fraction

The LOD values, presented in Table 2.2, were analyzed following the description above, but using two circular punches (2x ø 10mm), which were separated from the field blank filters of the stationary measurements. Comparably high LODs were found for the nitrite- and calcium-ions regarding the field blank filters of the stationary measurements.

Table 2.2 Limit of detection values of the water-soluble Ions quantified for the stationary measurements with a mean sampled air volume of 9.17 m^3

LOD values		stationary measurements
		tunnels/platforms
		PM_{10}
Cl^-	µg/m³	0.127
NO_2^-	µg/m³	0.147
NO_3^-	µg/m³	0.199
SO_4^-	µg/m³	0.016
Na^+	µg/m³	0.025
NH_4^+	µg/m³	0.005
Mg^{2+}	µg/m³	0.008
K^+	µg/m³	0.024
Ca^{2+}	µg/m³	0.104

2.3.2 Carbon analysis

2.3.3 Thermal-optical carbon analysis: TC, EC, OC

2.3.3.1 Methodology

A circular aliquot of the filters (ø 10 mm) was used for the quantification of the total carbon (TC), organic carbon (OC) and elemental carbon (EC) content. A thermal-optical method was employed using a Lab OC-EC Aerosol Analyzer by the Sunset Laboratory Incorporation, working with the EUSAAR-2 protocol and the obtained data was evaluated through the OCEC (Calc 415) software. The operating mode of the used thermal-optical carbon analysis method is based on the thermal desorption, sequentially under both inert (Helium) and then an oxidizing atmosphere (Helium + Oxygen), of the carbonaceous material (EC and OC) collected on the quartz fiber filters and their quantification (as CH_4) with a flame ionization detector, while utilizing the laser transmittance signal to correct the error caused by the partial charring of the OC fraction. At the end of each measurement, a fixed volume of external standard is injected as calibration gas (5V%CH_4 in He).

2.3.3.2 Limit of detection values

In Table 2.3, the organic carbon LOD values presented were evaluated via the field blank filters, while the elemental carbon LODs are the manufacturer-specified detection limits, since EC couldn`t be detected on field blank filters.

Table 2.3 Limit of detection values of the OC and EC fractions with a mean sampled air volume of 9.17 m^3

LOD values		stationary measurements tunnels and platforms
Cut-off		*PM_{10}*
OC	µg/m³	0.9
EC	µg/m³	0.5
TC	µg/m³	1.4

2.3.4 Elemental analysis

2.3.4.1 Methodology

ICP-MS: Fe, Cr, Mn, Zn, Sb, Cd, Ni, Pb, Cu, Be, Ba, V, Sb

The evaluation of iron, chromium, manganese, zinc, antimony, cadmium, nickel, lead, copper, beryllium, barium, and vanadium was performed by inductively coupled plasma mass spectrometry using an iCap Q System instrument (Figure 2.22) produced by the company Thermo Fisher Scientific.

Figure 2.15 Glass punch

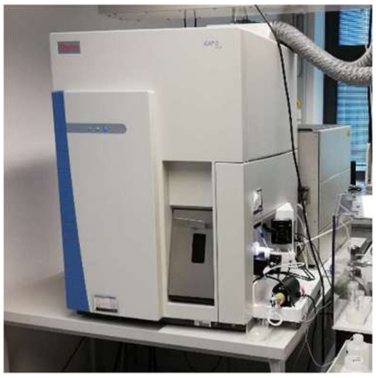

Figure 2.16 ICP-MS instrument

In order to minimize the contaminations introduced during the aliquoting of the filter samples, a glass punch (Figure 2.15) was refined from a glass tube by the university`s glass blower. Utilizing this glass punch, circular filter pieces (ø 12 - 13 mm) were cut out from the filter samples and were acid digested in 6 – 7 ml conc. aqua regia at 170 – 230 °C by using microwave technology. The obtained solution was decanted, and the Teflon reaction tubes, containing the remaining undigested filter portions, were washed using ultrapure water of "Type 1" to make up a volume of approximately 14 ml. The diluted digestions were gravimetrically measured for each sample using a microbalance, to estimate the gravimetric dilution factors. Further dilutions were prepared using 1 wt% aqua regia to get 1:25 dilutions for the analysis of the trace elements and 1:1250 dilutions for the determination of the most abundant component in the subway samples, iron. The dilutions were further spiked with 1 µg/kg Indium as internal standard, to recognize and correct errors caused by an instrumental sensitivity drift or an altered sample introduction performance during the measurements. The "kinetic energy discrimination" (KED) operation mode was applied to reduce the polyatomic isobaric interferences introduced by the argon plasma. An external calibration, ranging from 0.05 to 20 µg/kg, was performed for the quantification of every measurement, using dilutions created from certified reference materials (ICP multi-element standard stock solutions VIII, Sb and V from Merck KGaA, Certipur© Certified Reference Material) diluting again with 1 wt% aqua regia and using 1 µg/kg In as internal standard.

2.3.4.2 Limit of detection values

Figure 2.17 Microwave A (left) and microwave B (right) used for the filter digestions

Two microwaves (Figure 2.17) were employed for the digestions of the filter samples, since a malfunction of the "Microwave A" occurred amid the digestion of the filters sampled during the stationary measurements and another one (referred to as "Microwave B") had to be used. It is for this reason that there are two values presented for the LOD values regarding the stationary measurements. Inspecting the LODs of the tunnel and platform measurements presented in Table 2.4, it can be seen, that the limit of detection values were varying depending on the set-up used for the acid digestions of the same field blank filters. By comparison of the results from the two microwaves, a striking difference concerning the LOD values of manganese, copper and iron was noticed. These elevated limit of detection values for the acid digestions assisted by the "Microwave B" can be explained by a memory effect, since this microwave was previously used by the research group for the digestion of comparably great amounts of sedimented dust, originating likewise from the subway system of Vienna. Considering that these elements can be expected to be the most abundant components of the dust generated by the mechanical friction of the wheels and rails, these results are quite plausible. Further on elevated limit of detection values were detected for cobalt, zinc, cadmium, and aluminum. A possible aluminum source can be traced back to the grinding stone, routinely used by the maintenance workers at the Wiener Linien at the rail polishing operations, which mainly consists of corundum (Al_2O_3) and cryolite (Na_3AlF_6). For lead, barium, antimony, strontium, and beryllium lower LOD values were reached in the microwave B, while a significant change regarding the limit of detection values for the other trace elements was not observable.

Table 2.4 Limit of detection values of the elemental fraction with a mean sampled air volume of 9.17 m^3

LOD values		**stationary measurements**	
		tunnels and platforms	
		PM_{10}	
		Microwave A	**Microwave B**
Be	ng/m³	1.2	0.1
Al		279	430
V		134	28
Cr		3.7	7
Mn		26	550
Co		0.2	1.7
Ni		23	4.7
Cu		11	57
Zn		32	120
Sr		2.5	0.1
Cd		0.5	1.4
Sb		1.9	1.3
Ba		118	38
Pb		8.4	3.9
Fe		193	943

Chapter 3) Results and discussion

3.1 Filter analysis

3.1.1 PM_{10} mass concentrations

Mean PM_{10} mass concentration of each monitoring period (52 to 56 hours) were determined gravimetrically using the LVS-filters. The resulting concentrations ranged between 97 µg/m³ and 341 µg/m³, while the 4-hour means showed a greater variation, with extreme values of 24.5 µg/m³ and 538 µg/m³. Table 3.1 summarizes the total means, operation period means, mean values of the night-time hours, representing reduced operation (between 12 am and 4 am) and the extrema of the 4h mean PM_{10} values.

Table 3.1 Overview of the estimated mean PM_{10} mass concentration values

LVS	mean PM_{10} mass concentrations			Extrema	
	total	operation	reduced operation	Min	Max
			[µg/m³]		
tunnel Karlsplatz U1	341	381	63.0	45.8	538
tunnel Rochusgasse U3	96,6	103	56.2*	55.7	161
tunnel Praterstern U2	193	221	NA	NA	308
platform Karlsplatz U1	183	211	31.9	30.6	319
platform Rochusgasse U3	217	246	37.6	35.4	305
platform Stubentor U3	132	145	28.6	24.5	200

** Weekend – i.e., during night-operation of trains*

As expected, the highest mean value and the highest single 4h mean value were found in the tunnel Karlsplatz U1, which represents the measuring site of this campaign with the greatest depth (the deepest point of the station Karlsplatz U1 lies 23.7 m below Kärntner Straße) and the narrowest tunnel. The lowest mean PM_{10} mass concentration was determined within the tunnel Rochusgasse U3, possibly due to the wide, open tunnel design and comparably low depth with 13.8 m below Erdbergstraße. This influence of tunnel design was already assessed by other studies as contributing factors to air quality levels inside subway systems (Moreno et al., 2014). Looking at the 4h mean PM_{10} values, the lowest ones were measured during the periods of reduced operation and at the platform monitoring sites. The lowest individual value was obtained at the platform of the station Stubentor U3.

By comparing the mean values of the various monitoring sites, the speculated difference between tunnel and platform PM_{10} concentrations cannot be confirmed based on the limited data set available. The measurements at the two stations Karlsplatz U1 and Rochusgasse U3, where both tunnel and platform samplings were conducted thereby allowing a direct comparison, resulted in opposing outcomes. The mean PM_{10} concentration within the tunnel at Karlsplatz U1 is higher than the platform value, while at the site Rochusgasse U3 the opposite can be seen. This observation can be explained again by the open tunnel design at the station Rochusgasse U3, which possesses a greater air volume than the narrow tunnels at the station Karlsplatz U1. Furthermore, the sampling campaign at Rochusgasse was performed during the weekend period with reduced train frequency.

Comparison of the mean PM_{10} concentration values in the Viennese subway system with data from other cities, listed in Table 1.3 and Table 1.4, reveals a mid-range position of PM concentrations for the Austrian underground system. The majority of assessed PM_{10} mass concentration levels of European subway platforms range between 103 $\mu g/m^3$ and 407 $\mu g/m^3$ for Prague (Branǐs, 2006) and Rome (Ripanucci et al., 2006), respectively, while the concentration levels in the London Underground, known also as the oldest metro system in the world, are distinctly higher with concentrations between 1000-1500 $\mu g/m^3$ (Seaton et al., 2005). Looking at values assessed in metropoles of other continents, both the highest and lowest loadings of PM_{10}

were measured in Asia, with mean mass concentration values of 49 µg/m^3 and 366 µg/m^3 measured in Taipei (Cheng et al., 2008) and Shanghai (Ye et al., 2010), correspondingly. However, a direct comparison of these worldwide values should be carried out cautiously, as many of the mentioned studies derived their results from optical particle counters, omitting additional corrections through gravimetric measurements. Furthermore, measurement data from the literature were generated mainly at underground stations, platforms, or trains.

As most measurements were conducted during weekdays, trends relating to operating and non-operating hours (approximated by the sampling periods between 12 am and 4 am) can be visualized. Unsurprisingly, the night-time samples show lower PM_{10} concentrations than the values reached in operating hours during the day with enhanced train frequencies. Figure 3.1 shows the daily trends observed with the gravimetric results, ignoring the non-identic sampling dates. At the tunnel sites, the starting point of the sampling was set to 4 am, because the instruments had to be set up during the non-operating hours after 1am. The beginning of each platform measurement was initiated slightly later, between 12pm and 4pm. Characteristic repetitive daily trends of the PM_{10} mass concentration, already shown in the case of other subway systems (Cusack et al., 2015; Martins, Moreno, Mendes, et al., 2016; Reche et al., 2017; Salma et al., 2007), with a minimum during the night hours, are clearly visible from the gravimetric results. During this nighttime period, characterized by reduced train frequency between 12 am and 1 am and a total stop of operation between 1 am and 4 am, the lack of emissions, generally derived by mechanical wear and abrasion of the rail tracks and wheels during operating hours (Minguillón et al., 2018) and the resuspension of the generated PM due to the movement of the trains (Colombi et al., 2013), results in significantly lower mass concentrations than during the day. These night hours allow the sedimentation of particulate matter, providing an effective elimination process of the coarse airborne particles generated and resuspended during the day. With the resumption of the train service during the morning hours, the air pollution levels quickly rise again, producing morning and evening peaks due to high train operation frequencies and large passenger numbers. These daily trends are further discussed in the section describing the data obtained by the online instruments with better temporal resolutions (see 3.2.2).

The ratio of the mass concentrations (4 h mean values) of the night-time period to the operating hours (20 h mean values) were comparable with values between 5.1 and 6.5. Apart from the measuring site at the tunnel Rochusgasse U3, no notable difference was recognizable among the tunnel and platform locations. The measurement campaign at the tunnel Rochusgasse U3, as already mentioned, was conducted during the weekend with trains operating the entire night on Friday and Saturday, yielding a significantly lower ratio, which represents the concentration values for reduced, but continued train service. Due to a faulty gravimetric analysis of the night-time filters (12 am to 4 am) sampled at tunnel Praterstern U2, the corresponding ratio couldn`t be evaluated.

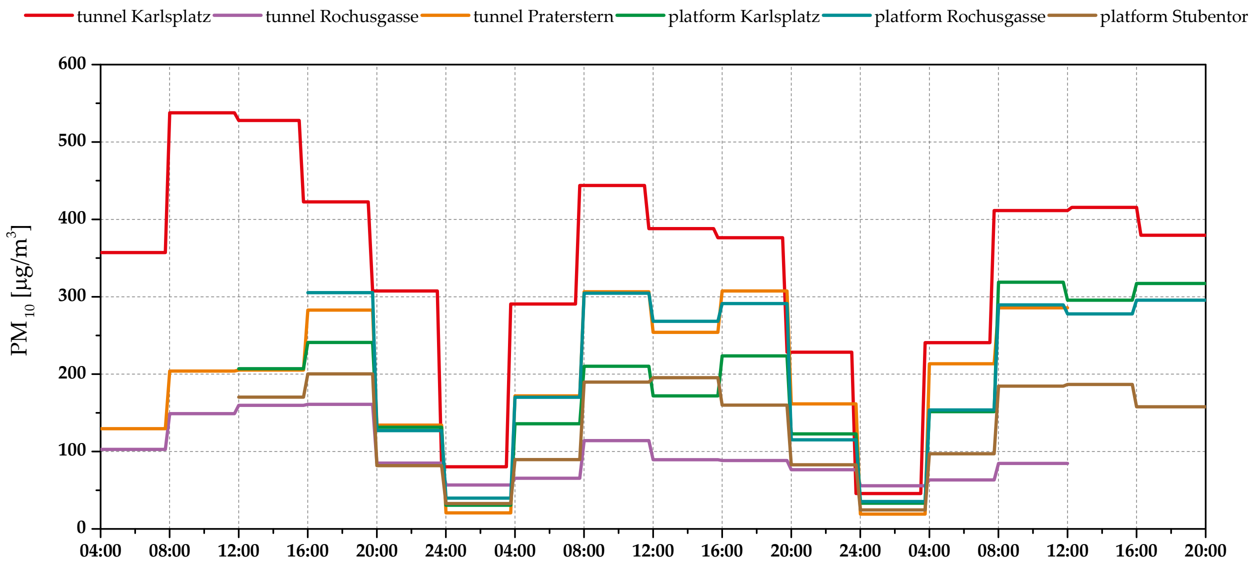

Figure 3.1 Temporal pattern of the PM_{10} mass concentration levels of all measuring sites (gravimetrically evaluated from the sampled LVS filters)

3.1.2 Comparison of subway and ambient PM_{10} mass concentrations

As expected, the comparison of the results from the particulate matter measurements in the subway system with the simultaneous values recorded by the ambient air network of Vienna reveals substantial differences in the PM_{10} mass concentration levels. The air pollution in the underground tunnel and platform microenvironments reaches a distinctly higher level than the levels measured in the outdoor environment. The measured values are summarized in Table 3.2. The ambient values of Vienna presented are mean values of the recorded levels at the monitoring sites of Taborstraße, A23-Wehlistraße and Gaudenzdorf, provided by the Vienna Municipal Department or Environmental Matters (MA22). Due to the late date of the measurements at the monitoring site of the tunnel Praterstern U2, no comparison was done for this period.

In addition to the daily mean values presented in the Table 3.2, Figure 3.2 shows the comparison of the diurnal concentration variations of the tunnel PM values sampled by the LVS at the station Karlsplatz U1 with the simultaneous 4 h mean ambient particulate matter levels, recorded by the ambient air network of Vienna. Looking at these illustrations, it can be concluded that the temporal mass concentration variations are independent from each other, even though concentration peaks can be observed during the morning rush hours in individual cases. The absence of a significant correlation between underground and ambient PM_{10} loadings was further on confirmed by a Pearson correlation coefficient of 0.05, which was calculated using the 4 h mean ambient and underground concentration values. This demonstrates the negligible impact of the ambient concentration levels to the semi-isolated microenvironment of the underground subway system, also confirmed by the results of the chemical analysis presented in the following sub-chapter. Thus, a correlation between outdoor and indoor air quality, shown in other studies (Martins, Moreno, Mendes, et al., 2016; Pan et al., 2019), couldn`t be confirmed with the dataset gathered in this work.

Table 3.2 Comparison of the ambient daily mean PM_{10} mass concentration values recorded by the MA22 (mean values of the levels recorded at the monitoring sites Taborstraße, A23-Wehlistraße and Gaudenzdorf) and at the subway measuring sites

Pearson`s r=0.05	platform			tunnel		
	Date	**ambient** PM_{10} **daily mean value [µg/m³]**	**LVS**	**Date**	**ambient** PM_{10} **daily mean value [µg/m³]**	**LVS**
Karlsplatz	4.11.19	7.5	186	11.11.11	17.2	431
	5.11.19	9.6	149	12.11.11	16.2	301
	6.11.19	7.4	223	13.11.11	7.4	233
Rochusgasse	19.11.19	20.4	216	15.11.11	20.4	143
	20.11.19	38.8	198	16.11.11	14.1	82
	21.11.19	17.4	210	17.11.11	23.3	68
Stubentor	28.10.19	14.1	151			
	29.10.19	19.3	125			
	30.10.19	21.7	130			

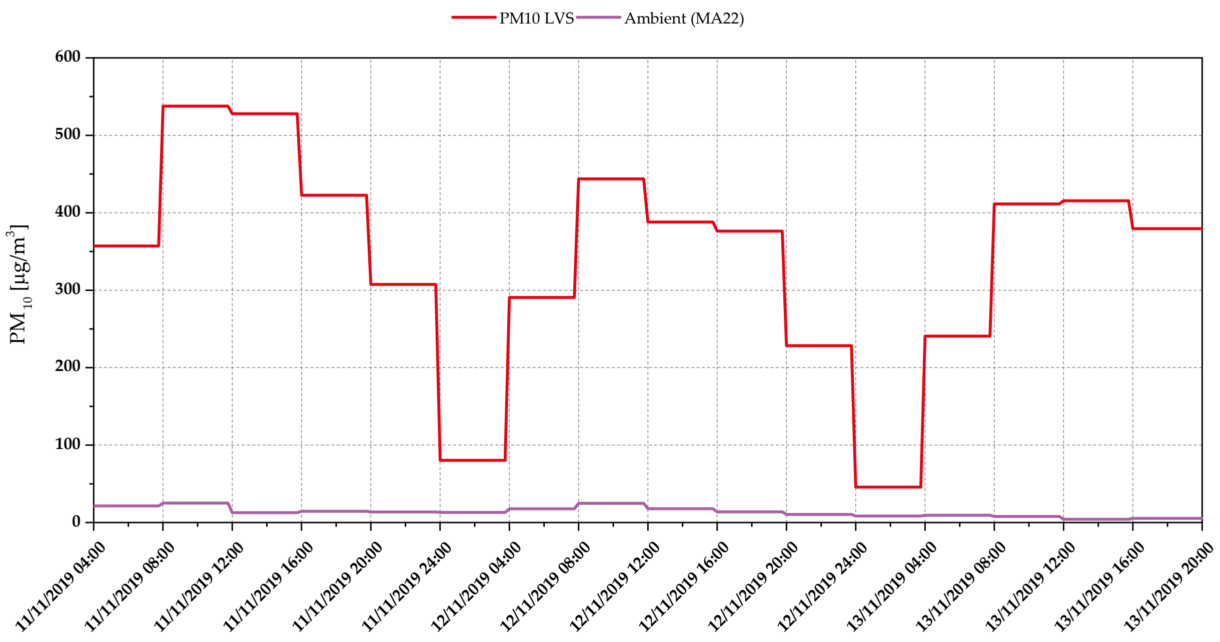

Figure 3.2 Comparison of the temporal patterns of the ambient and subway PM_{10} mass concentration levels. Ambient levels were recorded by the MA22 and the mean of the measuring sites of Taborstraße, A23-Wehlistraße and Gaudenzdorf is shown here, while subway pollution levels were recorded at the tunnel of the station Karlsplatz U1(gravimetrically evaluated from the sampled LVS filters)

3.1.3 Chemical composition of the subway PM_{10}

Most of the chemicals, amounting to the airborne particulate matter in the subway system, could be identified via the chemical analysis of the metal-, carbon- (presented as total carbon content) and water-soluble ion-content of the samples. Table 3.3 presents the mass concentration values of these substance groups and their percentual contribution to the total amount of PM_{10}.

Assessing the mean concentration values of the six monitoring sites, the iron content already amounts 56 - 72 % of the airborne particulates. The contribution of the trace elements (1 - 3 %), the carbonaceous particles (4 - 7 %) and the water-soluble ions (2 - 6 %) to the overall mass concentrations are significantly lower, but comparable with the results of other studies (Aarnio et al., 2005; Chillrud et al., 2011; Murruni et al., 2009). The remaining non-identified part includes mainly heteroatoms, primarily oxygen associated with the corresponding oxides, but also moisture. As a result of the usage of quartz fiber filters during the sampling campaign, the quantity of silicon couldn`t be determined. Since the quantification of the elemental components was conducted by ICP-MS, the characterization of the element species was not possible, however an estimation of the iron oxide species will be assessed subsequently.

Table 3.3 Overview of the mean mass concentration values of iron, trace element, water-soluble ion and total carbon content and their percentual contribution to the total PM_{10} concentration of all tunnel and platform measurements (faulty gravimetric measurements)*

Mean pollution levels		Fe		Trace metals		ws -Ions		TC		Identified
		[µg/m³]	%	[µg/m³]	%	[µg/m³]	%	[µg/m³]	%	%
tunnel Karlsplatz	total	223	65	5.3	2	6.4	2	14.2	4	73
	operation	250	66	5.8	2	6.9	2	15.2	4	73
	Reduced operation	33.5	53	1.4	2	3.4	5	7.1	11	72
tunnel Rochusgasse	total	60.3	62	2.8	3	6.2	6	7.1	7	79
	operation	65.6	64	2.8	3	6.1	6	7.4	7	79
	night operation	27.7	49	1.9	3	6.7	12	5.2	9	74
tunnel Praterstern	total	140	73	3.3	2	3.6	2	8.3	4	81
	operation	160	73	3.7	2	3.8	2	7.9	4	79
	Reduced operation	19.0	NA*	0.7	NA*	2.8	NA*	10.8	NA*	NA*
platform Karlsplatz	total	109	59	2.5	1	3.2	2	11.7	6	68
	operation	125	59	2.6	1	3.5	2	12.4	6	68
	Reduced operation	13.4	42	1.8	6	1.5	5	7.4	23	75
platform Rochusgasse	total	137	63	3.6	2	7.8	4	11.6	5	74
	operation	157	64	4.0	2	8.1	3	12.3	5	73
	Reduced operation	17.8	47	0.9	2	5.9	16	7.6	20	85
platform Stubentor	total	73.9	56	1.8	1	7.0	5	8.6	6	69
	operation	85.1	57	1.9	1	7.2	5	9.2	6	69
	Reduced operation	6.86	24	0.3	1	6.0	21	4.9	17	63

In the course of a precursor project, the ratio of the iron metal particles, hematite (Fe_2O_3) and magnetite (Fe_3O_4) present in the PM of the subway system of Vienna, were identified (Ott et al. `pers. Comm.`). The results showed a contribution of non-oxidized iron particles at 44 %, along with hematite at 35 % and magnetite at 21 %. Other studies investigating PM at platform areas of the subway systems in Barcelona and Stockholm (Querol et al. 2012) (Karlsson et al., 2008) (Karlsson et al., 2005) revealed the presence of iron oxides, identifying hematite as the predominant species. By taking the relative ratios of the determined iron species via the previous investigations in Vienna into account, the percentage of the iron compounds ($\sum$ (Fe, Fe_2O_3, Fe_3O_4))

increases to 69 – 90 %, regarding the total particulate matter mass. This conversion further increases the total identified PM_{10} amount to 82 – 98 %. Taking an even higher hematite content for this conversion, would decrease the non-identified part further. The non-classified chemical share can be reduced again by including the partially oxidized form of the determined trace elements, heteroatoms incorporated with the carbonaceous aerosols and moisture. The converted iron percentages are summarized in the Table 3.4, alongside the unmodified values of the trace metals, water-soluble ions and total carbon content already presented in Table 3.3.

Table 3.4 Overview of the mean mass concentration values of iron (estimated elemental and oxide fraction), trace element, water-soluble ion and total carbon content and their percentual contribution to the total PM_{10} concentration of all tunnel and platform measurements (faulty gravimetric measurements)*

Mittlere Belastung		**∑ (Fe, Fe_2O_3 und Fe_3O_4)**		**Trace metals**		**ws-Ionen**		**TC**		**Identified**
		[µg/m³]	%	[µg/m³]	%	[µg/m³]	%	[µg/m³]	%	%
tunnel Karlsplatz	total	274	80	5.3	2	6.4	2	14.2	4	88
	operation	307	81	5.8	2	6.9	2	15.2	4	88
	Reduced operation	41.2	65	1.4	2	3.4	5	7.1	11	84
tunnel Rochusgasse	total	74.2	77	2.8	3	6.2	6	7.1	7	94
	operation	80.7	78	2.8	3	6.1	6	7.4	7	94
	Reduced operation	34.1	61	1.9	3	6.7	12	5.2	9	85
tunnel Praterstern	total	173	90	3.3	2	3.6	2	8.3	4	98
	operation	197	89	3.7	2	3.7	2	7.9	4	96
	Reduced operation	23.4	NA*	0.7	NA*	2.8	NA*	10.8	NA*	NA*
platform Karlsplatz	total	134	73	2.5	1	3.2	2	11.7	6	82
	operation	154	73	2.6	1	3.5	2	12.4	6	82
	Reduced operation	16.5	52	1.8	6	1.5	5	7.4	23	85
platform Rochusgasse	total	168	78	3.6	2	7.7	4	11.6	5	88
	operation	193	78	4.0	2	8.0	3	12.3	5	88
	Reduced operation	21.9	58	0.9	2	5.9	16	7.6	20	96
platform Stubentor	total	90.9	69	1.8	1	7.0	5	8.6	7	82
	operation	105	70	1.9	1	7.2	5	9.2	6	82
	Reduced operation	8.4	30	0.2	1	6.0	21	4.9	17	68

In addition to Table 3.4, the PM_{10} mass concentration values of iron, other metals, water-soluble ions and total carbon are visualized in Figure 3.3, while Figure 3.4 illustrates their relative contribution to the total PM_{10} concentration. Looking at these graphs, the predominance of the iron quota becomes evident, followed by smaller contribution derived through the carbonaceous particles, the water-soluble ions, and the trace elements. A noteworthy variation of air pollution levels, between operating period and night-time (no operation or reduced night operation in the case of the tunnel Rochusgasse U3 in the weekend), and a substantial change of the relative abundance regarding the analyzed compound classes are also recognizable.

Further on, a common trend of the iron mass concentrations and their relative amount to the total PM_{10} is observable along all the measuring sites regarding the operating and non-operating hours. At night-time, the lack of iron emission sources, like mechanical wear and friction processes, and the absence of motion, responsible for the resuspension of dust particles, ensures the effective sedimentation of the coarse fraction, also containing particles of higher density. Thus the percentages of the iron fraction ($\sum$ (Fe, Fe_2O_3, Fe_3O_4)) during the day stretches between 70 – 89 %, while decreasing at night to 30 – 65 %. By comparing the operating and non-operating hours of the tunnel and platform measurements, a higher abundance of the iron compounds at the tunnel locations (78 – 89 %) than at the platform sites (70 – 78 %) is detectable throughout the entire monitoring course.

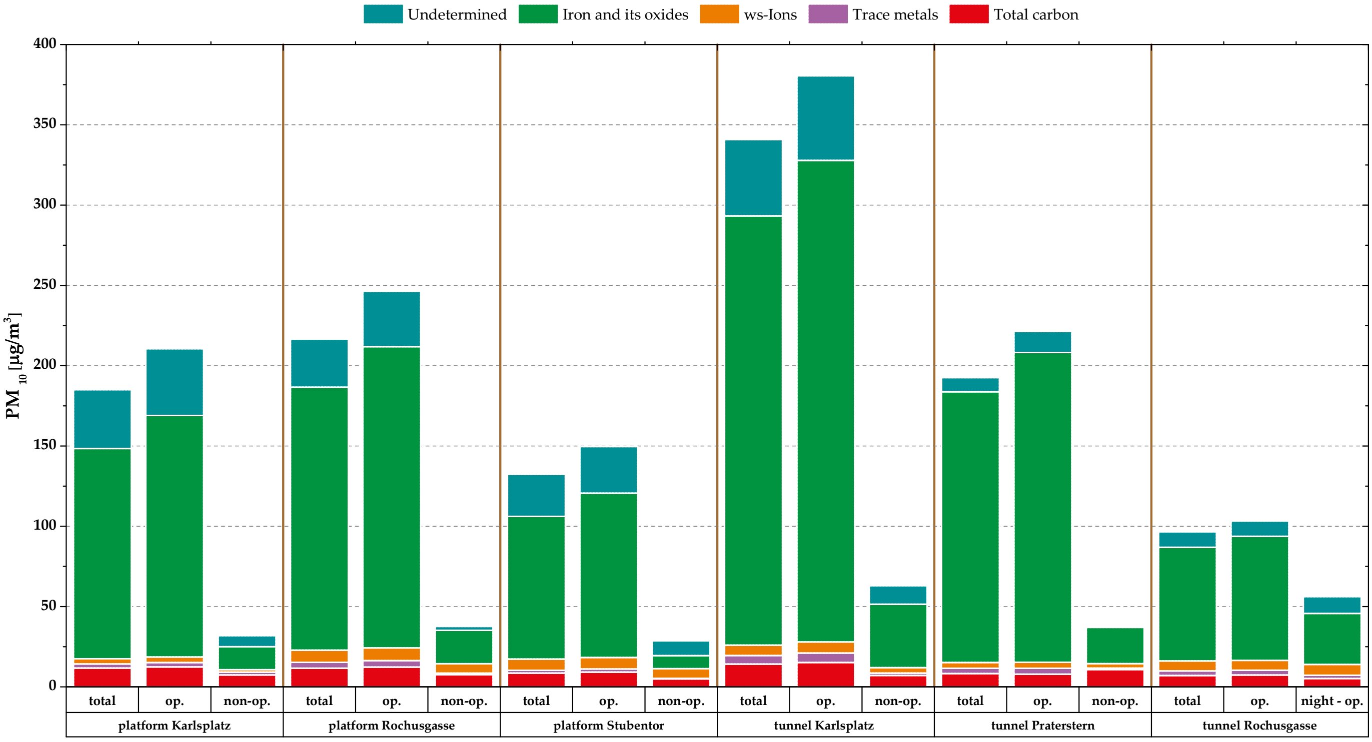

Figure 3.3 Illustration of the absolute PM_{10} mass concentration values measured at all tunnel and platform measuring sites and its absolute share on the quantified components (iron and its oxides, trace elements, water soluble ions and total carbon content)

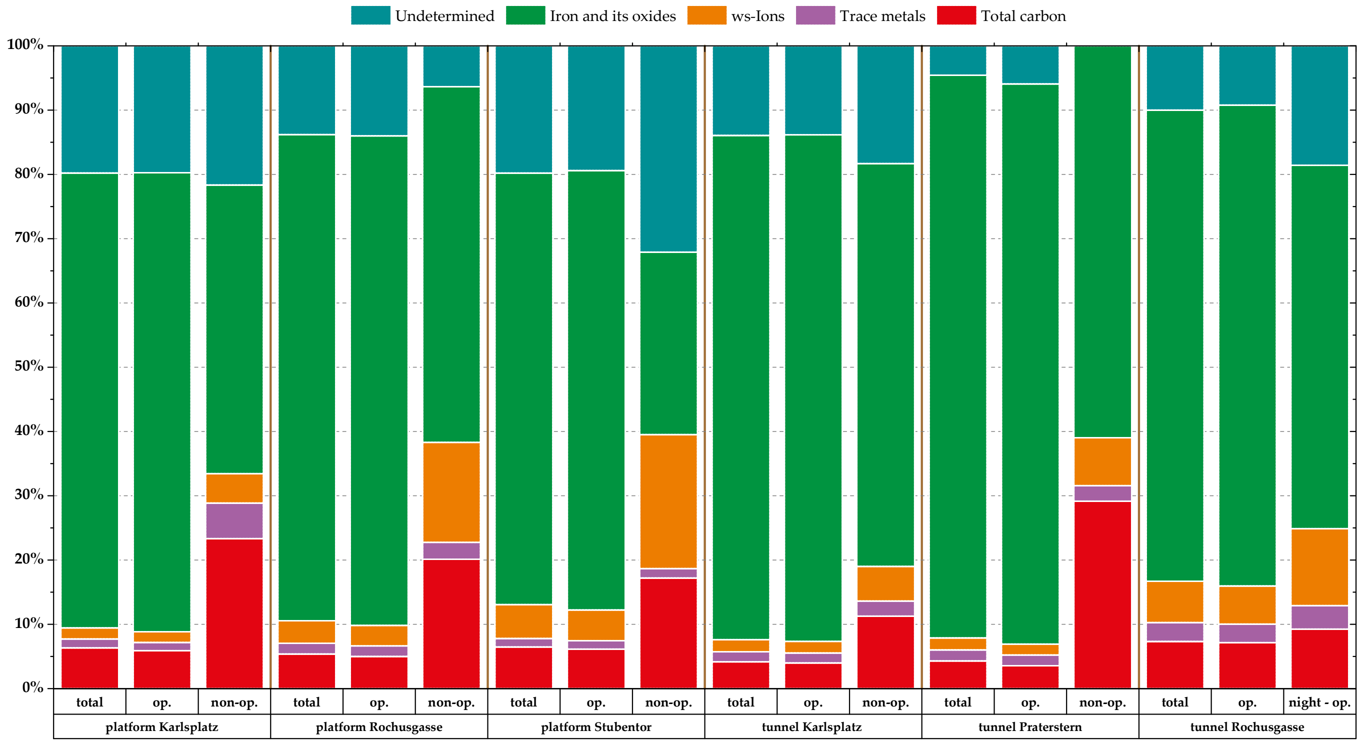

Figure 3.4 Illustration of the relative shares of the quantified components (iron and its oxides, trace elements, water soluble ions and total carbon content) on the total PM_{10} mass concentration values measured at all tunnel and platform measuring sites

Similarly, as for the case of the airborne iron particles, the emission of the trace elements is mainly occurring during the operation time of subway system (Minguillón et al., 2018). The cumulative PM_{10} mass concentration of the trace metals is correspondingly lower at all measuring sites during the non-operating hours. On the other hand, the relative amount of the trace metal fraction increases during the night hours, indicating a smaller aerodynamic diameter of these particles in comparison with the airborne iron particles. Due to their smaller aerodynamic sizes, these particles have lower deposition velocities (Noll et al., 1994). One exception represents the chemical results obtained at the platform Stubentor U3, where both the relative amount and the mean mass concentration values of the trace elements are lower during the night hours than during the operating hours. The cumulative parameter of the trace metals is primarily characterized by its aluminum, chromium, manganese, and copper content, being the most abundant elements quantified of this fraction, comparable to the findings of other studies (Aarnio et al., 2005; Loxham et al., 2013; Martins et al., 2017). Still the tendencies described above are also valid for the other trace elements, which can be seen in Table 3.5, showing the comparison of the mean PM_{10} mass concentration values for all individual components. The only exceptions are the results regarding cadmium and barium, although it can be generally stated, that the results of the cadmium measurements provided very low mass concentration values, some very close to the detection limits. At the station Karlsplatz U1, the mean concentration value of barium during the non-operating hours is exceeding the mean value measured from the samples collected during the operating hours. This is valid for both the tunnel and the platform samples.

The measured mass concentrations of beryllium were below the limit of detection values of 1 ng/m^3, thus they are not presented in Table 3.5.

The term carbonaceous compounds (TC) include the organic (OC) and elemental (EC) forms of carbon particles. Looking at Table 3.5, presenting these parameters separately, it gets clear, that the organic fraction contributes predominantly to the carbonaceous fraction of the subway aerosols, corresponding to other measurements conducted also in the colder season at Barcelona (Martins, Moreno, Minguillón, et al., 2016). The employed thermal-optical analysis method is a widely used reference method for the quantification of organic and elemental carbon concentrations in ambient air, even so the high abundance of hematite in the airborne subway particles can trigger an early evolution of EC due to heightened oxidation and catalysis rates (Chow et al., 2004). Further on the intrinsic color of iron oxides can influence the correct optical determination of the OC/EC split. Despite these known interferences, the thermal-optical method has been utilized by investigations concentrating on the chemical characterization of airborne subway PM of various cities (Querol et al., 2012)(Martins, Moreno, Minguillón, et al., 2016). For the following results the automatic OC/EC split-point, proposed by the OCEC (Calc 415) software, was used. Still, the OC and EC results obtained this way may only be interpreted as guidelines pinpointing to the actual ratio of organic and elemental carbon, because of the mentioned interferences causing systematic differences in their evaluation. A follow up study on the determination of clearer OC/EC split-points, regarding aerosol samples with varying iron oxide contents, is a work in progress at the Institute of Chemical Technologies and Analytics (TU Wien). The obtained EC/OC rates were close to or equal to 0.2 and were not dependent on the time of the day the samples were collected. On the contrary, the total carbon content, which can be quantified flawlessly using this method, decreases in most of the cases (with the exemption of tunnel Praterstern U2) during the non-operating hours, while its relative contribution to the total PM_{10} mass concentration rises to approximately 20 % (17 – 23 %) at the platform measuring sites. The iron concentration decreases in accordance with the increase of the carbon content during this period.

Levels of water-soluble ions were consistently low at every measuring site. However, a similar trend of concentration alteration was recognizable between the operating and non-operating hours, as for the carbonaceous aerosols. The mean mass concentration values of the water-soluble ions dropped during the night, but their relative contribution increased up to 21 %, due to the sedimentation of a substantial fraction of the airborne particulate matter. Still, the concentration of the water-soluble ions did not reach the ambient levels. Looking at the distinguished components of the water – soluble ions in the Table 3.5, it becomes evident that nitrate-, sulphate-, ammonium- and calcium- ions contribute the most to the mass concentration levels, showing concentration variations for different stations and sampling periods, respectively. Similar results were found in other studies investigating different subway systems (Lee et al., 2018; Martins, Moreno, Minguillón, et al., 2016). Through the examination of the individual measuring sites, it becomes clear that sulphate-, nitrate- and ammonium ions dominate the water-soluble ion fraction of the airborne particulate matter during the night, while during operating hours calcium is the most abundant component. This can be explained due to an emission source in the subway system, like abrasion of calcium rich construction materials or resuspension of sedimented dust, likely generated during preceding construction works. The relative contribution levels of calcium-ions to the total particulate mass stay throughout the measuring sites rather constant, while the sulphate-, nitrate- and ammonium-ion ratios are elevated at the station Rochusgasse U3 (tunnel and platform levels mutually).

Table 3.5 Overview of the mean PM_{10} mass concentration values measured on all tunnel and platform monitoring sites

		tunnel Karlsplatz			tunnel Rochusgasse			tunnel Praterstern			platform Karlsplatz			platform Rochusgasse			platform Stubentor		
Mean		total	op.	non-op.	total	op.	night-op.	total	op.	non-op.	total	op.	non-op.	total	op.	non-op.	total	op.	non-op.
PM_{10}	µg/m³	341	381	63	97	103	56	193	221	20	185	211	32	217	246	38	132	150	29
Fe	µg/m³	217	244	32	58	63	26	137	157	18	106	122	12	133	152	17	72	83	7
TC		14.2	15.2	7.1	7.1	7.4	5.2	8.3	7.9	10.8	11.7	12.4	7.4	11.6	12.3	7.6	8.6	9.2	4.9
OC	µg/m³	11.9	12.7	6.3	6.2	6.5	4.4	7.3	6.9	10.0	10.2	11.0	5.9	9.7	10.4	6.0	7.2	7.7	4.2
EC		2.3	2.5	0.8	0.9	0.9	0.8	0.9	1.0	0.8	1.5	1.5	1.6	1.9	2.0	1.5	1.4	1.5	0.8
ws-Cl^-		0.15	0.17	0.05	0.05	0.05	0.04	0.24	0.25	0.20	0.10	0.12	0.03	0.09	0.10	0.01	0.21	0.22	0.14
ws-NO_3^-		0.87	0.94	0.40	1.15	1.05	1.77	0.74	0.71	0.90	0.40	0.43	0.28	1.98	2.07	1.48	1.86	1.81	2.12
ws-SO_4^-		1.71	1.72	1.60	2.62	2.57	2.93	0.60	0.61	0.56	0.69	0.75	0.31	2.41	2.37	2.65	1.88	1.92	1.66
ws-NH_4^+		0.29	0.25	0.53	0.81	0.77	1.04	0.15	0.11	0.35	0.05	0.06	0.05	0.76	0.69	1.22	0.68	0.67	0.73
ws-Ca^{2+}	µg/m³	2.58	2.87	0.56	1.30	1.40	0.75	1.38	1.55	0.35	1.48	1.62	0.59	1.87	2.13	0.31	1.73	1.90	0.74
ws-Mg^{2+}		0.11	0.12	0.05	0.08	0.08	0.05	0.12	0.13	0.05	0.10	0.11	0.05	0.12	0.13	0.03	0.18	0.19	0.14
ws-Na^+		0.48	0.54	0.10	0.07	0.08	0.04	0.25	0.25	0.22	0.22	0.25	0.05	0.10	0.11	<0.025	0.32	0.32	0.33
ws-K^+		0.25	0.27	0.10	0.13	0.13	0.11	0.13	0.14	0.12	0.15	0.16	0.10	0.26	0.27	0.16	0.13	0.13	0.10
Al		1087	1160	577	562	607	292	557	614	215	699	648	1001	855	929	411	427	461	220
V		<28	<28	<28	35	34	41	<28	<28	<28	<28	<28	<28	<28	<28	<28	<28	<28	<28
Cr		619	687	146	309	335	158	494	565	69	358	407	60	554	635	67	226	259	23
Mn		1848	2070	288	536	578	280	1093	1229	275	888	1011	148	1120	1270	225	737	849	68
Co		12.5	13.9	2.4	9.8	11.0	2.6	6.1	6.9	1.4	4.8	5.4	1.1	8.0	9.1	1.2	4.2	4.9	0.2
Ni		168	185	56	238	228	301	112	129	12	92	97	64	276	305	103	42	47	12
Cu	ng/m³	725	821	48	396	427	211	679	749	257	195	220	40	354	411	17	122	141	5.6
Zn		420	468	82	508	579	86	317	360	60	148	156	104	254	278	110	34	37	16
Sr		13.1	13.7	8.7	12.0	12.5	9.0	7.0	8.0	1.3	7.0	7.2	6.1	12.2	13.0	8.0	3.0	3.3	1.2
Cd		2.0	2.0	2.3	2.1	2.1	2.2	5.9	6.8	0.7	2.7	3.0	0.8	1.9	1.9	1.8	1.5	0.5	7.8
Sb		7.2	7.9	1.6	5.2	5.9	0.8	6.4	7.3	0.6	6.6	7.3	2.2	11.0	12.5	2.0	7.0	8.0	1.0
Ba		162	156	201	182	106	637.3	<38	<38	<38	97.9	62.4	311	140	157	39.1	93.0	98.6	59.2
Pb		270	299	68.3	46.9	49.0	34.3	6.6	7.4	1.9	69.8	76.9	27.4	25.7	29.0	5.8	45.9	52.8	4.2

Concerning the mean mass concentration levels of the trace elements at the monitored subway stations, a relatively uniform image can be recognized, illustrated in the following Figure 3.5. The mean concentration variations of aluminum, chromium and manganese reflect virtually the change of PM_{10} levels, reaching the highest abundance at the tunnel Karlsplatz U1 and the lowest at the tunnel Rochusgasse U3 and at the platform Stubentor U3. For copper, the pattern of concentration distribution is slightly different, with higher concentrations measured at the tunnel Rochusgasse U3 and the tunnel Praterstern U2. The nickel levels at the station Rochusgasse U3 surpass the expected concentration levels moderately. Levels of zinc at the measuring point tunnel Rochusgasse U3 are significantly increased, while its abundance at the other sites follow the trend already mentioned above. There are elevated concentration levels of lead at tunnel Karlsplatz, then comparably low levels at the tunnel Praterstern U2 and at the platform Rochusgasse U3. Levels of barium show noticeably reduced values at the tunnel Praterstern U2. Vanadium could only be detected at the tunnel Rochusgasse U3 (presented in Table 3.5).

As already mentioned in 1.4.3, the sources of trace metals like Mn, Cr, Cu, Sb, Ba, Zn, Mo, Ni, Cd, as well as the dominating Fe, can be traced back to emission processes inside the subway MEs (Cusack et al., 2015; Minguillón et al., 2018). A detailed allocation of the elements C, Fe, Cr, Mn, Cu, Ni, Sb, V and Al to subway emission sources can be found in In Table 3.6, the elemental compositions of the alloys regarding rails, wheel tires, pantographs, and conductor rails, utilized inside the Viennese subway system are listed. Due to their mode of application, these compartments are all possible PM emission sources inside the underground ME. As already mentioned before, iron is the dominating constituent (between 97 % and 98 %) of these materials, with smaller differences in its contribution to the overall mass percentages regarding rails, wheel tires and pantographs, while for the conductor rails, the contribution of iron is somewhat smaller at 89 %. Regarding chromium, the conductor rails contain the highest mass percentage with 10 %, the wheel tires and pantographs contain around 0.6 % and the rails only 0.15 %. For manganese, the mass percentages of pantographs and conductor rails are identical at 0.6 %, while the contribution to the rails and wheel tires are bit higher with 0.95 % and 0.9 %, respectively. The elemental carbon content is the highest for the alloy used for the rails with 0.72 %, followed by the wheel tires, pantographs, and conductor rails with 0.65 %, 0.35 % and 0.05 %, accordingly. The copper content of the wheel tires and pantographs are equal at 0.3 %, while the rails contain somewhat less with 0.15 %. For the nickel and vanadium content, only the rails and wheel tires were specified. The wheel tires contain 0.3 % nickel and 0.05 % vanadium, while their contribution to the rail composition is smaller at 0.1 % and 0.03 %, respectively. Furthermore, only the rails contain antimony and aluminum with 0.02 % and 0.004 %, accordingly.

Table 3.6Additionally, some of these elements can be attributed to ambient anthropogenic sources as well, like V, Al, Cr, Cd, Fe, Ni, Cu, Zn and Pb, generated via processes associated with traffic emissions (Slezakova et al., 2007)(Chernyshev et al., 2019)(Shafer et al., 2012). Here, Vanadium is mainly emitted during the combustion of fossil fuels (Shafer et al., 2012). Non-exhaust traffic related emissions, like break abrasion is marked by elevated Fe, Cu, Zn and Sb contribution to PM_{10} emissions, while Zn and Cu are emitted amid the erosion of tires, as well (Grigoratos & Martini, 2014). Further on, elements like Mg, Al, Si, Ca, K and Ba can be related to crustal and road abrasion origins (Slezakova et al., 2007).

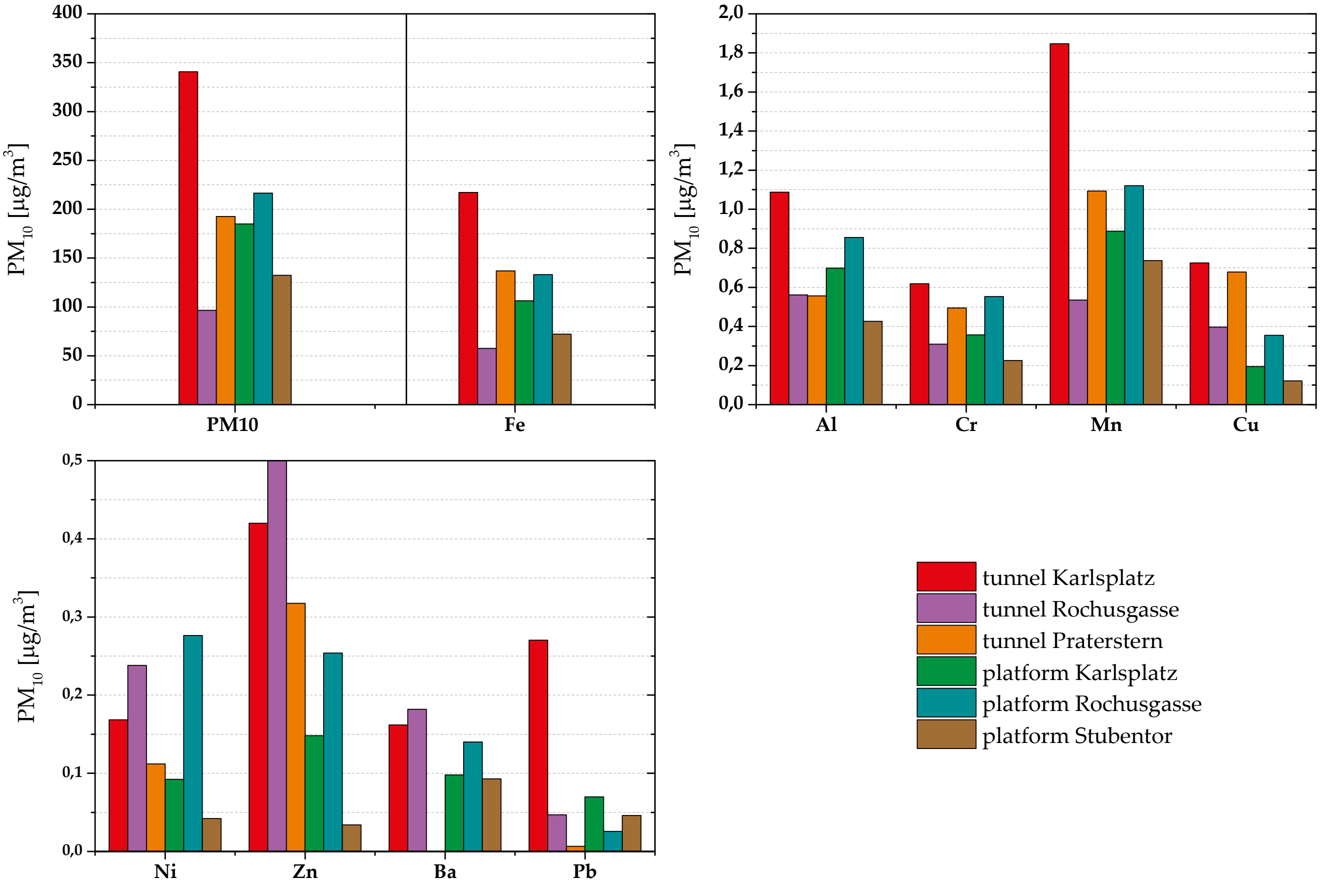

Figure 3.5 Comparison of the estimated mean mass concentration values of the investigated elements regarding all the monitoring sites

Looking at Table 3.5, it also becomes apparent that none of the maximum allowable concentration (MAK) levels defined in the Austrian Limit Value Ordinance of 2018 were exceeded during this measuring campaign. This is also the case for beryllium, which could not be quantified in the samples, due to lower concentration levels than its detection limit values.

3.1.4 Source analysis

In Table 3.6, the elemental compositions of the alloys regarding rails, wheel tires, pantographs, and conductor rails, utilized inside the Viennese subway system are listed. Due to their mode of application, these compartments are all possible PM emission sources inside the underground ME. As already mentioned before, iron is the dominating constituent (between 97 % and 98 %) of these materials, with smaller differences in its contribution to the overall mass percentages regarding rails, wheel tires and pantographs, while for the conductor rails, the contribution of iron is somewhat smaller at 89 %. Regarding chromium, the conductor rails contain the highest mass percentage with 10 %, the wheel tires and pantographs contain around 0.6 % and the rails only 0.15 %. For manganese, the mass percentages of pantographs and conductor rails are identical at 0.6 %, while the contribution to the rails and wheel tires are bit higher with 0.95 % and 0.9 %, respectively. The elemental carbon content is the highest for the alloy used for the rails with 0.72 %, followed by the wheel tires, pantographs, and conductor rails with 0.65 %, 0.35 % and 0.05 %, accordingly. The copper content of the wheel tires and pantographs are equal at 0.3 %, while the rails contain somewhat less with 0.15 %. For the nickel and vanadium content, only the rails and wheel tires were specified. The wheel tires contain 0.3 % nickel and 0.05 % vanadium, while their contribution to the rail composition is smaller at 0.1 % and 0.03 %, respectively. Furthermore, only the rails contain antimony and aluminum with 0.02 % and 0.004 %, accordingly.

Table 3.6 Mean mass percentual chemical compositions of subway modules (thus potential emission sources), given by the Wiener Linien

Mean composition	**C**	**Fe**	**Cr**	**Mn**	**Cu**	**Ni**	**Sb**	**V**	**Al**
					m%				
rail	0.72	97.88	0.15	0.95	0.15	0.1	0.02	0.03	0.004
wheel tire	0.65	97.2	0.6	0.9	0.3	0.3	NA*	0.05	NA*
pantograph	0.35	98.15	0.6	0.6	0.3	NA*	NA*	NA*	NA*
conductor rail	0.05	89.15	10.2	0.6	NA*	NA*	NA*	NA*	NA*

NA= not specified*

3.1.4.1 Comparison of the mass concentration normalized elemental ambient and subway concentrations

To compare the elemental composition of the subway PM and ambient PM composition taken from literature, the mean mass concentration values of each element for every tunnel and platform monitoring station were normalized against the respective PM_{10} mean mass concentration values, determined through the gravimetric measurements of the filters. The resulting relative contributions of each element to the total mass for each station was further on averaged, to calculate the corresponding overall ratios in the subway ME. In order to compare these values with ambient measurements, the Viennese PM_{10} mineral composition data, assessed by (Limbeck et al., 2009) at two urban sites Rinnböckstraße and Kendlerstraße, were normalized regarding the average gravimetric PM_{10} mass concentration values and averaged as well. Subsequently, the normalized contribution of each element for the subway PM_{10} was put in relation to the respective ambient contribution, thereby determining the ratios displayed in Figure 3.6.

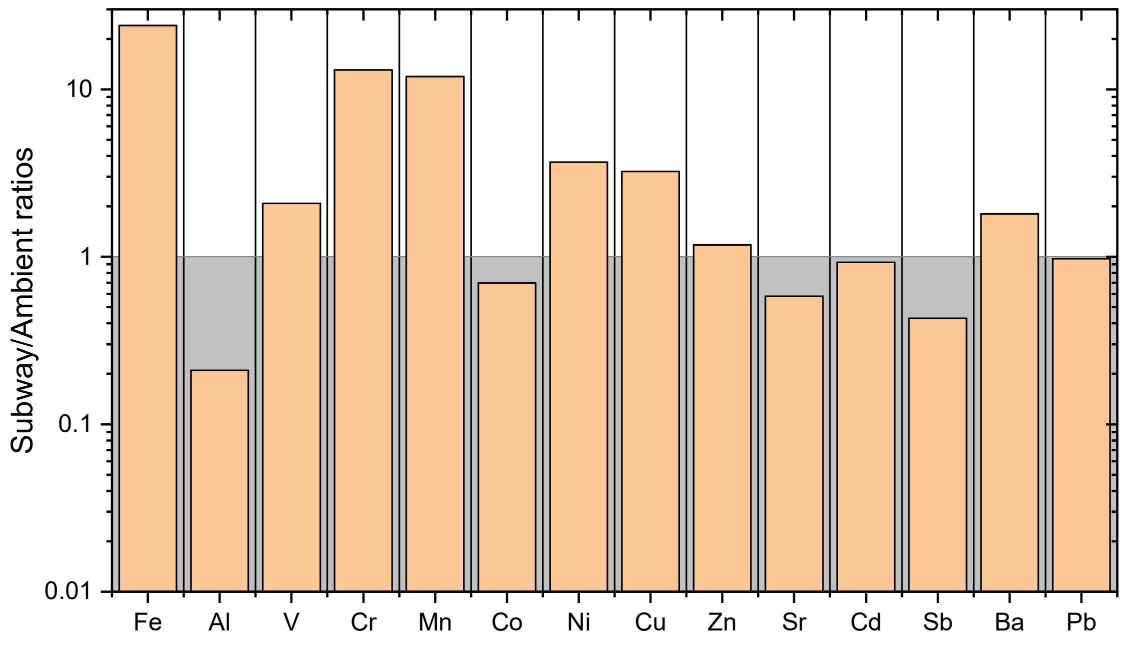

Figure 3.6 The determined normalised subway vs. ambient ratios for the measured mineral components

High contributions of iron, chromium, and manganese to the subway PM, with 24-fold, 13-fold and 12-fold corresponding relative enrichments, in regard to ambient PM can be noted. These elements are abundant in potential subway emission sources, listed already in Table 3.6. Further on, the contributions of nickel and copper are 4 and 3 times higher in the subway PM, than in the ambient PM, coherent with the composition of rails, wheel tires and pantographs, subjected to friction during the operating hours. The vanadium and barium concentrations in the subway ME are approximately 2 times higher than the ambient, while zinc is only slightly enhanced by 18 %. The source of vanadium can be appointed to the elemental composition of the subway rails, while barium could be a potential component of the brakes used (Moreno, Martins, et al., 2015), although an exact composition of the subway brakes in Vienna was not available. On the other hand, the influence of traffic as a source for vanadium cannot be neglected. Even though zinc is not stated as a main component of the Viennese rails, other studies suggested rails and catenaries as potential sources inside the subway ME (Minguillón et al., 2018). Relative contributions of lead and cadmium are comparable for both environments, with ratios of 0.98 and 0.93. In contrast, aluminum, antimony, strontium, and cobalt contribute more to the relative ambient PM mass concentrations by 4.77, 2.33, 1.72 and 1.44 times, accordingly. As aluminum is an abundant crustal element, its main emission sources can be of both natural and anthropogenic origins in the urban environment, thereby explaining its higher contributions to the ambient PM than the concentrations encountered in the subway ME, characterized by less potential Al sources (Aksu, 2015). The source of antimony emissions is mainly related to traffic emissions, produced by break wear (Smichowski, 2008). Like Al, strontium is a common crustal element, emitted to the atmosphere mainly by natural means, for example by abrasion of crustal material and resuspension mechanisms (Pathak & Gupta, 2020). Cobalt can both have natural and anthropogenic origins, ranging from crustal erosion, forest fires to exhaust emissions, industrial processes and incinerator emissions, inter alia (Faroon et al., 2004).

3.1.4.2 Elemental ratios of the highly enriched components Fe, Cr, Mn

Furthermore, the elemental ratio characteristics of iron and chromium to manganese were investigated, by plotting the Fe/Mn and Cr/Mn (Figure 3.7) values obtained from the tunnel and platform samples and their slopes were compared to the ratios typically found in crustal material. Particulate Fe was strongly correlated with particulate Mn ($R^2 = 0.96$) and provided an elemental ratio value of Fe/Mn = 113, by the evaluation of the slope of the linear regression model, which is twice as high as the crustal ratio described in the literature (Fe/Mn = 55) (Chillrud et al., 2011) and similar to the values given by (D. Park et al., 2014) and references therein.

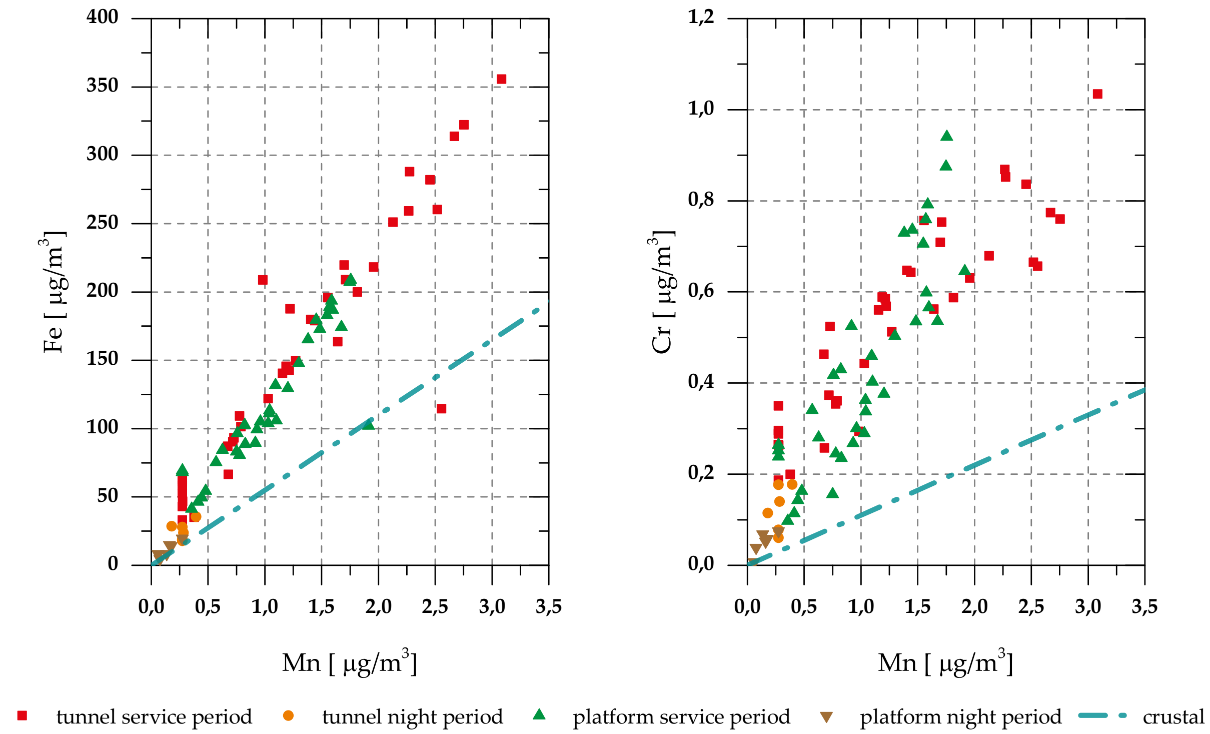

Figure 3.7 Comparison of the crustal and subway Fe/Mn and Cr/Mn ratios

The slope of the Cr/Mn regression model ($R^2 = 0.94$) provided an elemental ratio of 0.38, which is almost 3. 5 times the crustal ratio. These elemental ratios are consistent with other studies investigating the elevated particulate matter levels in other subway systems (Chillrud et al., 2011) and support the interpretations of the determined normalized subway vs. ambient ratios determined in the previous section 3.1.4.1 identifying the subway system as the main emission source of these elements.

3.1.4.3 Comparison of the sedimented vs. airborne subway aerosol composition

Quasi-enrichment factors (qEFs) were further calculated, to compare the results obtained by the parallel project analyzing the composition of the sedimented dust collected at the stations Karlsplatz U1, Rochusgasse U3 and Praterstern U2. Enrichment factors (EFs) are commonly used in the literature to differentiate between anthropogenic and natural origins regarding the occurrence of various elements in environmental samples, taking the crustal composition as a reference. The limitations of this approach have already been discussed extensively (Reimann & Caritat, 2005), thereby enabling only a cautious interpretation of the respective results. Enrichment factors can be calculated by utilizing the concentration of a reference element for the normalization against an element concentration in the particulate matter sample. Herein, only qEFs were determined, replacing the crustal ratios with the elemental ratios measured in the sedimented subway dust. Thus, it can be evaluated whether resuspension of sedimented dust is the main emission source for airborne particulate matter. qEFs were calculated using a modified Equation 3-1, based on (Barbieri, 2016). Since iron turned out to be the most abundant and conservative element in both the airborne and sedimented dust fractions, it was used as the reference metal for the enrichment estimations, presented in the following Table 3.8 for each measuring site separately.

$$qEF = \frac{\left[\frac{C(x)}{C(ref)}\right] \rightarrow subway\ airborne\ PM}{\left[\frac{C(x)}{C(ref)}\right] \rightarrow subway\ sedimented\ dust}$$

Equation 3-1 Calculation of the quasi- Enrichment Factors

Enrichment categories were identified using the following Table 3.7 proposed by modifying contamination classes used by different studies regarding elemental enrichment investigations of particulate matter (Barbieri, 2016; Yongming et al., 2006)

Table 3.7 Proposed enrichment categories

	Enrichment categories based on EF values
EF<2	Deficiency to minimal enrichment
EF=2-10	Moderate enrichment
EF=10-40	Significant enrichment
EF>40	High enrichment

Table 3.8 Overview of qEFs calculated via the elemental concentration values measured in the sedimented and airborne subway dust

		tunnel		**platform**	
		operation	non-operating hours	operation	non-operating hours
Karlsplatz	Al	0.4	1.3	0.4	6.4
	Mn	0.7	0.8	0.7	1.1
	Cr	1.1	1.8	1.3	2.1
	Pb	0.2	0.3	0.1	0.4
	Cu	1.7	0.7	0.9	1.7
	Zn	0.6	0.8	0.4	2.7
	Ni	0.8	1.7	0.8	5.5
	Cd	0.02	0.2	0.1	0.2
		operation	reduced operation	operation	non-operating hours
Rochusgasse	Al	0.5	0.5	0.3	1.2
	Mn	0.8	1.0	0.7	1.2
	Cr	0.8	0.9	0.6	0.6
	Pb	3.5	8.2	1.2	NA
	Cu	4.2	5.1	1.7	0.6
	Zn	2.4	2.3	1.3	4.5
	Ni	3.7	12.0	2.1	6.3
	Cd	0.1	0.3	0.04	0.3
		operation			
Praterstern	Al	0.2			
	Mn	0.8			
	Cr	0.7			
	Pb	NA			
	Cu	1.5			
	Zn	0.6			
	Ni	0.8			
	Cd	0.1			

Overall, most of the elemental concentration levels of the airborne particulates are very similar or slightly reduced in comparison with the sedimented dust. A general pattern can be noticed that if visible, the moderate enrichment is more pronounced during the non-operating hours compared to the service period of the subway trains. An interpretation could be that the air movement during operating hours leads to continuous resuspension of deposited particles, while size dependent deposition of particles becomes more relevant during the non-operating hours and the enhanced elements are more frequent in the smaller size range. Moderate enhancement of concentration values can be seen for aluminum and nickel at the platform site of Karlsplatz U1 during the non-operating hours. At the station Rochusgasse U3 the nickel levels show a comparable behavior, with moderately enriched values during the operating hours at both the tunnel and platform locations and a significant enrichment with an EF of 12 during the weekend period with continuous service at the tunnel measurement site. Further on, the EFs of lead, copper and zinc show moderate enhancement for this specific weekend period for the monitoring site at tunnel Rochusgasse U3. The results obtained for the tunnel Praterstern U2 do not show any enrichment. The EFs of lead for the non-operating hours at the platform of Rochusgasse U3 and at the tunnel at Praterstern U2 are not presented, as their concentration levels in the airborne particulate matter samples were below the limit of detection values.

3.1.4.4 Correlation analysis

To further analyze possible correlations between the investigated chemical components in the subway PM samples, Pearson and Spearman correlation matrices were generated via Datalab. While the Pearson coefficient can indicate the strength and direction of a linear correlation, the Spearman coefficient enables the recognition of the strength and direction, regarding a monotonic relationship between two variables (Schober et al., 2018). Both correlation coefficients can produce values between -1 and 1, indicating a perfect negative or positive relationship, accordingly, while values around zero indicate no statistical relationship. To recognize noteworthy correlations, the threshold value in Datalab was set to ± 0.7. The resulting correlation matrices are shown in Figure 3.8 and Figure 3.9.

As expected, high correlation coefficients were found between the PM_{10} mass concentration values and the Fe, Cr, Mn and TC concentrations, regarding both the Pearson`s and Spearman`s coefficients. Additionally, PM_{10} concentrations were correlated to Co and `ws`-Ca, concerning the respective Spearman correlation coefficients. Cr, Mn and TC were highly correlated with Fe, indicating a common source inside the subway system, like the emissions produced during the abrasion of materials listed in Table 3.6. Additionally, Co had a positive significant monotonic correlation to Fe. Furthermore, Zn and Sr had significant linear correlation both to V and Co concentrations. Due to their common occurrence in subway materials, exposed to abrasion, Mn and Cr both produced high Pearman`s and Spearman`s correlation coefficients, while Cu and Co showed positive monotonic correlations to the Cr concentrations. Further on, `ws`-Ca showed significant monotonic correlations to Cr and Mn.

4:12	PM10	Al	V	Cr	Mn	Co	Ni	Cu	Zn	Sr	Cd	Sb	Ba	Pb	Fe	Cl	NO2	NO3	SO4	Na	NH4	Mg	K	Ca	TC
PM10	**1.0000**																								
Al	0.4989	**1.0000**																							
V	-0.0336	0.4263	**1.0000**																						
Cr	**0.8248**	0.5088	0.0992	**1.0000**																					
Mn	**0.8912**	0.6235	0.2242	**0.8959**	**1.0000**																				
Co	0.4004	0.6284	**0.8448**	0.4876	0.6232	**1.0000**																			
Ni	0.2169	0.2900	0.1144	0.3696	0.2610	0.3072	**1.0000**																		
Cu	0.3051	0.2342	0.2515	0.4019	0.3879	0.4704	0.3203	**1.0000**																	
Zn	0.1600	0.4511	**0.7806**	0.2999	0.3519	**0.8240**	0.2815	0.6828	**1.0000**																
Sr	0.2862	0.6193	**0.7350**	0.3515	0.4321	**0.8139**	0.4200	0.4509	**0.7791**	**1.0000**															
Cd	0.0469	0.0136	0.1146	0.0546	0.0366	0.1066	-0.0158	0.3523	0.0829	0.0842	**1.0000**														
Sb	0.5028	0.4188	0.2249	0.5698	0.4856	0.4245	0.1166	0.1989	0.2752	0.2772	0.0482	**1.0000**													
Ba	-0.0600	0.0402	-0.0415	-0.0968	-0.0225	0.0113	0.5821	-0.0156	-0.0664	0.1871	-0.0272	-0.3377	**1.0000**												
Pb	0.4785	0.3445	0.1236	0.3961	0.5159	0.3685	0.1494	0.4311	0.3605	0.3597	-0.0354	0.1866	0.0672	**1.0000**											
Fe	**0.9479**	0.5451	-0.0111	**0.9046**	**0.9377**	0.4189	0.2382	0.3422	0.1934	0.2908	0.0274	0.4783	-0.0970	0.4471	**1.0000**										
Cl	0.3877	0.1116	-0.0569	0.3148	0.3974	0.1503	-0.1829	0.1557	0.0498	-0.0056	0.1416	0.2428	-0.1109	0.0147	0.4063	**1.0000**									
NO2	0.0521	0.0663	-0.0299	0.1572	0.0467	-0.0081	0.0466	-0.0465	-0.0382	0.0054	0.0925	0.3901	-0.0984	-0.0497	0.0700	-0.0905	**1.0000**								
NO3	-0.0227	-0.0366	-0.0443	-0.0593	-0.0580	-0.0098	0.2382	-0.0295	-0.0388	-0.0271	-0.0629	0.0783	0.2989	-0.0820	-0.1059	0.1171	-0.0032	**1.0000**							
SO4	-0.0374	0.1237	0.1997	0.0030	0.0086	0.1807	0.4065	-0.0148	0.1413	0.2601	-0.0484	0.1295	0.3259	0.0851	-0.0915	-0.1945	0.0241	0.6141	**1.0000**						
Na	0.5715	0.3512	-0.0457	0.2801	0.4711	0.1889	-0.1438	0.1500	0.1018	0.2182	0.0278	0.1872	-0.1004	0.3562	0.5514	0.5741	-0.0530	-0.0117	-0.1090	**1.0000**					
NH4	-0.3029	-0.0557	0.1513	-0.2409	-0.2336	0.0240	0.2921	-0.1097	0.0376	0.1098	-0.0564	-0.0164	0.3462	-0.0854	-0.3582	-0.2520	-0.0173	0.6626	**0.9214**	-0.2925	**1.0000**				
Mg	0.4466	0.2174	0.0039	0.4364	0.4966	0.2316	-0.0906	0.1325	0.0438	0.0052	0.0368	0.4642	-0.1928	0.0871	0.4590	0.6274	0.0582	0.3083	0.0637	0.4164	-0.0213	**1.0000**			
K	0.6180	0.4668	-0.0183	0.4970	0.5110	0.2689	0.2553	0.1722	0.1352	0.2746	0.0443	0.3645	0.0126	0.3045	0.5661	0.2620	0.0775	0.4537	0.2963	0.4767	0.0847	0.2957	**1.0000**		
Ca	0.6809	0.4888	0.0482	0.6007	0.6751	0.3473	0.1172	0.1775	0.1162	0.1747	-0.0261	0.4309	-0.1543	0.3415	0.6858	0.3199	0.0671	0.0483	0.0884	0.4085	-0.1241	0.5986	0.5244	**1.0000**	
TC	**0.7665**	0.5235	-0.0076	0.6439	**0.7575**	0.3605	0.1591	0.1743	0.1081	0.2300	0.0018	0.3952	-0.0109	0.4730	**0.7515**	0.3189	0.1511	0.0086	0.0607	0.4970	-0.1764	0.4127	0.6865	0.6891	**1.0000**

Figure 3.8 Pearson`s correlation matrix

4:12	PM10	Al	V	Cr	Mn	Co	Ni	Cu	Zn	Sr	Cd	Sb	Ba	Pb	Fe	Cl	NO2	NO3	SO4	Na	NH4	Mg	K	Ca	TC
PM10	**1.0000**																								
Al	0.5394	**1.0000**																							
V	-0.0284	0.1866	**1.0000**																						
Cr	**0.8452**	0.5883	0.1093	**1.0000**																					
Mn	**0.8892**	0.6190	0.1727	**0.9104**	**1.0000**																				
Co	**0.7925**	0.6327	0.2083	**0.7812**	**0.8470**	**1.0000**																			
Ni	0.4141	0.4734	0.1487	0.5977	0.4539	0.5007	**1.0000**																		
Cu	0.5914	0.5484	0.1772	**0.7632**	0.6948	0.6238	0.6277	**1.0000**																	
Zn	0.3945	0.5456	0.1890	0.5735	0.4084	0.4413	0.6116	0.6477	**1.0000**																
Sr	0.4822	0.6496	0.2102	0.5370	0.5124	0.5715	0.6235	0.5711	0.4931	**1.0000**															
Cd	0.0593	0.0899	0.3253	0.0824	0.0867	0.1399	0.1080	0.0723	0.1205	0.1465	**1.0000**														
Sb	0.5974	0.4800	0.1948	0.6353	0.5909	0.5490	0.2614	0.3922	0.3624	0.2459	0.0505	**1.0000**													
Ba	-0.0182	0.2125	-0.0572	-0.0882	0.0630	0.1219	0.2093	-0.0225	-0.1149	0.2916	0.0348	-0.3555	**1.0000**												
Pb	0.4938	0.4635	0.1564	0.4050	0.4773	0.4744	0.3466	0.3461	0.1607	0.4470	0.1145	0.2609	0.3413	**1.0000**											
Fe	**0.9401**	0.5778	0.0240	**0.9263**	**0.9448**	**0.8018**	0.4528	0.6899	0.4730	0.4937	0.0508	0.6125	-0.0746	0.4313	**1.0000**										
Cl	0.4752	0.1916	-0.0525	0.3634	0.5079	0.4154	-0.1200	0.2616	0.0740	0.0862	0.1033	0.3268	-0.0365	-0.0755	0.5021	**1.0000**									
NO2	0.0428	-0.0109	-0.0370	0.0642	0.0470	0.0114	-0.0568	-0.0929	-0.0807	0.0224	0.1630	0.1911	-0.1106	-0.0285	0.0418	-0.0568	**1.0000**								
NO3	-0.0353	0.0465	-0.0109	-0.0746	-0.0303	0.0390	0.1434	0.0271	-0.0215	-0.0074	0.0510	0.0726	0.0969	-0.1048	-0.0990	0.1562	0.0082	**1.0000**							
SO4	0.0359	0.2018	0.1639	0.0468	0.0875	0.1809	0.3685	0.0732	0.0725	0.2160	0.1479	0.1388	0.1958	0.2520	-0.0179	-0.1094	0.0266	**0.7469**	**1.0000**						
Na	0.5983	0.2248	-0.0328	0.3842	0.5876	0.4584	-0.1632	0.1889	-0.0322	0.0683	0.0944	0.3231	-0.0020	0.2466	0.5909	**0.7818**	0.0242	0.0387	-0.0815	**1.0000**					
NH4	-0.2780	-0.0153	0.1464	-0.2119	-0.1899	-0.0874	0.1967	-0.0915	-0.0301	0.0059	0.0957	-0.0671	0.1647	-0.0962	-0.3073	-0.1601	-0.0275	**0.7928**	**0.8842**	-0.2761	**1.0000**				
Mg	0.4976	0.3350	0.0109	0.4690	0.5759	0.4613	-0.0123	0.2459	0.0881	0.0608	0.0467	0.5329	-0.1013	0.0128	0.5287	0.6731	0.0719	0.3643	0.1981	0.6117	0.0811	**1.0000**			
K	0.6166	0.4935	0.0109	0.5530	0.5648	0.5271	0.4230	0.3747	0.2816	0.3390	0.2335	0.3767	0.0582	0.4372	0.5771	0.3050	0.0894	0.3249	0.3624	0.3587	0.1124	0.3353	**1.0000**		
Ca	**0.7634**	0.5653	0.1071	**0.7710**	**0.8068**	0.6968	0.3174	0.5479	0.3283	0.3360	-0.0069	**0.7336**	-0.1640	0.3808	**0.8066**	0.4700	0.0382	0.1437	0.2265	0.5149	-0.0411	**0.7689**	0.5557	**1.0000**	
TC	**0.7157**	0.5601	0.0022	0.6159	**0.7133**	0.6424	0.2790	0.3731	0.1862	0.3404	0.0887	0.4897	0.0793	0.5850	**0.7035**	0.3841	0.0803	-0.0034	0.1560	0.5128	-0.1349	0.4195	**0.7403**	0.6993	**1.0000**

Figure 3.9 Spearman`s correlation matrix

Looking at the ionic components, NH_4^+ and SO_4^{2-} showed high Pearson`s and Spearman`s correlation coefficients, indicating $(NH_4)_2SO_4$ as their common source from the ambient air entering the subway system. Also, the Spearman`s rank coefficient between the NH_4^+ and NO_3^- was significant, implying ammonium nitrate as their common source, being a major atmospheric PM component from anthropogenic processes. The significantly high monotonic correlation between NO_3^- and SO_4^{2-} can be explained, due to their general occurrence as secondary inorganic aerosols in the atmosphere (Lefer & Talbot, 2001). Further on, Na^+ and Cl^- show a significant monotonic relationship. The monotonic correlation of Mg^{2+} and Ca^{2+} could also point to their common source as crustal material aerosols (A. Kumar & Sarin, 2009). As K^+ is a commonly used indicator of biomass burning, the monotonic relationship with the TC content is also reasonable (Pachon et al., 2013). Albeit, as already mentioned above, TC is further on correlated with Fe, thus a clear connection of the total carbon content to biomass burning cannot be confirmed.

3.1.4.5 PCA

Principal component analysis (PCA) was performed with the DataLab (Version 4.100) software (Epina Gmbh) and applied on the whole dataset provided by the chemical analysis. For samples where specific components couldn`t be quantified due to concentration levels below detection limits, the respective LOD value was divided by two and added to the dataset. PCA is a helpful tool, often used for the characterization of emission sources and their respective input to assessed PM concentrations (Baker, 2003).

Using the standardized dataset consisting of the 86 samples obtained from the stationary measurements, the principal components (PCs) were calculated. Beryllium and nitrite were excluded, since their concentration levels were below the detection limits for most of the samples. Further on the concentration values of vanadium, barium, lead, aluminum and antimony were ignored, considering that more than 20% of the respective values were below the respective detection limits. All PCs with an eigenvalue over 1 were extracted from the analysis, therefore the results regarding the first 5 PCs are going to be examined subsequently. The resulting eigenvalues of the 19 calculated PCs are shown in Figure 3.10, with the first five, chosen for further interpretations, displayed in colors.

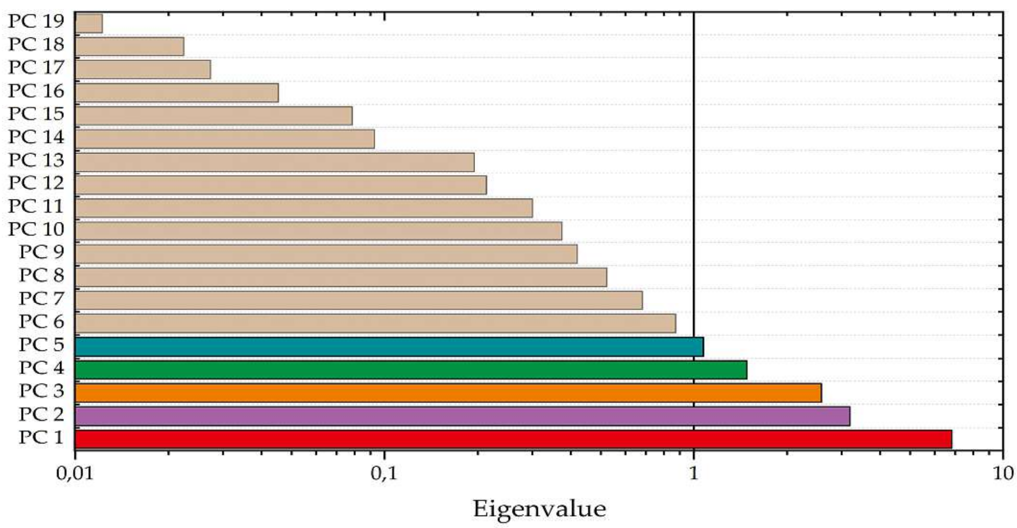

Figure 3.10 Resulting eigenvalues of the PCA model displayed on a logarithmical scale

The first 5 principal components could account for 79.7 % of the total variance. PC1 explains 35.9 % of the information, thereby describing a major part of the variance contained in the dataset. PC1 is characterized by a rather large group of components, with the loading values smeared among them. The highest loadings of PC1 are dominated by Mn, Fe, and Cr, supporting the results of the enrichment factor calculations, pinpointing to a common source for the three elements inside the subway system. Additionally, PC1 contains relatively high loadings of the variables OC, EC, Ca, and K which could imply a common source within the subway system, derived from the abrasion of the rails and wheels inside, but also the resuspension of crustal dust derived from building materials. On the other hand, the loadings of Cd as well as NO_3^-, SO_4^{2-} and NH_4^+ are negligible. These components are indicators of traffic emissions and secondary aerosols, formed outside of the subway system, and presumably transported with the ambient air via the ventilation system. PC2 accounts for an additional 16.8 % of the total variance and is characterized by the loadings of sulphate, nitrate, and ammonium ions, implying their common source as secondary aerosols entering the subway stations from the ambient air. Further on, elevated loadings can be noticed for the elements Ni, Sr and Zn, which can be associated with traffic derived metals (Handler et al., 2008; Hjortenkrans, 2008). PC3, which accounts for a further 13.6 % of the variance, has on the one hand again notably high, but negative loadings for NO_3^-, NH_4^+ and SO_4^{2-} , accompanied by lower negative loadings of K, Mg and EC, thereby pointing again to outside sources like secondary aerosols, mineral dust, and traffic emissions. On the other hand, high positive loadings can be noticed for Zn, Cu, Co, Sr, and Cd, which in principle can also be linked to traffic related emissions. Still, the opposite loading points to the fact that in case of the subway tunnel these compounds are not related to the influence of ambient air. In sum, the first three PCs could explain 66.3 % of the total variance, while PC4 and PC5 only account for a further 13.4%. Therein, PC4 explains an additional 7.8 % of the total variance and is characterized by high Cl, Mg, Cd, NO_3^- and Na, which could show more likely the contribution of road salt, traffic, and secondary aerosol emissions. An influence of sea salt aerosols (Viana et al., 2008) is less likely, due to the geographic location. PC5, describing only 5.6 % of the variance, is again characterized by high loadings of , like Cd, Cu and Ni.

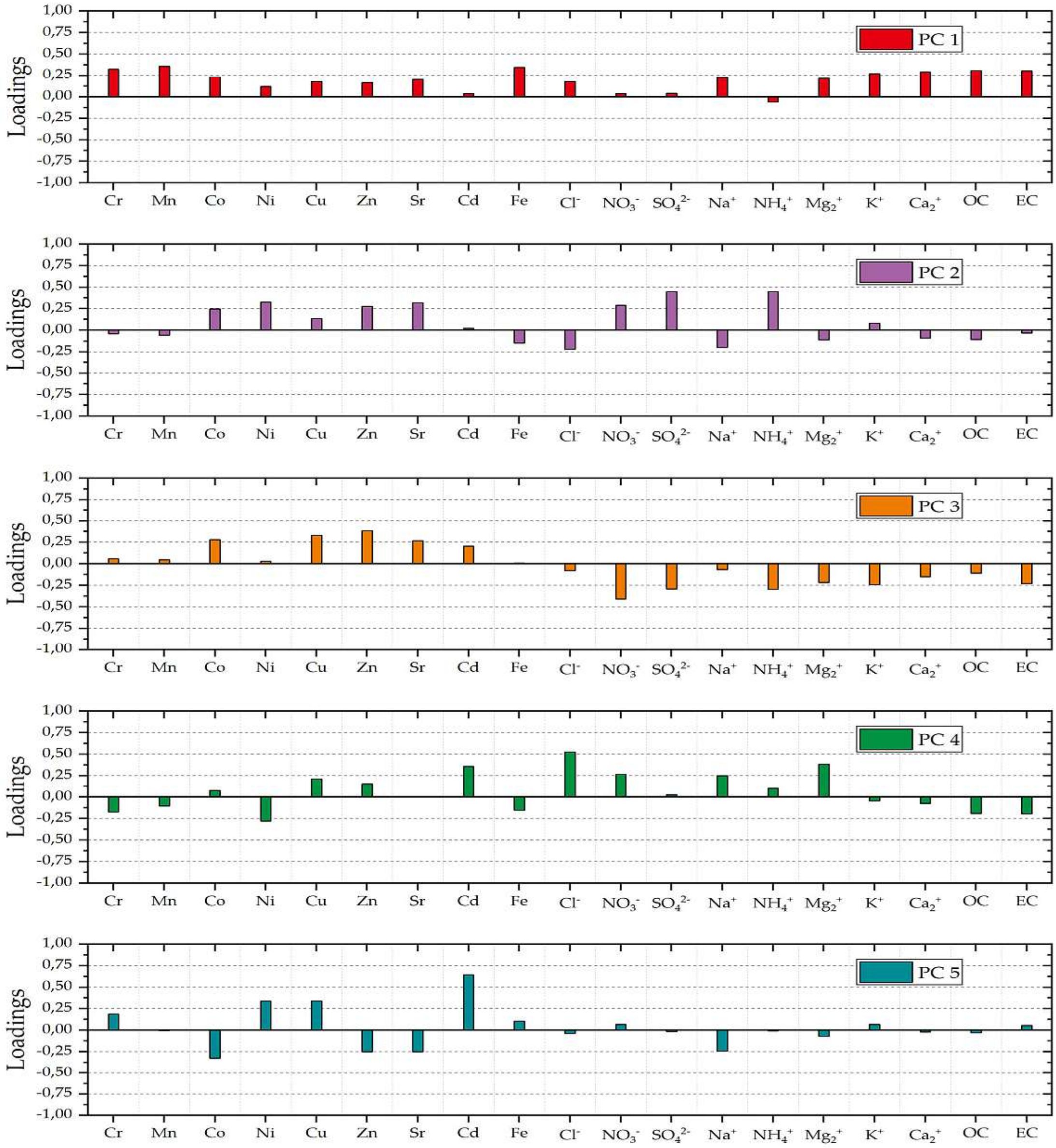

Figure 3.11 Loadings of the first five Principal components

Overall, the first 5 principal components of the PCA analysis could achieve a moderately good source appointment, with a remaining unexplained variance of 20.3 %. The main components of subway materials like Mn, Fe and Cr dominated the first PC, corresponding to the principal component explaining the highest variance and related to sources inside the subway system. Additionally, PC2 and PC3 could be associated with ambient PM sources.

3.2 Online measurements

In the following sub-chapter, the data obtained by the high temporal resolution measurements via the optical particle counter (OPC) and the electrical low-pressure impactor (ELPI) are discussed.

3.2.1 Evaluation of the correction factor for the optical particle counter

As already mentioned in section 2.2.2, the operation method of optical particle counter used, is based on the direct measurement of the particle number concentration and particle size, merging the results into a particle number distribution dataset. The resulting particle number concentration is then converted internally by an integrating algorithm, taking the assumption that the measured particles are spherical and possess a mean density uniform to the particles found in typical ambient air samples. Additionally, the optical particle counter model MINI-LAS 11E is equipped with a filter chamber for exchangeable PTFE filters, not only for the protection of the internal pump, but above all serving as a dust collector for the gravimetric control of the gained measurement results. As previously stated, the differing nature of the aerosols found in the microenvironment of the subway system necessitated the gravimetric evaluation of the employed PTFE-filter, by weighing the filters before and after each monitoring site to estimate the mass of the dust collected and relate it to the mass calculated internally amid the measuring period, to calculate the correction factor (C-factor) via the Equation 3-2, provided in the manufacturer`s manual.

$$Correction\ factor = \frac{Collected\ dust\ mass\ on\ the\ PTFE\ filter}{internally\ calculated\ dust\ mass}$$

Equation 3-2 Correction factor calculation, taken from the optical particle counter`s manual

The correction factors obtained this way were calculated for all the monitoring sites and resulted in factors of 3.3, 3.9, 4.0 and 4.7 for the platform Karlsplatz U1, tunnel Rochusgasse U3, tunnel Karlsplatz U1, and platform Rochusgasse U3, accordingly, while an additional comparably high value of 6.2 at the tunnel Praterstern U2 was acquired. For the platform Stubentor U3 no correction factor could be evaluated as the pre-weighting of the PTFE filter wasn`t carried out. These correction factors were then compared with the correction factors acquired by the simultaneous gravimetric LVS measurements. This was accomplished by plotting the measured

LVS 4 hour mean PM_{10} mass concentration levels against the uncorrected OPC PM_{10} mass concentrations of the same measuring period and by the investigation of the resulting slope of the modelled linear regression for each monitoring site, respectively. The regression models were forced through their origins; thus their intercept equals zero. The illustrations of these comparisons can be seen in Figure 3.12.

By the investigation of the resulting slopes of the six monitoring sites, three groups were obtained by calculating the mean values of the sites with similar slopes. The resulting groups and their associated correction factors can be seen in Table 3.9. These correction factors are quite well comparable with the C-factors obtained via Equation 3.2. as the correlation based on the LVS measurements allowed to include more data points, the factors listed in Table 3.9 were then used for the recalculation of the data obtained by the optical particle counter for each site, correspondingly. An exception to the good comparability of the correction factors obtained by the two methods can be noticed for the tunnel Rochusgasse U3, where the gravimetric determination via the OPC filter resulted in a much lower C-factor, in comparison to the value acquired by the LVS measurements. As evaluation of the PTFE filter of the OPC might have been erroneous as it relies on one measurement only, the comparison with the LVS was used for further correction.

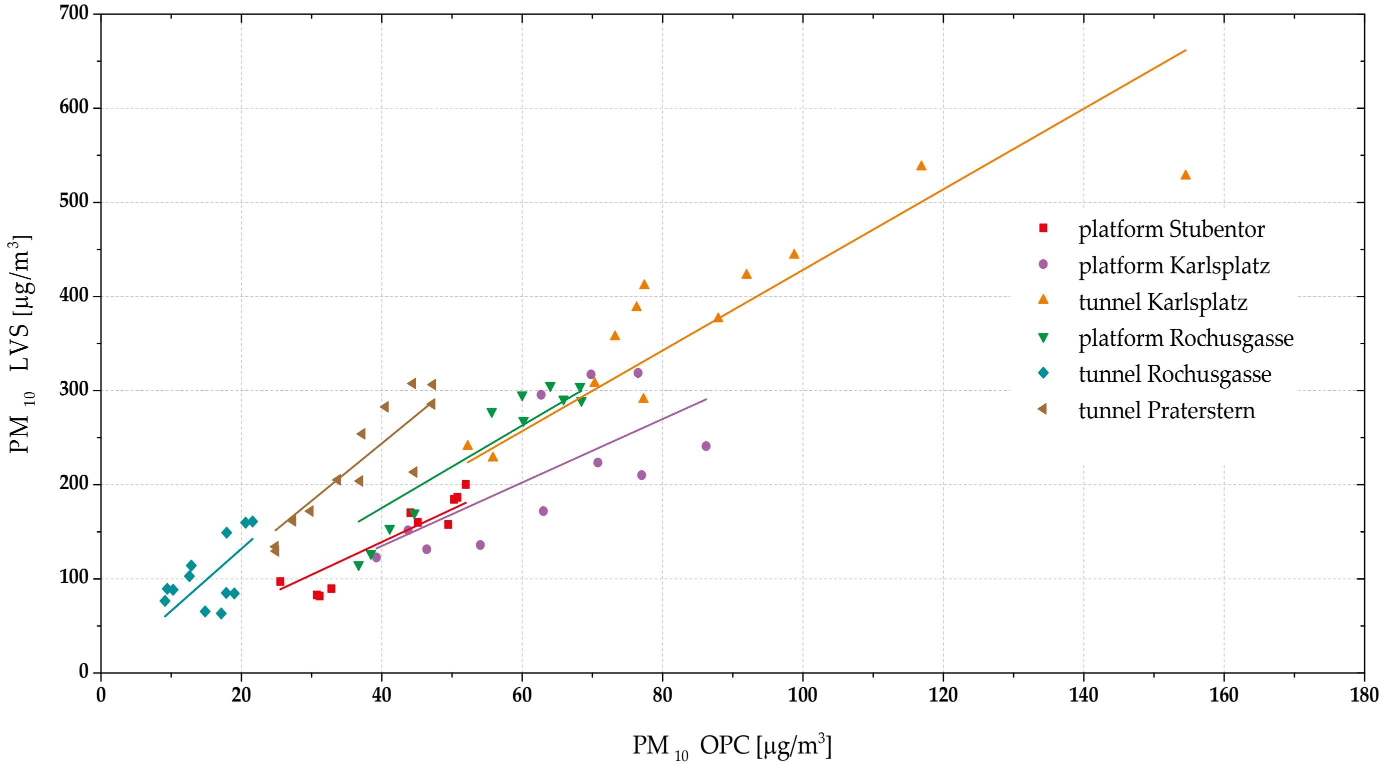

Figure 3.12 Correlation of the PM_{10} mass concentration levels obtained by the OPC vs. the values determined by the LVS for each monitoring site collected during the operating hours

Table 3.9 Overview of the evaluated correction factors for each group, containing two monitoring sites, respectively

	platform Stubentor	platform Karlsplatz	tunnel Karlsplatz	platform Rochusgasse	tunnel Rochusgasse	tunnel Praterstern
Intercept			*0*			
Slope	3.5	3.4	4.3	4.4	6.6	6.1
Standard error	±0.14	±0.24	±0.18	±0.15	±0.57	±0.21
R^2	*0.98*	*0.95*	*0.98*	*0.99*	*0.92*	*0.99*
Grouped mean slopes, resulting in the used correction factors	**3.4**		**4.3**		**6.3**	

Further evaluation of the dataset revealed, that for the monitoring periods without train service a lower correction factor of 2 ±0.2 ($R^2 = 0.92$) must be adopted, which is plausible regarding the results of the chemical analysis of the night samples, revealing a significantly reduced iron fraction in the subway air samples of the night periods. The relation of the OPC and LVS night-samples is presented in Figure 3.13. The estimated high correction factors for the service periods can be attributed to the high elemental fraction with higher density and differing refraction index of the subway aerosols. Since only two night samples were collected by the LVS for each monitoring site, individual night correction factors couldn`t be estimated for the respective locations. The night correction factor was not used for the data recalculation of the measuring site tunnel Rochusgasse U3, considering that this measurement occurred during the weekend with non-stop train service. Further on the correction factors for the $PM_{2.5}$ and PM_1 fractions couldn`t be evaluated, because the reference gravimetric sample collection was only conducted using an inlet with a PM_{10} cut-off.

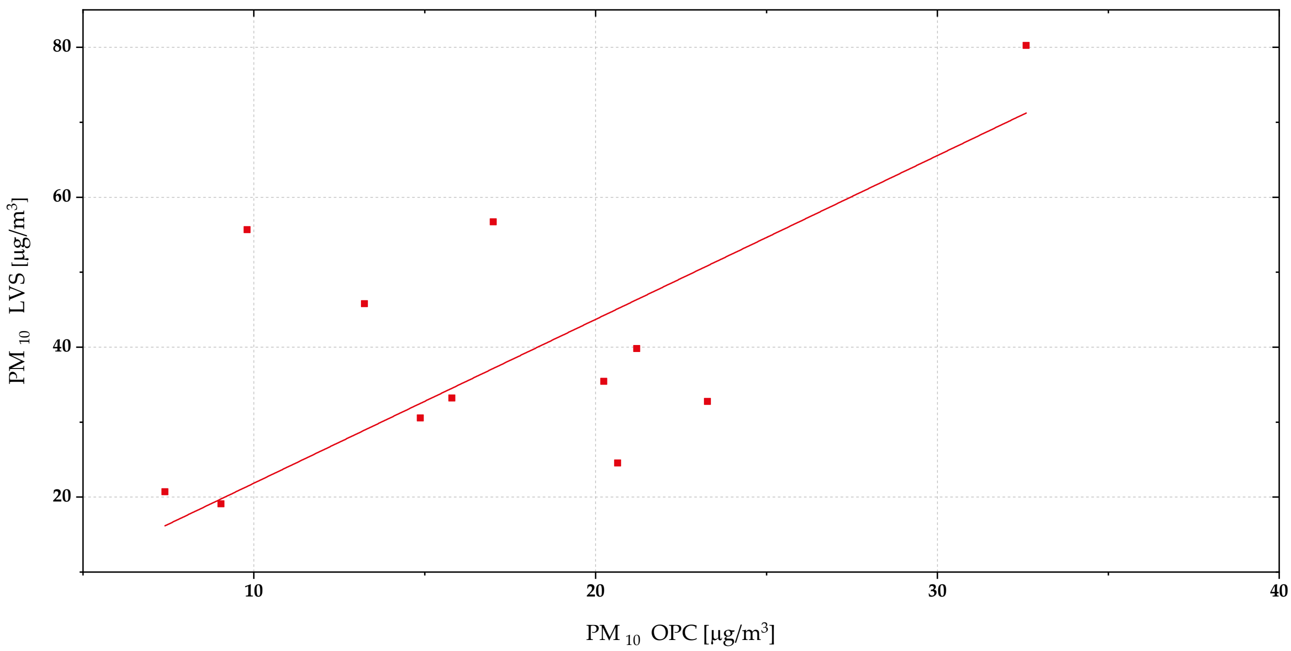

Figure 3.13 Correlation of the PM_{10} mass concentration levels obtained by the OPC vs. the values determined by the LVS for each monitoring site collected during the non- operating hours

3.2.2 <u>Temporal variations</u>

After the correction of the OPC data with the above-mentioned correction factors, the dataset was used to expose the temporal PM_{10} concentration variations throughout the measurement campaign, allowing the interpretation of the main factors causing the diurnal variations.

The following illustrations from Figure 3.14 to Figure 3.19 show the variation of PM_{10} levels (15 min resolution) measured by the OPC compared to the concentration levels sampled by the LVS on the platform and tunnel locations. The LVS measurements were limited to 14 filters, due to the maximum capacity of filters supported by the automatic filter changing system, restricting the sampling time to 56 hours, while the OPC was able to monitor the aerosol concentrations for a longer time. An overview of the descriptive statistics (mean values, medians, extreme values based on resolution of 15min PM_{10} values) can be found in the appendix (see section 6.5).

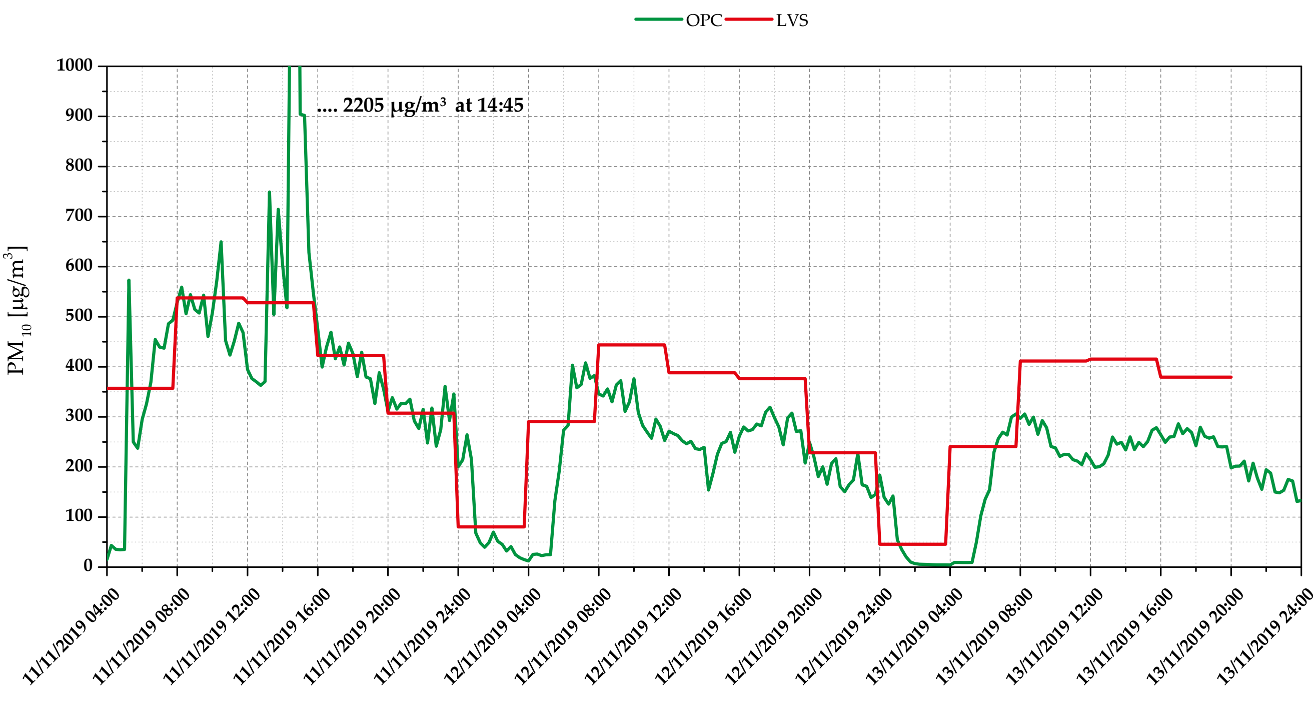

Figure 3.14 Comparison of the PM_{10} temporal variations recorded by the OPC (15min means) vs. LVS (4 hour means) at the monitoring site tunnel Karlsplatz U1

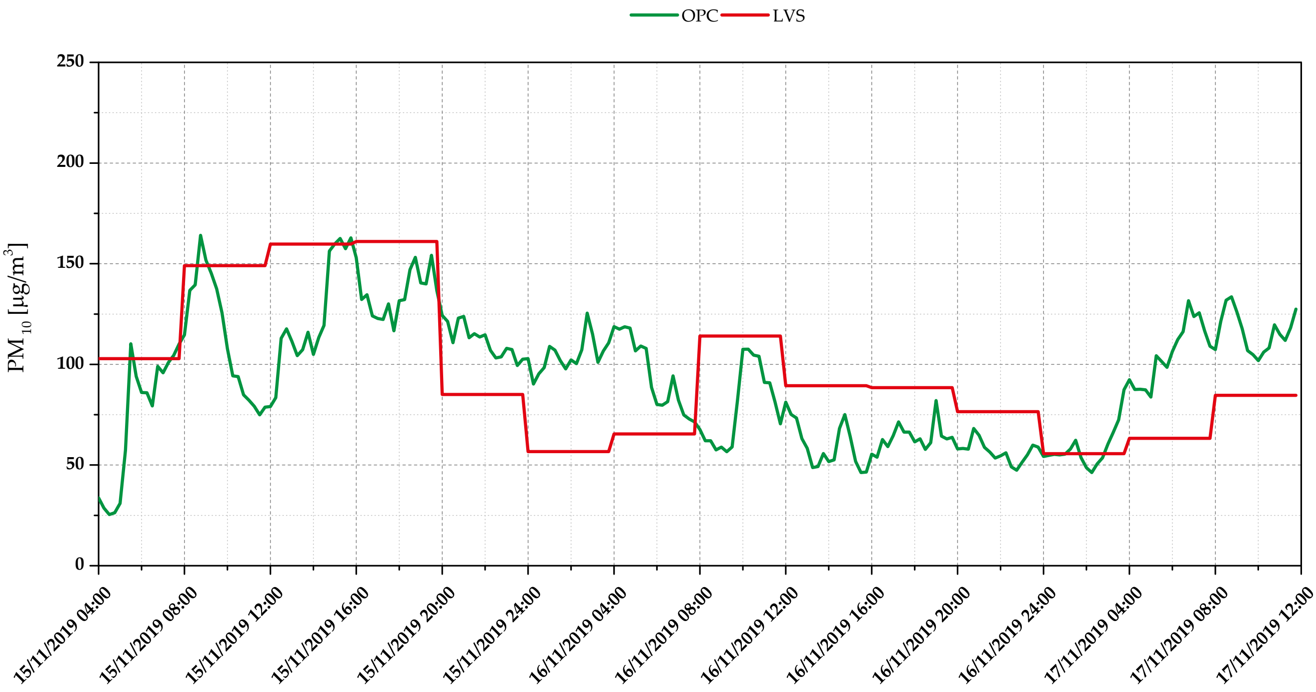

Figure 3.15 Comparison of the PM10 temporal variations recorded by the OPC (15min means) vs. LVS (4 hour means) at the monitoring site tunnel Rochusgasse U3

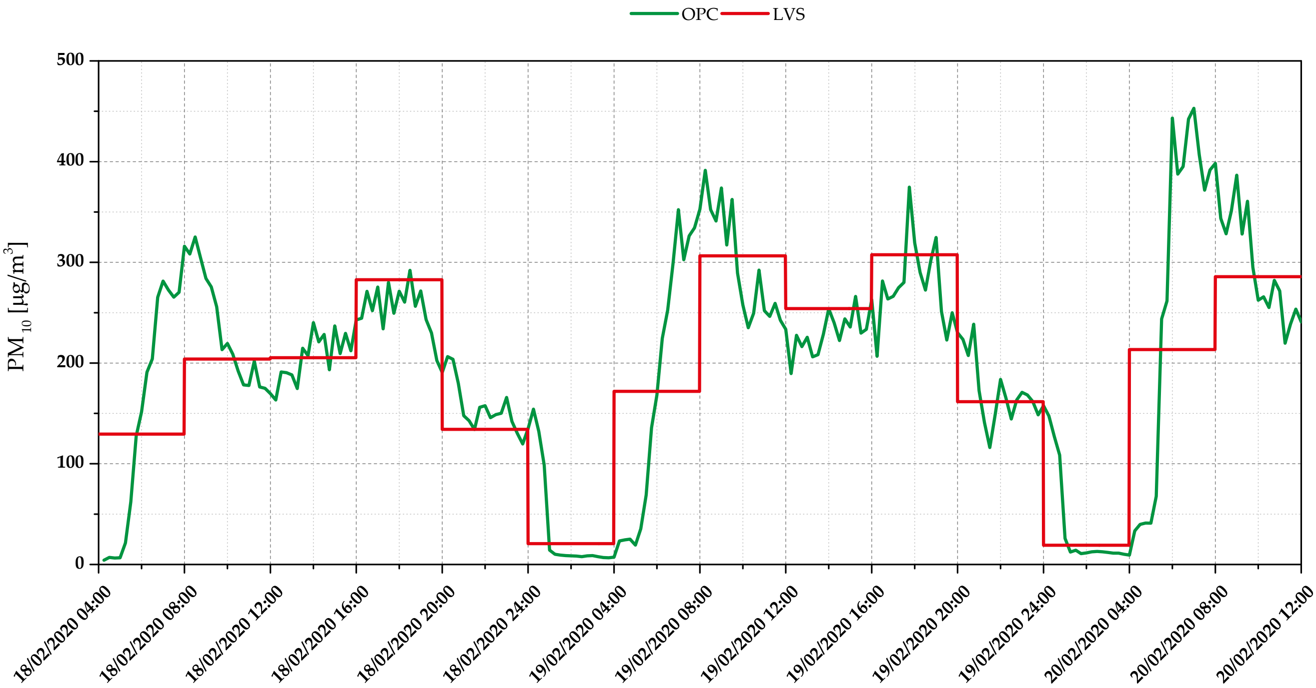

Figure 3.16 Comparison of the PM10 temporal variations recorded by the OPC (15min means) vs. LVS (4 hour means) at the monitoring site tunnel Praterstern U2

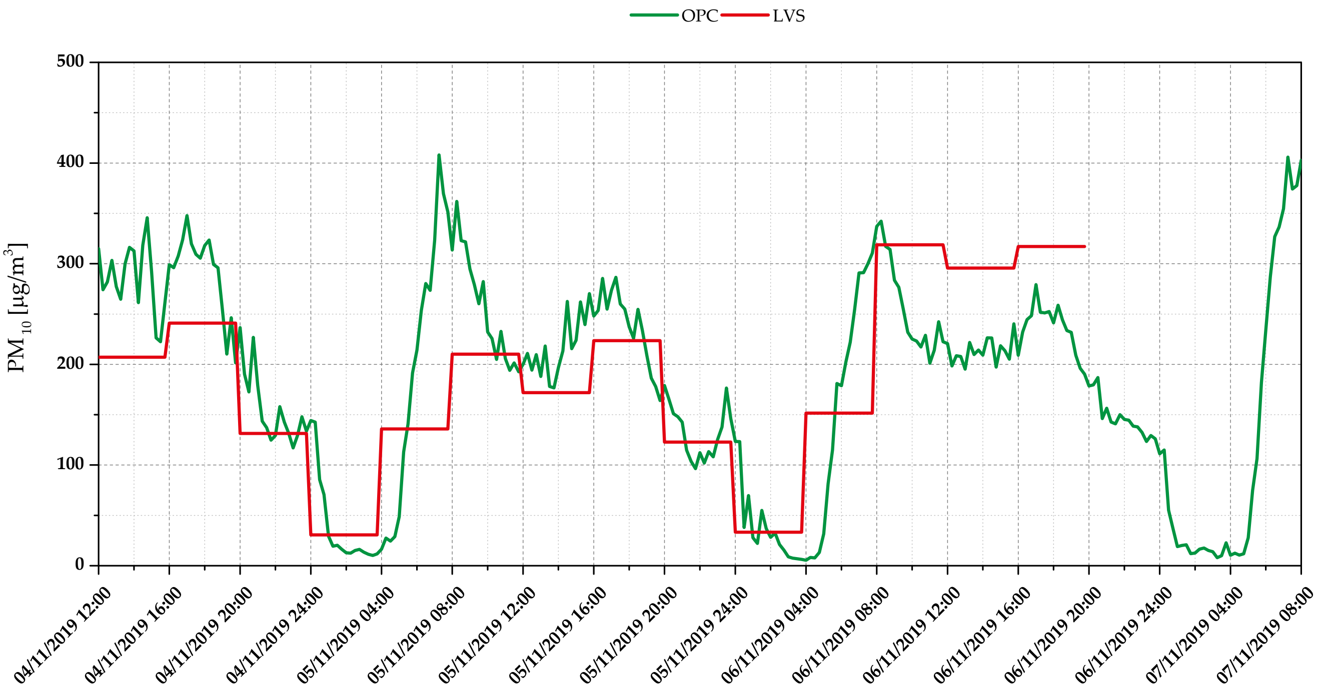

Figure 3.17 Comparison of the PM_{10} temporal variations recorded by the OPC (15min means) vs. LVS (4 hour means) at the monitoring site platform Karlsplatz U1

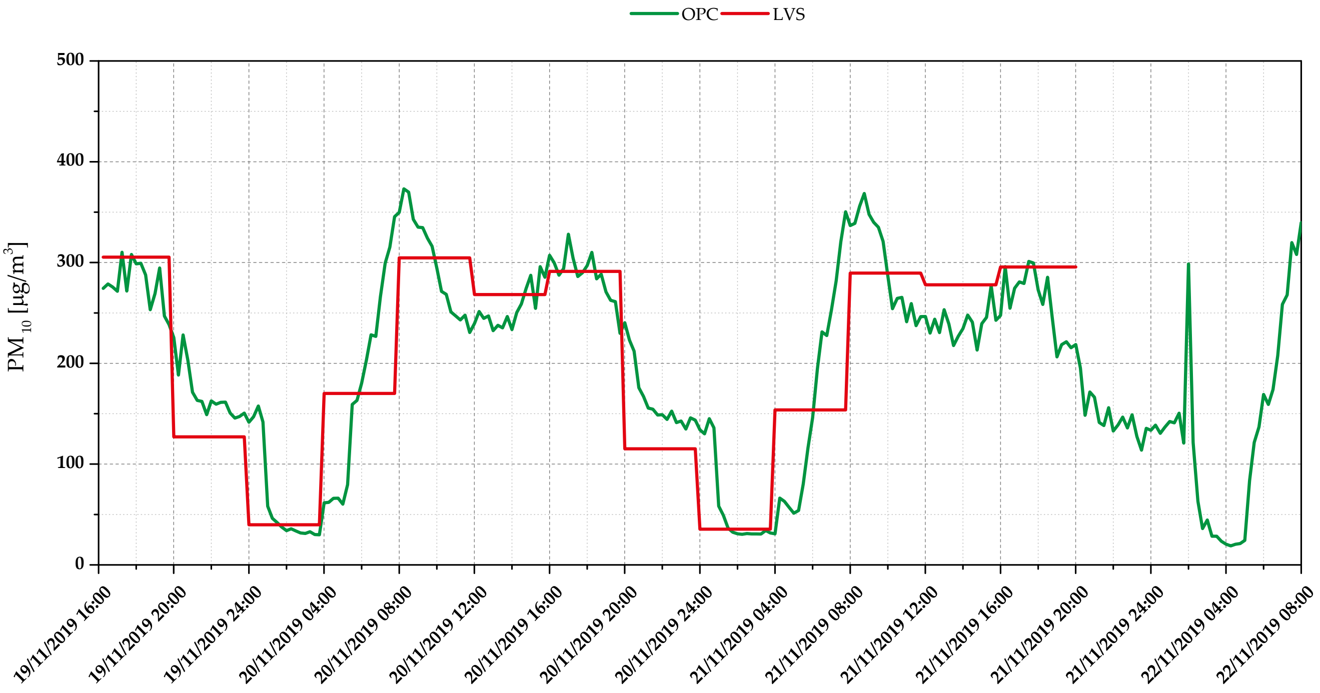

Figure 3.18 Comparison of the PM_{10} temporal variations recorded by the OPC (15min means) vs. LVS (4 hour means) at the monitoring site platform Rochusgasse U3

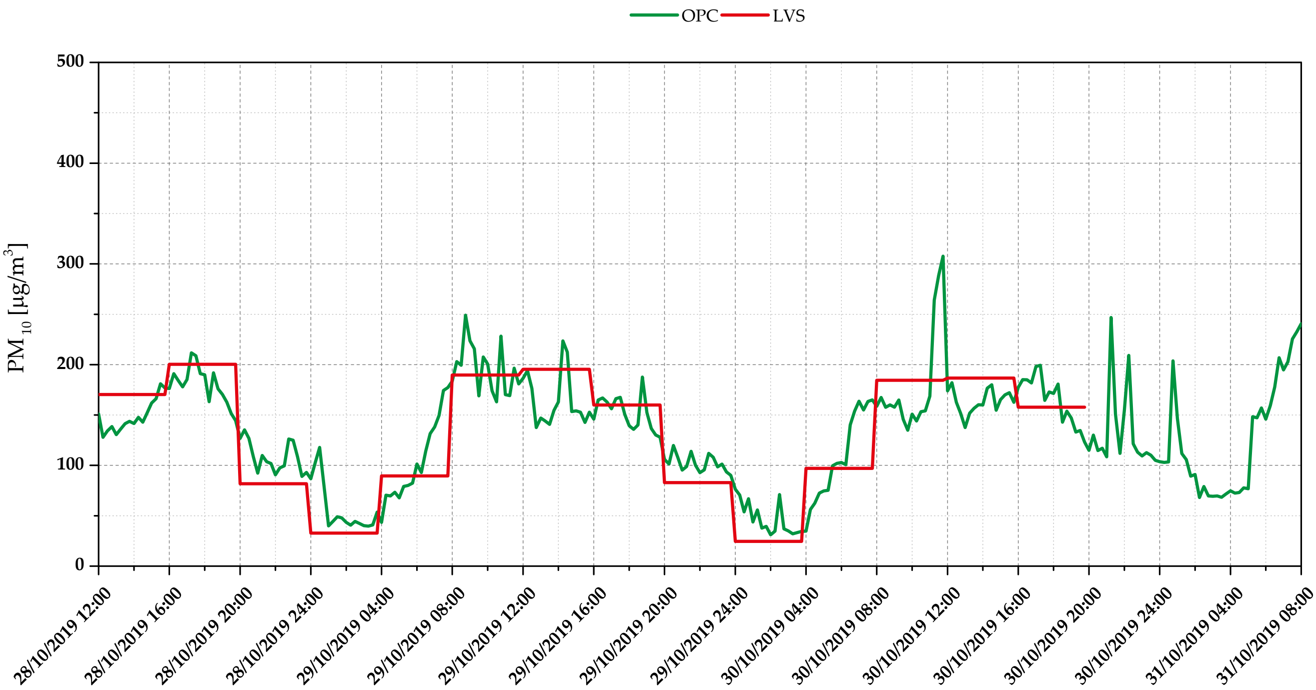

Figure 3.19 Comparison of the PM_{10} temporal variations recorded by the OPC (15min means) vs. LVS (4 hour means) at the monitoring site platform Stubentor U3

Looking at these graphs, an acceptable correlation between the concentration values gathered by the LVS and OPC is apparent, although the high resolution OPC data enables a more precise visualization of the two maxima, one between 7 am and 9 am and the other around 5 pm, caused by the morning and afternoon rush hours. It is also visible that the filters sampled by the LVS between 12 am and 4 am don`t cover the non-operating hours perfectly, since the train service ends somewhere between half past 12 am and 1 am, depending on the individual subway station, while the opening hour is around 5 am in the morning. At some stations, the diurnal variation patterns are sculpted by short periods of either elevated or reduced pollution levels.

At the measuring point tunnel Rochusgasse U3, the correlation between the data obtained by the OPC and the LVS is less coinciding. The measurements at this station were conducted during a weekend, monitoring an operation mode with lower train frequency, which explains the absence of the rush hour peaks and night-time operation. Compared to the other measurement sites the PM_{10} levels are noticeably low, this result may have been due to the open-cut construction design of the tunnel at Rochusgasse U3. Further reasons for the poor quality of the correlation between the two measurement methods couldn`t be found.

In the following illustrations from Figure 3.22 to Figure 3.27, the comparison between the PM_{10} concentration values, measured by the OPC, and the actual number of trains per hour are plotted against each other. From the comparability of these two parameters, it can be deduced that the train frequency impacts the pollution level fluctuations substantially. Still, by examining the individual subway stations in contrast, it can be stated that the influence of the train frequency is varying from station to station. This effect is best illustrated in the Figure 3.20, illuminating the proportionately high impact of train frequency at the station (tunnel and platform) Karlsplatz U1. Again, the poorest correlation between train frequency and hourly PM_{10} concentrations with a comparably low slope can be noticed for the tunnel Rochusgasse U3, listed in Table 3.10. A very similar trend can be recognized by the comparison of the measured gravimetric PM_{10} mass concentrations with the four-hour train frequencies, displayed in Figure 3.21. Here, the resulting slope at the platform Rochusgasse U3 is the second lowest after the tunnel Rochusgasse U3, while the slope of the regression model at the tunnel Praterstern U2 is slightly higher, even if the corresponding standard errors don`t suggest a substantial distinction. In general, the respective coefficients of determination point to a better correlation of the gravimetric PM_{10} data with the corresponding four-hour train frequencies, indicating some difficulties regarding the OPC measurements in view of the influence of the passing trains. The only exception regarding a better correlation of the OPC data can be seen for the platform Karlsplatz U1.

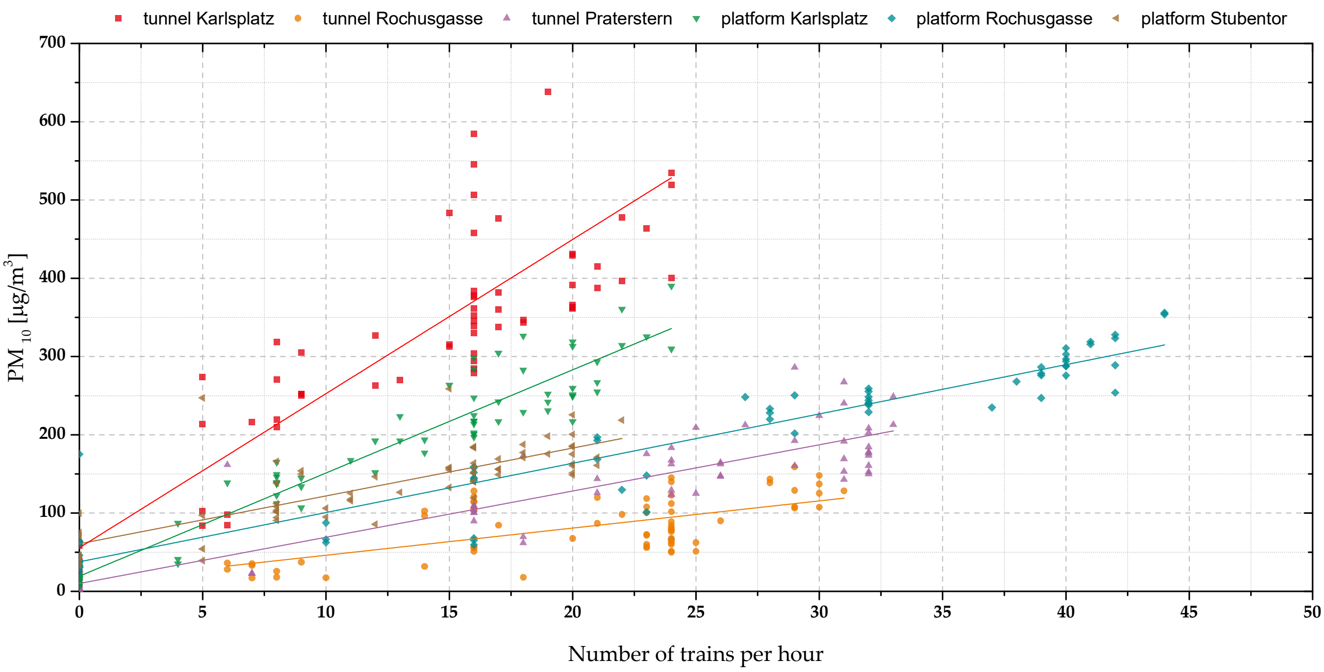

Figure 3.20 Scatter-plot of the hourly mean PM10 mass concentration values by the OPC versus the number of trains passing by in that hour

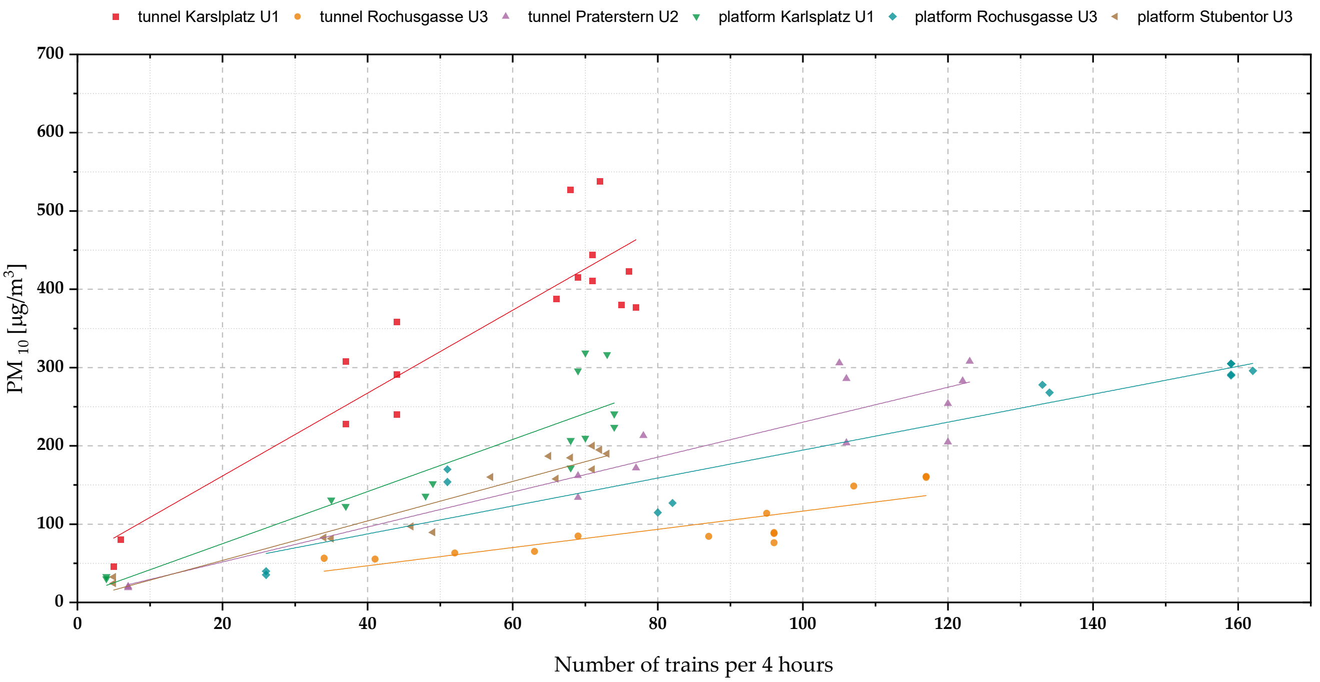

Figure 3.21 Scatter-plot of the 4-hour gravimetric PM10 mass concentration values measured with the LVS versus the number of trains passing by in that hour

Table 3.10 Results of the linear regression models generated from the train frequency and PM10 mass concentration measured by the OPC and LVS, respectively

	OPC			LVS		
	Intercept	Slope	R^2	Intercept	Slope	R^2
tunnel Karslplatz U1	55.7 ±25.8	19.7 ±1.8	0.64	55.7 ±37.9	5.3 ±0.6	0.81
tunnel Rochusgasse U3	11.4 ±11.5	3.5 ±0.5	0.39	0.3 ±18.8	1.2 ±0.2	0.70
tunnel Praterstern U2	10.1 ±10.4	5.9 ±0.4	0.77	7.1 ±25.2	2.2 ±0.3	0.85
platform Karlsplatz U1	19.4 ±6.8	13.2 ±0.5	0.92	8.5 ±28.0	3.3 ±0.5	0.78
platform Rochusgasse U3	37.7 ±7.8	6.3 ±0.3	0.89	16.1 ±20.3	1.8 ±0.2	0.90
platform Stubentor U3	60.8 ±7.4	6.1 ±0.5	0.65	3.2 ±11.6	2.5 ±0.2	0.92

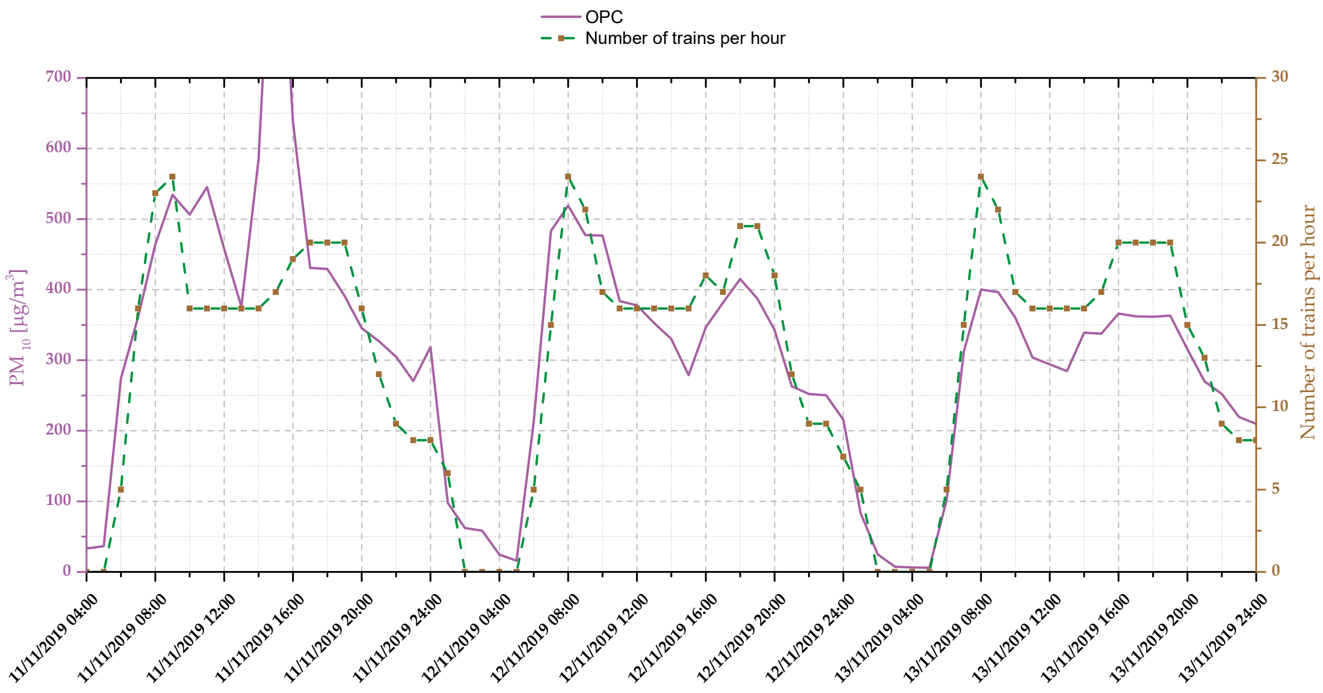

Figure 3.22 Comparison of the temporal variations of PM10 mass concentrations recorded by the OPC and the train frequency at the monitoring site tunnel Karlsplatz U1

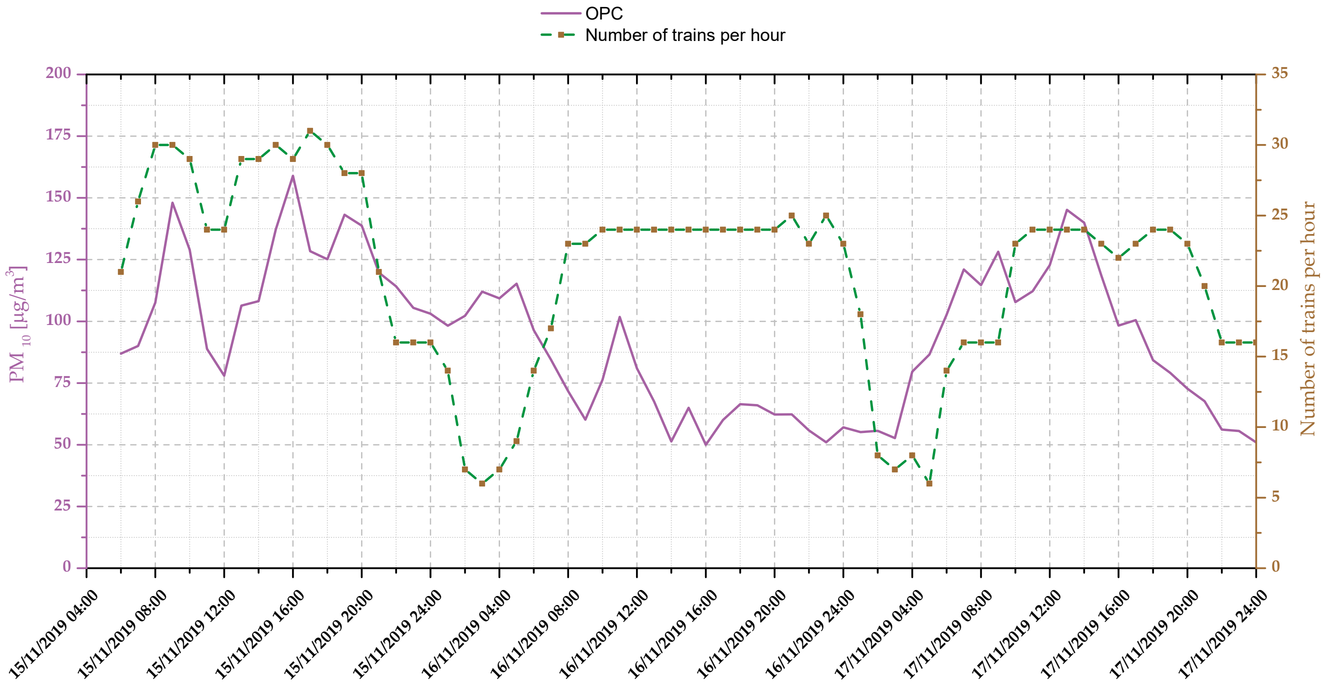

Figure 3.23 Comparison of the temporal variations of PM10 mass concentrations recorded by the OPC and the train frequency at the monitoring site tunnel Rochusgasse U3

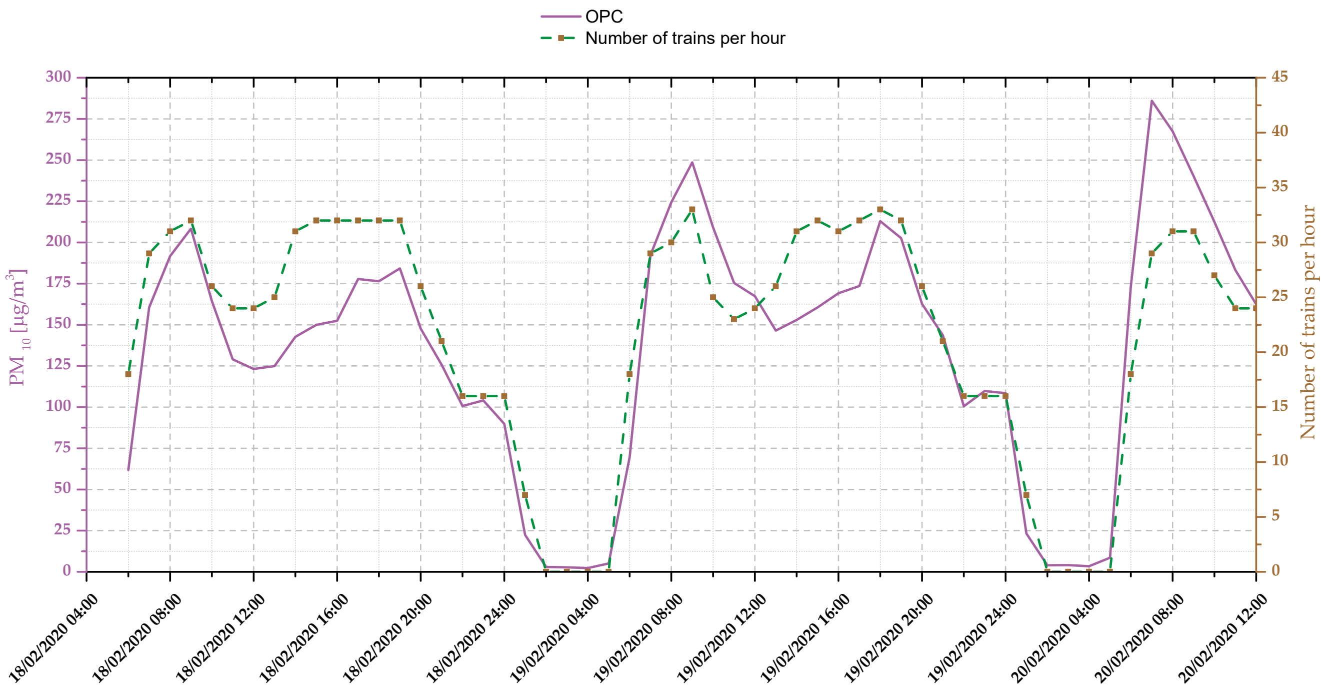

Figure 3.24 Comparison of the temporal variations of PM10 mass concentrations recorded by the OPC and the train frequency at the monitoring site tunnel Praterstern U2

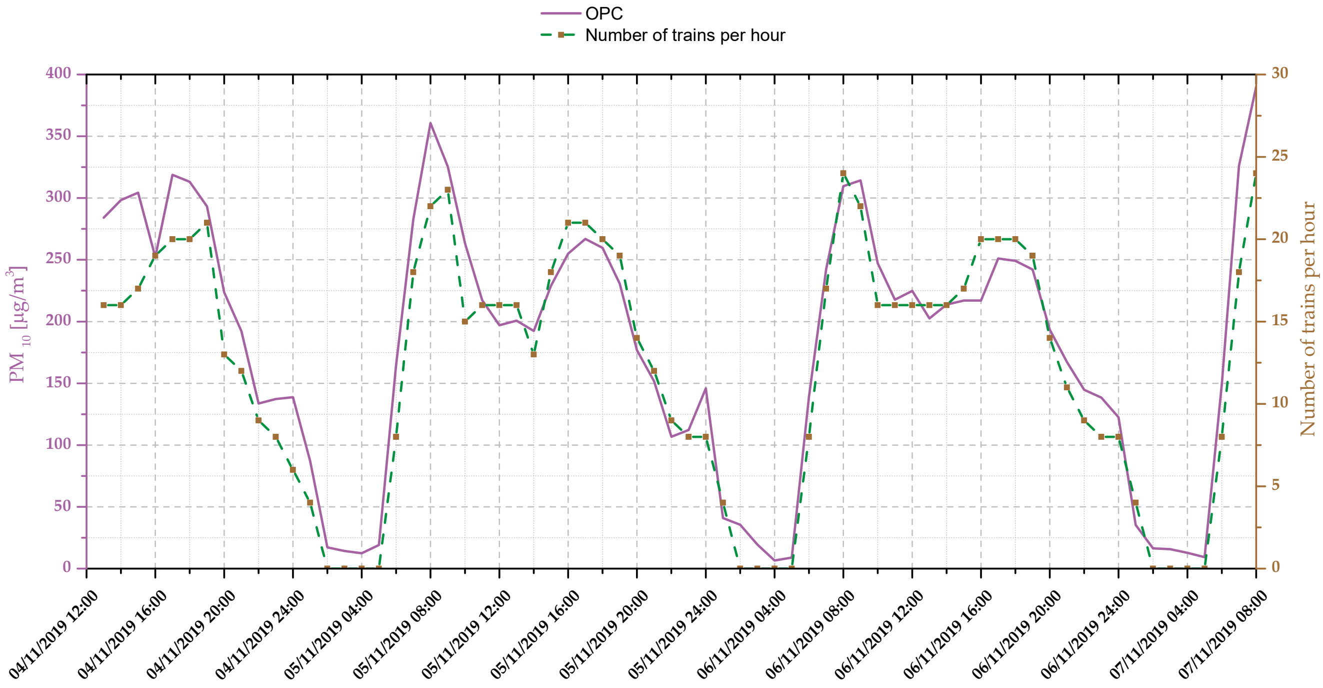

Figure 3.25 Comparison of the temporal variations of PM10 mass concentrations recorded by the OPC and the train frequency at the monitoring site platform Karlsplatz U1

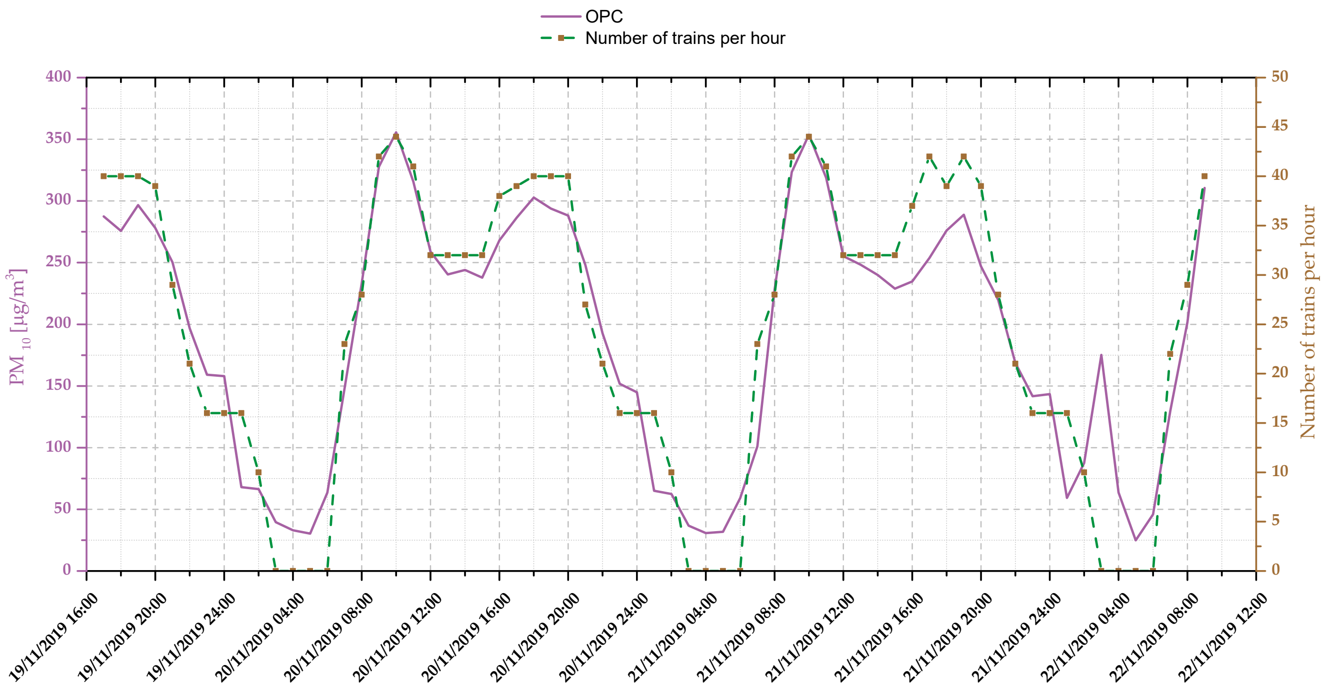

Figure 3.26 Comparison of the temporal variations of PM10 mass concentrations recorded by the OPC and the train frequency at the monitoring site platform Rochusgasse U3

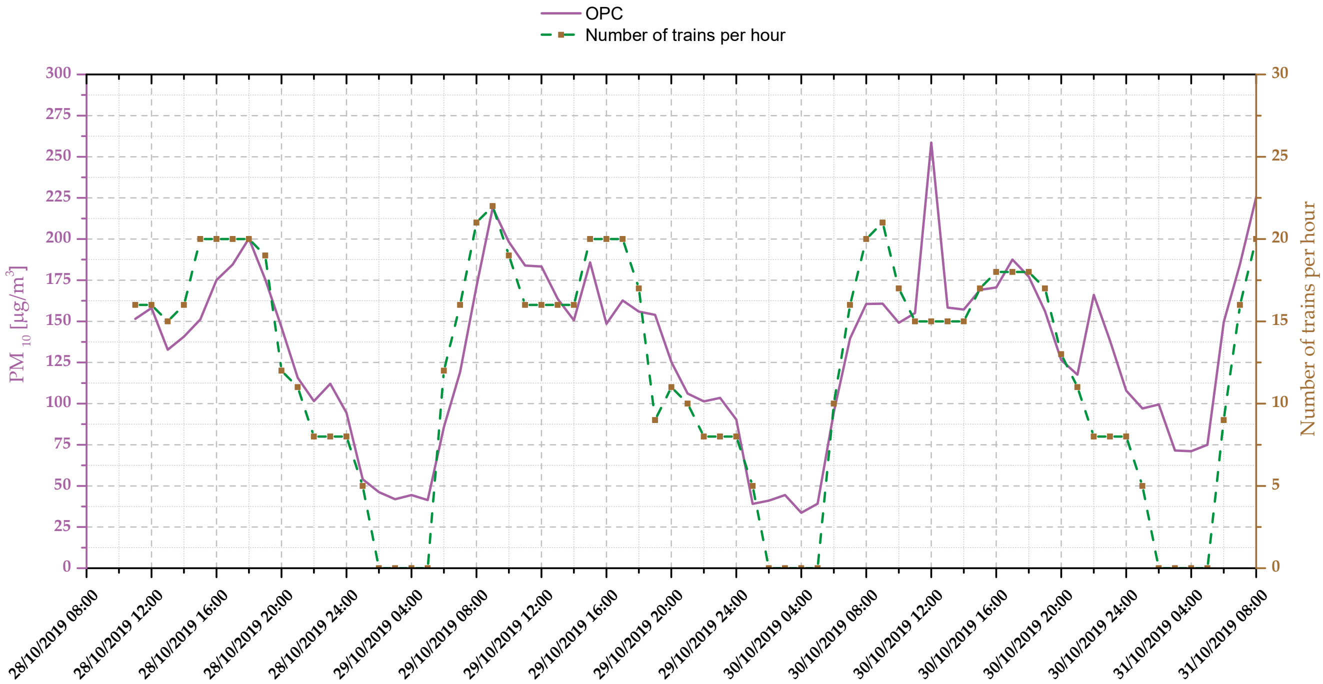

Figure 3.27 Comparison of the temporal variations of PM_{10} mass concentrations recorded by the OPC and the train frequency at the monitoring site platform Stubentor U3

As already mentioned before, there were short discrete events observed with elevated concentration levels regarding the diurnal variations. These spikes indicate other factors influencing the pollution levels in the subway system, like the influx of passengers or resuspension by the movements of trains or maintenance staff (Martins et al., 2015; Querol et al., 2012). Examples for these events can be found in the early afternoon (14:45) on the 11th of November 2019 at the tunnel Karlsplatz U1, in the night from 21st to 22nd of November 2019 at the platform Rochusgasse U3 and at the platform Stubentor U3 in the night from 30th to 31st of October 2019 and at noon on the 30th of October 2019. The high-resolution data collected by the OPC is optimally suited for the identification and visualization of these special events. To clarify the origin of these events, additional information about possible activities in these periods was requested from the Wiener Linien. Still, it was not possible to shed light on all the causes. For the night between the 21st and 22nd of November 2019, the passage of a subway monitoring train could account for the elevated PM_{10} levels at the platform Rochusgasse U3. The other events couldn`t be identified yet.

A further example of possible factors, likewise able to influence the aerosol concentration levels in the subway system, can be seen in Figure 3.28. Due to a defective train on the 19th of November 2019, all the passengers had to disembark shortly before noon onto the platform at the station Rochusgasse U3, causing a significant increase of the measured air pollution levels, most likely due to resuspension of PM. This period is missing from the temporal variation figures discussed beforehand, since the measurements concerning the spatial variations across the platform (see 3.2.3) were conducted at that time and thus no mean value for the platform is available.

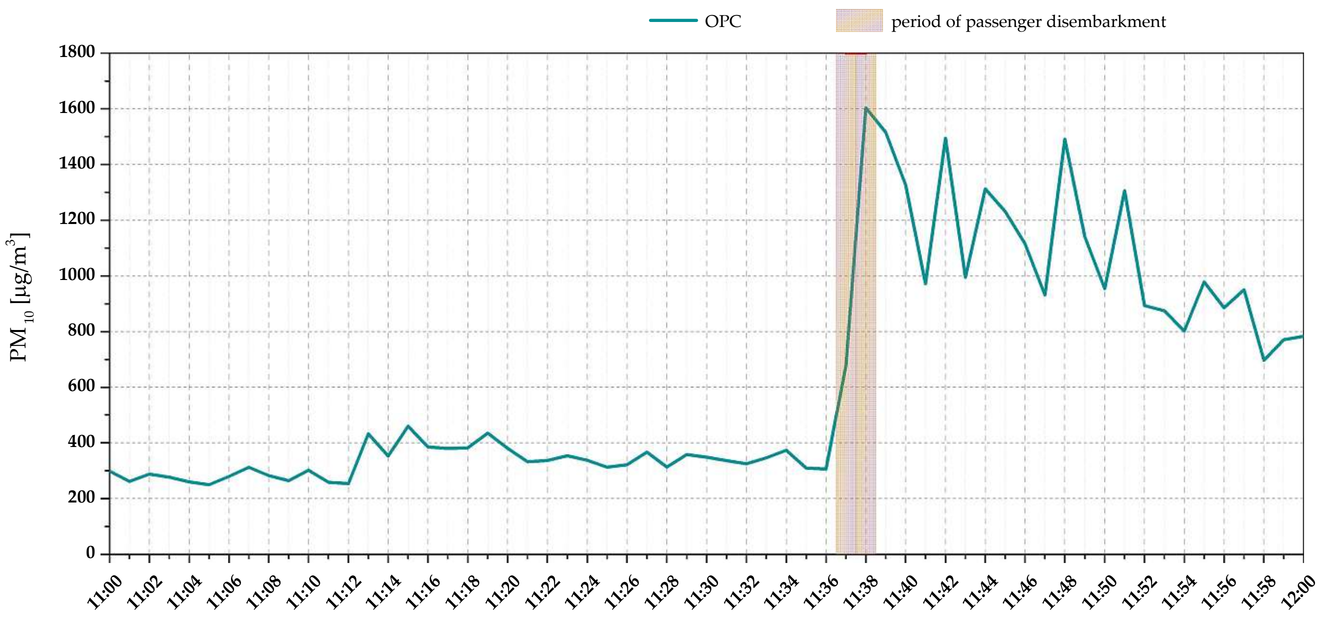

Figure 3.28 Increase of air pollution levels due to a malfunctioning train, forcing all passengers to leave the train and gather at the platform Rochusgasse U3 (red mark represents the time of disembarkment)

3.2.3 Spatial and temporal variations on the platform areas

To identify spatial gradients in the particulate matter exposure levels along the subway platform and to assess the representativity of the stationary measurements, the optical particle counter was furtherly deployed at three different positions at the platforms of all three stations monitored. The positions were chosen to monitor the PM levels at the front, middle and end (rear) of the platforms, regarding the direction of motion of the trains passing through the stations. In consideration of the diurnal fluctuations regarding the particulate matter mass concentration occurring in the subway system, the measurements for the estimation of the spatial variations was conducted within a total period of 3 hours at all platform locations, monitoring the three separate platform areas for approximately 20 minutes with a temporal resolution of 6 seconds, repeating the measurements three times, resulting in a total monitoring time of 1 hour for each platform position for the three platform stations investigated. Due to beforementioned train malfunctioning and subsequent passenger disembarkment at platform Rochusgasse U3, only shorter monitoring periods were used for the calculations of the following results. Thus, at the platform Rochusgasse U3, the investigated time intervals were reduced to 41 minutes, 35 minutes, and 15 minutes for the OPC measurements collected in the front, middle and rear of the platform, respectively. The resulting descriptive statistics are displayed in Table 3.11 and visualized by boxplots in Figure 3.29.

Table 3.11 Descriptive statistics of the OPC measurements regarding the spatial variations on the platforms of Karlsplatz Rochusgasse and Stubentor

	platform Karlsplatz U1			**platform Rochusgasse U3**			**platform Stubentor U3**		
	Front	Middle	Rear	Front	Middle	Rear	Front	Middle	Rear
Mean	288	302	332	304	323	357	183	216	188
Standard Deviation	±52.5	±63.6	±70.8	±75.4	±63.3	±66.3	±48.8	±49.3	±51.0
Minimum	164	172	162	168	165	241	80.6	96.6	104
1st Quartile (Q1)	250	256	277	250	283	305	147	180	154
Median	287	293	326	295	322	342	179	211	183
3rd Quartile (Q3)	323	335	384	344	362	405	214	243	212
Maximum	526	625	591	661	514	512	403	394	866

Looking at Figure 3.29, significant differences regarding the spatial variations of PM at the various platform stations become apparent. A very similar pattern can be noticed for the platform Karlsplatz U1 and Stubentor U3, where the PM_{10} concentrations increase from the front to the platform end, with more pronounced effects regarding the platform Stubentor U3. The mass concentrations measured at the front, middle and end of the platform segments at the station Karlsplatz U1 yielded mean values of 288 µg/m³, 302 µg/m³ and 332 µg/m³, respectively, with the greatest standard deviation of ±70.8 µg/m³ determined for the measurements conducted at the end of the platform. For the station Rochusgasse U3, the respective values resulted in concentrations of 304 µg/m³, 323 µg/m³, and 357 µg/m³ for the measuring points in the front, middle and end, although contrary to the station Karlsplatz U1, the highest standard deviation of ±75.4 µg/m³ was measured in the front. These results could be partly explained by the piston effect, drawing PM-rich air from the tunnel section amid the trains entering the station, deteriorating the air quality levels to a higher grade at the end of the platform (Moreno et al., 2014; Salma et al., 2007). Further on, both stations have similar designs, regarding the partition walls between two parallel tracks, and passages in-between, although the main passenger entrances are located differently. The influence of these factors on the spatial variability of PM levels encountered at subway stations have already been shown by other studies (Martins, Moreno, Mendes, et al., 2016). The station Karlsplatz U1 possesses two main entrances, one located exactly in the middle of the platform, the other one at the end. Meanwhile the main entrance at the station Rochusgasse U3 is located at the end of the platform, connecting the subway platform to a market aboveground, thus probably representing a more frequented entrance, while the second entrance is in the front. Moreover, the two tracks at the station Rochusgasse U3 are closer to each other than at the station Karlsplatz U1, therefore a higher influence of the trains passing by on track #2 on the air quality at track #1 can`t be ruled out. Meanwhile, the station Stubentor U3 has a differing design, with the two platforms located above each other, without a total separation of the two tracks, thereby providing a comparably voluminous vertical space and therefore potentially different air distribution dynamics, even if a mutual arrangement is given for all three stations, regarding the evenly distributed air supply and exhaust systems along the whole platforms (source: Wiener Linien foremen of the respective stations reached via phone). Here the highest PM_{10} loading was determined in the middle of the platform with a mean concentration value of 216 µg/m³, while the concentrations in the front and end of the platform were quite comparable at 183 µg/m³ and 188 µg/m³, respectively. At the station Stubentor U3, the entrances are located at the front and end of the platform, without any passage in the middle, where the elevated PM_{10} mass concentrations were determined. Like the platform Karlsplatz U1, the highest standard deviation was measured at the end of the platform Stubentor U3. Further air flow measurements and CFD simulations, not provided in this work, could yield deeper understandings of the underlying air flow and thereby pollutant distribution mechanisms, influencing the spatial variability of PM_{10} concentrations, affected by passenger movements, train movements or ventilation system designs and settings (Pan et al., 2013; Reche et al., 2017) . Still the variations determined within the single platforms do not change or mask the fundamental conclusion about PM concentrations, which can be deduced from a fixed site at any position of the platform, considering the basic constructional situation.

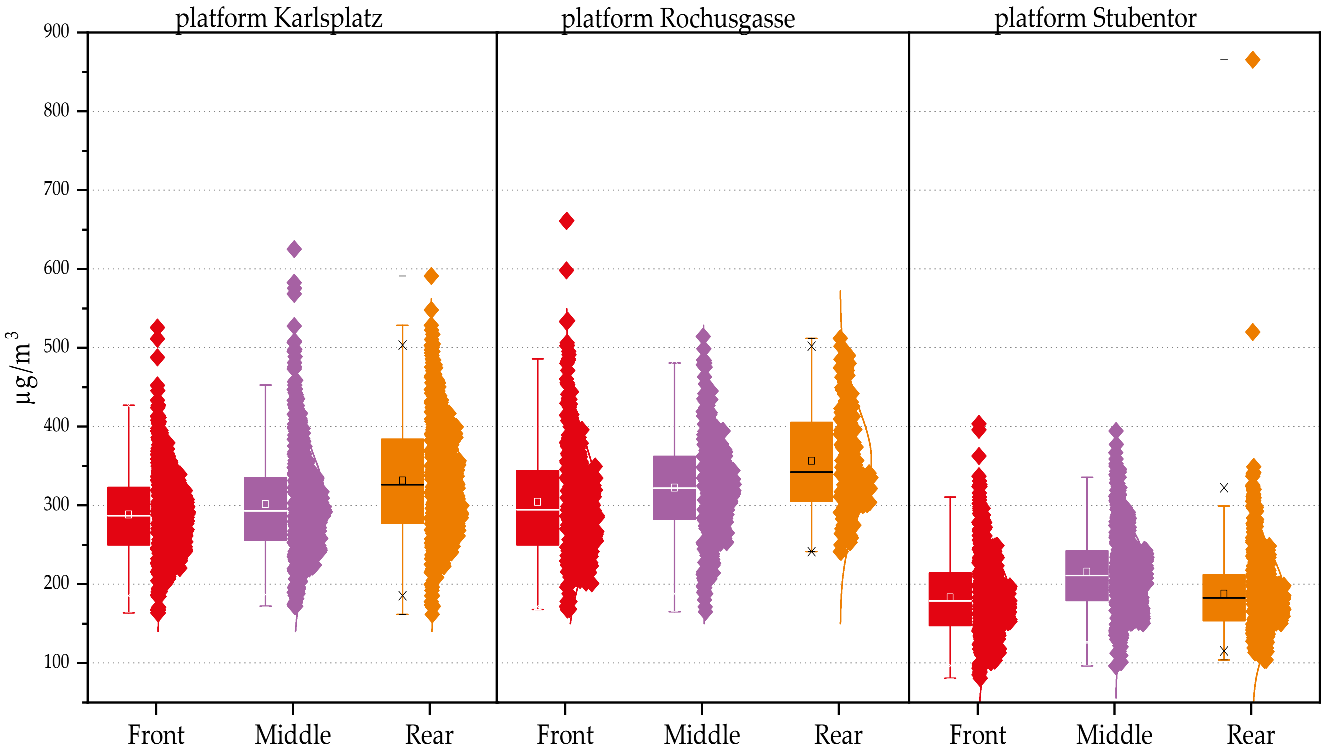

Figure 3.29 Boxplots of the 6s mean values recorded via the OPC during the spatial variability measurements at platform Karlsplatz U1, platform Rochusgasse U3 and platform Stubentor U3

In addition to the analysis of the spatial concentration variability at the subway platforms, the recorded 6 s mean PM_{10} concentration values were investigated, regarding the influences of the arriving and leaving trains. Other studies have associated enhanced mass concentration values with train arrival, and decreasing values with train departure (Salma et al., 2007)(Martins et al., 2015). In Figure 3.30, the temporal variations of recorded mass concentrations are shown for selected time intervals at the front, middle and end of the platform Karlsplatz U1, with the periods of trains arriving and leaving the station highlighted in green and purple, accordingly. No clear concentration trends can be derived from the respective data. This was also the case for the other two platform monitoring stations, not illustrated here, thus the results of the beforementioned studies couldn`t be reproduced with the experimental setting applied.

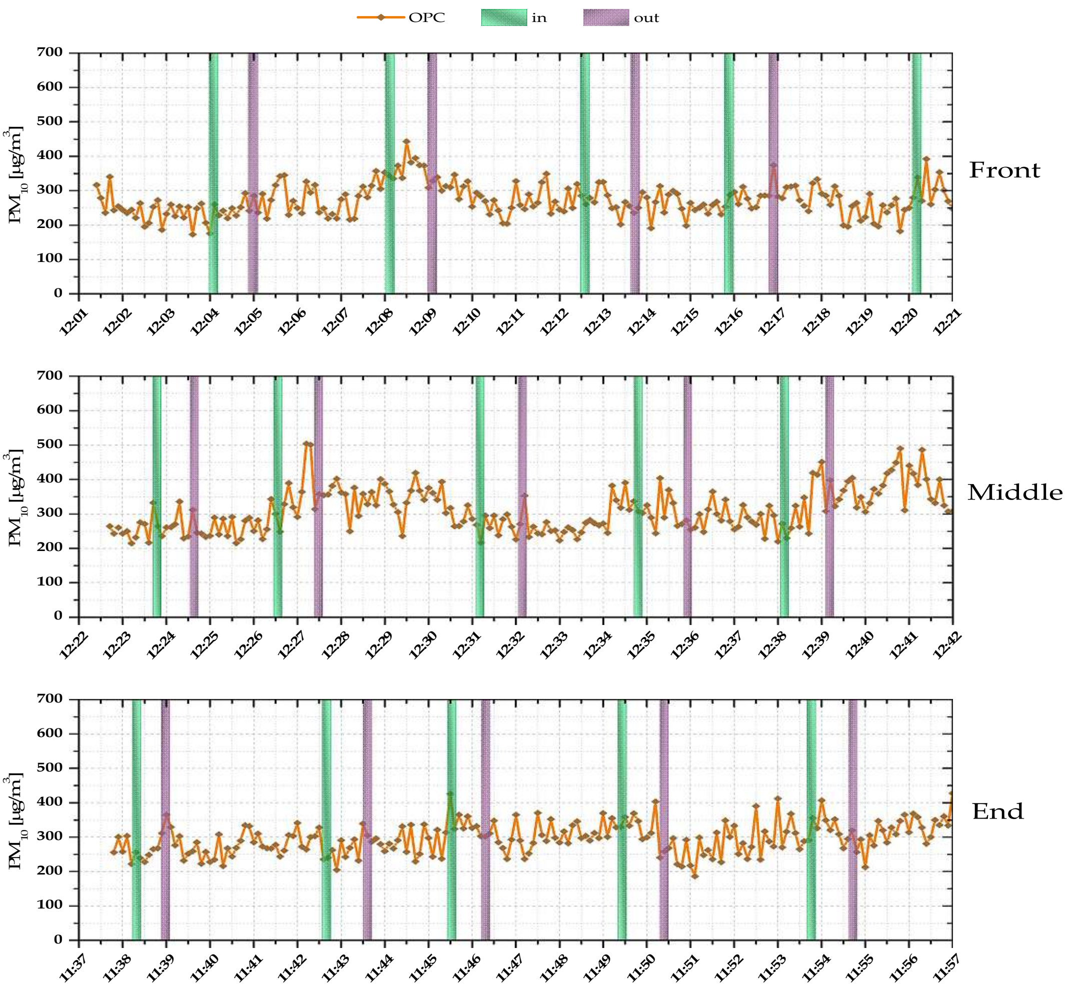

Figure 3.30 Temporal variation of the monitored OPC PM_{10} 6s mean values, recorded at station Karlsplatz U1, with the periods of train arrivals and departures highlighted in green and purple, respectively

3.2.4 Mass concentration distributions

The size distribution evaluation of the airborne particulate matter encountered in the microenvironment of the subway system of Vienna was performed using the data collected by the electrical low-pressure impactor (ELPI). The ELPI was employed at all the platform measuring locations for a period of approximately four hours, while the tunnel location at Praterstern U2 was monitored for 3 days continuously. Generally, the OPC provides the opportunity of size classification as well, but previous studies have shown poor agreement comparing the size distribution results of optical particle counters and electrical low-pressure impactors regarding samples collected in subway systems (Reche et al., 2017). This deviation is mainly assigned to the different modus operandi of the two instruments, as the OPC`s evaluations are based on the optical diameter of the sampled particles, while the ELPI segregates them according to their aerodynamic diameter sizes. Since the size distribution evaluation via the optical diameter is greatly influenced by the particles` refractive indices and density, the complementary data collected by the electrical low-pressure impactor was used for the final assessments and interpretations.

Figure 3.31 to Figure 3.34 show the contour plots of the mass concentration distributions of the four sites generated via the data obtained by the ELPI. On these figures, the x-axis shows the time scale, the y-axis shows the aerodynamic diameter of the particles on a logarithmical scale, whereas the particle mass concentration is presented with color codes defined by the likewise logarithmically scaled bar on the right side.

Generally, the fraction of the airborne particles with higher aerodynamic diameters contributes the most to the total aerosol mass. The mass concentration size distributions at the platform Karlsplatz U1, Stubentor U3 and Rochusgasse U3 were monitored only during the operation of the train service and show a very similar picture with approximately 90 % of the total PM_{10} mass concentrated in the fraction with >1µm (a.d.), mainly dominated by the mass contribution of the particles with >2.47µm (a.d.). Throughout the observation period of approx. 5 hours on the platforms, no marked variations of the mass size distribution were observed, even though a pattern of short concentration peaks can be noticed mainly for the particulates in the course (>1µm a.d.) size range and to a lesser extent down to ≥0.01µm (a.d.). Still, these recurring elevated mass concentration events couldn`t be assigned only to the passing trains, thus other factors like the movements of commuters may have played an additional role. In contrast, Figure 3.34 allows further deductions based on the temporal variations of the size fractions dominating the mass concentration distribution of the aerosols, measured during both the operating and non-operating hours at the monitoring site tunnel Praterstern U2. During the night period between 1am and 5am, a significant decrease of the mass concentration values can be seen for the particles with >1µm (a.d.), and a moderate decrease for the <0.1µm (a.d.) fraction, which already contributes only minimally to the total PM_{10} mass during the service hours. Meanwhile the fraction between 0.1µm and 1µm (a.d.) stays rather unaffected, both during operating and non-operating hours, thereby dominating the PM_{10} mass concentration levels during the night period.

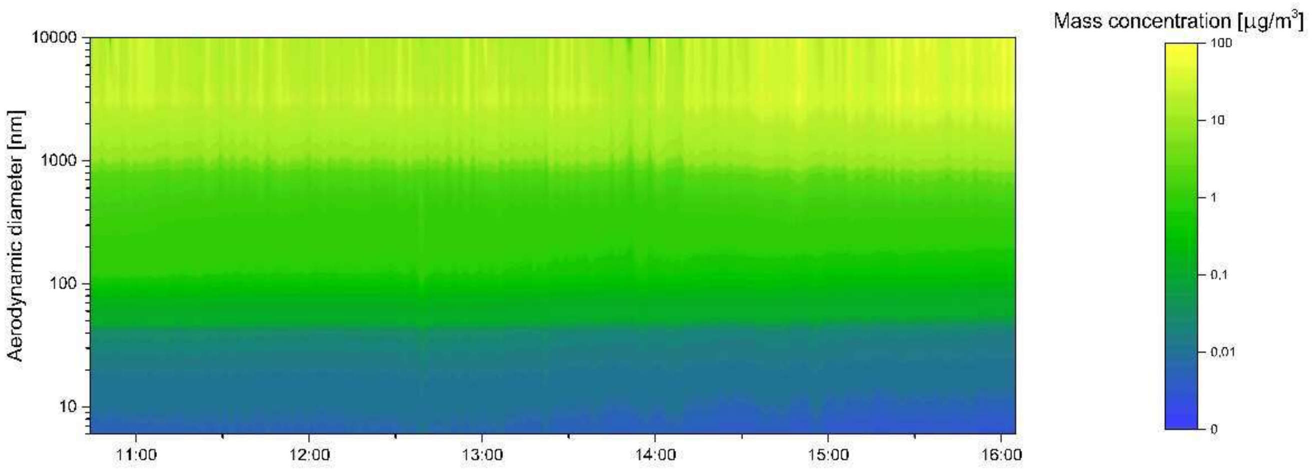

Figure 3.31 Temporal changes of the size distribution of PM mass concentrations measured at the platform Karlsplatz U1 with the ELPI

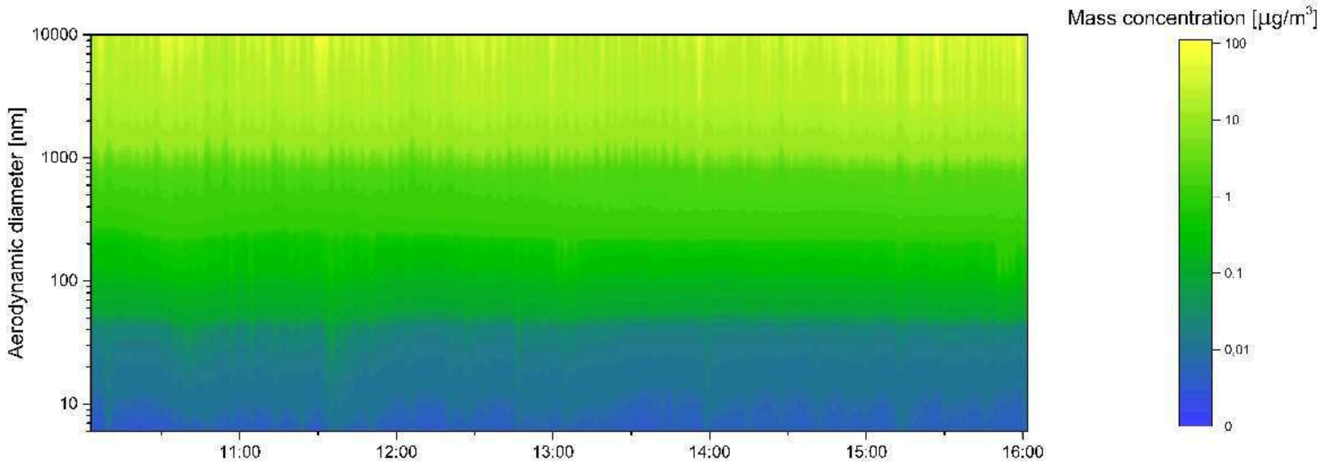

Figure 3.32 Temporal changes of the size distribution of PM mass concentrations measured at the platform Stubentor U3 with the ELPI

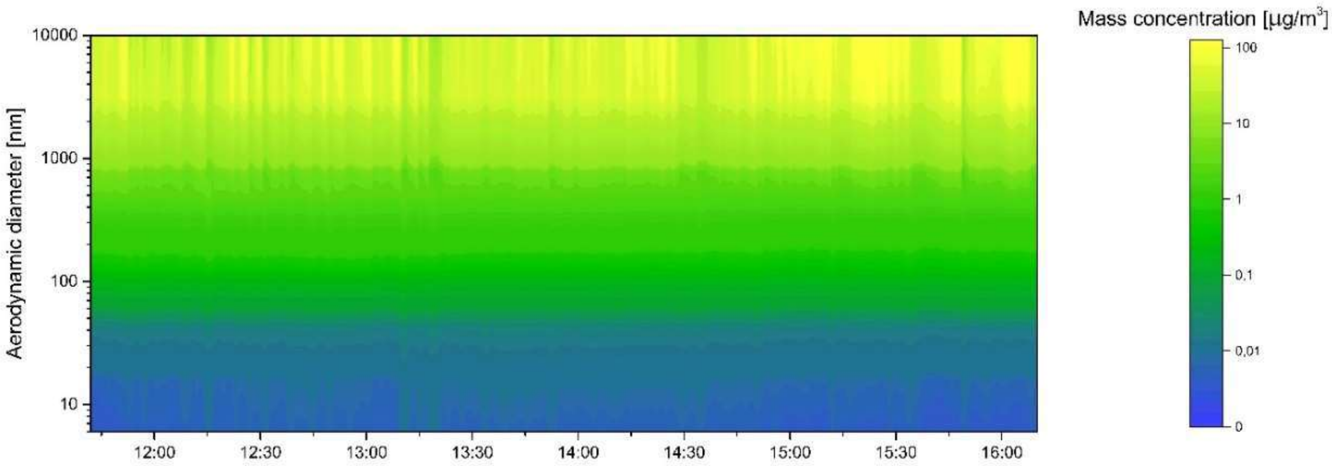

Figure 3.33 Temporal changes of the size distribution of PM mass concentrations measured at the platform Rochusgasse U3 with the ELPI

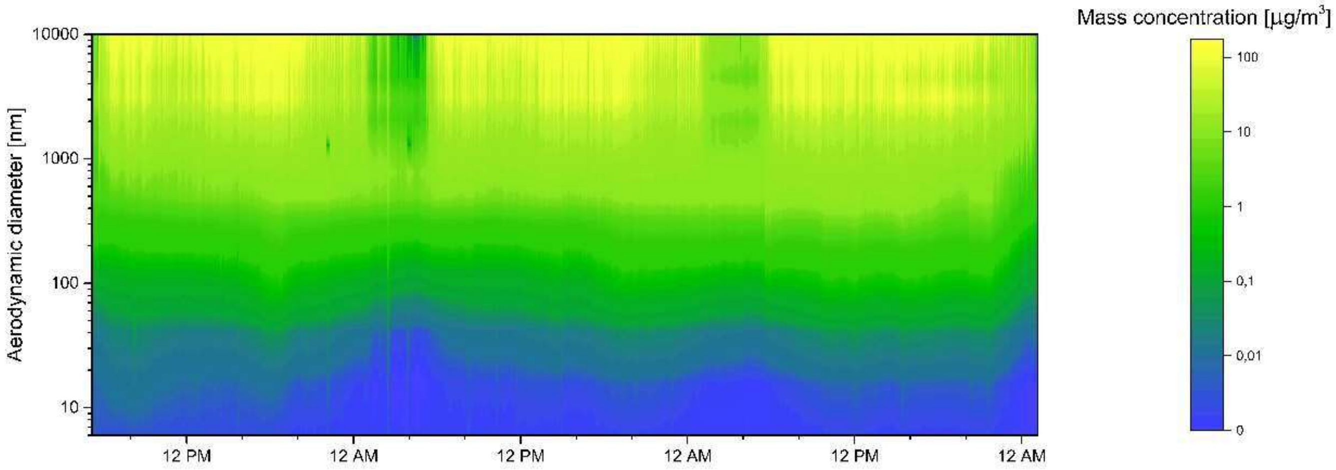

Figure 3.34 Temporal changes of the size distribution of PM mass concentrations measured at the tunnel Praterstern U2 with the ELPI

In addition to the contour plots above, Figure 3.35 illustrates the difference of the mass size distributions between operating and non-operating hours calculated from the data obtained by the measurements at tunnel Praterstern U2. In this illustrations, the total mean mass concentration values measured during the service period are compared to the total mean mass distribution during non-operating hours, distributed to 14 size channels with specific aerodynamic diameter size ranges, corresponding to the 14 impactor stages of the electrical low-pressure impactor. By the summation of the mass concentration values of the different impactor stages, the total PM_{10} mass concentration values can be calculated. Further on, to characterize the $PM_{2.5}$ and PM_1 fractions, the particles in the size ranges between 6 nm to 2.47 µm (a.d.) and 6 nm to 0.948 µm (a.d.) were applied, respectively. Table 3.12 summarizes the resulting mass concentration values of the individual monitoring locations and the $PM_{2.5}/PM_{10}$ ratios.

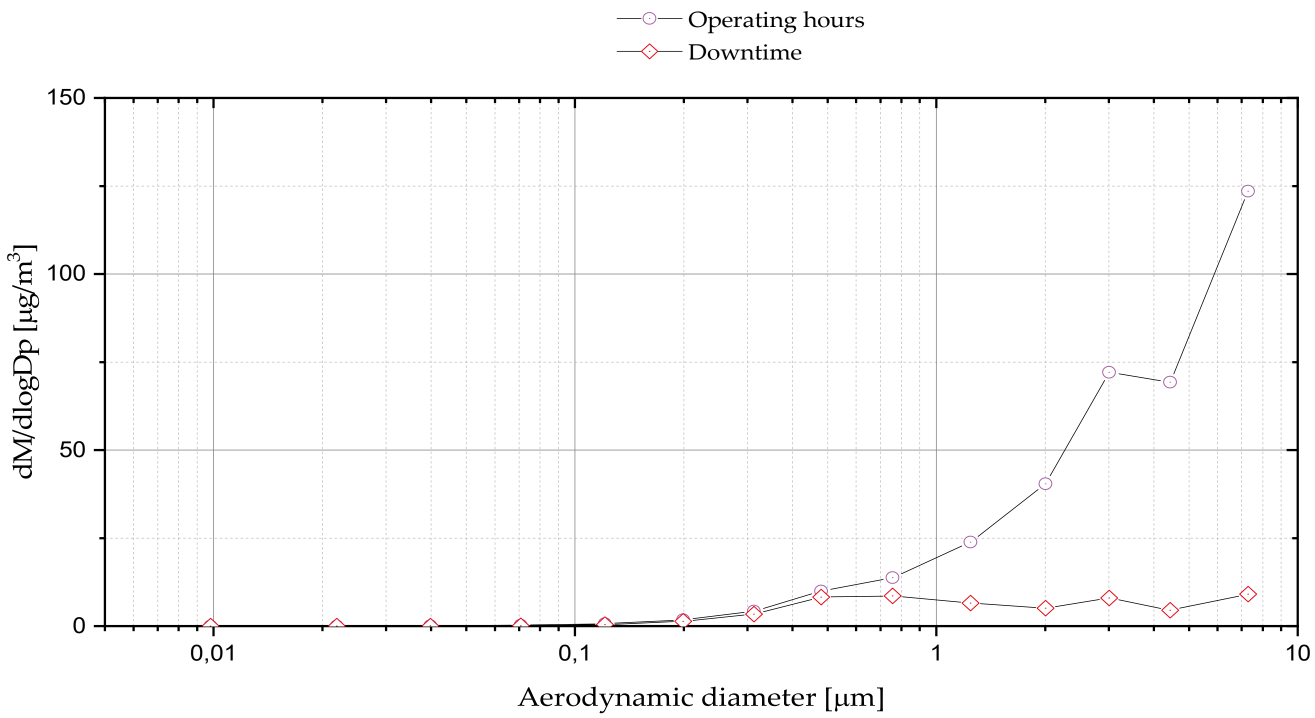

Figure 3.35 Praterstern mass size distribution of operating hours vs. non-operating hours

Table 3.12 Mass concentration values of the individual particulate matter fractions of all the stations, obtained from the evaluation of the data collected by the ELPI

			tunnel Praterstern	platform Stubentor	platform Karlsplatz	platform Rochusgasse
Total	PM_{10}	[µg/m³]	312			
	$PM_{2,5}$	[µg/m³]	85.3			
	$PM_{2,5}/PM_{10}$		*0.27*			
	PM_1	[µg/m³]	29.4			
Operating hours	PM_{10}	[µg/m³]	360	171	188	293
	$PM_{2,5}$	[µg/m³]	95.0	79.5	104	144
	$PM_{2,5}/PM_{10}$		*0.26*	*0.47*	*0.55*	*0.49*
	PM_1	[µg/m³]	30.7	21.3	25.1	36.1
Non-operating hours	PM_{10}	[µg/m³]	55.4			
	$PM_{2,5}$	[µg/m³]	33.7			
	$PM_{2,5}/PM_{10}$		*0.61*			
	PM_1	[µg/m³]	22.1			

Using the total (operating hours + non-operating hours) mean mass concentration values of the different particulate matter fractions, a $PM_{2.5}/PM_{10}$ ratio of 0.27 was estimated for the tunnel location Praterstern U2. This value is predominantly driven by the operating hours reflecting 84 % of the time and giving a similar ratio of 0.26. A significant elevation of the $PM_{2.5}$ fraction`s contribution to the PM_{10} fraction can be noticed during the non-operating hours, with a $PM_{2.5}/PM_{10}$ ratio of 0.61. At the platform locations, reflecting operating hours as well, the assessed $PM_{2.5}/PM_{10}$ ratios ranged between 0.47 and 0.55.

These estimated ratios correspond to the results presented in other studies (Cheng & Lin, 2010; Querol et al., 2012; Salma et al., 2007). The comparison of the $PM_{2.5}/PM_{10}$ ratios shows, that the PM_{10}-$PM_{2.5}$ fraction takes up the highest proportion of the airborne particulate matter mass in the tunnel area and during the service period. Without train service, the amount of coarse airborne particles decreases sharply. This corresponds to the trend observable in Figure 3.34, that the night periods are not only characterized by a general decline in mass concentration levels, but also a decline of the relative contribution to the PM_{10} mass concentration levels by the coarser fraction. As there are no emission sources or movements causing resuspension of PM during these intervals of service standstill, the deposition of the airborne dust via sedimentation processes is favored. The contribution of the $PM_{10-2.5}$ fraction during the operating hours is smaller at the platform monitoring sites than at the tunnel site, but higher than during the non-operating hours.

Usual air quality measurements of the ambient $PM_{2.5}/PM_{10}$ ratios in Austria result in values between 0.5 and 0.82 (Nagl & Spangl, 2020). Yet, the convergency of the measured ratios during the non-operating hours to these values doesn`t indicate a higher contribution of the outdoor air to the subway microenvironment, otherwise iron wouldn`t still be the dominating component in terms of mass concentrations, but rather a modulation of the size distribution pattern to the size distribution form seen in ambient samples, due to the decrease of particulate matter emission sources in the tunnel system.

The PM_1 fraction contributes clearly less to the mass of the airborne dust. Using the mean mass concentration values of the different monitoring sites, the PM_1/PM_{10} ratios can be calculated. The results show ratios of 0.085 and 0.094 for the operation hours and total mean value at the tunnel Praterstern U2, respectively, while the values for the platform stations range between 0.12 and 0.13. During the non-operation hours sampled at the monitoring site tunnel Praterstern U2, the PM_1/PM_{10} ratio increases to 0.42.

3.2.5 Particle number concentrations and distributions

The data obtained by the ELPI measurements was furtherly used for the evaluation of the number concentration distributions of particles within the subway aerosol. The illustrations from Figure 3.36 to Figure 3.39 show the time-series of the number particle size distribution at the three discrete platform monitoring sites, from late morning (start between 10am and 12pm) until 4pm, and at the tunnel location Praterstern U2, enclosing a campaign with three days of continuous measurement. On these figures, the x-axis shows the time scale, the y-axis shows the aerodynamic diameter of the particles on a logarithmical scale, whereas the particle number concentration is presented with color codes defined by the likewise logarithmically scaled bar on the right side.

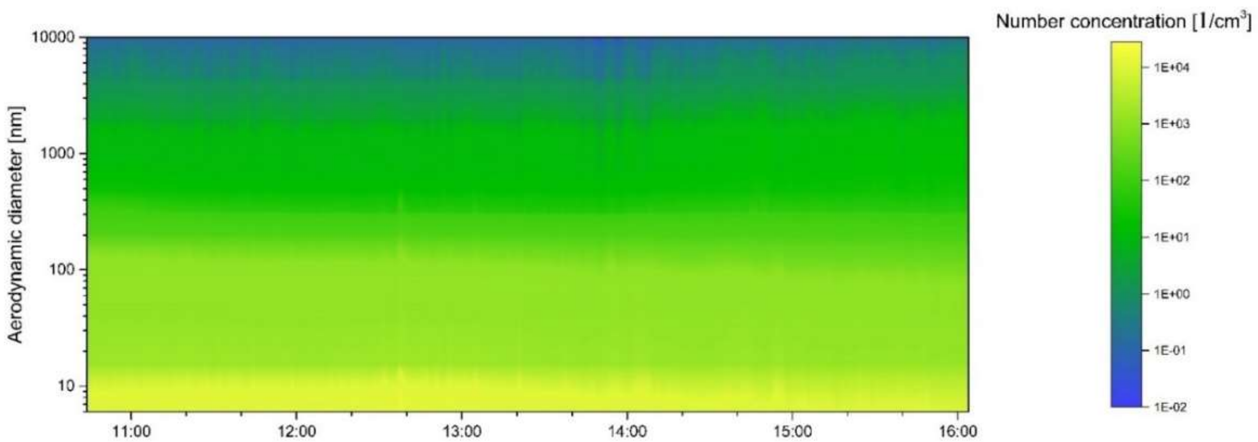

Figure 3.36 Temporal changes of the size distribution of PM number concentrations measured at the platform Karlsplatz U1 with the ELPI

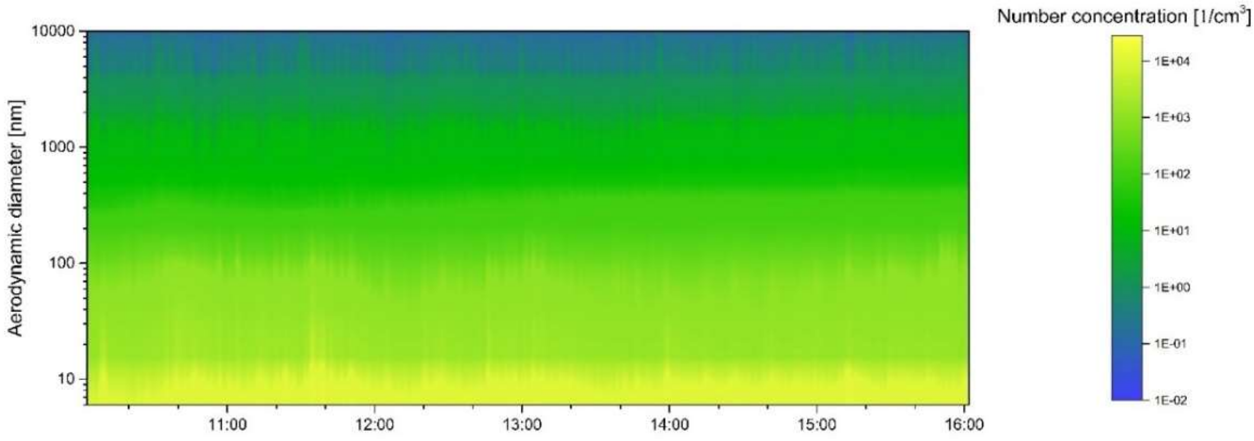

Figure 3.37 Temporal changes of the size distribution of PM number concentrations measured at the platform Stubentor U3 with the ELPI

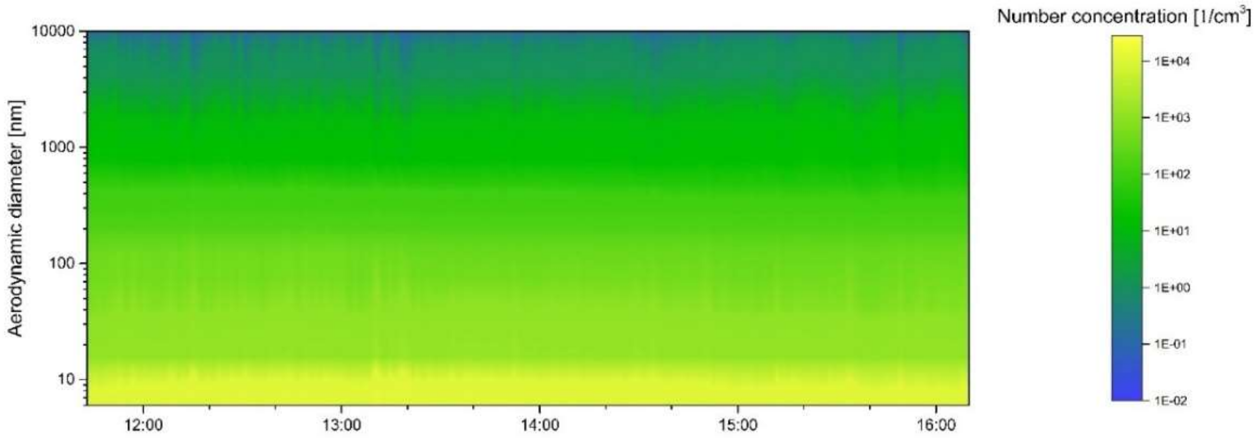

Figure 3.38 Temporal changes of the size distribution of PM number concentrations measured at the platform Rochusgasse U3 with the ELPI

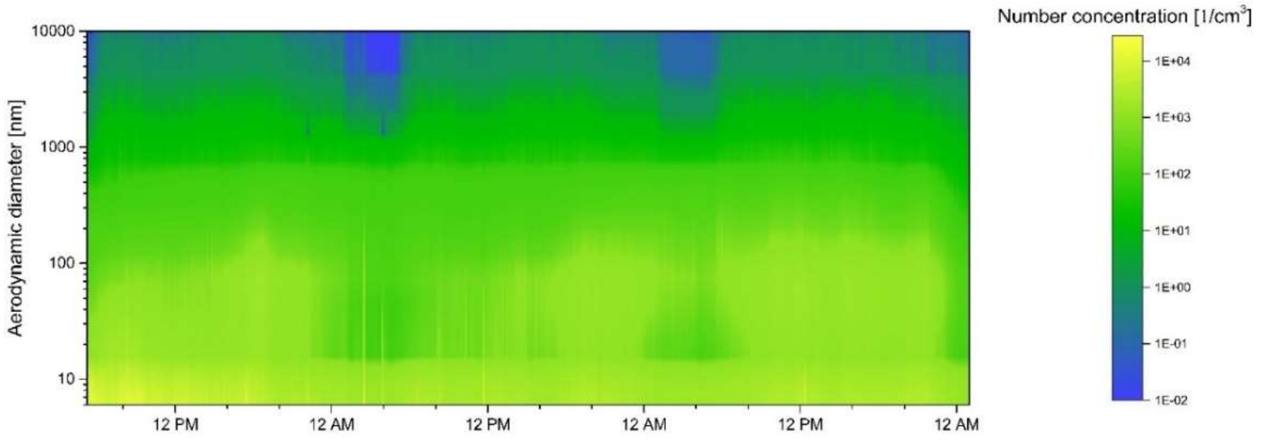

Figure 3.39 Temporal changes of the size distribution of PM number concentrations measured at the tunnel Praterstern U2 with the ELPI

As expected, the results show a completely different distribution pattern in comparison with the size distributions of mass concentrations discussed above. Generally, it can be stated, that the fine particles with an <300nm (a.d.) dictate the number concentration distribution mode in the subway system, displaying the dominance of the nano-sized (a.d.<100nm) aerosols` contribution to the total number concentration levels. The highest number concentration values are reached by particles in the size range below 10 nm (a.d.), where values above 10000 particles/cm^3 were measured, covering the major share of the estimated total mean number concentration values shown in Table 3.13.

The particle number concentration distributions observed on the platform levels during the early afternoon service periods, shown in Figure 3.36 to Figure 3.38, display a fairly steady pattern, although similarly to the temporal changes in the size distributions regarding the mass concentration levels (see 3.2.4), elevated number concentration events can be noticed as well, which couldn`t be appointed solely to train movements, thus other factors may play a substantial role in their origins. Meanwhile the investigation of the night periods (between 1am and 5am) at tunnel Praterstern U2, depicted in Figure 3.39, shows a more complex picture of the temporal number concentration variations. Here, a slight decrease of the number concentration amount can be observed at the aerodynamic diameter range between 20 and 100 nm, thus particulate formation processes could occur in this size range due to high temperatures amid the friction of the train system compartments during operation, also stated by (Loxham et al., 2013). Further on a significant drop of number concentration level can be seen for the coarse particles >1000 nm (a.d.), which already contributed only a minor share to the total number of particles during the day. The number concentration values of the particles with an aerodynamic diameter between 100 and 1000 nm hold a rather constant level both during the day and night period, which is similar to the related mass concentration pattern seen in Figure 3.34, while the particles below 10 nm (a.d.) dominate the contribution to the total number concentration of particles further on.

Table 3.13 summarizes the mean number concentration values encountered in the different subway platform levels during the service hours and additionally the total mean values measured during the operating and non-operating hours at the monitoring site tunnel Praterstern U2. The mean number concentration levels determined during the operating hours on the 3 platforms were quite similar, with the maximum mean value measured at the platform Karlsplatz U1. The mean number concentrations during the operating hours at the tunnel Praterstern U2 were rather low in comparison, which can be explained by the relatively voluminous space of the tunnel segment, where the measurements were conducted. The determined number concentration values are comparable with loadings in other subway systems from around the world (Levy et al., 2002; Moreno, Reche, et al., 2015; Ozgen et al., 2016; Suárez et al., 2014), listed in Table 1.5 (section 1.4.3). The usage of diesel fueled service and maintenance trains during the non-operating hours can further on play a role in the generation of UFP inside the subway system (Salma et al., 2007).

Table 3.13 Overview of the mean number concentration values at all monitoring sites observed by the ELPI

	PN [#particles/cm³]		
	Total	Operating hours	Non-operating hours
tunnel Praterstern U2	1.11E+04	1.12E+04	1.08E+04
platform Stubentor U3		1.98E+04	
platform Karlsplatz U1		2.02E+04	
platform Rochusgasse U3		1.96E+04	

In Figure 3.40, the temporal variations of the mass and number concentration values observed at the tunnel Praterstern U2 are plotted in parallel. A diurnal variation is noticeable for both parameters, although there is a less significant decline of the total number concentration levels during the tranquil night periods in comparison with the sharp drop at the mass concentration levels in the non-operating hours. There are also partially distinct patterns regarding the temporal variations of the two parameters noticeable during the service hours, which implies different factors impacting the mass and number concentration values in the subway system.

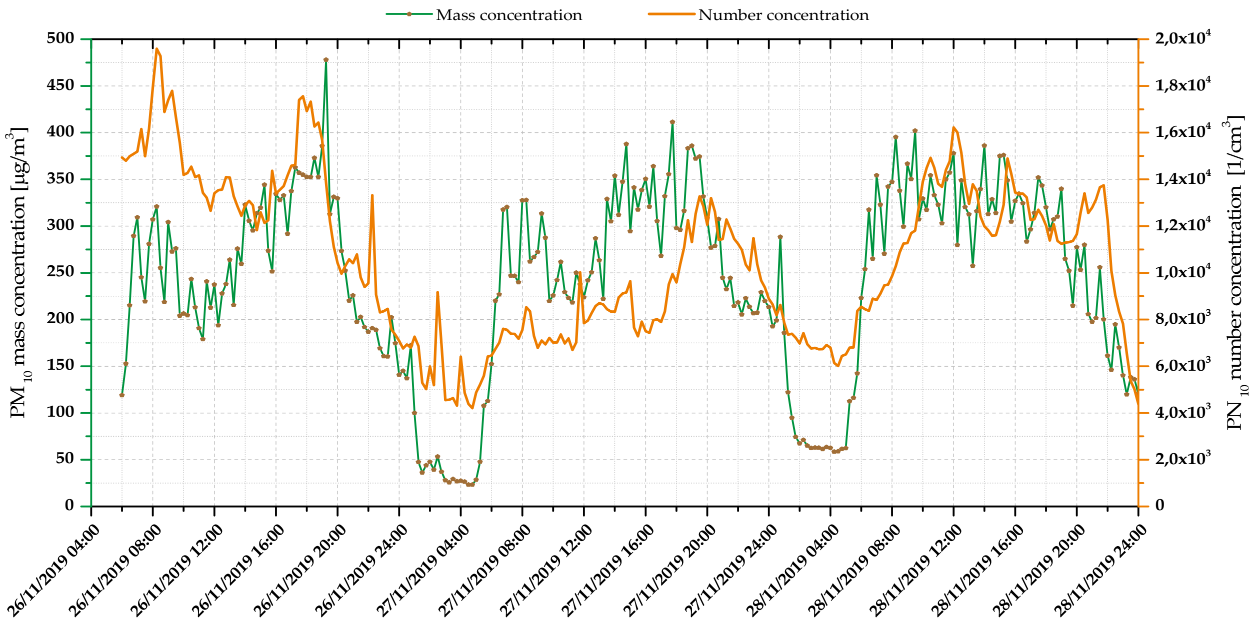

Figure 3.40 Temporal variations of the mass and number concentration levels measured by the ELPI at the tunnel location near the station Praterstern U2

Chapter 4) Summary and conclusions

Since its opening more than 40 years ago, the subway system in Vienna affirmed itself as an elemental part of the capital`s infrastructure, serving a total of 440 million commuters every year since 2015. While subway systems are offering a convenient and environmentally friendly option of getting around in major cities all around the world, recent studies of air quality in these microenvironments (MEs) discussed the elevated particulate matter concentration levels.

As part of an extensive study, a measurement campaign was conducted, starting in October 2019 and ending with March 2020, at four different Viennese underground metro stations in three platform (Karlsplatz U1, Rochusgasse U3 and Stubentor U3) and three tunnel locations (Karlsplatz U1, Rochusgasse U3 and Praterstern U2) to evaluate and characterize the PM_{10} levels using a Low Volume Sampler for gravimetric and chemical analysis, side by side with an Optical Particle Counter and an Electric Low Pressure Impactor to identify the impact on air quality by various factors, like train frequency, ventilation system, station depth and design.

As expected, the findings of the present study display elevated particulate matter mass concentrations in respect to common ambient levels, detected in the urban background of Vienna. The mean PM_{10} concentrations ranged between 97 $\mu g/m^3$ and 341 $\mu g/m^3$ for the monitored platform and tunnel locations, comparable with the analysis results from other metro systems around the world.

The highest mass concentration levels were measured at the tunnel location Karlsplatz U1, while the measurements at the tunnel Rochusgasse U3 revealed a less polluted ME. This outcome is in accordance with deduced trends in the literature, displaying the major impacts of station design, depth and age on the particulate matter concentrations encountered. Comparing the air pollution levels of the tunnel and platform locations, increased PM values were determined for the tunnel location of Karlsplatz U1, nevertheless the analogous observation for the station Rochusgasse U3 presented the inverse trend, thereby restricting a universal verdict of elevated pollution levels in the tunnel areas. Nonetheless, the gravimetric PM_{10} measurements showed higher mean concentration values for the tunnel samples, possessing a greater concentration range as well. Further on, the train frequency could be identified as the primary influencing factor in the distinct diurnal variations of the PM_{10} concentration levels, in agreement with the literature. Some spatial differences of PM loadings on the platform stations could be assessed, explained mainly by differing station designs and train motion.

The highest contribution to the PM_{10} mass fraction is given by the contribution of the proportionately coarser particles. According to location, between 45 % to 70 % of the particulate matter mass can be linked to the $PM_{10-2.5}$ fraction, which is generally more present in the operating hours than in the tranquil night hours, characterized by reduced PM mass concentration values in the absence of train service. In contrast, the particle number concentration levels are dominated by particles with a mean aerodynamic diameter less than 0.3 μm, reaching values between $1 – 2 * 10^4$ #/cm^{-3}.

The chemical composition of the particulate matter was mainly dominated by elemental iron and its oxides (69 – 90 %), next to further metalliferous elements, like Manganese, Aluminum, Chromium, Copper, Zinc, Lead, Barium, Antimony, Strontium, Cadmium and Vanadium, with minor contribution to the PM mass, however with crucial information regarding the toxic potential of the subway airborne dust. Overall, none of the maximum allowable concentration values (MAK) were exceeded for either of the particulate matter components. The rest of the PM mass is formed by water-soluble inorganic ions (2 - 6%) and carbonaceous compounds (4 – 7 %), accompanied by further non-measured constituents, like water moisture and other crustal elements.

Sources of the subway PM could be appointed via different analysis tools, like elemental ratios, correlation matrices and PCA, mainly to inside emissions, generated mainly by material abrasion, but also outside ambient sources like traffic emissions, resuspended dust and abundant secondary inorganic aerosols.

Chapter 5) References

Aarnio, P., Yli-Tuomi, T., Kousa, A., Mäkelä, T., Hirsikko, A., Hämeri, K., Räisänen, M., Hillamo, R., Koskentalo, T., & Jantunen, M. (2005). The concentrations and composition of and exposure to fine particles (PM2.5) in the Helsinki subway system. *Atmospheric Environment*, *39*(28), 5059–5066. https://doi.org/10.1016/j.atmosenv.2005.05.012

Adams, H. S., Nieuwenhuijsen, M. J., Colvile, R. N., McMullen, M. A. S., & Khandelwal, P. (2001). Fine particle (PM2.5) personal exposure levels in transport microenvironments, London, UK. *Science of the Total Environment*, *279*(1–3), 29–44. https://doi.org/10.1016/S0048-9697(01)00723-9

Adar, S. D., Davey, M., Sullivan, J. R., Compher, M., Szpiro, A., & Liu, L. S. (2008). Predicting airborne particle levels aboard Washington State school buses. *Atmospheric Environment*, *42*(33), 7590–7599. https://doi.org/10.1016/j.atmosenv.2008.06.041

Aksu, A. (2015). Sources of metal pollution in the urban atmosphere (A case study: Tuzla, Istanbul). *Journal of Environmental Health Science and Engineering*, *13*(1), 1–10. https://doi.org/10.1186/s40201-015-0224-9

Awe, Y., Bank, W., Hagler, G. S. W., States, U., Protection, E., & Klopp, J. M. (2017). *Filling the Gaps : Improving Measurement of Ambient Air Quality in Low and Middle Income Countries Draft preliminary guidance for low and middle income countries on. September.*

Badelt, C. (2021). *Austria's Economic Policy in the Time of COVID-19 and Beyond. An Assessment at the Turn of the Year 2020-21*.

Baker, J. E. (2003). *Source Apportionment of Polycyclic Aromatic Hydrocarbons in the Urban Atmosphere : A Comparison of Three Methods*. *37*(9), 1873–1881.

Barbieri, M. (2016). *The Importance of Enrichment Factor (EF) and Geoaccumulation Index (Igeo) to Evaluate the Soil Contamination*. *5*(1), 1–4. https://doi.org/10.4172/2381-8719.1000237

Bensch, S. (2013). Wiener Linien - Zahlen, Daten, Fakten. *CNE.Fortbildung*, *7*(01), 2–4. https://doi.org/10.1055/s-0033-1356810

BMAS. (2021). Technische Regeln für Gefahrenstoffe (TRGS 900). *Bundesministerium Für Arbeit Und Soziales*, *70*(25), 1–70.

Borghi, F., Spinazzè, A., Fanti, G., Campagnolo, D., Rovelli, S., Keller, M., Cattaneo, A., & Cavallo, D. M. (2020). Commuters' personal exposure assessment and evaluation of inhaled dose to different atmospheric pollutants. *International Journal of Environmental Research and Public Health*, *17*(10). https://doi.org/10.3390/ijerph17103357

Braniš, M. (2006). The contribution of ambient sources to particulate pollution in spaces and trains of the Prague underground transport system. *Atmospheric Environment*, *40*(2), 348–356. https://doi.org/10.1016/j.atmosenv.2005.09.060

Brown, J. S., Gordon, T., Price, O., & Asgharian, B. (2013). *Thoracic and respirable particle definitions for human health risk assessment*. 1–12.

Brugge, D., Durant, J. L., & Rioux, C. (2007). *Near-highway pollutants in motor vehicle exhaust : A review of epidemiologic evidence of cardiac and pulmonary health risks*. *12*, 1–12. https://doi.org/10.1186/1476-069X-6-23

Bui, K. V. H., Moon, J., Chae, M., Park, D., & Lee, Y. (2020). *Prediction of Aerosol Deposition in the Human Respiratory Tract via Computational Models : A Review with Recent Updates*. *February*. https://doi.org/10.3390/atmos11020137

Cartenì, A., Cascetta, F., & Campana, S. (2015). Underground and ground-level particulate matter concentrations in an Italian metro system. *Atmospheric Environment*, *101*, 328–337. https://doi.org/10.1016/j.atmosenv.2014.11.030

CEN. (1993). *Workplace Atmospheres - Size Fraction Definitions for Measurement of Airborne Particles*. European Comitee for Standardization.

Cepeda, M., Schoufour, J., Freak-Poli, R., Koolhaas, C. M., Dhana, K., Bramer, W. M., & Franco, O. H. (2017). Levels of ambient air pollution according to mode of transport: a systematic review. *The Lancet Public Health*, *2*(1), e23–e34. https://doi.org/10.1016/S2468-2667(16)30021-4

Chan, L. Y., Lau, W. L., Lee, S. C., & Chan, C. Y. (2002). Commuter exposure to particulate matter in public transportation modes in Hong Kong. *Atmospheric Environment*, *36*(21), 3363–3373. https://doi.org/10.1016/S1352-2310(02)00318-7

Chan, L. Y., Lau, W. L., Zou, S. C., Cao, Z. X., & Lai, S. C. (2002). *Exposure level of carbon monoxide and respirable suspended particulate in public transportation modes while commuting in urban area of Guangzhou , China*. *36*, 5831–5840.

Cheng, Y. H., & Lin, Y. L. (2010). Measurement of particle mass concentrations and size distributions in an underground station. *Aerosol and Air Quality Research*, *10*(1), 22–29. https://doi.org/10.4209/aaqr.2009.05.0037

Cheng, Y. H., Lin, Y. L., & Liu, C. C. (2008). Levels of PM10 and PM2.5 in Taipei Rapid Transit System. *Atmospheric Environment*, *42*(31), 7242–7249. https://doi.org/10.1016/j.atmosenv.2008.07.011

Chernyshev, V. V., Zakharenko, A. M., Ugay, S. M., Hien, T. T., Hai, L. H., Olesik, S. M., Kholodov, A. S., Zubko, E., Kokkinakis, M., Burykina, T. I., Stratidakis, A. K., Mezhuev, Y. O., Sarigiannis, D. A., Tsatsakis, A., & Golokhvast, K. S. (2019). Morphological and chemical composition of particulate matter in buses exhaust. *Toxicology Reports*, *6*(October 2018), 120–125. https://doi.org/10.1016/j.toxrep.2018.12.002

Chillrud, S. N., Epstein, D., Ross, J. M., Sax, S. N., Pederson, D. E. E., Spengler, J. D., & Kinney, P. L. (2011). Elevated Airborne Exposures of Teenagers to Manganese, E Chromium, and Iron from Steel Dust and New York City's Subway System. *Environ Sci Technol.*, *38*(3), 732–737. https://doi.org/10.1021/es034734y

Chow, J. C., Watson, J. G., Chen, L. W. A., Arnott, W. P., Moosmüller, H., & Fung, K. (2004). Equivalence of elemental carbon by thermal/optical reflectance and transmittance with different temperature protocols. *Environmental Science and Technology*, *38*(16), 4414–4422. https://doi.org/10.1021/es034936u

City of Vienna. (2019). *Quality of living - Vienna remains the number one.* https://www.wien.gv.at/english/politics/international/comparison/mercer-study.html

City of Vienna. (2020). *Vienna's population 2020 - facts and figures on migration and integration.* https://www.wien.gv.at/english/social/integration/facts-figures/population-migration.html

Colombi, C., Angius, S., Gianelle, V., & Lazzarini, M. (2013). Particulate matter concentrations, Physical characteristics and elemental composition in the Milan underground transport system. *Atmospheric Environment*, *70*, 166–178. https://doi.org/10.1016/j.atmosenv.2013.01.035

Cusack, M., Talbot, N., Ondráček, J., Minguillón, M. C., Martins, V., Klouda, K., Schwarz, J., & Ždímal, V. (2015). Variability of aerosols and chemical composition of PM10, PM2.5 and PM1 on a platform of the Prague underground metro. *Atmospheric Environment*, *118*, 176–183. https://doi.org/10.1016/j.atmosenv.2015.08.013

ECA. (2020). *Special report 06/2020: Sustainable Urban Mobility in the EU: No substantial improvement is possible without Member States' commitment*.

EEA. (2019). *Air quality in Europe — 2019 report* (Issue 10).

EPA. (2019). *Integrated Science Assessment for Particulate Matter*.

Faroon, O. M., Abadin, H., Keith, S., Osier, M., Chappell, L. L., Diamond, G., & Sage, G. (2004). TOXICOLOGICAL PROFILE FOR COBALT. *Agency for Toxic Substances and Disease Registry*, *April*.

Farrow, A., & Miller, K. A. (2020). *TOXIC AIR : The price of fossil fuels* (Issue February).

Gerber, A., Bohn, J., Groneberg, D. A., Schulze, J., & Bundschuh, M. (2014). Airborne particulate matter in public transport: A field study at major intersection points in Frankfurt am Main (Germany). *Journal of Occupational Medicine and Toxicology*, *9*(1), 13–16. https://doi.org/10.1186/1745-6673-9-13

Goel, R., Gani, S., Guttikunda, S. K., Wilson, D., & Tiwari, G. (2015). On-road PM2.5 pollution exposure in multiple transport microenvironments in Delhi. *Atmospheric Environment*, *123*, 129–138. https://doi.org/10.1016/j.atmosenv.2015.10.037

Gómez-Perales, J. E., Colvile, R. N., Nieuwenhuijsen, M. J., Fernández-Bremauntz, A., Gutiérrez-Avedoy, V. J., Páramo-Figueroa, V. H., Blanco-Jiménez, S., Bueno-López, E., Mandujano, F., Bernabé-Cabanillas, R., & Ortiz-Segovia, E. (2004). Commuters' exposure to PM2.5, CO, and benzene in public transport in the metropolitan area of Mexico City. *Atmospheric Environment*, *38*(8), 1219–1229. https://doi.org/10.1016/j.atmosenv.2003.11.008

Grass, D. S., Ross, J. M., Family, F., Barbour, J., James Simpson, H., Coulibaly, D., Hernandez, J., Chen, Y., Slavkovich, V., Li, Y., Graziano, J., Santella, R. M., Brandt-Rauf, P., & Chillrud, S. N. (2010). Airborne particulate metals in the New York City subway: A pilot study to assess the potential for health impacts. *Environmental Research*, *110*(1), 1–11. https://doi.org/10.1016/j.envres.2009.10.006

Grigoratos, T., & Martini, G. (2014). Non-exhaust traffic related emissions. Brake and tyre wear PM. In *European Commission Joint Research Centre Institute of Energy and Transport*. https://doi.org/doi:10.2790/21481

Handler, M., Puls, C., Zbiral, J., Marr, I., Puxbaum, H., & Limbeck, A. (2008). Size and composition of particulate emissions from motor vehicles in the Kaisermühlen-Tunnel, Vienna. *Atmospheric Environment*, *42*(9), 2173–2186. https://doi.org/10.1016/j.atmosenv.2007.11.054

Health Effects Institute. (2019). *State of Global Air 2019*.

Heiler, G., Reisch, T., Hurt, J., Forghani, M., Omani, A., Hanbury, A., & Karimipour, F. (2021). *Country-wide Mobility Changes Observed Using Mobile Phone Data During COVID-19 Pandemic*.

Hjortenkrans, D. (2008). *Road traffic metals – sources and emissions*.

Hunkin, S., & Krell, K. (2019). *Promoting Active Modes of Transport*. *February*.

Hussein, T., Puustinen, A., & Aalto, P. P. (2004). *and Physics Urban aerosol number size distributions*. *1999*, 391–411.

Hyeong, J., Youn, P., Son, S., & Kim, K. H. (2018). *A review of traditional and advanced technologies for the removal of particulate matter in subway systems*. *September*, 177–191. https://doi.org/10.1111/ina.12532

Ji, W., Li, X., & Wang, C. (2021). Composition and exposure characteristics of PM 2 . 5 on subway platforms and estimates of exposure reduction by protective masks. *Environmental Research*, *197*(October 2020), 111042. https://doi.org/10.1016/j.envres.2021.111042

Johansson, C., & Johansson, P. Å. (2002). Particulate matter in the underground of Stockholm. *Advances in Air Pollution*, *11*, 541–549.

Jung, H., Kim, B. W., Malek, A., Sung, Y., Hoon, J., & Son, Y. (2012). Chemical speciation of size-segregated floor dusts and airborne magnetic particles collected at underground subway stations in Seoul , Korea. *Journal of Hazardous Materials*, *213–214*, 331–340. https://doi.org/10.1016/j.jhazmat.2012.02.006

Jung, H., Kim, B. W., Ryu, J. Y., Maskey, S., Kim, J. C., Sohn, J., & Ro, C. U. (2010). Source identification of particulate matter collected at underground subway stations in Seoul, Korea using quantitative single-particle analysis. *Atmospheric Environment*, *44*(19), 2287–2293. https://doi.org/10.1016/j.atmosenv.2010.04.003

Kam, W., Cheung, K., Daher, N., & Sioutas, C. (2011). *Particulate matter (PM) concentrations in underground and ground-level rail systems of the Los Angeles Metro*. *45*, 1506–1516. https://doi.org/10.1016/j.atmosenv.2010.12.049

Kamani, H., Hoseini, M., Seyedsalehi, M., Mahdavi, Y., Jaafari, J., & Safari, G. H. (2014). Concentration and characterization of airborne particles in Tehran's subway system. *Environmental Science and Pollution Research*, *21*(12), 7319–7328. https://doi.org/10.1007/s11356-014-2659-4

Karlsson, H. L., Nilsson, L., & Möller, L. (2005). Subway particles are more genotoxic than street particles and induce oxidative stress in cultured human lung cells. *Chemical Research in Toxicology*, *18*(1), 19–23. https://doi.org/10.1021/tx049723c

Kim, B. W., Jung, H., Song, Y. C., Lee, M. J., Kim, H. K., Kim, J. C., Sohn, J., & Ro, C. U. (2010). Characterization of summertime aerosol particles collected at subway stations in seoul, korea using low-Z particle electron probe X-ray microanalysis. *Asian Journal of Atmospheric Environment*, *4*(2), 97–105. https://doi.org/10.5572/ajae.2010.4.2.097

Kim, K. H., Ho, D. X., Jeon, J. S., & Kim, J. C. (2012). A noticeable shift in particulate matter levels after platform screen door installation in a Korean subway station. *Atmospheric Environment*, *49*, 219–223. https://doi.org/10.1016/j.atmosenv.2011.11.058

Knibbs, L. D., & de Dear, R. J. (2010). Exposure to ultrafine particles and PM2.5 in four Sydney transport modes. *Atmospheric Environment*, *44*(26), 3224–3227. https://doi.org/10.1016/j.atmosenv.2010.05.026

Kumar, A., & Sarin, M. M. (2009). Mineral aerosols from western India: Temporal variability of coarse and fine atmospheric dust and elemental characteristics. *Atmospheric Environment*, *43*(26), 4005–4013. https://doi.org/10.1016/j.atmosenv.2009.05.014

Kumar, P., Morawska, L., Birmili, W., Paasonen, P., Hu, M., Kulmala, M., Harrison, R. M., Norford, L. K., & Britter, R. (2014). Ultrafine particles in cities. *Environment International*, *66*, 1–10. https://doi.org/10.1016/j.envint.2014.01.013

Kwon, S. B., Jeong, W., Park, D., Kim, K. T., & Cho, K. H. (2015). A multivariate study for characterizing particulate matter (PM10, PM2.5, and PM1) in Seoul metropolitan subway stations, Korea. *Journal of Hazardous Materials*, *297*, 295–303. https://doi.org/10.1016/j.jhazmat.2015.05.015

Lee, Y., Lee, Y., Kim, T., Choi, J. S., & Park, D. (2018). Sources and Characteristics of Particulate Matter in Subway Tunnels in Seoul , Korea. *Environmental Research and Public Health*, *15*(2534), 1–17. https://doi.org/10.3390/ijerph15112534

Lefer, B. L., & Talbot, R. W. (2001). Summertime measurements of aerosol nitrate and ammonium at a northeastern U.S. site. *Journal of Geophysical Research*, *106*(2000).

Levy, J. I., Dumyahn, T., & Spengler, J. D. (2002). Particulate matter and polycyclic aromatic hydrocarbon concentrations in indoor and outdoor microenvironments in Boston, Massachusetts. *Journal of Exposure Analysis and Environmental Epidemiology*, *12*(2), 104–114. https://doi.org/10.1038/sj.jea.7500203

Li, T. T., Bai, Y. H., Liu, Z. R., & Li, J. L. (2007). In-train air quality assessment of the railway transit system in Beijing: A note. *Transportation Research Part D: Transport and Environment*, *12*(1), 64–67. https://doi.org/10.1016/j.trd.2006.11.001

Limbeck, A., Handler, M., Puls, C., Zbiral, J., Bauer, H., & Puxbaum, H. (2009). Impact of mineral components and selected trace metals on ambient PM10 concentrations. *Atmospheric Environment*, *43*(3), 530–538. https://doi.org/10.1016/j.atmosenv.2008.10.012

Lippmann, M., Yeates, D. B., & Albert, R. E. (1980). *Deposition , retention , and clearance of inhaled particles*. *September 1979*, 337–362.

Loxham, M., Cooper, M. J., Gerlofs-Nijland, M. E., Cassee, F. R., Davies, D. E., Palmer, M. R., & Teagle, D. A. H. (2013). Physicochemical characterization of airborne particulate matter at a mainline underground railway station. *Environmental Science and Technology*, *47*(8), 3614–3622. https://doi.org/10.1021/es304481m

Loxham, M., & Nieuwenhuijsen, M. J. (2019). *Health effects of particulate matter air pollution in underground railway systems – a critical review of the evidence*. *2*, 1–24.

Lu, S., Liu, D., Zhang, W., Liu, P., Fei, Y., Gu, Y., Wu, M., Yu, S., Yonemochi, S., Wang, X., & Wang, Q. (2015). Physico-chemical characterization of PM2.5 in the microenvironment of Shanghai subway. *Atmospheric Research*, *153*, 543–552. https://doi.org/10.1016/j.atmosres.2014.10.006

Martins, V., Minguillón, M. C., Moreno, T., & Mende. (2017). Characterisation of Airborne Particulate Matter in Different European Subway Systems. *Urban Transport Systems*, *February*. https://doi.org/10.5772/65364

Martins, V., Moreno, T., Mendes, L., Eleftheriadis, K., Diapouli, E., Alves, C. A., Duarte, M., Miguel, E. De, Capdevila, M., Querol, X., & Cruz, M. (2016). Factors controlling air quality in different European subway systems. *Environmental Research*, *146*, 35–46. https://doi.org/10.1016/j.envres.2015.12.007

Martins, V., Moreno, T., Minguillón, M. C., Amato, F., de Miguel, E., Capdevila, M., Querol, X., Cruz, M., Amato, F., Miguel, E. De, Capdevila, M., & Querol, X. (2015). Exposure to airborne particulate matter in the subway system. *Science of the Total Environment*, *511*, 711–722. https://doi.org/10.1016/j.scitotenv.2014.12.013

Martins, V., Moreno, T., Minguillón, M. C., Van Drooge, B. L., Reche, C., Amato, F., De Miguel, E., Capdevila, M., Centelles, S., & Querol, X. (2016). Origin of inorganic and organic components of PM2.5 in subway stations of Barcelona, Spain. *Environmental Pollution*, *208*, 125–136. https://doi.org/10.1016/j.envpol.2015.07.004

Mattha Busby, Martin Belam, Sarah Marsh, Alison Rourke, K. R. and M. F. (2020). Europe on alert as four more Covid-19 deaths reported in Italy. *The Guardian*. https://www.theguardian.com/world/live/2020/feb/25/coronavirus-live-updates-outbreak-latest-news-italy-italia-deaths-symptoms-china-stocks-wall-street-dow-jones-economy-falls?page=with:block-5e550afd8f086a28115b2205

Minguillón, M. C., Reche, C., Martins, V., Amato, F., de Miguel, E., Capdevila, M., Centelles, S., Querol, X., & Moreno, T. (2018). Aerosol sources in subway environments. *Environmental Research*, *167*(May), 314–328. https://doi.org/10.1016/j.envres.2018.07.034

Mitsakou, C., Adamson, J. P., Doutsi, A., Brunt, H., Jones, S. J., Gowers, A. M., & Exley, K. S. (2021). Assessing the exposure to air pollution during transport in urban areas – Evidence review. *Journal of Transport & Health*, *21*(March), 101064. https://doi.org/10.1016/j.jth.2021.101064

Moore, K., Krudysz, M., Pakbin, P., Hudda, N., Moore, K., Krudysz, M., Pakbin, P., Hudda, N., & Sioutas, C. (2009). *Intra-Community Variability in Total Particle Number Concentrations in the San Pedro Harbor Area (Los Angeles , California) Intra-Community Variability in Total Particle Number Concentrations in the San Pedro Harbor Area (Los Angeles , California)*. *6826*. https://doi.org/10.1080/02786820902800900

Moreno, T., Martins, V., Querol, X., Jones, T., Bérubé, K., Minguillón, M. C., Amato, F., Capdevila, M., Miguel, E. De, Centelles, S., & Gibbons, W. (2015). A new look at inhalable metalliferous airborne particles on rail subway platforms. *Science of the Total Environment*, *505*, 367–375. https://doi.org/10.1016/j.scitotenv.2014.10.013

Moreno, T., Pérez, N., Reche, C., Martins, V., de Miguel, E., Capdevila, M., Centelles, S., Minguillón, M. C., Amato, F., Alastuey, A., Querol, X., Gibbons, W., Miguel, E. De, Capdevila, M., Centelles, S., Minguillón, M. C., Amato, F., Alastuey, A., Querol, & Gibbons, W. (2014). Subway platform air quality.Assessing the influences of tunnel ventilation, train piston effect and station design. *Atmospheric Environment*, *92*(March 2015), 461–468. https://doi.org/10.1016/j.atmosenv.2014.04.043

Moreno, T., Reche, C., Rivas, I., Minguillón, M. C., Martins, V., Vargas, C., Buonanno, G., Parga, J., Pandol, M., Brines, M., Ealo, M., So, A., Amato, F., Sosa, G., Capdevila, M., Miguel, E. De, Querol, X., & Gibbons, W. (2015). *Urban air quality comparison for bus , tram , subway and pedestrian commutes in Barcelona*. *142*, 495–510. https://doi.org/10.1016/j.envres.2015.07.022

Mugica-Álvarez, V., Figueroa-lara, J. J., Romero-romo, M., Sepúlveda-Sánchez, J., & Moreno, T. (2012). Concentrations and properties of airborne particles in the Mexico City subway system. *Atmospheric Environment*, *49*, 284–293. https://doi.org/10.1016/j.atmosenv.2011.11.038

Munster, V. J., Feldmann, F., Williamson, B. N., van Doremalen, N., Pérez-Pérez, L., Schulz, J., Meade-White, K., Okumura, A., Callison, J., Brumbaugh, B., Avanzato, V. A., Rosenke, R., Hanley, P. W., Saturday, G., Scott, D., Fischer, E. R., & de Wit, E. (2020). Respiratory disease in rhesus macaques inoculated with SARS-CoV-2. *Nature*, *585*(7824), 268–272. https://doi.org/10.1038/s41586-020-2324-7

Murruni, L. G., Solanes, V., Debray, M., Kreiner, A. J., Davidson, J., Davidson, M., Vázquez, M., & Ozafrán, M. (2009). Concentrations and elemental composition of particulate matter in the Buenos Aires underground system. *Atmospheric Environment*, *43*(30), 4577–4583. https://doi.org/10.1016/j.atmosenv.2009.06.025

Nagl, C., & Spangl, W. (2020). *Umweltbundesamt Report-0713 - JAHRESBERICHT DER LUFTGÜTEMESSUNGEN IN ÖSTERREICH 2019*. https://www.umweltbundesamt.de/abfallaufkommen#textpart-1

Nazelle, A. De, Bode, O., & Pablo, J. (2017). Comparison of air pollution exposures in active vs . passive travel modes in European cities : A quantitative review. *Environment International*, *99*, 151–160. https://doi.org/10.1016/j.envint.2016.12.023

Nieuwenhuijsen, M. J., Gómez-Perales, J. E., & Colvile, R. N. (2007). Levels of particulate air pollution, its elemental composition, determinants and health effects in metro systems. *Atmospheric Environment*, *41*(37), 7995–8006. https://doi.org/10.1016/j.atmosenv.2007.08.002

No, I. Z. A. D. P., Giménez-nadal, J. I., Velilla, J., Giménez-nadal, J. I., & Velilla, J. (2020). *Trends in Commuting Time of European Workers : A Cross-Country Analysis Trends in Commuting Time of European Workers : A Cross-Country Analysis*. *12916*.

Noll, K. E., Lin, J. J., Noll, K. E., Holsen, T. M., Lin, J. J., Noll, K. E., Holsen, T. M., Deposition, D., Lin, J. J., Noll, K. E., & Holsen, T. M. (1994). Dry Deposition Velocities as a Function of Particle Size in the Ambient Atmosphere. *Aerosol Science and Technology*, *6826*(3), 239–252. https://doi.org/10.1080/02786829408959680

Onat, B., & Stakeeva, B. (2014). Assessment of fine particulate matters in the subway system of Istanbul. *Indoor and Built Environment*, *23*(4), 574–583. https://doi.org/10.1177/1420326X12464507

Ozgen, S., Ripamonti, G., Malandrini, A., S. Ragettli, M., & Lonati, G. (2016). Particle number and mass exposure concentrations by commuter transport modes in Milan, Italy. *AIMS Environmental Science*, *3*(2), 168–184. https://doi.org/10.3934/environsci.2016.2.168

Pachon, J. E., Weber, R. J., Zhang, X., Mulholland, J. A., Russell, A. G., & Pachon, J. E. (2013). Revising the use of potassium (K) in the source apportionment of PM2.5. *Atmospheric Pollution Research*, *4*(1), 14–21. https://doi.org/10.5094/APR.2013.002

Pan, S., Du, S., Wang, X., Zhang, X., Xia, L., Liu, J., Pei, F., & Wei, Y. (2019). Analysis and interpretation of the particulate matter (PM10 and PM2.5) concentrations at the subway stations in Beijing, China. *Sustainable Cities and Society*, *45*(November 2018), 366–377. https://doi.org/10.1016/j.scs.2018.11.020

Pan, S., Fan, L., Liu, J., Xie, J., Sun, Y., Cui, N., Zhang, L., & Zheng, B. (2013). *A Review of the Piston Effect in Subway Stations*. *2013*. https://doi.org/10.1155/2013/950205

Park, D., Lee, T., Hwang, D., Jung, W., Lee, Y., Cho, K. C., Kim, D., & Lee, K. (2014). Identification of the sources of PM10 in a subway tunnel using positive matrix factorization. *Journal of the Air and Waste Management Association*, *64*(12), 1361–1368. https://doi.org/10.1080/10962247.2014.950766

Park, D. U., & Ha, K. C. (2008). Characteristics of PM10, PM2.5, CO2 and CO monitored in interiors and platforms of subway train in Seoul, Korea. *Environment International*, *34*(5), 629–634. https://doi.org/10.1016/j.envint.2007.12.007

Pathak, P., & Gupta, D. K. (2020). *Strontium Contamination in the Environment*. Springer. https://doi.org/10.1007/978-3-030-15314-4

Patwa, A., & Shah, A. (2015). Anatomy and physiology of respiratory system relevant to anaesthesia. *Indian Journal of Anaesthesia*, 533–541. https://doi.org/10.4103/0019-5049.165849

Pfeifer, G. D., Harrison, R. M., & Lynam, D. R. (1999). Personal exposures to airborne metals in London taxi drivers and office workers in 1995 and 1996. *Science of the Total Environment*, *235*(1–3), 253–260. https://doi.org/10.1016/S0048-9697(99)00201-6

Pope, C. A. (2000). Epidemiology of Fine Particulate Air Pollution and Human Health : Biologic Mechanisms and Who ' s at Risk ? *Environmental Health Perspectives*, *108 Suppl*(October), 713–723. https://doi.org/10.1289/ehp.00108s4713

Pope, C. A., & Dockery, D. W. (2006). Health Effects of Fine Particulate Air Pollution : Lines that Connect Health Effects of Fine Particulate Air Pollution : Lines that Connect. *Journal of the Air & Waste Management Association*, *56*(6), 709–742. https://doi.org/10.1080/10473289.2006.10464485

Posselt, K. P., Neuberger, M., & Köhler, D. (2019). Fine and ultrafine particle exposure during commuting by subway in Vienna. *Wiener Klinische Wochenschrift*, *131*(15–16), 374–380. https://doi.org/10.1007/s00508-019-1516-3

Pupajim, Gyver, M., Rootystep, & Merry. (2017). *My Research*. The Shift, STAND HIGH RECORDS.

Qiao, T., Xiu, G., Zheng, Y., Yang, J., & Wang, L. (2015). Characterization of PM and microclimate in a Shanghai subway tunnel, China. *Procedia Engineering*, *102*, 1226–1232. https://doi.org/10.1016/j.proeng.2015.01.250

Qiao, T., Xiu, G., Zheng, Y., Yang, J., Wang, L., Yang, J., & Huang, Z. (2015). Preliminary investigation of PM1, PM2.5, PM10 and its metal elemental composition in tunnels at a subway station in Shanghai, China. *Transportation Research Part D: Transport and Environment*, *41*, 136–146. https://doi.org/10.1016/j.trd.2015.09.013

Querol, X., Moreno, T., Karanasiou, A., Reche, C., Alastuey, A., Viana, M., Font, O., Gil, J., de Miguel, E., Capdevila, M., & Miguel, E. De. (2012). Variability of levels and composition of PM 10 and PM 2.5 in the Barcelona metro system. *Atmospheric Chemistry and Physics*, *12*(11), 5055–5076. https://doi.org/10.5194/acp-12-5055-2012

Ramos, C. A., Wolterbeek, H. T., & Almeida, S. M. (2016). Air pollutant exposure and inhaled dose during urban commuting: a comparison between cycling and motorized modes. *Air Quality, Atmosphere and Health*, *9*(8), 867–879. https://doi.org/10.1007/s11869-015-0389-5

Ramos, M. J., Vasconcelos, A., & Faria, M. (2015). Comparison of particulate matter inhalation for users of different transport modes in Lisbon. *Transportation Research Procedia*, *10*(July), 433–442. https://doi.org/10.1016/j.trpro.2015.09.093

Raut, J. C., Chazette, P., & Fortain, A. (2009). Link between aerosol optical, microphysical and chemical measurements in an underground railway station in Paris. *Atmospheric Environment*, *43*(4), 860–868. https://doi.org/10.1016/j.atmosenv.2008.10.038

Reche, C., Moreno, T., Martins, V., Minguillón, M. C., Jones, T., de Miguel, E., Capdevila, M., Centelles, S., Querol, X., Miguel, E. De, Reche, C., Moreno, T., Martins, V., Minguillón, M. C., Capdevila, M., Centelles, S., & Querol, X. (2017). Factors controlling particle number concentration and size at metro stations. *Atmospheric Environment*, *156*, 169–181. https://doi.org/10.1016/j.atmosenv.2017.03.002

Reimann, C., & Caritat, P. De. (2005). *Distinguishing between natural and anthropogenic sources for elements in the environment : regional geochemical surveys versus enrichment factors*. *337*, 91–107. https://doi.org/10.1016/j.scitotenv.2004.06.011

Ripanucci, G., Grana, M., Vicentini, L., Magrini, A., & Bergamaschi, A. (2006). Dust in the underground railway tunnels of an Italian town. *Journal of Occupational and Environmental Hygiene*, *3*(1), 16–25. https://doi.org/10.1080/15459620500444004

Ryu, K., & Juraeva, M. (2012). Ventilation Efficiency in the Subway Environment for the Indoor Air Quality. *International Journal of Computer and Systems Engineering*, *6*(3), 34–38. http://scholar.google.com/scholar?hl=en&btnG=Search&q=intitle:Ventilation+Efficiency+in+the+Subway+Environment+for+the+Indoor+Air+Quality#0

Şahin, Ü. A., Onat, B., Stakeeva, B., Ceran, T., & Karim, P. (2012). PM10 concentrations and the size distribution of Cu and Fe-containing particles in Istanbul's subway system. *Transportation Research Part D: Transport and Environment*, *17*(1), 48–53. https://doi.org/10.1016/j.trd.2011.09.003

Salma, I., Weidinger, T., & Maenhaut, W. (2007). Time-resolved mass concentration, composition and sources of aerosol particles in a metropolitan underground railway station. *Atmospheric Environment*, *41*(37), 8391–8405. https://doi.org/10.1016/j.atmosenv.2007.06.017

Schober, P., Boer, C., & Schwarte, L. A. (2018). *Correlation Coefficients: Appropriate Use and Interpretation*. *XXX*(Xxx), 1–6. https://doi.org/10.1213/ANE.0000000000002864

Seaton, A., Cherrie, J., Dennekamp, M., Donaldson, K., Hurley, J. F., & Tran, C. L. (2005). The London Underground: Dust and hazards to health. *Occupational and Environmental Medicine*, *62*(6), 355–362. https://doi.org/10.1136/oem.2004.014332

Shafer, M. M., Toner, B. M., Overdier, J. T., Schauer, J. J., Fakra, S. C., Hu, S., Herner, J. D., & Ayala, A. (2012). Chemical speciation of vanadium in particulate matter emitted from diesel vehicles and urban atmospheric aerosols. *Environmental Science and Technology*, *46*(1), 189–195. https://doi.org/10.1021/es200463c

Slezakova, K., Reis, M. A., Pereira, M. C., & Alvim-Ferraz, M. C. (2007). Influence of traffic on the elemental composition of PM10 and PM2.5 in Oporto region. *WIT Transactions on Ecology and the Environment*, *101*, 59–68. https://doi.org/10.2495/AIR070061

Smichowski, P. (2008). *Antimony in the environment as a global pollutant : A review on analytical methodologies for its determination in atmospheric aerosols*. *75*, 2–14. https://doi.org/10.1016/j.talanta.2007.11.005

Son, Y., Jeon, J. S., Lee, H. J., Ryu, I. C., & Kim, J. C. (2014). Installation of platform screen doors and their impact on indoor air quality: Seoul subway trains. *Journal of the Air and Waste Management Association*, *64*(9), 1054–1061. https://doi.org/10.1080/10962247.2014.923350

Son, Y., Salama, A., Jeong, H. S., Kim, S., Jeong, J. H., Lee, J., Sunwoo, Y., & Kim, J. C. (2013). The effect of platform screen doors on PM10 levels in a subway station and a trial to reduce PM10 in tunnels. *Asian Journal of Atmospheric Environment*, *7*(1), 38–47. https://doi.org/10.5572/ajae.2013.7.1.038

Spangl, W. (2018). *Luftgütemessungen und meteorologische Messungen*. Umweltbundesamt GmbH.

Spangl, W., & Nagl, C. (2018). *Luftgütemessungen in Österreich*.

Strasser, G., Hiebaum, S., & Neuberger, M. (2018). Commuter exposure to fine and ultrafine particulate matter in Vienna. *Wiener Klinische Wochenschrift*, *130*(1–2), 62–69. https://doi.org/10.1007/s00508-017-1274-z

Suárez, L., Mesías, S., Iglesias, V., Silva, C., Cáceres, D. D., & Ruiz-Rudolph, P. (2014). Personal exposure to particulate matter in commuters using different transport modes (bus, bicycle, car and subway) in an assigned route in downtown Santiago, Chile. *Environmental Sciences: Processes and Impacts*, *16*(6), 1309–1317. https://doi.org/10.1039/c3em00648d

The European Commission. (2004). Directive 2004/107/EC of the European Parliament and of the Council of 15 December 2004 relating to arsenic, cadmium, mercury, nickel and polycyclic aromatic hydrocarbons in ambient air. *Official Journal of the European Union*, *1882*.

The European Commission. (2008). DIRECTIVE 2008/50/EC OF THE EUROPEAN PARLIAMENT AND OF THE COUNCIL. *Official Journal of the European Union.*, *August*, 1–62.

The European Commission. (2013). *Impact Assessment of the clean air policy package*.

The European Commission. (2015). Commission Directive (EU) 2015/1480 of 28 August 2015 amending several annexes to Directives 2004/107/EC and 2008/50/EC of the European Parliament and of the Council laying down the rules concerning reference methods, data validation and location of sampl. *Official Journal of the European Union*, *219*, 4–11.

Tirachini, A., & Cats, O. (2020). COVID-19 and public transportation: Current assessment, prospects, and research needs. *Journal of Public Transportation*, *22*(1), 1–34. https://doi.org/10.5038/2375-0901.22.1.1

United Nations. (2015). *World urbanization prospects: The 2014 revision*.

Viana, M., Kuhlbusch, T. A. J., Querol, X., Alastuey, A., Harrison, R. M., Hopke, P. K., Winiwarter, W., Vallius, M., Szidat, S., Prévôt, A. S. H., Hueglin, C., Bloemen, H., Wåhlin, P., Vecchi, R., Miranda, A. I., Kasper-Giebl, A., Maenhaut, W., & Hitzenberger, R. (2008). Source apportionment of particulate matter in Europe: A review of methods and results. *Journal of Aerosol Science*, *39*(10), 827–849. https://doi.org/10.1016/j.jaerosci.2008.05.007

Vitrano, C. (2020). COVID-19 and Public Transportation. In *K2 WORKING PAPER*. https://scholarcommons.usf.edu/jpt/vol22/iss1/1/

Wang, B. Q., Liu, J. F., Ren, Z. H., & Chen, R. H. (2016). Concentrations, properties, and health risk of PM2.5 in the Tianjin City subway system. *Environmental Science and Pollution Research*, *23*(22), 22647–22657. https://doi.org/10.1007/s11356-016-7444-0

Wang, X. R., & Oliver Gao, H. (2011). Exposure to fine particle mass and number concentrations in urban transportation environments of New York City. *Transportation Research Part D: Transport and Environment*, *16*(5), 384–391. https://doi.org/10.1016/j.trd.2011.03.001

Wen, Y., Leng, J., Shen, X., Han, G., Sun, L., & Yu, F. (2020). Environmental and health effects of ventilation in subway stations: A literature review. In *International Journal of Environmental Research and Public Health* (Vol. 17, Issue 3). https://doi.org/10.3390/ijerph17031084

Wiener Linien. (2018). *40 Facts zu 40 Jahre Wiener U-Bahn*. https://blog.wienerlinien.at/40-facts-zu-40-jahre-wiener-u-bahn/

Wiener Linien. (2020). *Das größte Verkehrsnetz Österreichs*. https://www.wienerlinien.at/media/files/2015/betriebsangaben_2014_151135.pdf

World Bank and Institute for Health Metrics and Evaluation. (2016). *The Cost of Air Pollution: Strengthening the Economic Case for Action*.

World Health Organization. (2005). Air quality guidelines for particulate matter, ozone, nitrogen dioxide and sulfur dioxide. *WHO Air Quality Guidelines*, *195*(2), 491–498.

World Health Organization. (2013). Health Effects of Particulate Matter. *World Health Organization Regional Office for Europe Copenhagen*, *91*(2), 106–113. https://doi.org/10.3904/kjm.2016.91.2.106

World Health Organization. (2016). *Ambient air pollution: A global assessment of exposure and burden of disease*.

Xu, B., & Hao, J. (2017). Air quality inside subway metro indoor environment worldwide : A review. *Environment International*, *107*(March), 33–46. https://doi.org/10.1016/j.envint.2017.06.016

Yang, F., Kaul, D., Chun, K., Westerdahl, D., Sun, L., Ho, K., Tian, L., Brimblecombe, P., & Ning, Z. (2015). *Heterogeneity of passenger exposure to air pollutants in public transport microenvironments*. *109*, 42–51. https://doi.org/10.1016/j.atmosenv.2015.03.009

Ye, X., Lian, Z., Jiang, C., Zhou, Z., & Chen, H. (2010). Investigation of indoor environmental quality in Shanghai metro stations, China. *Environmental Monitoring and Assessment*, *167*(1–4), 643–651. https://doi.org/10.1007/s10661-009-1080-9

Yongming, H., Peixuan, D., Junji, C., & Posmentier, E. S. (2006). *Multivariate Analysis of Heavy Metal Contamination in Urban Dusts of Multivariate analysis of heavy metal contamination in urban dusts of Xi ' an , Central China*. *March*. https://doi.org/10.1016/j.scitotenv.2005.02.026

Youn, K., Shin, Y., Man, Y., Min, C., & Nyon, C. (2008). *Spatial distribution of particulate matter (PM 10 and PM 2 . 5) in Seoul Metropolitan Subway stations*. *154*, 440–443. https://doi.org/10.1016/j.jhazmat.2007.10.042

Zhu, N., Zhang, D., Wang, W., Li, X., Yang, B., Song, J., Zhao, X., Huang, B., Shi, W., Lu, R., Niu, P., Zhan, F., Ma, X., Wang, D., Xu, W., Wu, G., Gao, G. F., & Tan, W. (2020). A Novel Coronavirus from Patients with Pneumonia in China, 2019. *New England Journal of Medicine*, *382*(8), 727–733. https://doi.org/10.1056/nejmoa2001017

Zuurbier, M., Hoek, G., Oldenwening, M., Lenters, V., Meliefste, K., van den Hazel, P., & Brunekreef, B. (2010). Commuters' exposure to particulate matter air pollution is affected by mode of transport, fuel type, and route. *Environmental Health Perspectives*, *118*(6), 783–789. https://doi.org/10.1289/ehp.0901622

Chapter 6) Appendix

6.1 Gravimetric PM_{10} Mass concentrations obtained with the LVS

Table 6.1 Overview of the results obtained by the LVS measurements at tunnel Karlsplatz U1

ID	Sampling period	Date	Resulting weight	Sample volume	PM_{10} mass concentration
			[µg]	[m³]	[µg/m³]
TU-KP-1	*4-8h*	11.11.19	3275	9.16	358
TU-KP-2	*8-12h*	11.11.19	4925	9.16	538
TU-KP-3	*12-16h*	11.11.19	4835	9.17	527
TU-KP-4	*16-20h*	11.11.19	3875	9.17	423
TU-KP-5	*20-24h*	12.11.19	2820	9.16	308
TU-KP-6	*0-4h*	12.11.19	735	9.17	80,2
TU-KP-7	*4-8h*	12.11.19	2665	9.16	291
TU-KP-8	*8-12h*	12.11.19	4065	9.16	444
TU-KP-9	*12-16h*	12.11.19	3555	9.17	388
TU-KP-10	*16-20h*	12.11.19	3450	9.15	377
TU-KP-11	*20-24h*	12.11.19	2090	9.16	228
TU-KP-12	*0-4h*	13.11.19	420	9.15	45,9
TU-KP-13	*4-8h*	13.11.18	2205	9.17	240
TU-KP-14	*8-12h*	13.11.19	3765	9.16	411
TU-KP-15	*12-16h*	13.11.19	3810	9.17	415
TU-KP-16	*16-20h*	13.11.19	3480	9.17	380
				total	341
		Mean		**operation**	381
				reduced operation	63.0

Table 6.2 Overview of the results obtained by the LVS measurements at tunnel Rochusgasse U3

ID	Sampling period	Date	Resulting weight	Sample volume	PM_{10} mass concentration
			[µg]	[m³]	[µg/m³]
TU-RO-1	*4-8h*	15.11.19	945	9.19	103
TU-RO-2	*8-12h*	15.11.19	1365	9.16	149
TU-RO-3	*12-16h*	15.11.19	1465	9.17	160
TU-RO-4	*16-20h*	15.11.19	1475	9.16	161
TU-RO-5	*20-24h*	15.11.19	780	9.17	85.1
TU-RO-6	*0-4h*	16.11.19	520	9.17	56.7
TU-RO-7	*4-8h*	16.11.19	600	9.17	65.4
TU-RO-8	*8-12h*	16.11.19	1045	9.16	114
TU-RO-9	*12-16h*	16.11.19	820	9.17	89.4
TU-RO-10	*16-20h*	16.11.19	810	9.16	88.4
TU-RO-11	*20-24h*	16.11.19	700	9.15	76.5
TU-RO-12	*0-4h*	17.11.19	510	9.16	55.7
TU-RO-13	*4-8h*	17.11.19	580	9.17	63.3
TU-RO-14	*8-12h*	17.11.19	775	9.16	84.6
				total	96.6
		Mean		**operation**	103
				reduced operation	56.2

Table 6.3 Overview of the results obtained by the LVS measurements at tunnel Praterstern U2

ID	Sampling period	Date	Resulting weight	Sample volume	PM_{10} mass concentration
			[µg]	[m³]	[µg/m³]
TU-PR-1	*4-8h*	18.02.20	1190	9.19	129
TU-PR-2	*8-12h*	18.02.20	1870	9.17	204
TU-PR-3	*12-16h*	18.02.20	1880	9.16	205
TU-PR-4	*16-20h*	18.02.20	2590	9.16	283
TU-PR-5	*20-24h*	18.02.20	1230	9.17	134
TU-PR-6	*0-4h*	19.02.20	190	9.17	20.7
TU-PR-7	*4-8h*	19.02.20	1575	9.16	172
TU-PR-8	*8-12h*	19.02.20	2810	9.17	306
TU-PR-9	*12-16h*	19.02.20	2330	9.17	254
TU-PR-10	*16-20h*	19.02.20	2820	9.17	308
TU-PR-11	*20-24h*	19.02.20	1480	9.16	162
TU-PR-12	*0-4h*	20.02.20	175	9.16	19.1
TU-PR-13	*4-8h*	20.02.20	1955	9.16	213
TU-PR-14	*8-12h*	20.02.20	2620	9.17	286
Mean				**total**	193
				operation	221
				reduced operation	19.9

Table 6.4 Overview of the results obtained by the LVS measurements at platform Karlsplatz U1

ID	Sampling period	Date	Resulting weight	Sample volume	PM_{10} mass concentration
			[µg]	[m³]	[µg/m³]
PL-KP-1	*12-16h*	4.11.19	1905	9.2	207
PL-KP-2	*16-20h*	4.11.19	2205	9.15	241
PL-KP-3	*20-24h*	4.11.19	1205	9.17	131
PL-KP-4	*0-4h*	5.11.19	280	9.16	30.6
PL-KP-5	*4-8h*	5.11.19	1245	9.16	136
PL-KP-6	*8-12h*	5.11.19	1925	9.16	210
PL-KP-7	*12-16h*	5.11.19	1575	9.16	172
PL-KP-8	*16-20h*	5.11.19	2050	9.17	224
PL-KP-9	*20-24h*	5.11.19	1125	9.16	123
PL-KP-10	*0-4h*	6.11.19	305	9.18	33.2
PL-KP-11	*4-8h*	6.11.19	1390	9.17	152
PL-KP-12	*8-12h*	6.11.19	2920	9.16	319
PL-KP-13	*12-16h*	6.11.19	2705	9.15	296
PL-KP-14	*16-20h*	6.11.19	2905	9.16	317
Mean				**total**	185
				operation	211
				reduced operation	31.9

Table 6.5 Overview of the results obtained by the LVS measurements at tunnel Rochusgasse U3

ID	Sampling period	Date	Resulting weight	Sample volume	PM_{10} mass concentration
			[µg]	[m³]	[µg/m³]
PL-RO-1	*12-16h*	19.11.19	3300	9.2	359
PL-RO-2	*16-20h*	19.11.19	2800	9.17	305
PL-RO-3	*20-24h*	19.11.19	1165	9.17	127
PL-RO-4	*0-4h*	20.11.19	365	9.17	39.8
PL-RO-5	*4-8h*	20.11.19	1560	9.17	170
PL-RO-6	*8-12h*	20.11.19	2790	9.16	305
PL-RO-7	*12-16h*	20.11.19	2460	9.17	268
PL-RO-8	*16-20h*	20.11.19	2670	9.17	291
PL-RO-9	*20-24h*	20.11.19	1055	9.16	115
PL-RO-10	*0-4h*	21.11.19	325	9.17	35.4
PL-RO-11	*4-8h*	21.11.19	1410	9.17	154
PL-RO-12	*8-12h*	21.11.19	2655	9.17	290
PL-RO-13	*12-16h*	21.11.19	2545	9.16	278
PL-RO-14	*16-20h*	21.11.19	2710	9.17	296
				total	217
	Mean			**operation**	246
				reduced operation	37.6

Table 6.6 Overview of the results obtained by the LVS measurements at platform Stubentor U3

ID	Sampling period	Date	Resulting weight	Sample volume	PM_{10} mass concentration
			[µg]	[m³]	[µg/m³]
PL-ST-1	*12-16h*	28.10.19	1565	9.19	170
PL-ST-2	*16-20h*	28.10.19	1835	9.16	200
PL-ST-3	*20-24h*	28.10.19	750	9.17	81.8
PL-ST-4	*0-4h*	29.10.19	300	9.16	32.8
PL-ST-5	*4-8h*	29.10.19	820	9.16	89.5
PL-ST-6	*8-12h*	29.10.19	1740	9.17	190
PL-ST-7	*12-16h*	29.10.19	1790	9.16	195
PL-ST-8	*16-20h*	29.10.19	1465	9.16	160
PL-ST-9	*20-24h*	29.10.19	760	9.17	82.9
PL-ST-10	*0-4h*	30.10.19	225	9.17	24.5
PL-ST-11	*4-8h*	30.10.19	890	9.17	97.1
PL-ST-12	*8-12h*	30.10.19	1690	9.16	185
PL-ST-13	*12-16h*	30.10.19	1710	9.16	187
PL-ST-14	*16-20h*	30.10.19	1445	9.16	158
				total	132
	Mean			**operation**	150
				reduced operation	28.6

6.2 Results of the IC analysis

6.2.1.1 Tunnel Karlsplatz U1

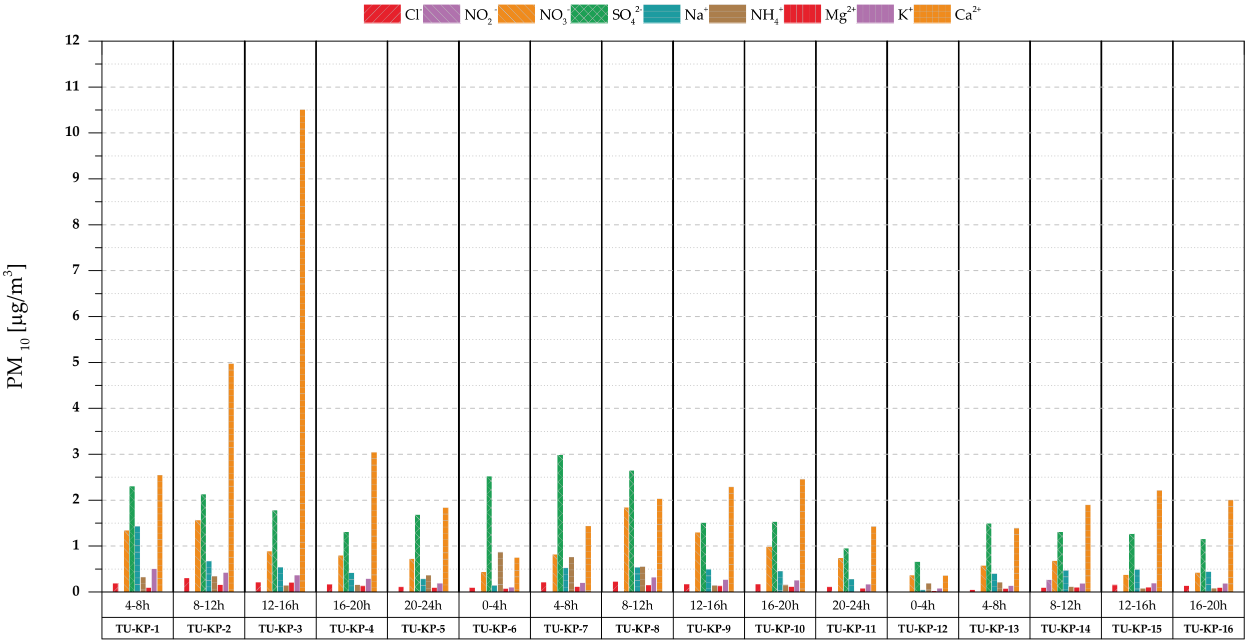

ID	Sampling period	Cl^-	NO_2^-	NO_3^-	SO_4^{2-}	Na^+	NH_4^+	Mg^{2+}	K^+	Ca^{2+}
						[µg/m³]				
TU-KP-1	*4-8h*	0.19	<LOD	1.35	2.31	1.44	0.33	0.10	0.51	2,55
TU-KP-2	*8-12h*	0.31	<LOD	1.57	2.14	0.68	0.35	0.17	0.43	4,98
TU-KP-3	*12-16h*	0.22	<LOD	0.90	1.79	0.55	0.15	0.21	0.37	10,51
TU-KP-4	*16-20h*	0.17	<LOD	0.80	1.32	0.42	0.17	0.14	0.30	3,05
TU-KP-5	*20-24h*	0.11	<LOD	0.73	1.69	0.29	0.37	0.10	0.19	1,84
TU-KP-6	*0-4h*	0.10	<LOD	0.44	2.53	0.15	0.87	0.08	0.11	0,76
TU-KP-7	*4-8h*	0.22	<LOD	0.82	2.99	0.53	0.77	0.12	0.20	1,44
TU-KP-8	*8-12h*	0.23	<LOD	1.85	2.66	0.54	0.56	0.15	0.32	2,04
TU-KP-9	*12-16h*	0.17	<LOD	1.30	1.51	0.50	0.15	0.14	0.27	2,30
TU-KP-10	*16-20h*	0.17	<LOD	0.99	1.53	0.46	0.16	0.12	0.26	2,46
TU-KP-11	*20-24h*	0.12	<LOD	0.75	0.96	0.28	<LOD	0.09	0.17	1,43
TU-KP-12	*0-4h*	<LOD	<LOD	0.37	0.67	0.05	0.19	0.03	0.08	0,36
TU-KP-13	*4-8h*	0.05	<LOD	0.58	1.50	0.41	0.22	0.08	0.14	1,40
TU-KP-14	*8-12h*	0.10	0.27	0.69	1.32	0.48	0.12	0.11	0.19	1,90
TU-KP-15	*12-16h*	0.16	<LOD	0.38	1.27	0.49	0.09	0.11	0.20	2,22
TU-KP-16	*16-20h*	0.14	<LOD	0.43	1.16	0.45	0.09	0.10	0.19	2,01
PM_{10} mean of total sampling period		**0.15**	**<LOD**	**0.87**	**1.71**	**0.48**	**0.29**	**0.11**	**0.25**	**2.58**
PM_{10} mean of operating period		**0.17**	**<LOD**	**0.94**	**1.72**	**0.54**	**0.25**	**0.12**	**0.27**	**2.87**
PM_{10} mean of downtime		**0.05**	**<LOD**	**0.40**	**1.60**	**0.10**	**0.53**	**0.05**	**0.10**	**0.56**

6.2.1.2 Tunnel Rochusgasse U3

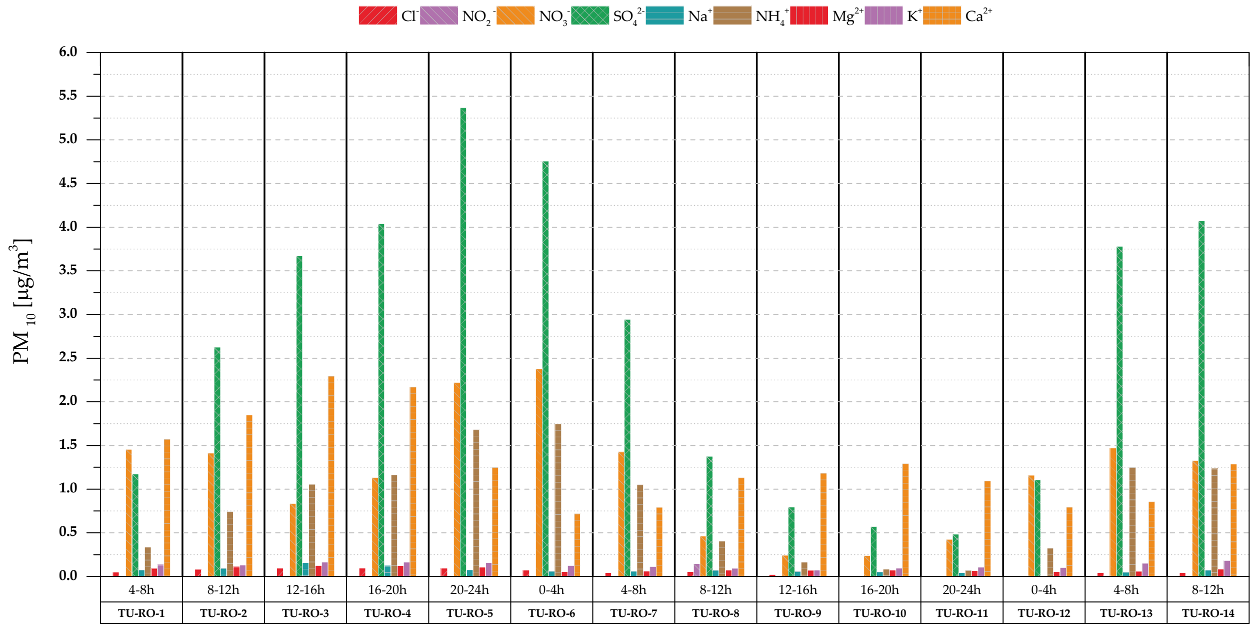

ID	Sampling period	Cl^-	NO_2^-	NO_3^-	SO_4^{2-}	Na^+	NH_4^+	Mg^{2+}	K^+	Ca^{2+}
						[µg/m³]				
TU-RO-1	*4-8h*	0.05	<LOD	1.45	1.17	0.07	0.34	0.09	0.13	1,57
TU-RO-2	*8-12h*	0.08	<LOD	1.41	2.62	0.09	0.74	0.11	0.13	1,85
TU-RO-3	*12-16h*	0.09	<LOD	0.83	3.67	0.16	1.06	0.12	0.16	2,29
TU-RO-4	*16-20h*	0.09	<LOD	1.13	4.04	0.12	1.16	0.12	0.16	2,17
TU-RO-5	*20-24h*	0.10	<LOD	2.22	5.36	0.08	1.68	0.10	0.16	1,25
TU-RO-6	*0-4h*	0.07	<LOD	2.38	4.75	0.06	1.75	0.05	0.12	0,72
TU-RO-7	*4-8h*	0.04	<LOD	1.43	2.94	0.06	1.05	0.06	0.11	0,79
TU-RO-8	*8-12h*	0.05	0.14	0.46	1.37	0.07	0.41	0.07	0.09	1,13
TU-RO-9	*12-16h*	0.02	<LOD	0.24	0.79	0.06	0.16	0.07	0.07	1,18
TU-RO-10	*16-20h*	<LOD	<LOD	0.24	0.57	0.05	0.08	0.07	0.09	1,29
TU-RO-11	*20-24h*	<LOD	<LOD	0.42	0.48	0.04	0.07	0.06	0.11	1,09
TU-RO-12	*0-4h*	<LOD	<LOD	1.16	1.11	<LOD	0.32	0.05	0.10	0,79
TU-RO-13	*4-8h*	0.04	<LOD	1.47	3.78	0.05	1.25	0.06	0.15	0,85
TU-RO-14	*8-12h*	0.04	<LOD	1.33	4.07	0.07	1.23	0.08	0.18	1,29
PM_{10} mean of total sampling period		**0.05**	**<LOD**	**1.15**	**2.62**	**0.07**	**0.81**	**0.08**	**0.13**	**1.30**
PM_{10} mean of operating period		**0.05**	**<LOD**	**1.05**	**2.57**	**0.08**	**0.77**	**0.08**	**0.13**	**1.40**
PM_{10} mean of downtime		**0.04**	**<LOD**	**1.77**	**2.93**	**0.04**	**1.04**	**0.05**	**0.11**	**0.75**

6.2.1.3 Tunnel Praterstern U2

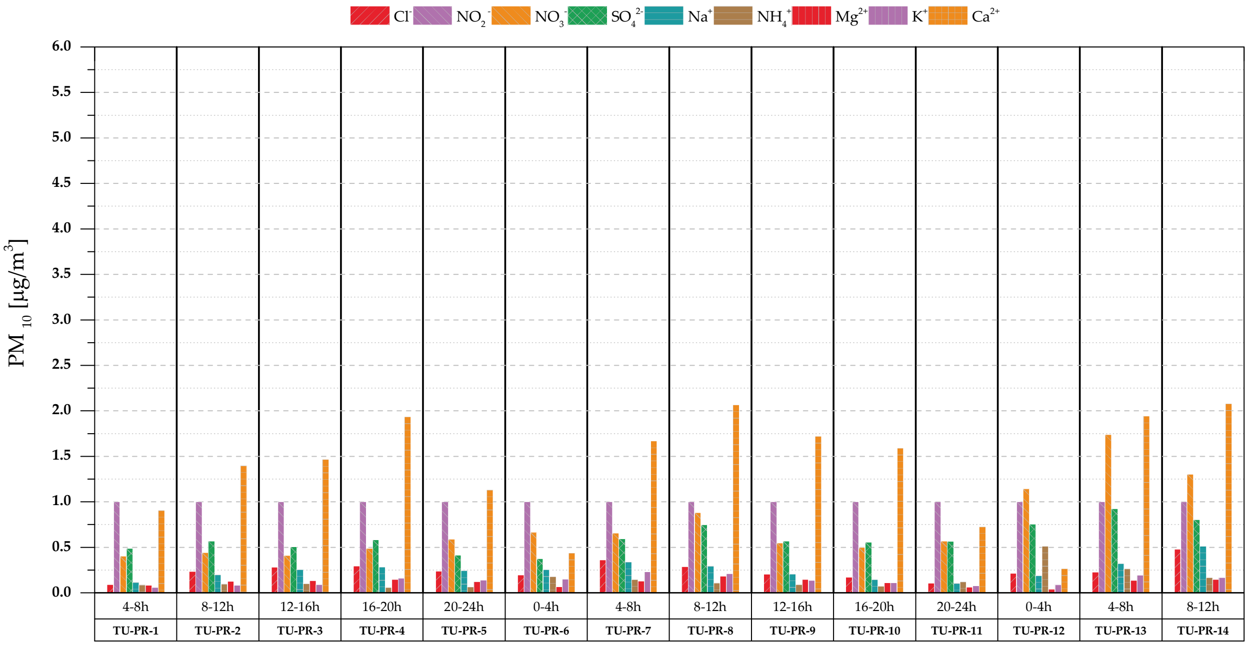

ID	Sampling period	Cl^-	NO_2^-	NO_3^-	SO_4^{2-}	Na^+	NH_4^+	Mg^{2+}	K^+	Ca^{2+}
						[µg/m³]				
TU-PR-1	*4-8h*	0.09	<LOD	0.40	0.49	0.11	0.09	0.08	0.06	0,91
TU-PR-2	*8-12h*	0.23	<LOD	0.44	0.57	0.20	0.10	0.12	0.08	1,40
TU-PR-3	*12-16h*	0.28	<LOD	0.41	0.50	0.26	0.10	0.13	0.09	1,47
TU-PR-4	*16-20h*	0.29	<LOD	0.49	0.58	0.28	0.06	0.15	0.16	1,93
TU-PR-5	*20-24h*	0.24	<LOD	0.59	0.41	0.24	0.06	0.12	0.14	1,13
TU-PR-6	*0-4h*	0.20	<LOD	0.66	0.37	0.25	0.18	0.07	0.15	0,44
TU-PR-7	*4-8h*	0.36	<LOD	0.66	0.59	0.34	0.15	0.13	0.23	1,67
TU-PR-8	*8-12h*	0.29	<LOD	0.88	0.75	0.29	0.11	0.18	0.21	2,07
TU-PR-9	*12-16h*	0.20	<LOD	0.55	0.57	0.21	0.09	0.15	0.14	1,72
TU-PR-10	*16-20h*	0.17	<LOD	0.50	0.55	0.15	0.07	0.11	0.11	1,59
TU-PR-11	*20-24h*	0.10	<LOD	0.57	0.56	0.10	0.12	0.06	0.08	0,73
TU-PR-12	*0-4h*	0.21	<LOD	1.14	0.75	0.19	0.51	0.04	0.09	0,26
TU-PR-13	*4-8h*	0.23	<LOD	1.74	0.92	0.32	0.26	0.14	0.19	1,94
TU-PR-14	*8-12h*	0.48	<LOD	1.30	0.80	0.51	0.17	0.15	0.17	2,08
PM_{10} mean of total sampling period		**0.24**	**<LOD**	**0.74**	**0.60**	**0.25**	**0.15**	**0.12**	**0.13**	**1.38**
PM_{10} mean of operating period		**0.25**	**<LOD**	**0.71**	**0.61**	**0.25**	**0.11**	**0.13**	**0.14**	**1.55**
PM_{10} mean of downtime		**0.20**	**<LOD**	**0.90**	**0.56**	**0.22**	**0.35**	**0.05**	**0.12**	**0.35**

6.2.1.4 Platform Karlsplatz U1

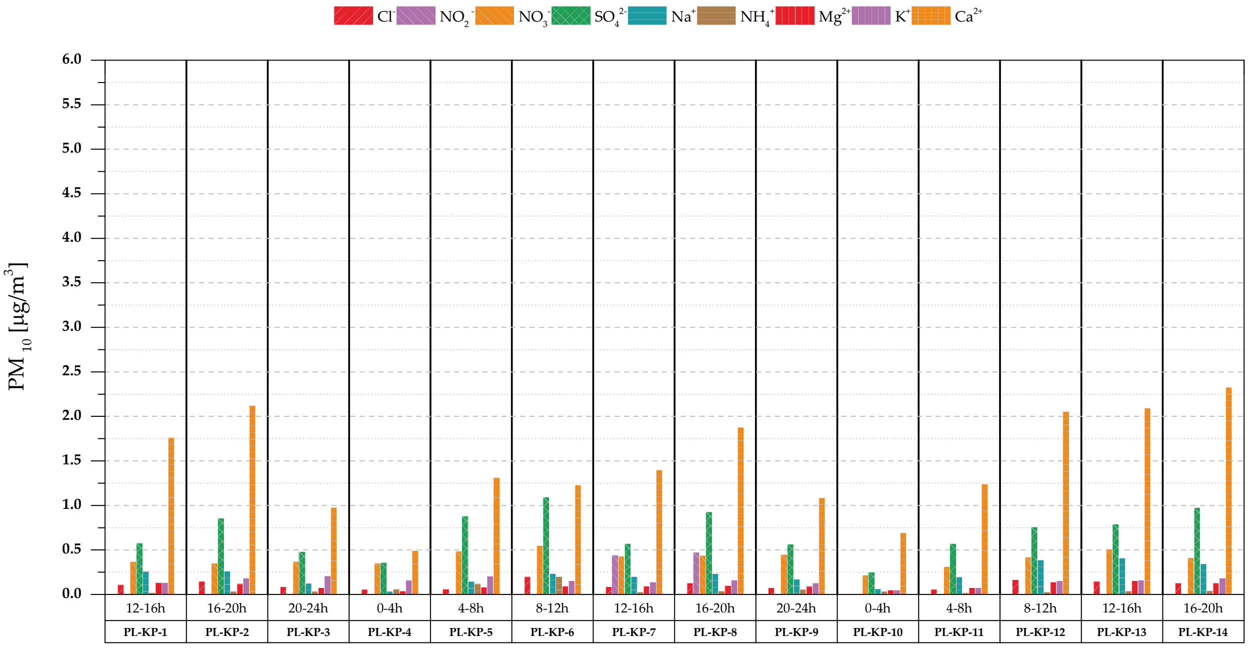

ID	Sampling period	Cl^-	NO_2^-	NO_3^-	SO_4^{2-}	Na^+	NH_4^+	Mg^{2+}	K^+	Ca^{2+}
						[µg/m³]				
PL-KP-1	*12-16h*	0.11	<LOD	0.37	0.58	0.26	0.02	0.13	0.13	1,76
PL-KP-2	*16-20h*	0.15	<LOD	0.35	0.86	0.26	0.04	0.12	0.19	2,12
PL-KP-3	*20-24h*	0.08	<LOD	0.37	0.48	0.13	0.04	0.08	0.21	0,98
PL-KP-4	*0-4h*	0.06	<LOD	0.35	0.36	0.04	0.06	0.04	0.16	0,49
PL-KP-5	*4-8h*	0.06	<LOD	0.49	0.88	0.15	0.12	0.08	0.20	1,31
PL-KP-6	*8-12h*	0.20	<LOD	0.55	1.09	0.23	0.20	0.09	0.16	1,23
PL-KP-7	*12-16h*	0.09	0.44	0.43	0.57	0.20	0.03	0.09	0.14	1,40
PL-KP-8	*16-20h*	0.13	0.47	0.44	0.93	0.23	0.04	0.10	0.16	1,88
PL-KP-9	*20-24h*	0.08	<LOD	0.45	0.56	0.17	0.06	0.09	0.13	1,08
PL-KP-10	*0-4h*	<LOD	<LOD	0.22	0.25	0.06	0.04	0.05	0.05	0,69
PL-KP-11	*4-8h*	0.06	<LOD	0.31	0.57	0.20	0.02	0.08	0.08	1,24
PL-KP-12	*8-12h*	0.17	<LOD	0.42	0.76	0.39	0.03	0.14	0.16	2,06
PL-KP-13	*12-16h*	0.15	<LOD	0.51	0.79	0.41	0.04	0.16	0.16	2,09
PL-KP-14	*16-20h*	0.13	<LOD	0.42	0.97	0.35	0.04	0.13	0.18	2,33
PM_{10} mean of total sampling period		**0.10**	**<LOD**	**0.40**	**0.69**	**0.22**	**0.05**	**0.10**	**0.15**	**1.48**
PM_{10} mean of operating period		**0.12**	**<LOD**	**0.43**	**0.75**	**0.25**	**0.06**	**0.11**	**0.16**	**1.62**
PM_{10} mean of downtime		**0.03**	**<LOD**	**0.28**	**0.31**	**0.05**	**0.05**	**0.05**	**0.10**	**0.59**

6.2.1.5 Platform Rochusgasse U3

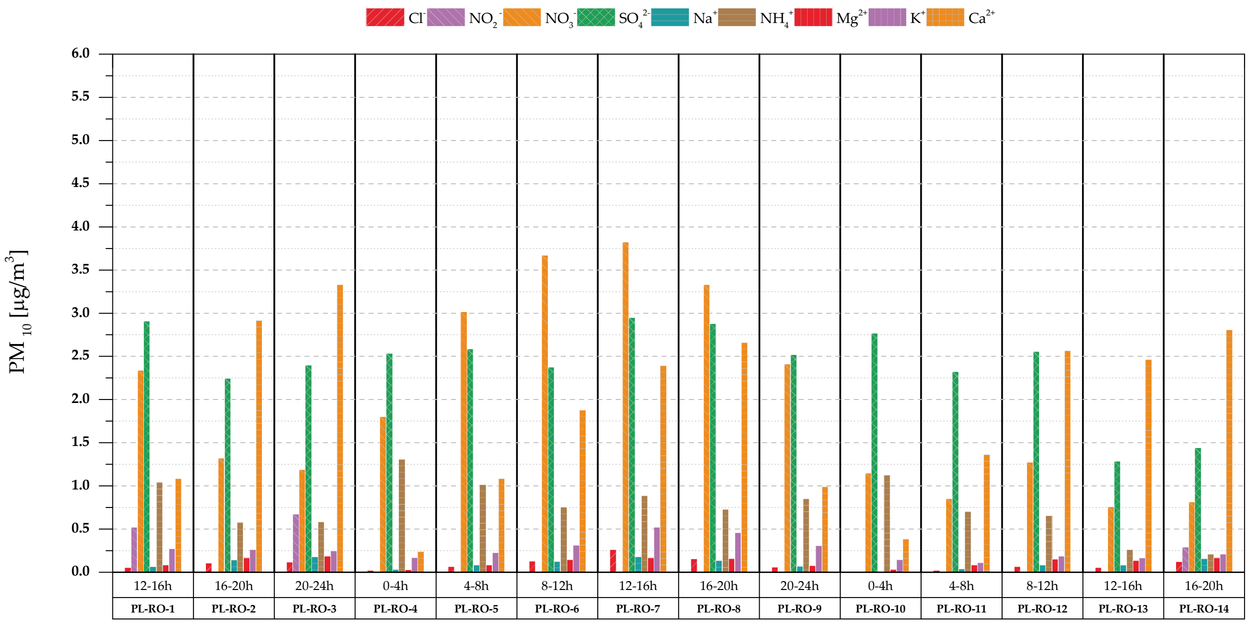

ID	Sampling period	Cl^-	NO_2^-	NO_3^-	SO_4^{2-}	Na^+	NH_4^+	Mg^{2+}	K^+	Ca^{2+}
						[µg/m³]				
PL-RO-1	*12-16h*	0.05	0.52	2.34	2.91	0.07	1.04	0.08	0.27	1,08
PL-RO-2	*16-20h*	0.11	<LOD	1.32	2.25	0.14	0.58	0.17	0.26	2,91
PL-RO-3	*20-24h*	0.12	0.67	1.19	2.40	0.18	0.58	0.18	0.24	3,33
PL-RO-4	*0-4h*	0.02	<LOD	1.80	2.53	0.03	1.31	0.03	0.17	0,24
PL-RO-5	*4-8h*	0.07	<LOD	3.01	2.58	0.09	1.02	0.08	0.22	1,09
PL-RO-6	*8-12h*	0.13	<LOD	3.67	2.37	0.13	0.75	0.14	0.31	1,88
PL-RO-7	*12-16h*	0.26	<LOD	3.82	2.95	0.18	0.89	0.17	0.52	2,39
PL-RO-8	*16-20h*	0.15	<LOD	3.33	2.88	0.14	0.73	0.16	0.46	2,66
PL-RO-9	*20-24h*	0.06	<LOD	2.41	2.52	0.07	0.85	0.08	0.31	0,99
PL-RO-10	*0-4h*	<LOD	<LOD	1.15	2.77	<LOD	1.13	0.03	0.14	0,38
PL-RO-11	*4-8h*	0.02	<LOD	0.85	2.32	0.04	0.70	0.09	0.11	1,36
PL-RO-12	*8-12h*	0.06	<LOD	1.27	2.56	0.08	0.66	0.15	0.19	2,56
PL-RO-13	*12-16h*	0.06	<LOD	0.76	1.29	0.08	0.26	0.14	0.16	2,46
PL-RO-14	*16-20h*	0.12	0.29	0.82	1.44	0.16	0.21	0.17	0.21	2,81
PM_{10} mean of total sampling period		**0.09**	**0.16**	**1.98**	**2.41**	**0.10**	**0.76**	**0.12**	**0.26**	**1.87**
PM_{10} mean of operating period		**0.10**	**0.17**	**2.07**	**2.37**	**0.11**	**0.69**	**0.13**	**0.27**	**2.13**
PM_{10} mean of downtime		**0.01**	**<LOD**	**1.48**	**2.65**	**<LOD**	**1.22**	**0.03**	**0.16**	**0.31**

6.2.1.6 Platform Stubentor U3

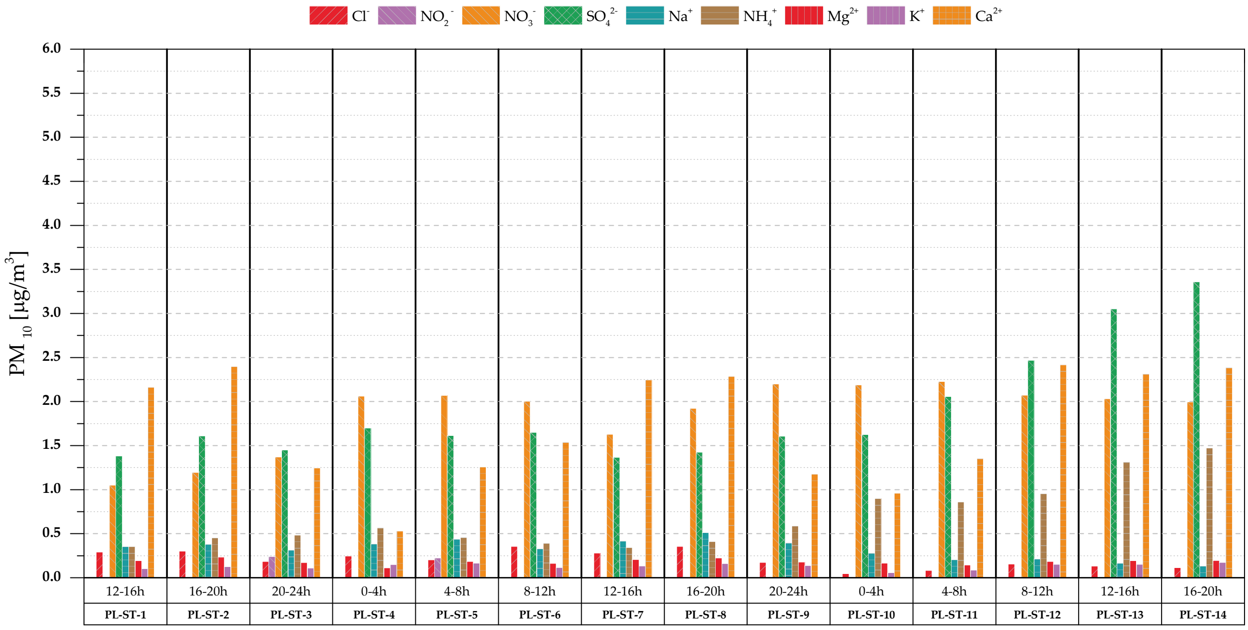

ID	Sampling period	Cl^-	NO_2^-	NO_3^-	SO_4^{2-}	Na^+	NH_4^+	Mg^{2+}	K^+	Ca^{2+}
		[µg/m³]								
PL-ST-1	*12-16h*	0.29	<LOD	1.05	1.38	0.35	0.35	0.19	0.10	2,16
PL-ST-2	*16-20h*	0.30	<LOD	1.19	1.61	0.38	0.45	0.23	0.13	2,40
PL-ST-3	*20-24h*	0.18	0.24	1.37	1.45	0.31	0.48	0.17	0.11	1,25
PL-ST-4	*0-4h*	0.24	<LOD	2.06	1.70	0.38	0.57	0.11	0.15	0,53
PL-ST-5	*4-8h*	0.20	0.22	2.07	1.61	0.44	0.46	0.18	0.17	1,26
PL-ST-6	*8-12h*	0.35	<LOD	2.00	1.65	0.33	0.39	0.16	0.12	1,54
PL-ST-7	*12-16h*	0.28	<LOD	1.63	1.36	0.42	0.34	0.21	0.13	2,24
PL-ST-8	*16-20h*	0.35	<LOD	1.92	1.42	0.51	0.41	0.23	0.16	2,28
PL-ST-9	*20-24h*	0.17	<LOD	2.20	1.61	0.39	0.59	0.18	0.14	1,18
PL-ST-10	*0-4h*	0.04	<LOD	2.19	1.62	0.28	0.90	0.16	0.06	0,96
PL-ST-11	*4-8h*	0.08	<LOD	2.23	2.05	0.20	0.86	0.14	0.09	1,35
PL-ST-12	*8-12h*	0.15	<LOD	2.07	2.47	0.21	0.95	0.18	0.15	2,42
PL-ST-13	*12-16h*	0.13	<LOD	2.03	3.05	0.16	1.31	0.19	0.15	2,31
PL-ST-14	*16-20h*	0.11	<LOD	1.99	3.36	0.13	1.47	0.20	0.17	2,38
PM_{10} mean of total sampling period		**0.21**	**<LOD**	**1.86**	**1.88**	**0.32**	**0.68**	**0.18**	**0.13**	**1.73**
PM_{10} mean of operating period		**0.22**	**<LOD**	**1.81**	**1.92**	**0.32**	**0.67**	**0.19**	**0.13**	**1.90**
PM_{10} mean of downtime		**0.14**	**<LOD**	**2.12**	**1.66**	**0.33**	**0.73**	**0.14**	**0.10**	**0.74**

6.3 Results of the Carbon analysis

6.3.1.1 Tunnel Karlsplatz U1

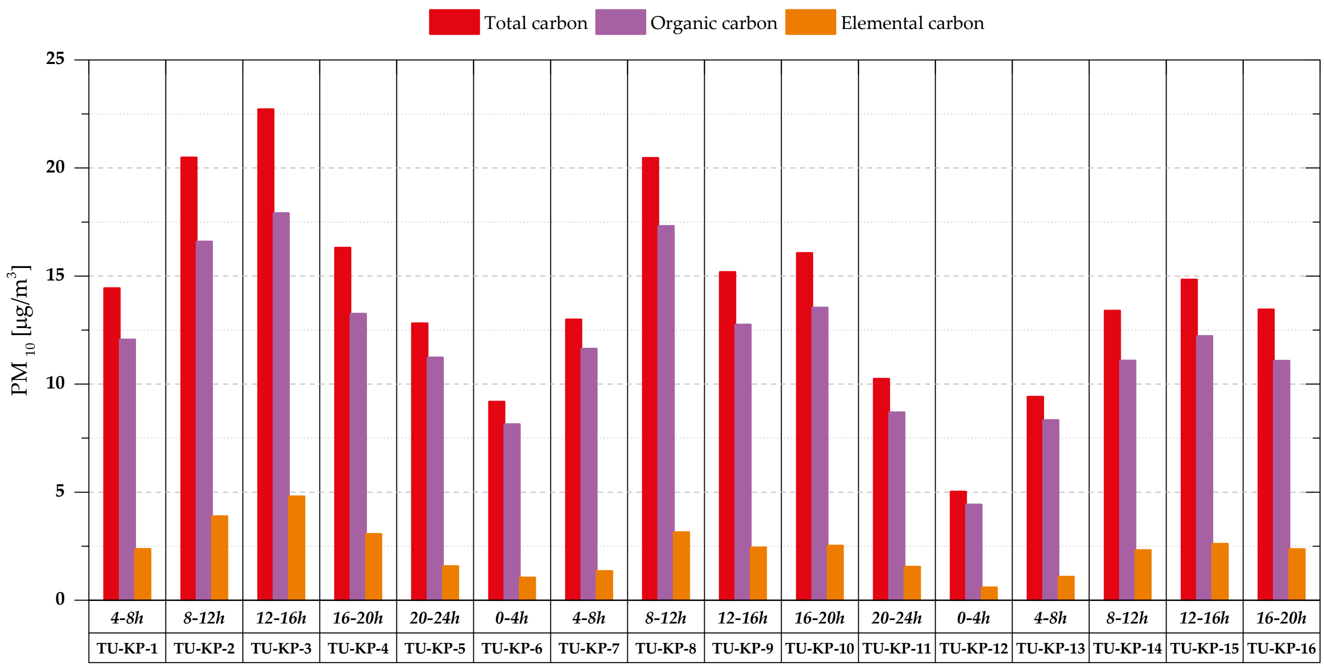

ID	Sampling period	TC	OC	EC
			[µg/m³]	
TU-KP-1	*4-8h*	14.44	12.06	2,38
TU-KP-2	*8-12h*	20.49	16.60	3,89
TU-KP-3	*12-16h*	22.72	17.91	4,81
TU-KP-4	*16-20h*	16.32	13.25	3,06
TU-KP-5	*20-24h*	12.81	11.23	1,58
TU-KP-6	*0-4h*	9.19	8.14	1,05
TU-KP-7	*4-8h*	12.99	11.64	1,35
TU-KP-8	*8-12h*	20.47	17.32	3,15
TU-KP-9	*12-16h*	15.19	12.75	2,44
TU-KP-10	*16-20h*	16.07	13.54	2,53
TU-KP-11	*20-24h*	10.25	8.70	1,55
TU-KP-12	*0-4h*	5.02	4.43	0,59
TU-KP-13	*4-8h*	9.42	8.34	1,08
TU-KP-14	*8-12h*	13.40	11.09	2,31
TU-KP-15	*12-16h*	14.83	12.22	2,61
TU-KP-16	*16-20h*	13.45	11.08	2,37
PM_{10} mean of total sampling period		**14.19**	**11.89**	**2.30**
PM_{10} mean of operating period		**15.20**	**12.70**	**2.51**
PM_{10} mean of downtime		**7.11**	**6.29**	**0.82**

6.3.1.2 Tunnel Rochusgasse U3

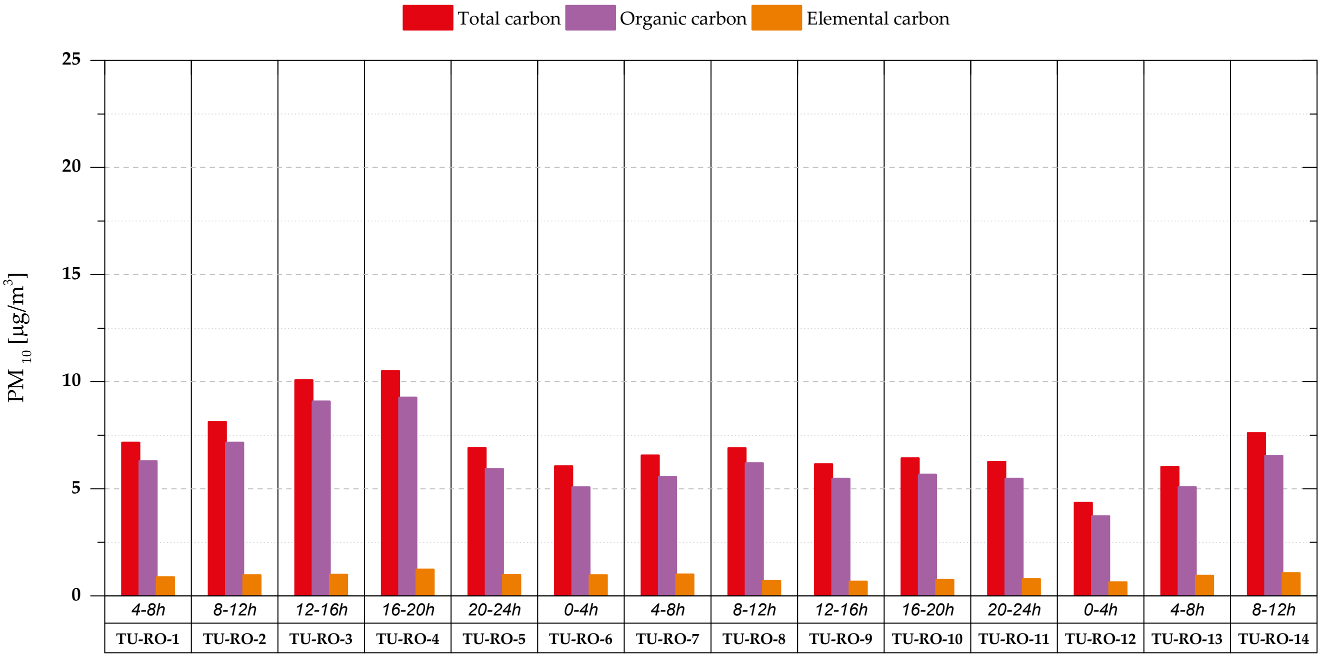

ID	Sampling period	TC	OC	EC
			[µg/m³]	
TU-RO-1	*4-8h*	7.16	6.29	0,87
TU-RO-2	*8-12h*	8.12	7.15	0,97
TU-RO-3	*12-16h*	10.07	9.08	0,99
TU-RO-4	*16-20h*	10.49	9.26	1,23
TU-RO-5	*20-24h*	6.91	5.93	0,98
TU-RO-6	*0-4h*	6.05	5.08	0,97
TU-RO-7	*4-8h*	6.55	5.56	0,99
TU-RO-8	*8-12h*	6.90	6.20	0,71
TU-RO-9	*12-16h*	6.15	5.48	0,67
TU-RO-10	*16-20h*	6.42	5.67	0,76
TU-RO-11	*20-24h*	6.26	5.47	0,79
TU-RO-12	*0-4h*	4.35	3.72	0,63
TU-RO-13	*4-8h*	6.02	5.09	0,94
TU-RO-14	*8-12h*	7.60	6.53	1,07
PM_{10} mean of total sampling period		**7.08**	**6.18**	**0.90**
PM_{10} mean of operating period		**7.39**	**6.48**	**0.91**
PM_{10} mean of downtime		**5.20**	**4.40**	**0.80**

6.3.1.3 Tunnel Praterstern U2

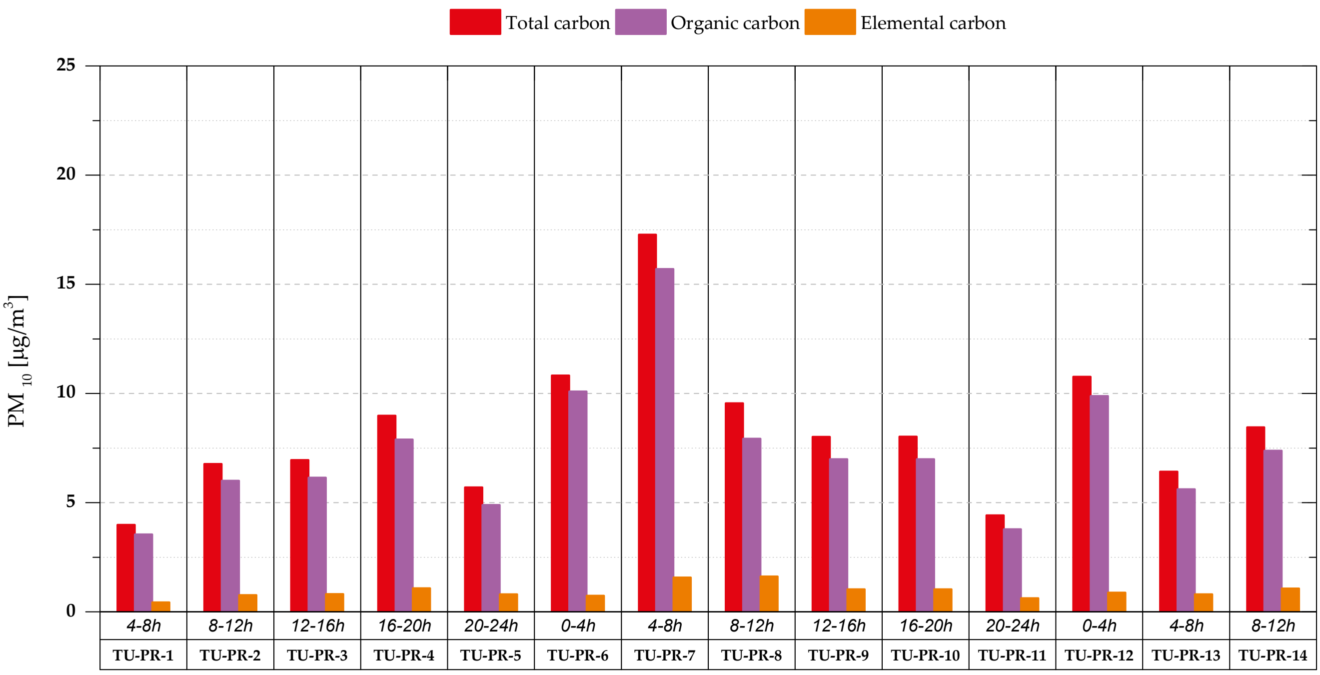

ID	Sampling period	TC	OC	EC
			[µg/m³]	
TU-PR-1	*4-8h*	3.99	3.55	0,44
TU-PR-2	*8-12h*	6.77	6.00	0,77
TU-PR-3	*12-16h*	6.96	6.15	0,81
TU-PR-4	*16-20h*	8.98	7.90	1,09
TU-PR-5	*20-24h*	5.70	4.90	0,81
TU-PR-6	*0-4h*	10.83	10.09	0,74
TU-PR-7	*4-8h*	17.27	15.70	1,57
TU-PR-8	*8-12h*	9.55	7.93	1,62
TU-PR-9	*12-16h*	8.02	6.99	1,03
TU-PR-10	*16-20h*	8.03	6.99	1,03
TU-PR-11	*20-24h*	4.42	3.79	0,63
TU-PR-12	*0-4h*	10.77	9.89	0,88
TU-PR-13	*4-8h*	6.43	5.62	0,81
TU-PR-14	*8-12h*	8.45	7.38	1,07
PM_{10} mean of total sampling period		**8.30**	**7.35**	**0.95**
PM_{10} mean of operating period		**7.88**	**6.91**	**0.97**
PM_{10} mean of downtime		**10.80**	**9.99**	**0.81**

6.3.1.4 Platform Karlsplatz U1

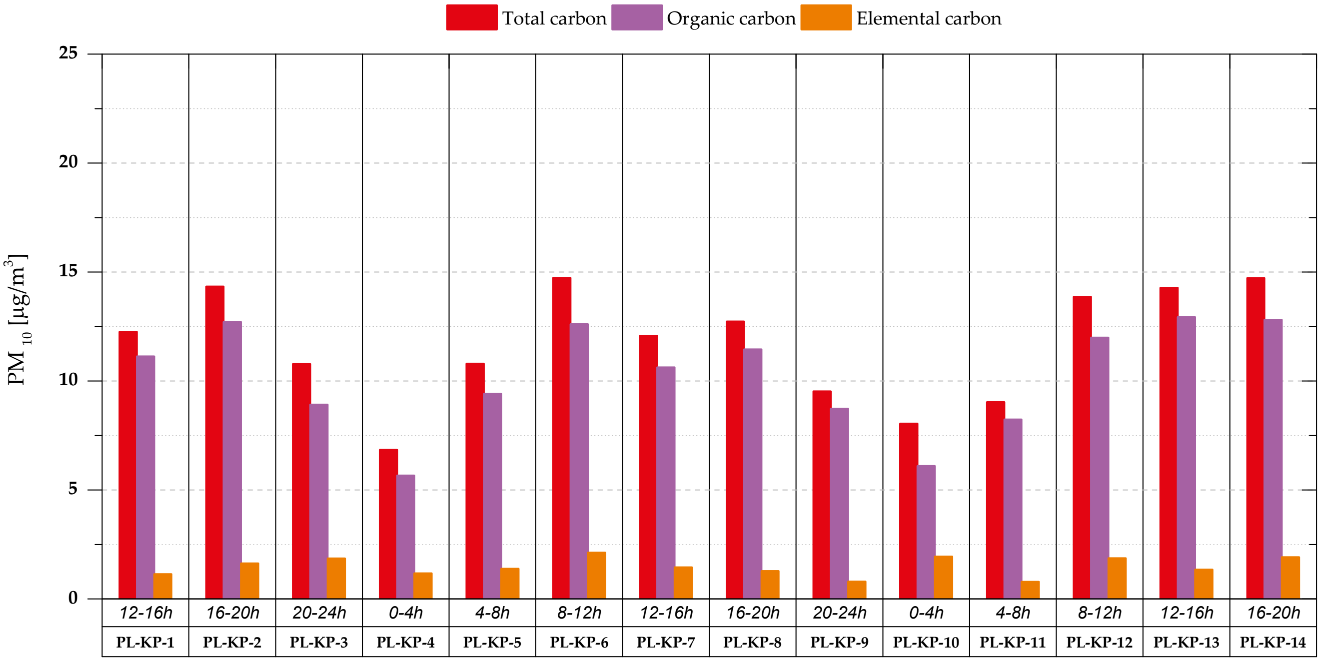

ID	Sampling period	TC	OC	EC
			[µg/m³]	
PL-KP-1	*12-16h*	12.26	11.13	1,13
PL-KP-2	*16-20h*	14.34	12.71	1,63
PL-KP-3	*20-24h*	10.78	8.92	1,86
PL-KP-4	*0-4h*	6.84	5.66	1,18
PL-KP-5	*4-8h*	10.79	9.41	1,38
PL-KP-6	*8-12h*	14.74	12.61	2,13
PL-KP-7	*12-16h*	12.07	10.62	1,45
PL-KP-8	*16-20h*	12.74	11.45	1,28
PL-KP-9	*20-24h*	9.52	8.73	0,80
PL-KP-10	*0-4h*	8.04	6.10	1,94
PL-KP-11	*4-8h*	9.03	8.24	0,79
PL-KP-12	*8-12h*	13.86	11.99	1,87
PL-KP-13	*12-16h*	14.28	12.93	1,35
PL-KP-14	*16-20h*	14.72	12.81	1,91
PM_{10} mean of total sampling period		11.72	10.24	1.48
PM_{10} mean of operating period		12.43	10.96	1.47
PM_{10} mean of downtime		7.44	5.88	1.56

6.3.1.5 Platform Rochusgasse U3

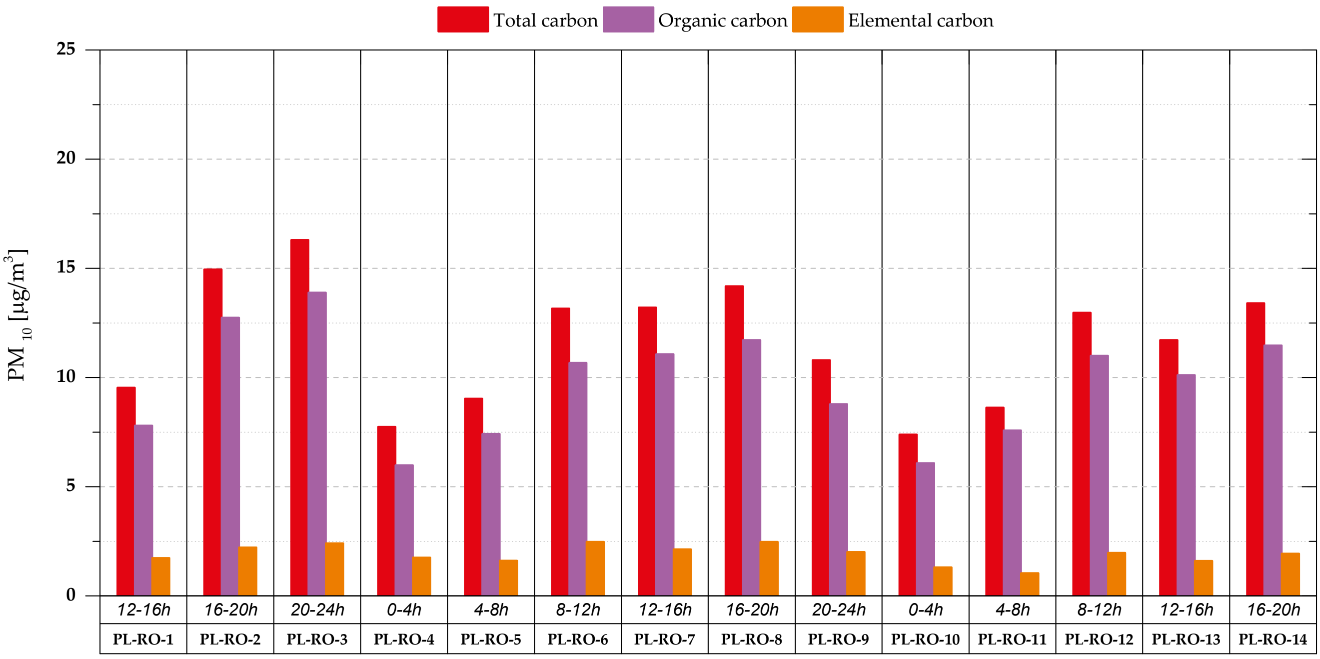

ID	Sampling period	TC	OC	EC
			[µg/m³]	
PL-RO-1	*12-16h*	9.54	7.80	1,74
PL-RO-2	*16-20h*	14.96	12.74	2,22
PL-RO-3	*20-24h*	16.30	13.89	2,41
PL-RO-4	*0-4h*	7.75	5.99	1,75
PL-RO-5	*4-8h*	9.04	7.42	1,61
PL-RO-6	*8-12h*	13.16	10.68	2,48
PL-RO-7	*12-16h*	13.21	11.08	2,13
PL-RO-8	*16-20h*	14.18	11.71	2,47
PL-RO-9	*20-24h*	10.79	8.78	2,01
PL-RO-10	*0-4h*	7.39	6.08	1,31
PL-RO-11	*4-8h*	8.63	7.58	1,04
PL-RO-12	*8-12h*	12.97	10.99	1,98
PL-RO-13	*12-16h*	11.72	10.11	1,61
PL-RO-14	*16-20h*	13.40	11.47	1,93
PM_{10} mean of total sampling period		11.64	9.74	1.91
PM_{10} mean of operating period		12.32	10.35	1.97
PM_{10} mean of downtime		7.57	6.04	1.53

6.3.1.6 Platform Stubentor U3

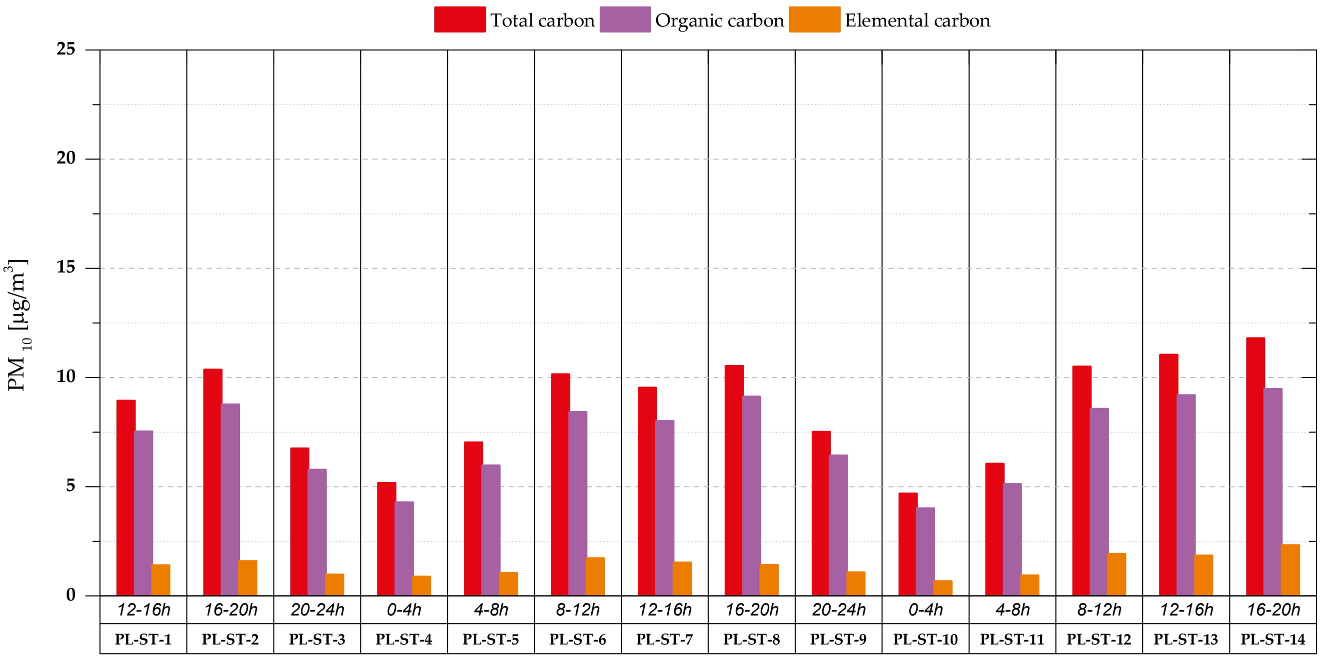

ID	Sampling period	TC	OC	EC
			[µg/m³]	
PL-ST-1	*12-16h*	8.94	7.53	1,41
PL-ST-2	*16-20h*	10.36	8.77	1,59
PL-ST-3	*20-24h*	6.75	5.77	0,98
PL-ST-4	*0-4h*	5.17	4.29	0,88
PL-ST-5	*4-8h*	7.03	5.98	1,05
PL-ST-6	*8-12h*	10.15	8.43	1,72
PL-ST-7	*12-16h*	9.53	8.00	1,53
PL-ST-8	*16-20h*	10.54	9.12	1,41
PL-ST-9	*20-24h*	7.51	6.43	1,08
PL-ST-10	*0-4h*	4.69	4.02	0,67
PL-ST-11	*4-8h*	6.06	5.12	0,94
PL-ST-12	*8-12h*	10.50	8.57	1,93
PL-ST-13	*12-16h*	11.04	9.20	1,85
PL-ST-14	*16-20h*	11.80	9.48	2,33
PM_{10} mean of total sampling period		**8.58**	**7.19**	**1.38**
PM_{10} mean of operating period		**9.18**	**7.70**	**1.48**
PM_{10} mean of downtime		**4.93**	**4.15**	**0.78**

6.4 Results of the elemental analysis

6.4.1.1 Tunnel Karlsplatz U1

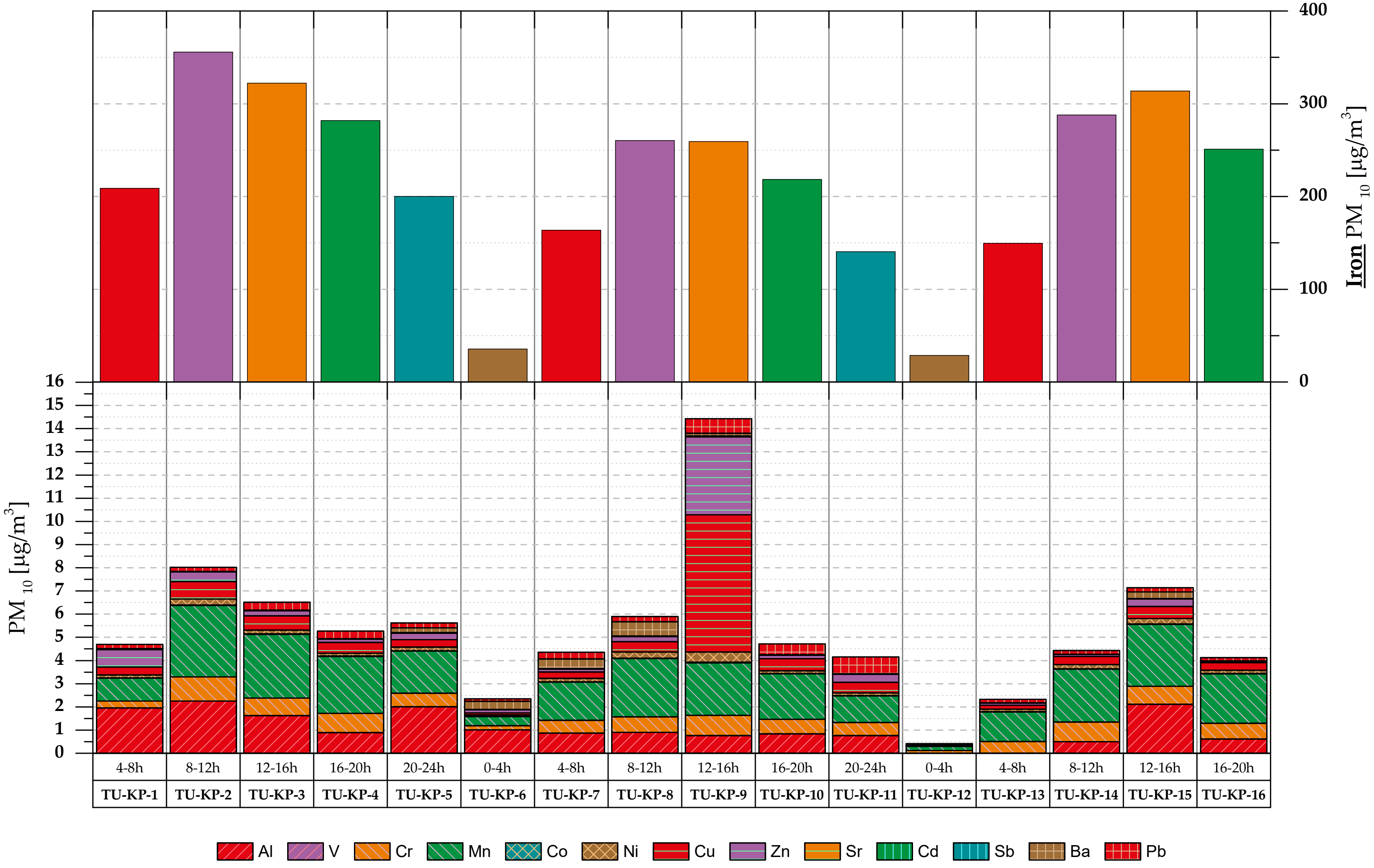

	Al	V	Cr	Mn	Co	Ni	Cu	Zn	Sr	Cd	Sb	Ba	Pb	Fe
	[µg/m³]	[ng/m³]	[µg/m³]	[ng/m³]										[µg/m³]
TU-KP-1	1.96	<LOD	0.29	984	11	135	339	749	38	2	6	<LOD	183	209
TU-KP-2	2.25	<LOD	1.03	3084	19	262	757	412	11	2	12	<LOD	172	356
TU-KP-3	1.62	<LOD	0.76	2753	16	161	617	217	14	1	11	<LOD	338	322
TU-KP-4	0.89	<LOD	0.84	2454	14	125	465	138	7	<LOD	11	<LOD	324	282
TU-KP-5	2.01	<LOD	0.59	1816	11	155	325	286	9	2	8	207	211	200
TU-KP-6	1.01	<LOD	0.18	394	4	66	90	132	13	4	<LOD	344	106	36
TU-KP-7	0.87	<LOD	0.56	1643	10	150	272	127	21	6	<LOD	415	280	164
TU-KP-8	0.90	<LOD	0.66	2519	16	259	454	216	23	5	<LOD	613	222	260
TU-KP-9	0.76	<LOD	0.87	2268	26	443	5918	3348	27	3	13	126	621	259
TU-KP-10	0.84	<LOD	0.63	1960	12	116	522	149	7	1	11	<LOD	473	218
TU-KP-11	0.76	<LOD	0.56	1156	10	112	456	355	9	2	9	<LOD	727	140
TU-KP-12	<LOD	<LOD	0.11	181	0	45	<LOD	33	4	<LOD	2	<LOD	30	29
TU-KP-13	<LOD	<LOD	0.51	1273	6	106	172	95	3	1	7	<LOD	152	150
TU-KP-14	0.50	<LOD	0.85	2274	13	182	356	77	8	<LOD	9	<LOD	159	288
TU-KP-15	2.12	<LOD	0.77	2671	17	235	518	316	12	2	8	293	180	314
TU-KP-16	0.62	<LOD	0.68	2130	13	143	329	68	<LOD	1	6	<LOD	143	251
PM_{10} mean of total sampling period	**1.09**	**<LOD**	**0.62**	**1848**	**12**	**168**	**725**	**420**	**13**	**2**	**7**	**162**	**270**	**217**
PM_{10} mean of operating period	**1.16**	**<LOD**	**0.69**	**2070**	**14**	**185**	**821**	**468**	**14**	**2**	**8**	**156**	**299**	**244**
PM_{10} mean of downtime	**0.58**	**<LOD**	**0.15**	**288**	**2**	**56**	**48**	**82**	**9**	**2**	**2**	**201**	**68**	**32**

6.4.1.2 Tunnel Rochusgasse U3

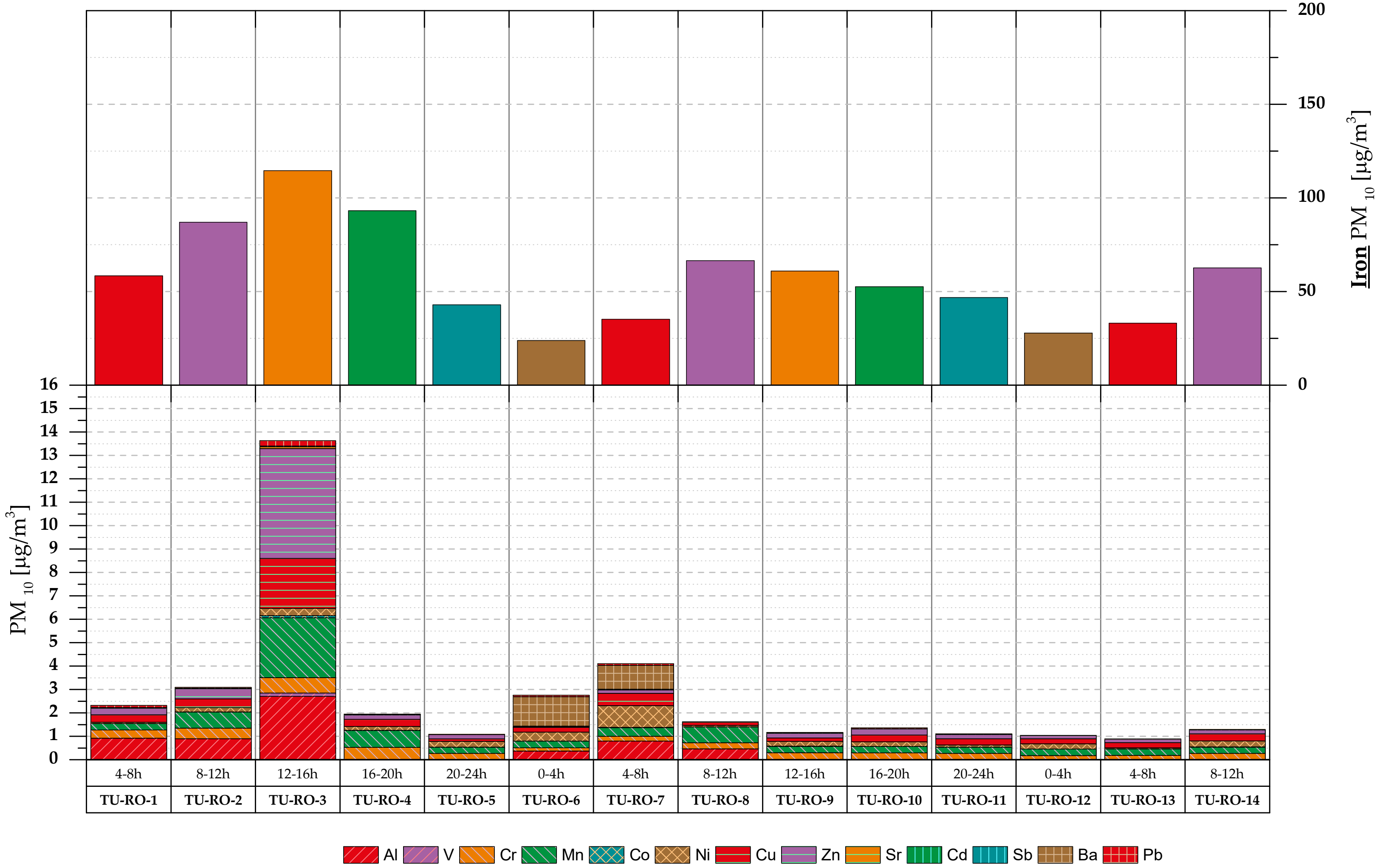

	Al	V	Cr	Mn	Co	Ni	Cu	Zn	Sr	Cd	Sb	Ba	Pb	Fe
	[µg/m³]	[ng/m³]	[µg/m³]	[ng/m³]										[µg/m³]
TU-RO-1	0.92	<LOD	0.35	274	2	57	316	293	6	1	6	<LOD	97	58
TU-RO-2	0.89	<LOD	0.46	674	7	194	362	437	6	3	10	<LOD	43	87
TU-RO-3	2.70	143	0.66	2557	100	301	2140	4693	79	11	23	<LOD	228	115
TU-RO-4	<LOD	<LOD	0.52	728	4	171	295	192	5	1	13	<LOD	16	93
TU-RO-5	<LOD	<LOD	0.26	275	1	239	103	186	3	1	7	<LOD	18	43
TU-RO-6	0.37	<LOD	0.14	285	4	378	204	33	18	4	<LOD	1255	58	24
TU-RO-7	0.80	<LOD	0.20	378	6	927	526	150	20	3	<LOD	1022	79	35
TU-RO-8	0.47	<LOD	0.26	679	5	53	147	<LOD	11	2	<LOD	<LOD	<LOD	66
TU-RO-9	<LOD	<LOD	0.30	275	2	207	148	204	12	1	3	<LOD	13	61
TU-RO-10	<LOD	<LOD	0.29	275	3	199	287	265	3	1	3	<LOD	42	53
TU-RO-11	<LOD	<LOD	0.26	276	1	85	273	182	3	1	2	<LOD	14	47
TU-RO-12	<LOD	<LOD	0.18	275	1	224	217	138	<LOD	1	<LOD	<LOD	11	28
TU-RO-13	<LOD	<LOD	0.19	275	1	38	228	144	<LOD	1	<LOD	<LOD	17	33
TU-RO-14	<LOD	<LOD	0.27	275	1	261	297	181	<LOD	1	3	<LOD	18	63
PM_{10} mean of total sampling period	**0.56**	**35**	**0.31**	**536**	**10**	**238**	**396**	**508**	**12**	**2**	**5**	**182**	**47**	**58**
PM_{10} mean of operating period	**0.61**	**34**	**0.33**	**578**	**11**	**228**	**427**	**579**	**13**	**2**	**6**	**106**	**49**	**63**
PM_{10} mean of downtime	**0.29**	**41**	**0.16**	**280**	**3**	**301**	**211**	**86**	**9**	**2**	**1**	**637**	**34**	**26**

6.4.1.3 Tunnel Praterstern U3

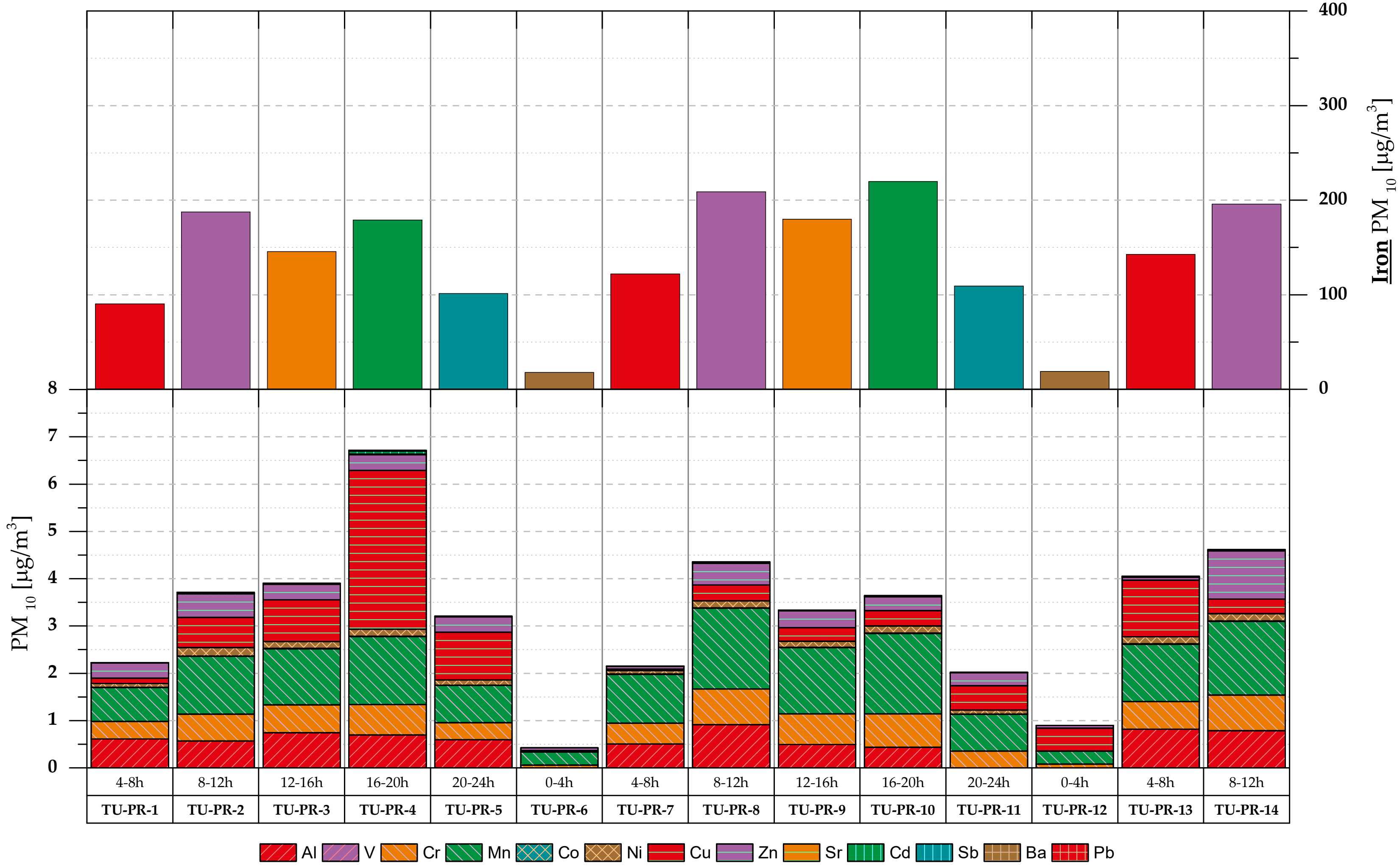

	Al	V	Cr	Mn	Co	Ni	Cu	Zn	Sr	Cd	Sb	Ba	Pb	Fe
	[µg/m³]	[ng/m³]	[µg/m³]	[ng/m³]										[µg/m³]
TU-PR-1	0.61	<LOD	0.37	720	2	84	108	323	8	1	2	<LOD	<LOD	90
TU-PR-2	0.57	<LOD	0.57	1223	8	177	639	497	9	3	5	<LOD	16	188
TU-PR-3	0.74	<LOD	0.59	1187	9	142	885	325	10	3	8	<LOD	<LOD	146
TU-PR-4	0.69	<LOD	0.64	1440	8	149	3356	331	11	64	10	<LOD	10	179
TU-PR-5	0.60	<LOD	0.36	790	3	108	1010	327	7	1	4	<LOD	<LOD	101
TU-PR-6	<LOD	<LOD	0.06	275	2	<LOD	28	60	<LOD	1	<LOD	<LOD	<LOD	18
TU-PR-7	0.50	<LOD	0.44	1031	7	73	29	60	4	1	6	<LOD	<LOD	122
TU-PR-8	0.91	<LOD	0.75	1711	10	147	336	454	8	2	9	<LOD	14	209
TU-PR-9	0.49	<LOD	0.65	1405	6	126	288	354	8	1	7	<LOD	<LOD	180
TU-PR-10	0.44	<LOD	0.71	1700	9	148	326	293	8	1	14	<LOD	<LOD	220
TU-PR-11	<LOD	<LOD	0.35	778	2	87	516	277	6	1	4	<LOD	<LOD	109
TU-PR-12	<LOD	<LOD	0.08	275	1	<LOD	486	60	<LOD	1	<LOD	<LOD	<LOD	19
TU-PR-13	0.82	<LOD	0.58	1214	9	149	1196	60	5	1	8	<LOD	12	143
TU-PR-14	0.78	<LOD	0.76	1556	9	158	303	1023	11	4	11	<LOD	<LOD	196
PM$_{10}$ mean of total sampling period	0.56	<LOD	0.49	1093	6	112	679	317	7	6	6	<LOD	7	137
PM$_{10}$ mean of operating period	0.61	<LOD	0.57	1229	7	129	749	360	8	7	7	<LOD	7	157
PM$_{10}$ mean of downtime	0.21	<LOD	0.07	275	1	12	257	60	1	1	1	<LOD	2	18

6.4.1.4 Platform Karlsplatz U1

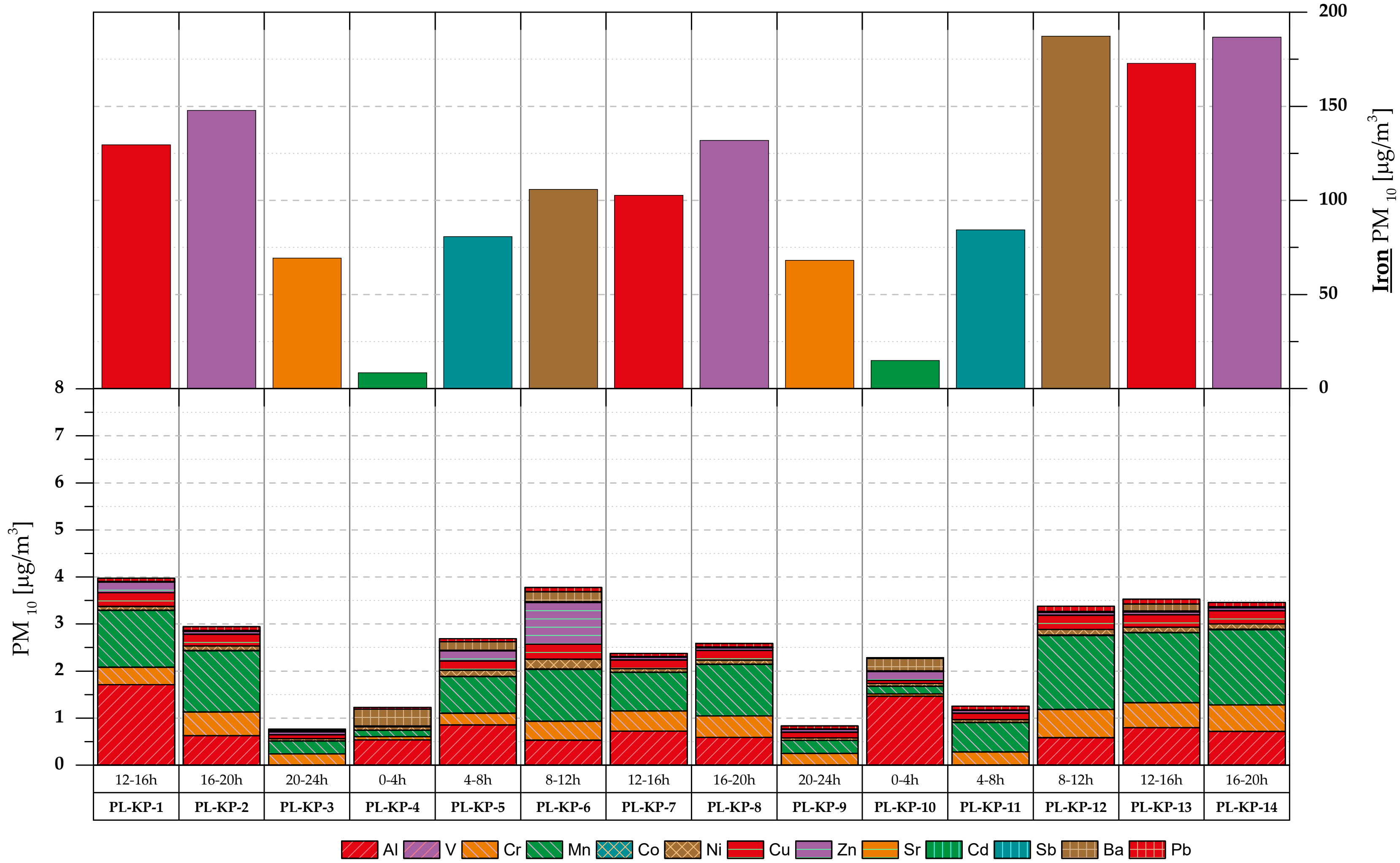

	Al	V	Cr	Mn	Co	Ni	Cu	Zn	Sr	Cd	Sb	Ba	Pb	Fe
	[µg/m^3]	[ng/m^3]	[µg/m^3]	[ng/m^3]										[µg/m^3]
PL-KP-1	1.71	<LOD	0.38	1202	7	80	293	225	7	2	7	<LOD	68	129
PL-KP-2	0.63	<LOD	0.50	1300	7	96	247	60	10	1	13	<LOD	81	148
PL-KP-3	<LOD	<LOD	0.24	275	1	51	81	60	3	26	4	<LOD	29	69
PL-KP-4	0.54	<LOD	0.07	137	1	70	13	<LOD	8	1	<LOD	357	36	8
PL-KP-5	0.86	<LOD	0.24	778	5	132	198	215	7	1	5	178	65	81
PL-KP-6	0.53	<LOD	0.40	1102	10	206	321	888	11	2	<LOD	211	91	106
PL-KP-7	0.72	<LOD	0.43	822	4	73	184	60	6	1	7	<LOD	66	103
PL-KP-8	0.59	<LOD	0.46	1095	6	80	209	60	6	1	7	<LOD	75	132
PL-KP-9	<LOD	<LOD	0.25	275	1	50	125	60	3	1	5	<LOD	62	68
PL-KP-10	1.46	<LOD	0.05	160	1	59	67	192	5	1	3	264	19	15
PL-KP-11	<LOD	<LOD	0.28	628	2	56	138	60	3	1	7	<LOD	79	84
PL-KP-12	0.59	<LOD	0.60	1575	8	119	300	60	8	1	11	<LOD	114	187
PL-KP-13	0.80	<LOD	0.53	1486	7	108	267	60	6	1	12	149	104	173
PL-KP-14	0.72	<LOD	0.57	1598	8	114	282	60	15	1	9	<LOD	90	187
PM_{10} mean of total sampling period	0.70	<LOD	0.36	888	5	92	195	148	7	3	7	98	70	106
PM_{10} mean of operating period	0.65	<LOD	0.41	1011	5	97	220	156	7	3	7	62	77	122
PM_{10} mean of downtime	1.00	<LOD	0.06	148	1	64	40	104	6	1	2	311	27	12

6.4.1.5 Platform Rochusgasse U3

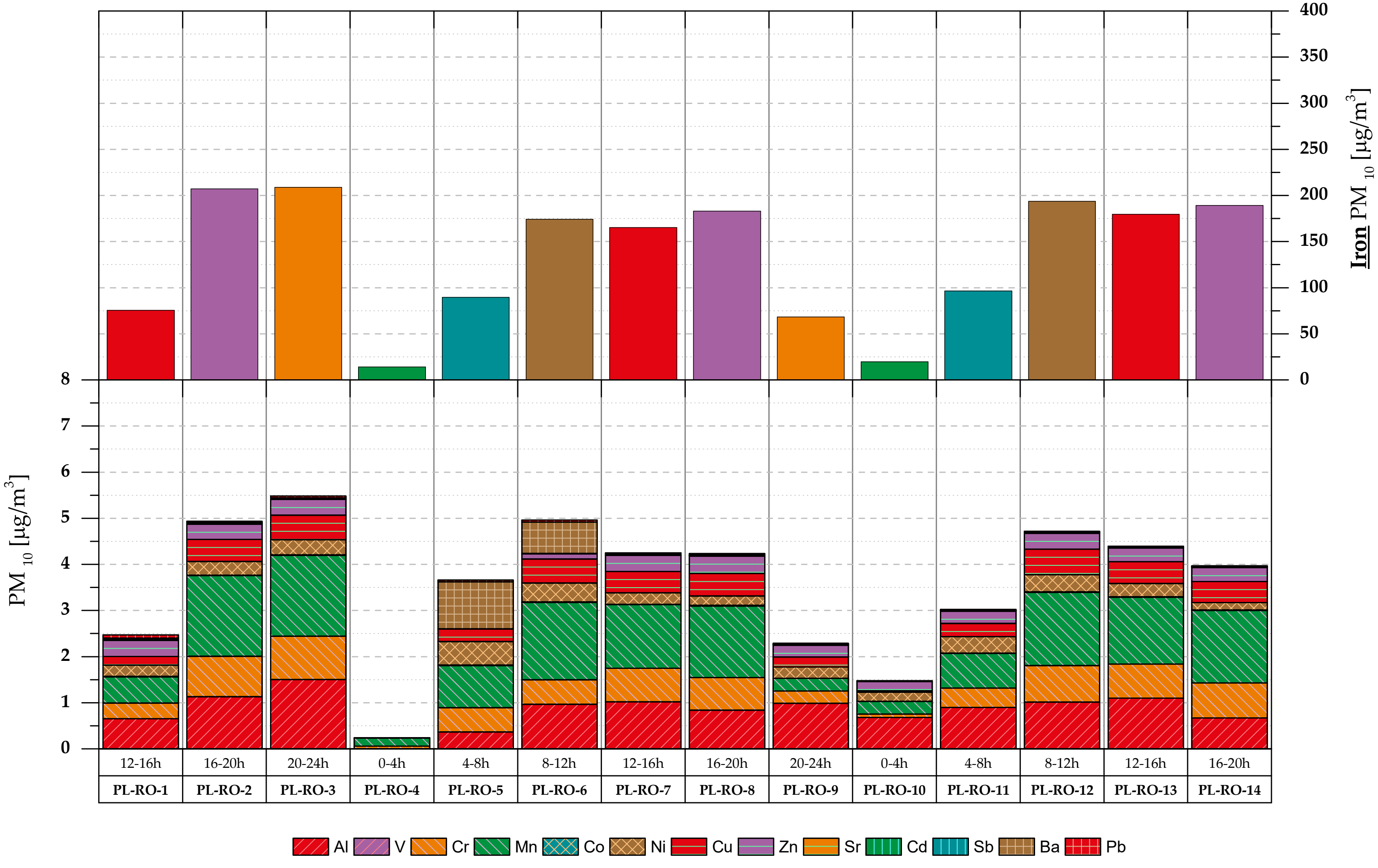

	Al	V	Cr	Mn	Co	Ni	Cu	Zn	Sr	Cd	Sb	Ba	Pb	Fe
	[µg/m^3]	[ng/m^3]	[µg/m^3]	[ng/m^3]										[µg/m^3]
PL-RO-1	0.65	<LOD	0.34	571	9	242	190	347	14	5	31	<LOD	69	75
PL-RO-2	1.13	<LOD	0.87	1748	10	297	480	326	13	2	22	<LOD	30	207
PL-RO-3	1.50	<LOD	0.94	1755	10	331	531	336	14	7	18	<LOD	38	209
PL-RO-4	<LOD	<LOD	0.06	175	2	<LOD	<LOD	<LOD	4	3	<LOD	<LOD	<LOD	14
PL-RO-5	0.37	<LOD	0.52	916	11	512	269	<LOD	7	<LOD	<LOD	1016	40	89
PL-RO-6	0.96	<LOD	0.54	1674	12	408	520	113	12	1	<LOD	678	45	174
PL-RO-7	1.02	<LOD	0.73	1380	8	249	459	354	13	2	16	<LOD	23	165
PL-RO-8	0.84	<LOD	0.71	1548	17	204	485	376	14	2	15	<LOD	23	183
PL-RO-9	0.99	<LOD	0.26	275	2	242	218	255	14	1	6	<LOD	23	68
PL-RO-10	0.68	<LOD	0.08	275	1	195	28	203	12	1	3	<LOD	<LOD	20
PL-RO-11	0.90	<LOD	0.42	757	5	353	288	268	15	3	7	<LOD	9	97
PL-RO-12	1.02	<LOD	0.79	1588	9	375	550	343	12	1	14	<LOD	20	194
PL-RO-13	1.10	<LOD	0.74	1452	8	286	477	294	14	1	10	<LOD	12	180
PL-RO-14	0.67	<LOD	0.76	1572	8	158	458	305	12	1	10	<LOD	15	189
PM_{10} mean of total sampling period	**0.86**	**<LOD**	**0.55**	**1120**	**8**	**276**	**354**	**254**	**12**	**2**	**11**	**140**	**26**	**133**
PM_{10} mean of operating period	**0.93**	**<LOD**	**0.63**	**1270**	**9**	**305**	**411**	**278**	**13**	**2**	**13**	**157**	**29**	**152**
PM_{10} mean of downtime	**0.41**	**<LOD**	**0.07**	**225**	**1**	**103**	**17**	**110**	**8**	**2**	**2**	**39**	**6**	**17**

6.4.1.6 Platform Stubentor U3

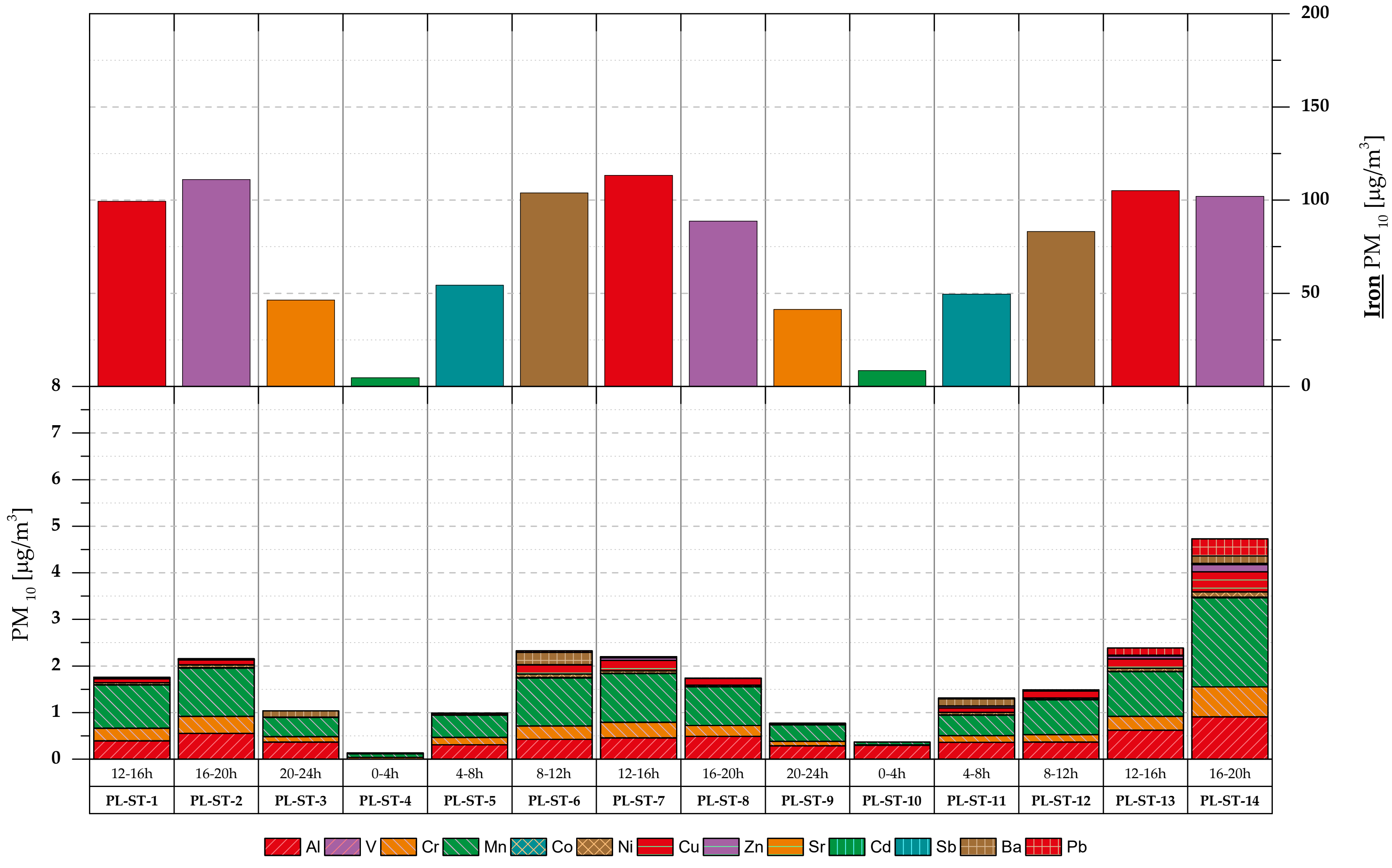

	Al	**V**	**Cr**	**Mn**	**Co**	**Ni**	**Cu**	**Zn**	**Sr**	**Cd**	**Sb**	**Ba**	**Pb**	**Fe**
	[µg/m³]	[ng/m³]	[µg/m³]	[ng/m³]										[µg/m³]
PL-ST-1	0.40	<LOD	0.27	930	6	44	83	<LOD	<LOD	1	22	<LOD	10	99
PL-ST-2	0.55	<LOD	0.36	1040	6	58	107	<LOD	3	1	12	<LOD	11	111
PL-ST-3	0.37	<LOD	0.11	412	2	<LOD	<LOD	<LOD	3	<LOD	6	131	<LOD	46
PL-ST-4	<LOD	<LOD	0.04	76	0	<LOD	<LOD	<LOD	<LOD	15	<LOD	<LOD	<LOD	5
PL-ST-5	0.31	<LOD	0.16	479	3	<LOD	31	<LOD	<LOD	<LOD	5	<LOD	<LOD	54
PL-ST-6	0.42	<LOD	0.29	1029	7	78	197	<LOD	5	1	<LOD	267	30	104
PL-ST-7	0.46	<LOD	0.34	1044	6	52	227	57	<LOD	1	9	<LOD	9	113
PL-ST-8	0.49	<LOD	0.24	826	5	33	143	<LOD	3	<LOD	5	<LOD	<LOD	89
PL-ST-9	0.29	<LOD	0.10	355	1	<LOD	31	<LOD	<LOD	<LOD	2	<LOD	<LOD	41
PL-ST-10	0.30	<LOD	0.01	60	<LOD	<LOD	<LOD	<LOD	<LOD	<LOD	<LOD	<LOD	<LOD	9
PL-ST-11	0.36	<LOD	0.14	445	2	53	100	37	<LOD	<LOD	4	155	13	50
PL-ST-12	0.37	<LOD	0.16	750	4	36	146	<LOD	<LOD	<LOD	9	<LOD	18	83
PL-ST-13	0.62	<LOD	0.30	962	6	63	199	67	6	<LOD	8	<LOD	156	105
PL-ST-14	0.91	<LOD	0.64	1915	11	116	428	155	13	1	12	157	370	102
PM_{10} mean of total sampling period	**0.43**	**<LOD**	**0.23**	**737**	**4**	**42**	**122**	**34**	**3**	**2**	**7**	**93**	**46**	**72**
PM_{10} mean of operating period	**0.46**	**<LOD**	**0.26**	**849**	**5**	**47**	**141**	**37**	**3**	**0**	**8**	**99**	**53**	**83**
PM_{10} mean of downtime	**0.22**	**<LOD**	**0.02**	**68**	**0**	**12**	**6**	**16**	**1**	**8**	**1**	**59**	**4**	**7**

6.5 Results of the measurements with the OPC

		Mean	Median	Min	Max	Stdev
		[µg/m³]				
Tunnel Karlsplatz	*total*	311	322	5	6142	±226
	operation	364	347	13	6142	±206
	downtime	27	16	5	318	±32
Tunnel Rochusgasse	*total*	82	79	8	222	±39
	operation	93	93	17	222	±32
	night operation	24	22	8	71	±11
Tunnel Praterstern	*total*	199	218	2	982	±113
	operation	237	235	6	982	±82
	downtime	13	10	2	42	±8
Platform Karlsplatz	*total*	186	201	4	735	±110
	operation	221	221	8	735	±86
	downtime	16	14	4	99	±11
Platform Rochusgasse	*total*	199	217	17	1122	±103
	operation	233	239	46	711	±76
	downtime	46	31	17	1122	±63
Platform Stubentor	*total*	133	137	26	810	±58
	operation	149	148	32	810	±49
	downtime	56	44	26	259	±28

6.6 Results of the measurements with the ELPI

6.6.1 Results of the measured mass concentration distributions

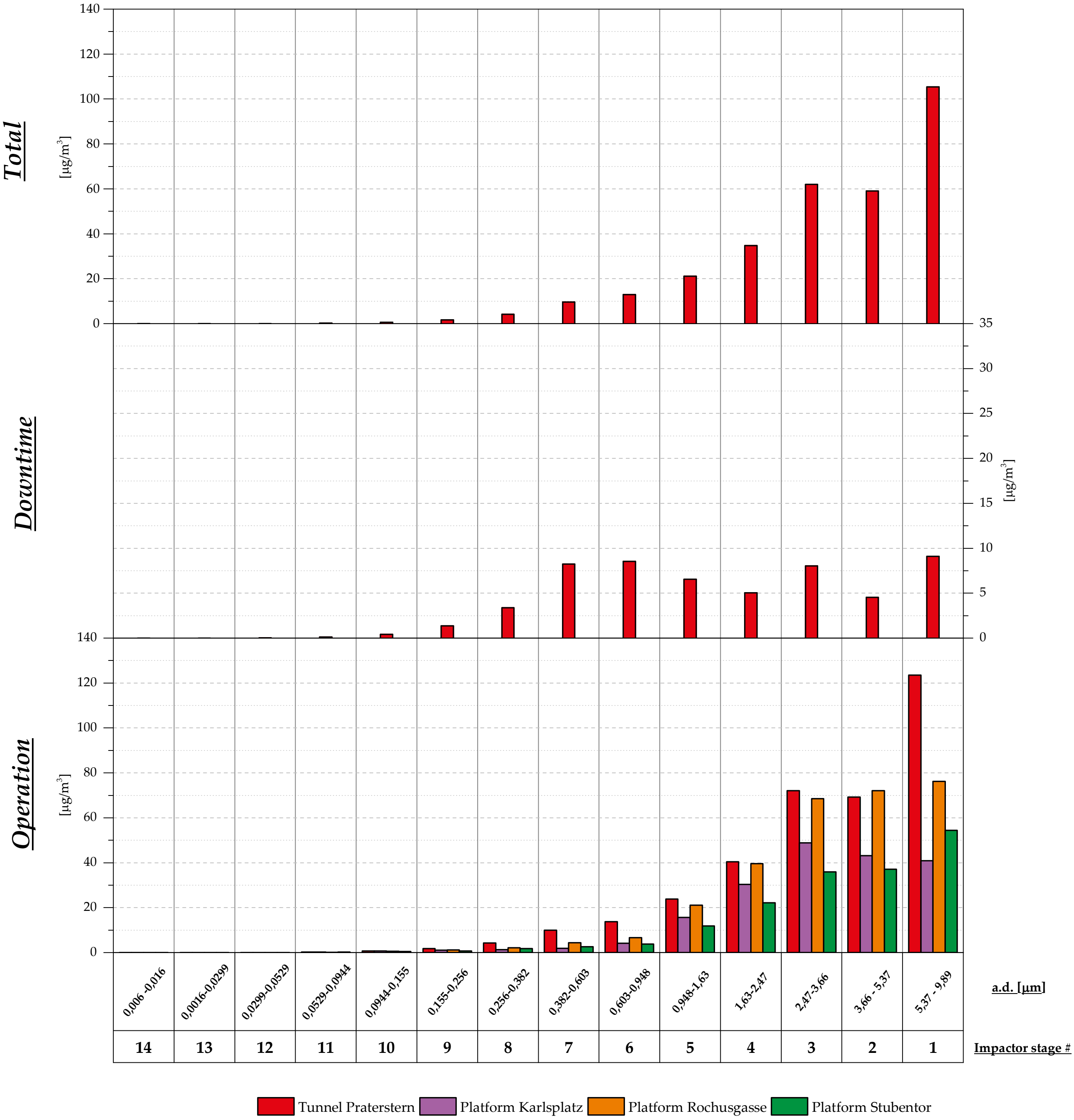

Impactor Stage	Particles` aerodynamic diameter range	Tunnel			Platform		
		Praterstern			Karlsplatz	Rochusgasse	Stubentor
		total	*operation*	*downtime*	*operation*		
#	*[µm]*	*[µg/m³]*					
14	*0.006 - 0.016*	0.00	0.00	0.00	0.01	0.01	0.01
13	*0.0016 - 0.0299*	0.01	0.01	0.00	0.01	0.01	0.01
12	*0.0299 - 0.0529*	0.04	0.04	0.02	0.05	0.03	0.04
11	*0.0529 - 0.0944*	0.22	0.24	0.11	0.26	0.13	0.18
10	*0.0944 - 0.155*	0.64	0.68	0.43	0.76	0.57	0.49
9	*0.155 - 0.256*	1.71	1.78	1.37	1.04	1.15	0.75
8	*0.256 - 0.382*	4.14	4.28	3.38	1.26	2.08	1.72
7	*0.382 - 0.603*	9.64	9.90	8.23	1.95	4.37	2.55
6	*0.603 - 0.948*	12.96	13.79	8.55	4.13	6.64	3.75
5	*0.948 - 1.63*	21.11	23.85	6.56	15.66	21.12	11.81
4	*1.63 - 2.47*	34.78	40.38	5.05	30.35	39.65	22.21
3	*2.47 - 3.66*	61.96	72.11	8.02	48.89	68.56	35.92
2	*3.66 - 5.37*	58.99	69.23	4.53	43.18	72.09	37.14
1	*5.37 - 9.89*	105.38	123.50	9.10	40.90	76.17	54.42

6.6.2 Results of the measured number concentration distributions

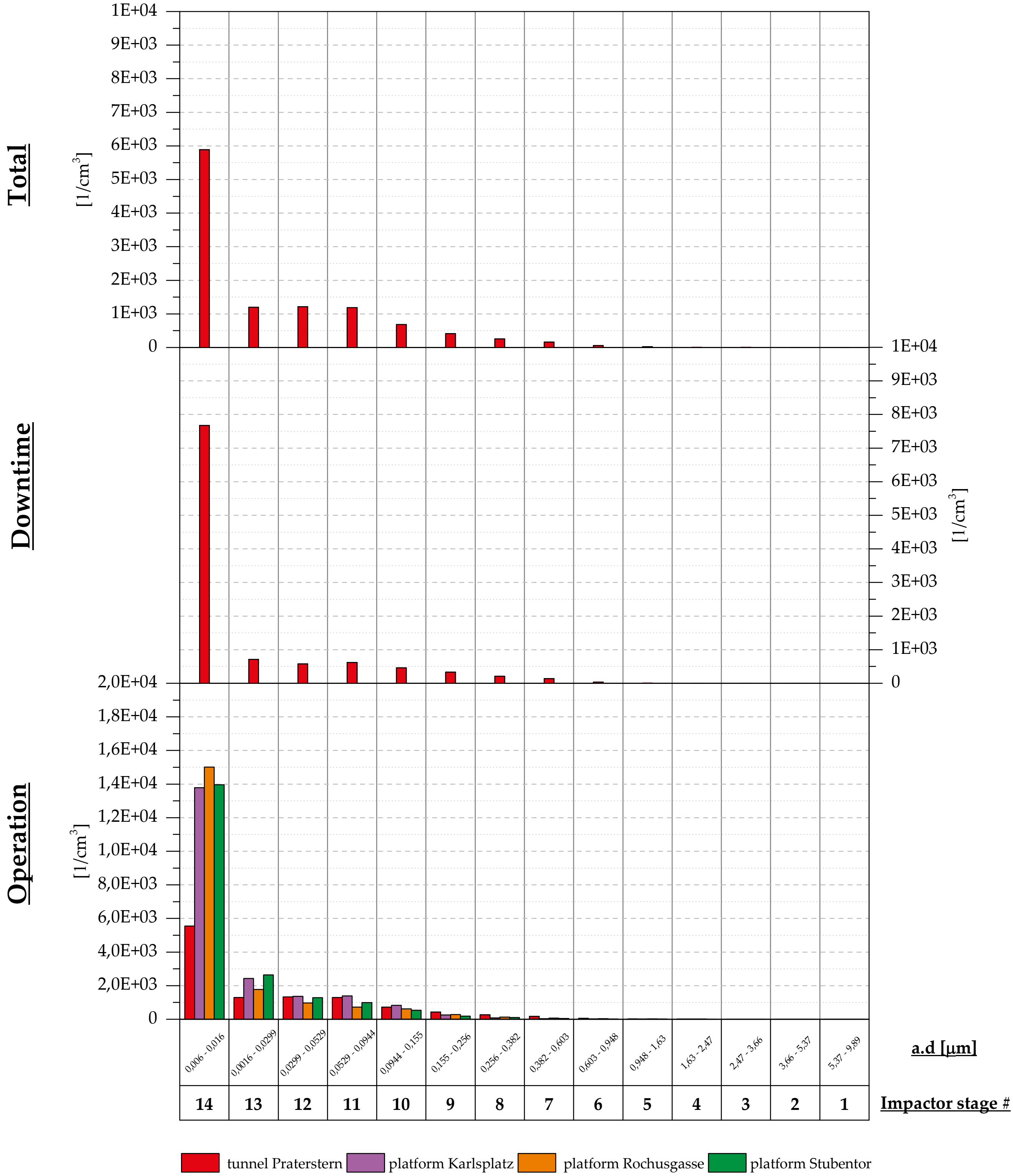

Impactor Stage	Particles` aerodynamic diameter range	Tunnel			Platform		
		Praterstern			Karlsplatz	Rochusgasse	Stubentor
		total	*operation*	*downtime*	*operation*		
#	*[µm]*	*[1/cm³]*					
14	*0.006 - 0.016*	5.89E+03	5.55E+03	7.67E+03	1.38E+04	1.50E+04	1.40E+04
13	*0.0016 - 0.0299*	1.20E+03	1.29E+03	7.10E+02	2.43E+03	1.78E+03	2.64E+03
12	*0.0299 - 0.0529*	1.21E+03	1.33E+03	5.80E+02	1.37E+03	9.68E+02	1.28E+03
11	*0.0529 - 0.0944*	1.19E+03	1.29E+03	6.17E+02	1.39E+03	7.22E+02	9.94E+02
10	*0.0944 - 0.155*	6.86E+02	7.28E+02	4.61E+02	8.24E+02	6.17E+02	5.32E+02
9	*0.155 - 0.256*	4.14E+02	4.29E+02	3.31E+02	2.51E+02	2.79E+02	1.81E+02
8	*0.256 - 0.382*	2.58E+02	2.67E+02	2.11E+02	7.84E+01	1.30E+02	1.07E+02
7	*0.382 - 0.603*	1.66E+02	1.71E+02	1.42E+02	3.37E+01	7.54E+01	4.41E+01
6	*0.603 - 0.948*	5.72E+01	6.09E+01	3.77E+01	1.83E+01	2.93E+01	1.66E+01
5	*0.948 - 1.63*	2.10E+01	2.37E+01	6.51E+00	1.56E+01	2.10E+01	1.17E+01
4	*1.63 - 2.47*	8.22E+00	9.54E+00	1.19E+00	7.17E+00	9.37E+00	5.25E+00
3	*2.47 - 3.66*	4.35E+00	5.06E+00	5.63E-01	3.44E+00	4.82E+00	2.52E+00
2	*3.66 - 5.37*	1.29E+00	1.52E+00	9.88E-02	9.47E-01	1.58E+00	8.14E-01
1	*5.37 - 9.89*	5.20E-01	6.09E-01	4.41E-02	2.02E-01	3.77E-01	2.69E-01